BioMed Research International

Cardiovascular Physiology

Guest Editors: Karim Bendjelid, Bruno Levy, and Alain Broccard

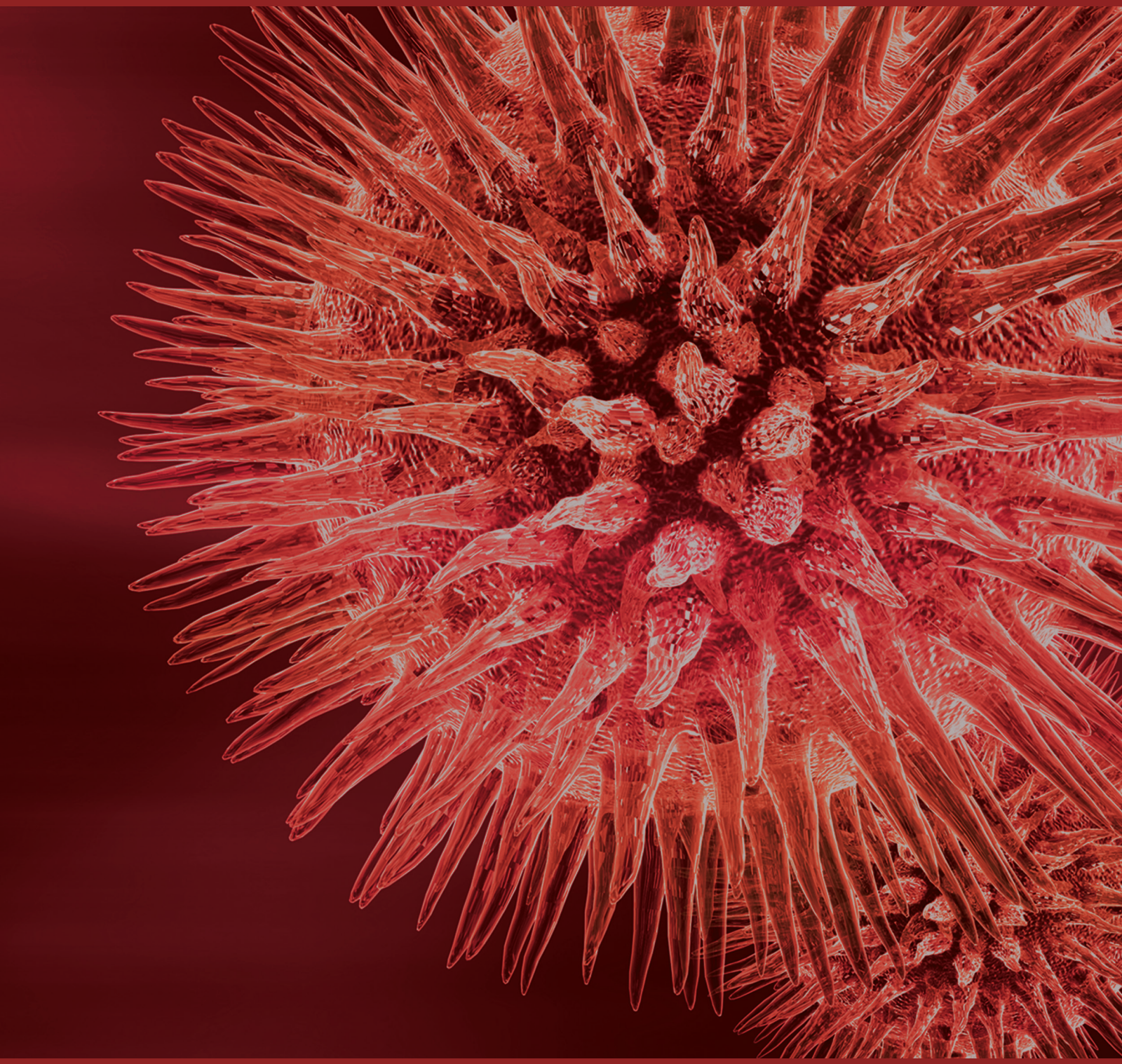

Cardiovascular Physiology

BioMed Research International

Cardiovascular Physiology

Guest Editors: Karim Bendjelid, Bruno Levy, and Alain Broccard

Contents

Hindawi Publishing Corporation
BioMed Research International
Volume 2015, Article ID 479134, 2 pages
http://dx.doi.org/10.1155/2015/479134

Editorial

Intensive Care Medicine Science: An Art Based on Applied Physiology?

Karim Bendjelid,[1,2] Bruno Levy,[3] and Alain Broccard[4]

[1]*Geneva Medical School, 1211 Geneva, Switzerland*
[2]*Intensive Care Service, Geneva University Hospitals, Geneva Medical School, 1211 Geneva, Switzerland*
[3]*Service de Réanimation Médicale Brabois, Vandoeuvre lès Nancy, France*
[4]*University of Minnesota, Regions Hospital Pulmonary and Critical Care Division, 640 Jackson Street, St. Paul, MN 55455, USA*

Correspondence should be addressed to Karim Bendjelid; karim.bendjelid@hcuge.ch

Received 30 September 2014; Accepted 30 September 2014

The provision of complex medical care in the intensive care unit (ICU) environment is challenging as the established goals of intensive care are to reduce the morbidity and mortality related to critical illness, maintain organ function, and restore health. Despite technological advances, the prevalence of death in the ICU remains a serious problem. Even if it is unlikely that intensive care medicine is recognized as an evidence-based process, the present reality reveals that scientific proof regarding patient management is very rare [1]. However, this medicine is pathophysiology based, and it necessitates the monitoring of physiological abnormalities to treat the patient. Indeed, outcome prediction models measuring the severity of illness of patients admitted to the ICU use physiological variables to predict hospital mortality. For instance, from the clinical and medical management perspective, the state-of-the-art Simplified Acute Physiology Score (SAPS) model is frequently used.

In the present state of medical knowledge, it is important to account for human physiology when treating critically ill patients, as these patients often present with circulatory failure. Understanding the properties of cardiovascular physiology is an excellent example of how general principles are useful in comprehending hemodynamic instability and shock states [2]. Therefore, from a physiological point of view, mastering the cardiovascular physiology and identifying the pathophysiological mechanisms and archetype involved in shock allow the physician to manage each situation according to the specific characteristics of the state of the patient.

In the first half of the 20th century, there was considerable confusion among physiologists regarding the combined role of the heart and vasculature in determining flow and pressure in the cardiovascular system [3]. Currently, our understanding of these subjects is constantly evolving. As part of the present special issue, respected researchers and physiologists provide an outline of the important advances in cardiovascular physiology and the great progress made in recent years within this discipline. The present papers take a deeper look at selected physiological principles and main beliefs that are the basis of intensive care medicine. In fact, the present papers investigate physiological principles using various techniques described in humans and animal experimentation. In addition, in the present issue, the use of mathematical and simulated models as alternative methods is highlighted as a potential way to study specific cases in diverse vessels. These papers, which describe numerical simulations of flow, ranging from the geometry of steady flow in rigid vessels to unsteady flow with elastic vessel walls, deserve further attention as several flow and wall models are compared. Finally, all of these works reinforce our use of these principles in clinical decision-making.

Thus, it must be established and accepted that specific cardiovascular physiology concepts are essential if and only if an appropriate form of intervention or treatment could be administered based on this knowledge. Indeed, it is important to note that our way of thinking about cardiovascular physiology in the ICU may sometimes be imperfect as views and understanding need to evolve [4]. Certainly, in the present state of knowledge, the most significant advantage of mastering cardiovascular physiology in critically ill patients

is the capability to recommend new methods of treatment for shock.

Karim Bendjelid
Bruno Levy
Alain Broccard

References

[1] J. B. West, "Making clinical decisions with insufficient evidence," *High Altitude Medicine & Biology*, vol. 11, no. 1, article 1, 2010.

[2] K. Bendjelid, "Right atrial pressure: determinant or result of change in venous return?" *Chest*, vol. 128, no. 5, pp. 3639–3640, 2005.

[3] N. Westerhof, J.-W. Lankhaar, and B. E. Westerhof, "The arterial windkessel," *Medical & Biological Engineering & Computing*, vol. 47, no. 2, pp. 131–141, 2009.

[4] S. Magder, "More respect for the CVP," *Intensive Care Medicine*, vol. 24, no. 7, pp. 651–653, 1998.

Hindawi Publishing Corporation
BioMed Research International
Volume 2015, Article ID 628416, 11 pages
http://dx.doi.org/10.1155/2015/628416

Clinical Study

Patient-Specific Simulation of Coronary Artery Pressure Measurements: An *In Vivo* Three-Dimensional Validation Study in Humans

Panagiotis K. Siogkas,[1] Michail I. Papafaklis,[2,3,4] Antonis I. Sakellarios,[1] Kostas A. Stefanou,[5] Christos V. Bourantas,[6] Lambros S. Athanasiou,[1] Themis P. Exarchos,[5] Katerina K. Naka,[2,4] Lampros K. Michalis,[2,4] Oberdan Parodi,[7] and Dimitrios I. Fotiadis[1,4,5]

[1] *Unit of Medical Technology and Intelligent Information Systems, Department of Materials Science, University of Ioannina, 45110 Ioannina, Greece*
[2] *Department of Cardiology, Medical School, University of Ioannina, 45110 Ioannina, Greece*
[3] *Harvard-MIT Division of Health Sciences & Technology, Massachusetts Institute of Technology, Cambridge, MA 02139, USA*
[4] *Michailideion Cardiac Center, University of Ioannina, 45110 Ioannina, Greece*
[5] *Biomedical Research Institute-FORTH, University of Ioannina, 45110 Ioannina, Greece*
[6] *Thoraxcenter, Erasmus Medical Center, 3000 CA Rotterdam, Netherlands*
[7] *Istituto di Fisiologia Clinica, Consiglio Nazionale delle Ricerche (IFC-CNR), 56124 Pisa, Italy*

Correspondence should be addressed to Dimitrios I. Fotiadis; fotiadis@cs.uoi.gr

Received 25 April 2014; Accepted 10 September 2014

Academic Editor: Karim Bendjelid

Pressure measurements using finite element computations without the need of a wire could be valuable in clinical practice. Our aim was to compare the computed distal coronary pressure values with the measured values using a pressure wire, while testing the effect of different boundary conditions for the simulation. Eight coronary arteries (lumen and outer vessel wall) from six patients were reconstructed in three-dimensional (3D) space using intravascular ultrasound and biplane angiographic images. Pressure values at the distal and proximal end of the vessel and flow velocity values at the distal end were acquired with the use of a combo pressure-flow wire. The 3D lumen and wall models were discretized into finite elements; fluid structure interaction (FSI) and rigid wall simulations were performed for one cardiac cycle both with pulsatile and steady flow in separate simulations. The results showed a high correlation between the measured and the computed coronary pressure values (coefficient of determination [r^2] ranging between 0.8902 and 0.9961), while the less demanding simulations using steady flow and rigid walls resulted in very small relative error. Our study demonstrates that computational assessment of coronary pressure is feasible and seems to be accurate compared to the wire-based measurements.

1. Introduction

Cardiovascular disease is the leading cause of mortality in developed countries. Atherosclerosis develops due to the accumulation of lipids in the arterial wall and the migration of smooth muscle cells to the intima and leukocyte infiltration, thereby forming plaques in the arterial wall. When the progression of atherosclerotic lesions exceeds the compensatory wall response, plaque protrudes into the lumen causing stenosis and obstructs blood flow to the distal myocardial bed.

Lumen obstruction may be hemodynamically significant causing stable angina in patients. One of the most common and efficient ways to assess the hemodynamic significance of coronary lesions is the measurement of the fractional flow reserve (FFR) [1]. FFR is defined as the maximal coronary flow in an arterial segment with a stenosis, divided by the maximal coronary flow in the same arterial segment if no

stenosis was present and is measured as the ratio of distal to proximal (i.e., aortic) coronary pressure under maximal vasodilation. Therefore, assessment of coronary pressure is critical for estimating FFR. The measurement of coronary pressure is currently performed invasively with the use of a dedicated pressure wire. However, the advent of technology has now enabled blood flow simulations in three-dimensional (3D) coronary artery reconstructions. Accurate calculation of coronary pressure using finite element simulations without using a pressure wire could be a valuable tool in the catheterization laboratory.

Blood flow simulations are demanding and depend on the applied boundary conditions. A critical boundary condition imposed during the simulation is the behavior of the arterial wall. There are two main approaches for simulating the behavior of the wall. One assumes that the arterial wall is rigid, not taking into consideration the interaction between the blood and the arterial wall [2–6], while the second assumes that arteries are elastic incorporating the interaction between the blood and the arterial walls into the simulation.

The first attempts of blood flow simulations in human arteries were made on 3D simplified tube-like geometries representing arterial segments. Following the advances in image processing, accurate 3D reconstructed arterial models were used for computational blood flow simulations, resulting in more precise results. The rigid wall assumption led to quick blood flow simulations since only the lumen needed to be discretized. However, in an effort to realistically simulate the complexity of the human vasculature, the interaction between the blood and the arterial wall was introduced by applying fluid structure interaction (FSI) models [2, 7–18]. According to these models, blood flow creates loads on the surface of the arterial wall forcing it to deform. The elastic nature of the arterial wall tends to restore the wall to its original state, thereby causing the deformation of the blood domain. Both the blood and the arterial wall domains are discretized and the equations of each domain are solved and used as initial conditions to the other domain. Due to the large number of equations that need to be solved, FSI simulations are very demanding in computational resources and very time-consuming compared to the rigid wall approach but are considered to provide more accurate results for the flow field. However, the differences in computed pressure values between the rigid wall and FSI approaches have not been previously studied.

Currently, we present a validation study for coronary artery pressure measurements using patient-specific 3D coronary artery reconstructions and investigate (a) the accuracy of the computed pressure results using the invasive pressure measurements as the gold standard and (b) the differences in computed pressure measurements between different critical boundary conditions (steady versus pulsatile flow and rigid wall versus FSI).

2. Methods

2.1. Patient Data. Six subjects underwent intravascular ultrasound (IVUS) and angiography examinations for angina symptoms at CNR (Institute of Clinical Physiology, Milan, Italy). The clinical and demographic patient characteristics are presented in Table 1. A coronary guide wire (0.014 inch diameter) with miniaturized tip transducers for pressure and flow measurements (Combo wire, Volcano Corp.) was used. The pressure-flow wire was inserted in the coronary artery until a stable recording of the flow velocity was obtained at a distal coronary location. The aforementioned parameters were measured at the baseline and during maximal coronary vasodilation (hyperemic conditions) which was achieved with the intravenous administration of adenosine (140 mcg/kg/min). The parameters measured under hyperemic conditions were used as boundary conditions for the simulations and are described in detail in Section 2.3.4. The final measurements included pressure values throughout three cardiac cycles at the proximal (guiding catheter at the ostium of the artery) and distal locations of each arterial segment, combined with flow velocity values at the distal location both at baseline and during maximal hyperemia. A 3-French catheter with a 64-crystal electronic ultrasound probe was used for IVUS examination (Eagle-Eye, Volcano Corp.). The catheter was placed in the distal part of the examined vessel and then a motorized pullback (speed 1 mm/sec) was performed. Following contrast injection two isocentric angiographic views were obtained to depict the position of the catheter inside the vessel before the start of the pullback. The IVUS probe was positioned distally at the same location where the distal coronary pressure-flow measurements were performed so that these measurements could be applied as boundary conditions for the blood flow simulations in 3D reconstructed arterial models as it is described below. Figure 1 shows the angiographic images with the exact locations of the acquired measurements for the right coronary artery (RCA) of patient 4.

2.2. Three-Dimensional Reconstruction. The 3D reconstruction of the 8 arterial segments was performed using a methodology which is based on the fusion of IVUS and biplane angiographic data [19]. The end-diastolic frames were selected for segmenting the lumen and the external elastic media (i.e., vessel wall) borders. Then, the corresponding angiographic end-diastolic images were used to reconstruct the 3D IVUS catheter path. The segmented frames were then placed onto the generated 3D catheter path and were appropriately oriented. Finally, two point clouds representing the lumen and vessel wall were derived for each artery and were processed to nonuniform rational B-spline (NURBS) 3D surfaces. Figure 2 depicts two 3D reconstructed models of two RCA segments. Our dataset includes 4 RCA and 4 LAD segments with mild or moderate lumen stenosis.

2.3. Blood Flow Simulation. Transient as well as steady flow simulations were carried out on all 8 arterial segments with either rigid or deformable wall assumptions. In total, four different approaches were used: FSI-transient, FSI-steady flow, rigid walls-transient and rigid walls-steady flow. The most demanding in terms of computational resources is the one using FSI models with transient flow as it is time

Table 1: Patient demographic and clinical characteristics.

Patient	Age	Sex	Familiarity	Hypertension	Hypercholesterolemia	Diabetes	Angina
01	73	M	N	Y	Y	Y	N
02	55	M	N	Y	Y	N	Y
03	56	M	Y	Y	Y	Y	N
04	56	M	N	Y	Y	Y	N
05	70	M	Y	Y	Y	N	N
06	75	M	N	Y	Y	N	N

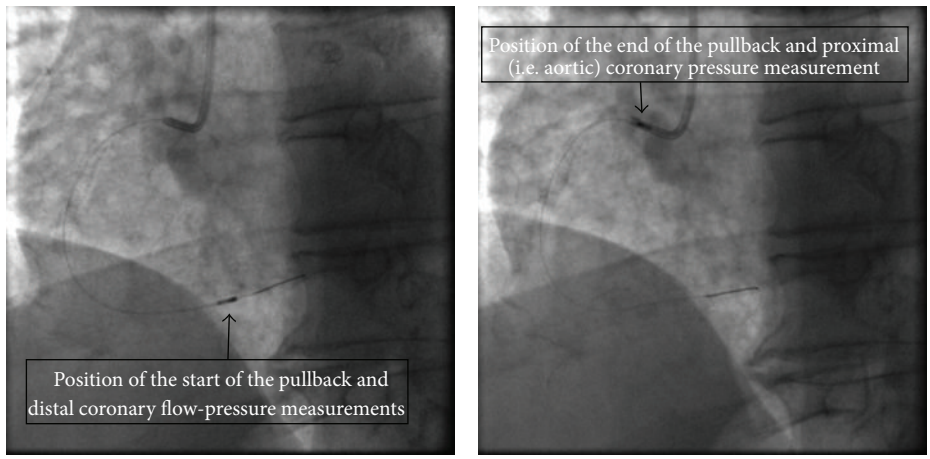

(a) (b)

Figure 1: The two views depict the exact locations of the start (a) and end (b) of the pullback procedure as well as the exact positions of the pressure and flow measurements acquisition.

dependent, whereas the lowest computational requirements are for the one with the rigid walls assumption and the steady flow. The computational approach and the boundary conditions for each type of simulation are presented in detail below.

2.3.1. Rigid Wall Assumption. Blood flow is modeled using the Navier-Stokes and the continuity equations:

$$\rho\frac{\partial \mathbf{v}}{\partial t} + \rho\left(\mathbf{v}\cdot\nabla\right)\mathbf{v} - \nabla\cdot\boldsymbol{\tau} = 0,$$
$$\nabla\cdot\left(\rho\mathbf{v}\right) = 0, \tag{1}$$

where $\mathbf{v}$ is the blood velocity vector, ρ the blood density, and $\boldsymbol{\tau}$ is the stress tensor, defined as

$$\boldsymbol{\tau} = -p\delta_{ij} + 2\mu\varepsilon_{ij}, \tag{2}$$

where δ_{ij} is the Kronecker delta, μ is the blood dynamic viscosity, p is the blood pressure, and ε_{ij} is the strain tensor calculated as

$$\varepsilon_{ij} = \frac{1}{2}\left(\nabla\mathbf{v} + \nabla\mathbf{v}^{T}\right). \tag{3}$$

Blood was treated as a Newtonian fluid having a density of 1060 kg/m^3 and a dynamic viscosity 0.0035 Pa·s. The blood flow was considered laminar with the Reynolds number ranging between 126 and 883.

2.3.2. Fluid Structure Interaction-Blood Domain. In FSI simulations, the interface between the lumen and the wall (i.e., the wall boundary of the fluid domain) deforms, and thus the equations governing fluid flow are expressed in terms of the fluid variables relative to the mesh movement. For the moving reference frame in FSI simulations, the momentum conservation equation for fluid flow is

$$\rho\frac{\partial \mathbf{v}}{\partial t} + \rho\left(\left(\mathbf{v}-\mathbf{w}\right)\cdot\nabla\right)\mathbf{v} - \nabla\cdot\boldsymbol{\tau} = 0, \tag{4}$$

where ρ is the density of the blood, $\mathbf{v}$ is the blood velocity vector, $\mathbf{w}$ is the vector of the moving mesh velocity (i.e., the velocity of the deformable wall boundary), and $\boldsymbol{\tau}$ is the stress tensor.

(a) Fluid Structure Interaction-Arterial Wall Domain. The following momentum conservation equation is used to model the arterial wall domain:

$$\nabla\boldsymbol{\tau}_s + \mathbf{f}_s^{\mathbf{B}} = \rho_s\ddot{\mathbf{d}}_s, \tag{5}$$

where $\boldsymbol{\tau}_s$ is the arterial wall stress tensor, $\mathbf{f}_s^{\mathbf{B}}$ are the body forces per unit volume, ρ_s is the density of the arterial wall, and $\ddot{\mathbf{d}}_s$ is the solid's local acceleration.

Due to lack of universal values for the parameters of the material properties of the arterial wall, we have used a nine-parameter Mooney-Rivlin model to describe the material

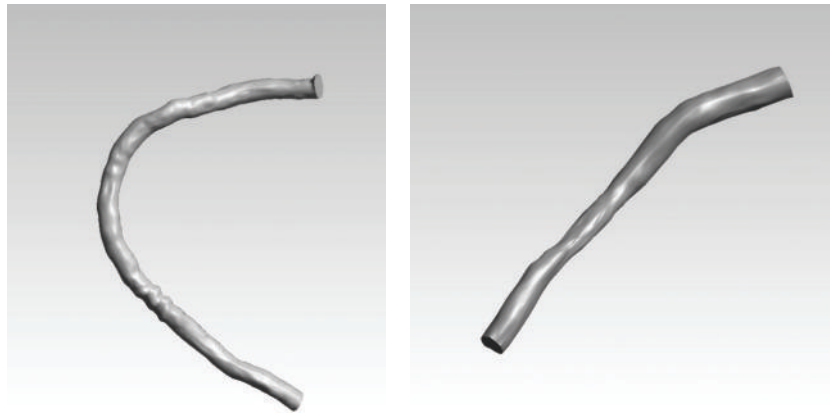

(a) (b)

Figure 2: Three-dimensional reconstruction of the lumen of a right coronary artery for patient #2 (a) and patient #1 (b).

properties of the wall. Despite the fact that the coronary arterial wall is considered to have an anisotropic and heterogeneous structure due to the complex composition (e.g., collagen fibers), we applied an isotropic and homogenous material model because of the absence of *in vivo* data regarding the fiber direction and the heterogeneity that describes the anisotropic behavior of the arterial tissue. The parameters of the Mooney-Rivlin model were set as previously described in FSI analyses in the human right coronary artery [18, 20]. The following equation is used to calculate the strain energy function:

$$\begin{aligned} W = {} & c_{10}\left(\bar{I}_1 - 3\right) + c_{01}\left(\bar{I}_2 - 3\right) + c_{20}\left(\bar{I}_1 - 3\right)^2 \\ & + c_{11}\left(\bar{I}_1 - 3\right)\left(\bar{I}_2 - 3\right) + c_{02}\left(\bar{I}_2 - 3\right)^2 \\ & + c_{30}\left(\bar{I}_1 - 3\right)^3 + c_{21}\left(\bar{I}_1 - 3\right)^2\left(\bar{I}_2 - 3\right) \\ & + c_{12}\left(\bar{I}_1 - 3\right)\left(\bar{I}_2 - 3\right)_2 + c_{03}\left(\bar{I}_2 - 3\right)^3 + \frac{1}{d}(J-1)^2. \end{aligned} \tag{6}$$

$\bar{I}_1$, $\bar{I}_2$ are the first and second deviatoric strain invariants, respectively, and J is the determinant of the elastic deformation gradient tensor. The rest of the parameters are set as in [18]: $c_{10} = 0.07$ MPa, $c_{20} = 3.2$ MPa, and $c_{21} = 0.0716$ MPa and the others are equal to zero. The compressibility parameter d is defined as

$$d = \frac{2}{K}, \tag{7}$$

where K is the bulk modulus (1×10^{-5}).

2.3.3. Fluid Structure Interaction-Coupling Equations. In order for the two domains to be solved together, the following displacement compatibility and traction equilibrium equations must be satisfied:

$$\boldsymbol{\tau}_s \cdot \hat{\mathbf{n}}_s = \boldsymbol{\tau}_f \cdot \hat{\mathbf{n}}_f \qquad (x, y, z) \in \Gamma^S_{\mathrm{FSI}} \cap \Gamma^F_{\mathrm{FSI}}, \tag{8}$$

$$\mathbf{d}_s = \mathbf{d}_f \qquad (x, y, z) \in \Gamma^S_{\mathrm{FSI}} \cap \Gamma^F_{\mathrm{FSI}}, \tag{9}$$

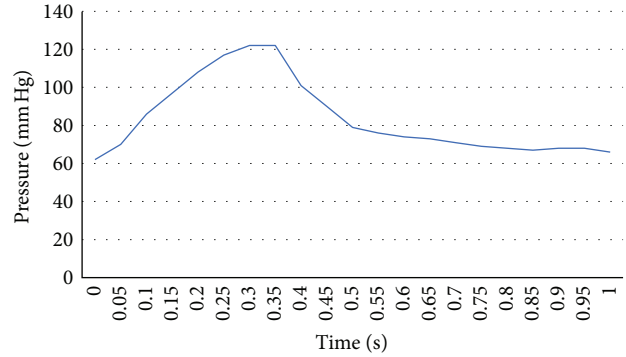

Figure 3: Measured pressure profile for patient #6 for a full cardiac cycle.

where Γ^S_{FSI} is a set of points on the arterial wall and Γ^F_{FSI} a set of points on the lumen.

The generated stresses from the fluid and the solid on the interface of the two domains must be in equilibrium (8) and the displacements of the two domains on their common surface must be equal (9).

2.3.4. Boundary Conditions

(i) Inlet. Regarding the inlet, a measured pressure profile in the catheterization laboratory was applied as a boundary condition. In particular, for the transient simulations, a full cardiac cycle (either the second or the third measured in order for the measurements to be stable and accurate) was divided into time steps of 0.05 seconds (Figure 3 exhibits the applied inlet pressure profile for patient 6), while for the steady flow simulations, the mean pressure value of the same cardiac cycle that was used in the transient ones was applied as the inlet boundary condition.

(ii) Outlet. Velocity profiles were available at the distal end of the reconstructed artery (measured invasively using the combo pressure-flow wire) and were prescribed as outlet

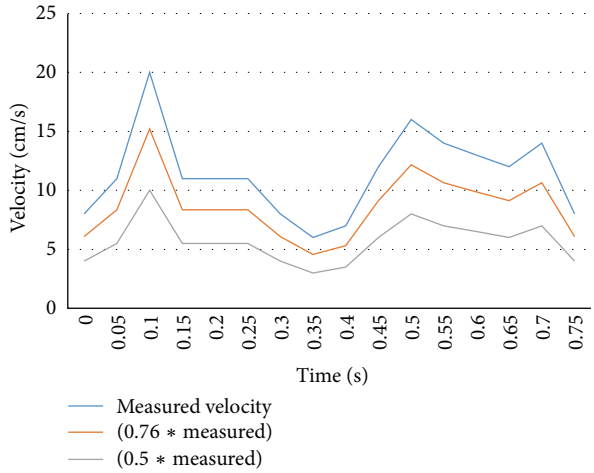

FIGURE 4: Mean velocity values calculated for patient #1 in order to determine the optimal velocity profile for validation.

boundary conditions. To capture the true nature of the velocity profile of the outlet, we used the developed flow (this has a paraboloid profile) derived from the 3D geometry and we defined the "magnitude" of the developed flow according to the flow measurements. To achieve that, we applied the mass flow rate profile for each case which was calculated as

$$\dot{m} = \rho \mathbf{v} A, \tag{10}$$

where ρ is the blood's density, $\mathbf{v}$ is the velocity of blood, and A is the cross-sectional area of the outlet. However, due to the nature of the Doppler wire measurements, we executed a parametric study regarding the accuracy of the measured velocity values. The measured velocity values from the wire cannot be considered to be the highest of the cross section due to the fact that either the wire is not aligned in the center of the vessel or due to the fact that the wire itself interrupts the flow. The velocity value that is inserted in the mass flow rate equation is the mean velocity value of the profile. We tried three different velocity profiles to examine which fits our problem best. In the first case scenario, the measured values from the Doppler wire as the mean profile value were used; in the second scenario a ratio of 0.76 ($\mathbf{v}_{\text{mean}} = 0.76 * \mathbf{v}_{\text{measured}}$) as it was previously suggested [21]; and in the third scenario a ratio of 0.5 which is common in the generalized Poiseuille flow. Figure 4 depicts the velocity profiles of the three cases for an RCA segment of patient 1. The closest results to the measured values were achieved by using the measured velocity values as the mean value of the profile. The results of the parametric study are presented in detail in Section 3.

(iii) Lumen Wall Interface. At the lumen wall, a no-slip boundary condition was applied, meaning that the blood had zero velocity relative to the solid-fluid interface.

(iv) Arterial Wall. The distal ends of the arterial wall (inlet and outlet) were assumed to be fixed on all directions so that motion was restricted at these sites.

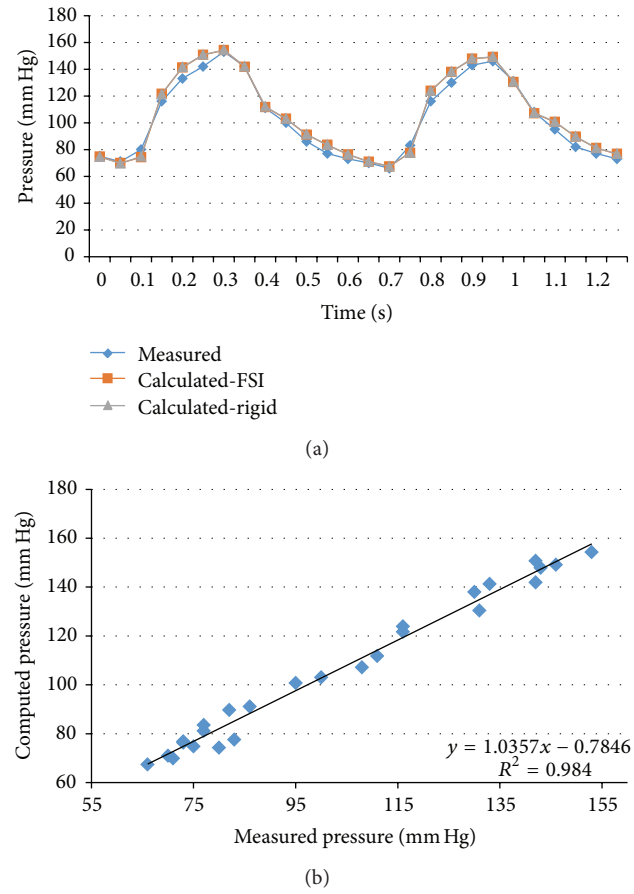

FIGURE 5: (a) depicts the pressure waveforms for the examined cardiac cycles (measured and calculated results) and (b) exhibits the linear regression analysis for patient #1.

2.3.5. Mesh. The lumen was discretized into hexahedral elements, with an element face size ranging from 0.09 to 0.12 mm, with an increased mesh density throughout the boundary layer of the flow close to the arterial wall. The arterial wall was discretized into tetrahedral elements with an element face size 0.09 mm and 15 layers of brick elements with a thickness of 0.03 mm at the interface with the lumen. The brick element layers were first generated from the interface of the wall and the lumen towards the outer perimeter of the wall and then the remaining volume was discretized into tetrahedral elements.

The mesh size both for the lumen and the wall was selected after performing a mesh (face size) sensitivity analysis. The sensitivity analysis was performed in a representative case both for the rigid (Table 4) and deformable (Table 5) wall assumption using steady-state flow. The mesh sensitivity analysis for the deformable wall simulation (Table 5) was performed using a face size of 0.09–0.12 mm for the lumen (as derived from the initial sensitivity analysis for the rigid wall assumption in Table 4). The analysis was based on the correlation between the mesh size and the produced results regarding the average wall shear stress of the same cross-section on 4 different mesh sizes. The mesh size with <5%

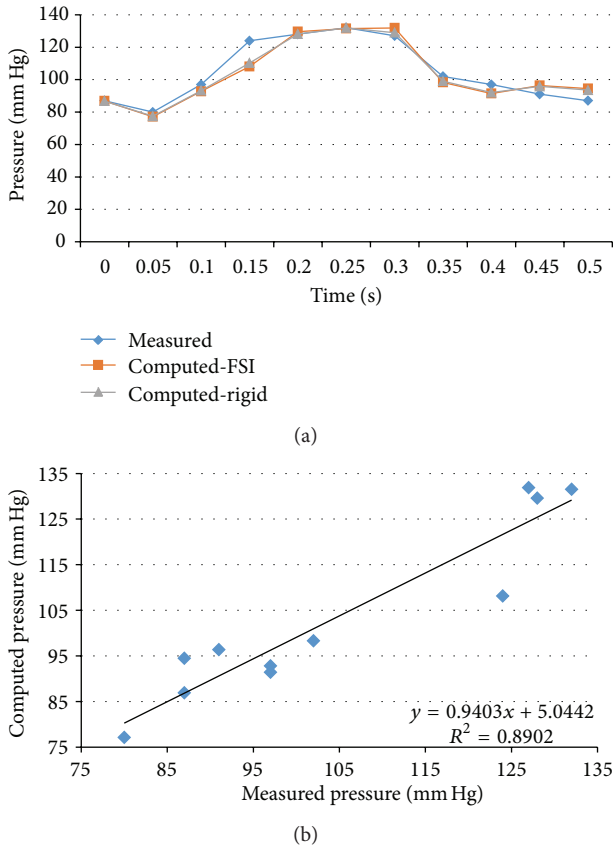

FIGURE 6: (a) depicts the pressure waveforms for the examined cardiac cycles (measured and computed results) and (b) exhibits the linear regression analysis for patient #2.

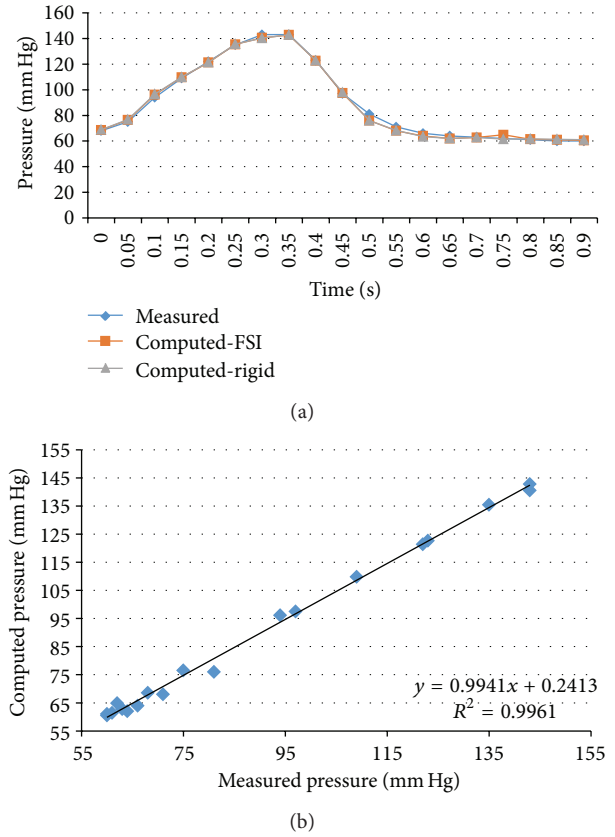

FIGURE 7: (a) depicts the pressure waveforms for the examined cardiac cycles (measured and computed results) and (b) exhibits the linear regression analysis for patient #3.

difference in wall shear stress values was used in the final simulations; of note, computed pressure values at the outlet, on which we focus in the current study, were also minimally influenced by the mesh size (<0.05% difference, Tables 4 and 5).

3. Results

A series of blood flow simulations using different assumptions and approaches was carried out, a linear regression analysis on all 8 vessels was performed, and the respective aggregate Bland-Altman plot was obtained in order to examine the correlation of the computed results to the measured ones.

3.1. Validation Results. We performed transient FSI simulations for one cardiac cycle. The produced results show excellent correlation between the measured and the calculated values with the worst case scenario having a coefficient of determination $r^2 = 0.8902$ and the best case scenario having an $r^2 = 0.9961$. The Bland-Altman plots also depict a high similarity between the measured and the computed values with almost all values being within the 1.96∗SD cut-offs. Figures 5, 6, 7, 8, 9, 10, 11, and 12 depict the pressure waveforms of the measured and the rigid wall computed as well as the FSI computed values and the linear regression analysis plots for all cases. Moreover, Figure 13 represents an aggregate Bland-Altman plot for all 8 cases with a mean difference close to zero.

3.2. Rigid Wall versus FSI Simulations. The calculated mean difference between the rigid wall and the FSI simulations for all cases reached the statistically negligible value of 0.26%. The rigid wall simulations produced slightly higher pressure values than the FSI simulations on most of the examined cases. Moreover, compared to the values measured in the catheterization laboratory, and the FSI simulations produced slightly more accurate results than the rigid wall ones. In Table 2, a comparison between the measured and the computed mean outlet pressure values for all cases is presented.

3.3. Transient versus Steady Flow Simulations. The computed pressure of the steady flow simulation was compared to the average pressure of the same cardiac cycle as it was computed from the transient simulation. Our results demonstrated a very close match between the steady flow and the transient results for both rigid and FSI simulations. In detail, the two simulation types exhibited a mean difference of 0.44%

Table 2: Comparison between the wire-based measured pressure values (P_{out}) and the computed values from the four types of simulations ($P_{out(comp)}$).

Patient #	P_{out} (mm Hg)	FSI-transient $P_{out(comp)}$ (mm Hg)	Rigid-transient $P_{out(comp)}$ (mm Hg)	FSI-steady state $P_{out(comp)}$ (mm Hg)	Rigid-steady state $P_{out(comp)}$ (mm Hg)
1-RCA	103.04	105.93	106.06	105.46	105.48
2-RCA	104.73	103.52	103.38	103.82	103.71
3-LAD	89.32	89.03	89	89.17	89.15
4-RCA	61.95	63.68	63.83	64.01	64.22
4-LAD	67.47	70.72	71.45	70.94	71.59
5-RCA	105.2	102.42	102.68	102.51	102.58
5-LAD	85.95	83.64	83.85	83.59	83.72
6-LAD	83.52	82.8	82.77	82.98	83.03

Table 3: Results of the parametric study concerning the velocity profiles (steady-state simulations).

Patient #	$P_{out(comp)}$ (mm Hg)	$P_{out}(v_{max})$ (mm Hg)	$P_{out}(0.76 * v_{max})$ (mm Hg)	$P_{out}(0.5 * v_{max})$ (mm Hg)
1-RCA	103.04	105.48	106.16	106.75
2-RCA	104.73	103.71	106.56	107.6
3-LAD	89.32	89.15	90.48	91.19
4-RCA	61.95	64.22	65.02	65.66
4-LAD	67.47	71.59	73.21	74.68
5-RCA	105.2	102.58	103.18	103.53
5-LAD	85.95	83.72	84.07	84.55
6-LAD	83.52	83.03	85.23	86.96

(Table 2). The results that were closest to the measured wire-based values were the ones obtained using the transient simulations as expected. Table 3 demonstrates the results of the parametric study related to the flow velocity values used in the mass flow rate equation for the outlet boundary condition. It seems that the optimal results were obtained when the measured flow velocity values from the combo wire were used as the maximum and not the mean values of the velocity profile.

4. Discussion

We presented a study on coronary artery pressure measurements using blood flow simulation in realistic 3D reconstructed coronary arteries. Our primary findings are the following: (I) computed distal coronary pressure values correlate very well with the measured ones using the pressure wire and (II) the assumption of rigid walls and steady flow results in negligible differences compared to the more demanding FSI and pulsatile simulations, respectively.

Several validation studies have been previously carried out to test the accuracy and validity of numerical methods. Phantom, simplified 3D models, or patient-specific arterial models have been previously employed in order to perform blood flow simulations. Left coronary artery bifurcations and carotid bifurcations, as well as mesenteric arterial segments were included. The computed velocity profiles were then compared to the measured ones resulting in a fairly good agreement between the measured and the computed values [22–27]. A recent study examined the correlation of flow and pressure patterns between the computed and the measured values for two deformable flow phantoms mimicking a normal and an obstructed aorta, respectively [28]. Good qualitative agreement was found between the measured and the computed values for flow, exhibiting a better correlation for the pressure results. The majority of those studies focus on the carotid vasculature due to the technical difficulty that arises when dealing with the coronary vasculature. Coronary arteries require invasive imaging methods in order to acquire information related to the size and complex anatomy of the obstruction. Therefore, there is a lack of data on the accuracy of the results regarding numerical simulations in human coronary arteries.

In our study, we focus on coronary arteries and use realistic patient-specific reconstructed coronary arteries derived from angiographic and IVUS data. Furthermore, we use *in vivo* data from invasive flow/pressure measurements in the catheterization laboratory for our validation purposes. The results exhibited a very high correlation of the computed pressure values compared to the measured ones. The pressure waveforms between the measured and the computed values distally in coronary arteries were very close to each other, and the mean computed pressure values for each case showed very small relative error values. Moreover, there was a very

Table 4: Results of the mesh sensitivity analysis in the lumen (rigid wall assumption).

Face size	Lumen mesh size (elements)	Outlet pressure (mm Hg)	Difference in pressure (%)	Cross-sectional WSS (Pa)	Difference in WSS (%)
0.13–0.15 mm	87 K	105.516	0.053	6.31	21.22
0.12–0.15 mm	176 K	105.512	0.049	7.14	10.86
0.09–0.12 mm	**400 K**	**105.483**	**0.022**	**7.78**	**2.87**
0.07–0.09 mm	657 K	105.460	—	8.01	—

WSS: wall shear stress.
The selected mesh size for the final simulations is indicated in bold font (<5% difference in WSS).

Table 5: Results of the sensitivity analysis in the deformable wall assumption (lumen face size was 0.09–0.12 mm).

Element size	Wall mesh size (elements)	Outlet pressure (mm Hg)	Difference in pressure (%)	Cross-sectional WSS (Pa)	Difference in WSS (%)
0.13 mm	292 K	105.494	0.048	6.38	21.62
0.10 mm	540 K	105.487	0.042	7.19	11.67
0.09 mm	**582 K**	**105.458**	**0.014**	**7.85**	**3.56**
0.07 mm	1.232 M	105.443	—	8.14	—

WSS: wall shear stress.
The selected mesh size for the final simulations is indicated in bold font (<5% difference in WSS).

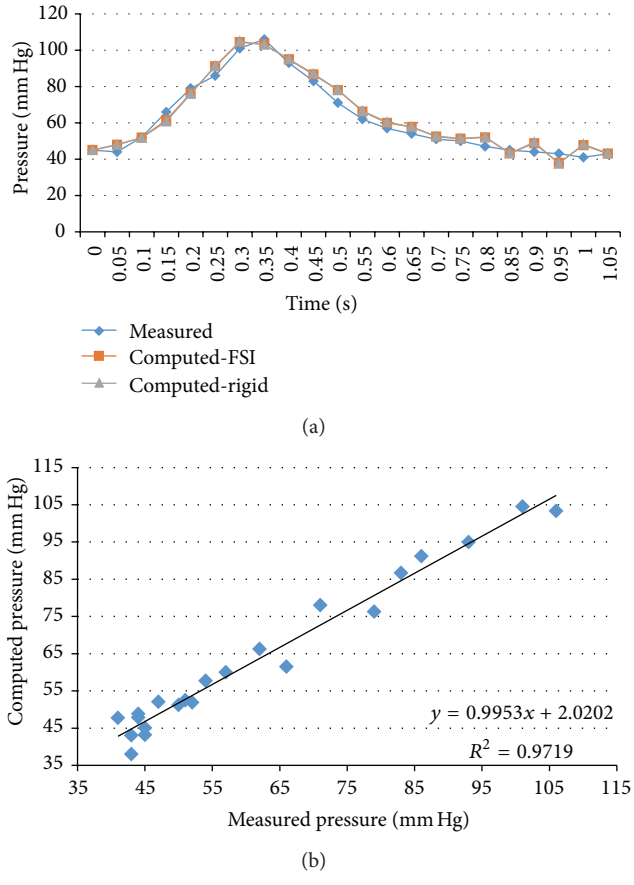

Figure 8: (a) depicts the pressure waveforms for the examined cardiac cycles (measured and computed results) and (b) exhibits the linear regression analysis for patient #4, right coronary artery.

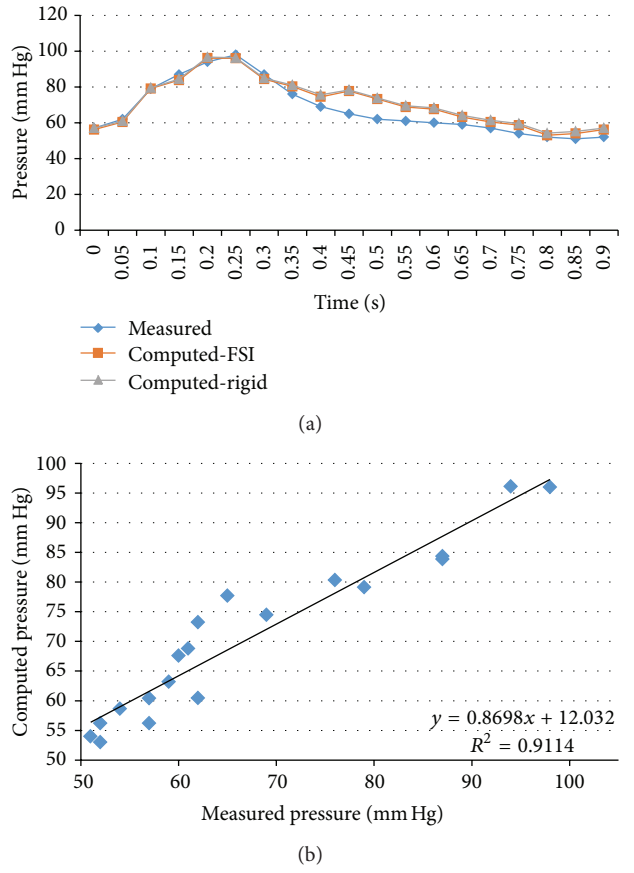

Figure 9: (a) depicts the pressure waveforms for the examined cardiac cycles (measured and computed results) and (b) exhibits the linear regression analysis for patient #4, left anterior descending coronary artery.

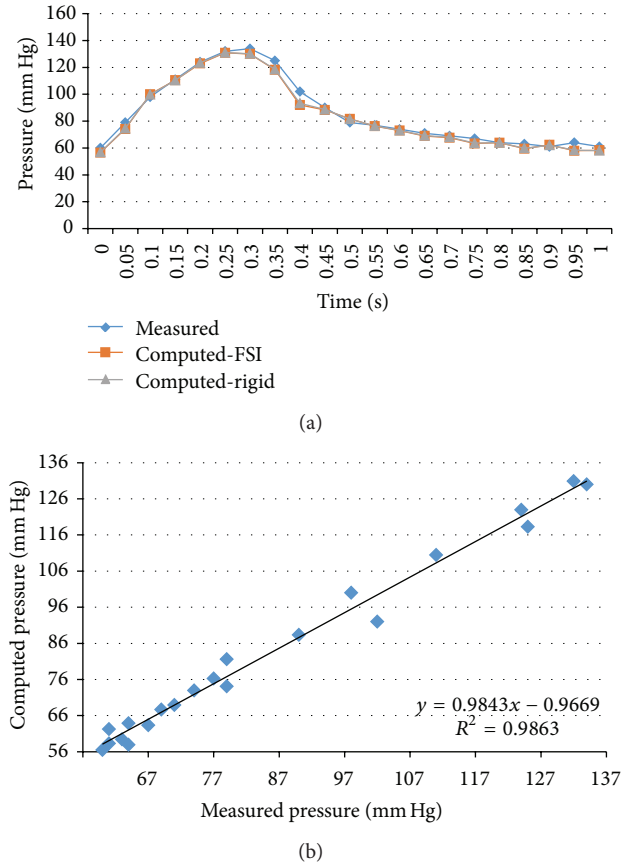

Figure 10: (a) depicts the pressure waveforms for the examined cardiac cycles (measured and computed results) and (b) exhibits the linear regression analysis for patient #5, right coronary artery.

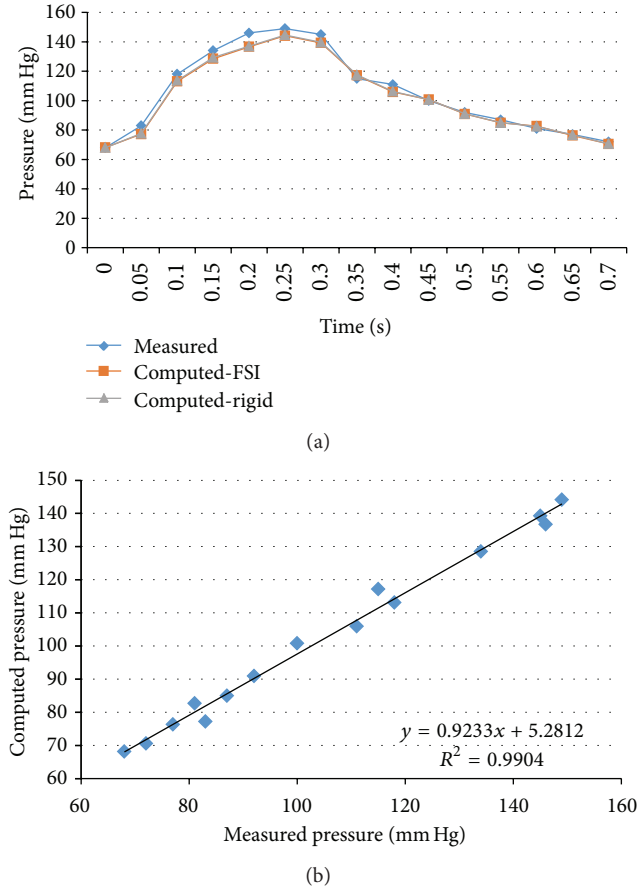

Figure 11: (a) depicts the pressure waveforms for the examined cardiac cycles (measured and computed results) and (b) exhibits the linear regression analysis for patient #5, left anterior descending coronary artery.

good agreement between the measured and the computed values. In addition, our findings demonstrate that the less demanding simulations using steady flow and rigid walls instead of pulsatile flow and FSI result in very small relative error. Therefore, our results support the use of the simpler and less time-consuming simulations for coronary artery pressure computation.

Clinical Implications and Challenges. Hemodynamic factors such as arterial pressure both proximal and distal to coronary stenoses are of great clinical importance. FFR, calculated as the ratio of distal to proximal coronary pressure under maximal vasodilation, has been shown to discriminate functionally significant stenoses and help in patient management leading to favorable clinical outcomes [29]. Our results support the use of numerical simulations for assessing distal coronary pressure in humans. This approach implemented in 3D realistic human coronary arteries could open the pathway to FFR assessment based on imaging data only without the need of a pressure wire. However, several challenges lie in the pathway of virtual FFR assessment including the "*a priori*" selection of the appropriate boundary condition for hyperemic flow, the incorporation of the resistance of the distal myocardial bed into the simulation, and the effect of flow division in the branched coronary tree. Although our results demonstrated that finite element simulation in realistic 3D coronary models may yield accurate distal pressure measurements if aortic pressure and coronary flow are known, further clinical studies are needed to test the accuracy of virtual pressure measurements when patient-specific hemodynamic conditions at the inlet are not known.

Limitations. The reconstructed segments in the current study neglect the presence of bifurcations which influence flow distribution. Moreover, the hemodynamic significance (i.e., pressure drop) of the coronary stenoses in the arteries studied was not large, and thus we did not have the opportunity to test the accuracy of the computed pressure values in cases with large pressure gradients.

5. Conclusions

Our study highlights the value of numerical simulations applied in 3D models for assessing hemodynamic factors such as coronary artery pressure. The accuracy of the computed results supports the use of this approach for virtual pressure

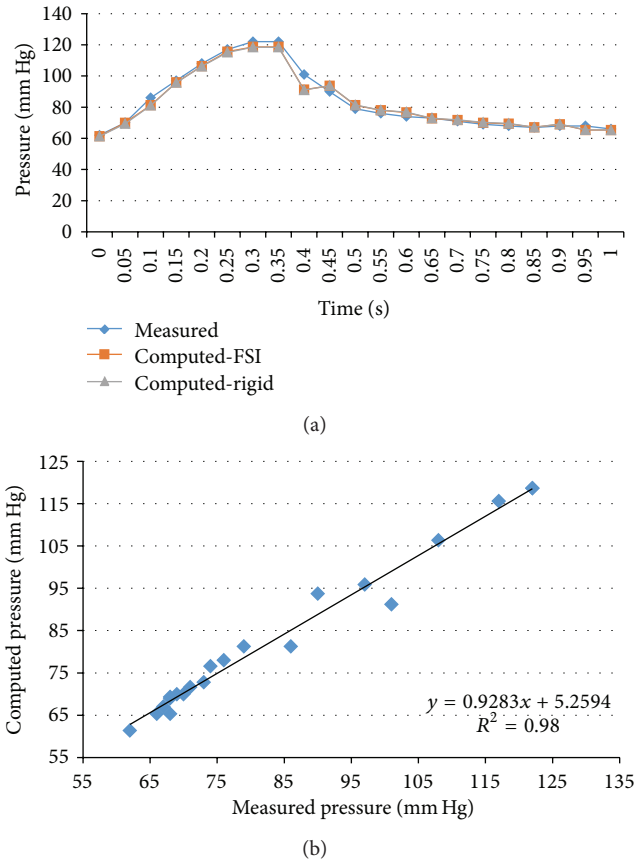

FIGURE 12: (a) depicts the pressure waveforms for the examined cardiac cycles (measured and computed results) and (b) exhibits the linear regression analysis for patient #6.

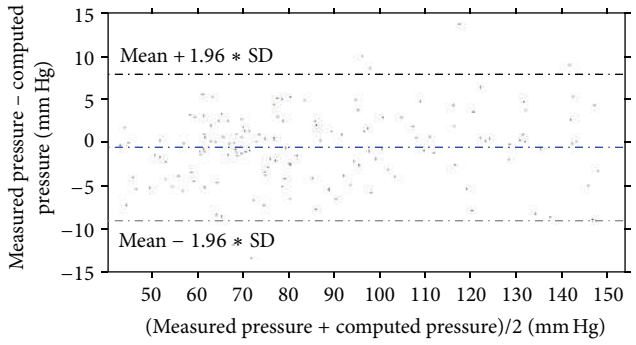

FIGURE 13: Bland-Altman plot for all 8 cases.

calculation which may have major clinical implications for assessing the hemodynamic significance of coronary stenoses without using a pressure wire in the catheterization laboratory.

Conflict of Interests

The authors declare that there is no conflict of interest regarding the publication of this paper.

Acknowledgments

This research project has been cofinanced by the European Union (European Regional Development Fund (ERDF)) and Greek National Funds through the Operational Program "Thessaly-Mainland Greece and Epirus-2007–2013" of the National Strategic Reference Framework (NSRF 2007–2013).

References

[1] M. J. Kern, A. Lerman, J. W. Bech et al., "Physiological assessment of coronary artery disease in the cardiac catheterization laboratory: a scientific statement from the American Heart Association Committee on diagnostic and interventional cardiac catheterization, council on clinical cardiology," *Circulation*, vol. 114, no. 12, pp. 1321–1341, 2006.

[2] M. Kojic, N. Filipovic, B. Stojanovic, and N. Kojic, *Computer Modeling in Bioengineering: Theoretical Background, Examples and Software*, John Wiley & Sons, New York, NY, USA, 2008.

[3] F. Kabinejadian and D. N. Ghista, "Compliant model of a coupled sequential coronary arterial bypass graft: effects of vessel wall elasticity and non-Newtonian rheology on blood flow regime and hemodynamic parameters distribution," *Medical Engineering & Physics*, vol. 34, no. 7, pp. 860–872, 2012.

[4] M. Malvè, A. García, J. Ohayon, and M. A. Martínez, "Unsteady blood flow and mass transfer of a human left coronary artery bifurcation: FSI vs. CFD," *International Communications in Heat and Mass Transfer*, vol. 39, no. 6, pp. 745–751, 2012.

[5] P. Vasava, P. Jalali, M. Dabagh, and P. J. Kolari, "Finite element modelling of pulsatile blood flow in idealized model of human aortic arch: study of hypotension and hypertension," *Computational and Mathematical Methods in Medicine*, vol. 2012, Article ID 861837, 14 pages, 2012.

[6] M. A. Ikbal, S. Chakravarty, Sarifuddin, and P. K. Mandal, "Unsteady analysis of viscoelastic blood flow through arterial stenosis," *Chemical Engineering Communications*, vol. 199, no. 1, pp. 40–62, 2012.

[7] J. R. Leach, V. L. Rayz, M. R. K. Mofrad, and D. Saloner, "An efficient two-stage approach for image-based FSI analysis of atherosclerotic arteries," *Biomechanics and Modeling in Mechanobiology*, vol. 9, no. 2, pp. 213–223, 2010.

[8] D. Bluestein, Y. Alemu, I. Avrahami et al., "Influence of microcalcifications on vulnerable plaque mechanics using FSI modeling," *Journal of Biomechanics*, vol. 41, no. 5, pp. 1111–1118, 2008.

[9] S. A. Kock, J. V. Nygaard, N. Eldrup et al., "Mechanical stresses in carotid plaques using MRI-based fluid-structure interaction models," *Journal of Biomechanics*, vol. 41, no. 8, pp. 1651–1658, 2008.

[10] A. Borghi, N. B. Wood, R. H. Mohiaddin, and X. Y. Xu, "Fluid-solid interaction simulation of flow and stress pattern in thoracoabdominal aneurysms: a patient-specific study," *Journal of Fluids and Structures*, vol. 24, no. 2, pp. 270–280, 2008.

[11] R. Torii, M. Oshima, T. Kobayashi, K. Takagi, and T. E. Tezduyar, "Fluid-structure interaction modeling of a patient-specific cerebral aneurysm: influence of structural modeling," *Computational Mechanics*, vol. 43, no. 1, pp. 151–159, 2008.

[12] M. X. Li, J. J. Beech-Brandt, L. R. John, P. R. Hoskins, and W. J. Easson, "Numerical analysis of pulsatile blood flow and vessel wall mechanics in different degrees of stenoses," *Journal of Biomechanics*, vol. 40, no. 16, pp. 3715–3724, 2007.

[13] B. Vahidi and N. Fatouraee, "Large deforming buoyant embolus passing through a stenotic common carotid artery: a computational simulation," *Journal of Biomechanics*, vol. 45, no. 7, pp. 1312–1322, 2012.

[14] S. H. Lee, H. G. Choi, and J. Y. Yool, "Finite element simulation of blood flow in a flexible carotid artery bifurcation," *Journal of Mechanical Science and Technology*, vol. 26, no. 5, pp. 1355–1361, 2012.

[15] X. H. Wang and X. Y. Li, "Fluid-structure interaction based study on the physiological factors affecting the behaviors of stented and non-stented thoracic aortic aneurysms," *Journal of Biomechanics*, vol. 44, no. 12, pp. 2177–2184, 2011.

[16] J. Lantz, J. Renner, and M. Karlsson, "Wall shear stress in a subject specific human aorta—influence of fluid-structure interaction," *International Journal of Applied Mechanics*, vol. 3, no. 4, pp. 759–778, 2011.

[17] V. Vavourakis, Y. Papaharilaou, and J. A. Ekaterinaris, "Coupled fluid-structure interaction hemodynamics in a zero-pressure state corrected arterial geometry," *Journal of Biomechanics*, vol. 44, no. 13, pp. 2453–2460, 2011.

[18] R. Torii, N. B. Wood, N. Hadjiloizou et al., "Fluid-structure interaction analysis of a patient-specific right coronary artery with physiological velocity and pressure waveforms," *Communications in Numerical Methods in Engineering with Biomedical Applications*, vol. 25, no. 5, pp. 565–580, 2009.

[19] C. V. Bourantas, M. I. Papafaklis, L. Athanasiou et al., "A new methodology for accurate 3-dimensional coronary artery reconstruction using routine intravascular ultrasound and angiographic data: implications for widespread assessment of endothelial shear stress in humans," *EuroIntervention*, vol. 9, no. 5, pp. 582–593, 2013.

[20] N. Koshiba, J. Ando, X. Chen, and T. Hisada, "Multiphysics simulation of blood flow and LDL transport in a porohyperelastic arterial wall model," *Journal of Biomechanical Engineering*, vol. 129, no. 3, pp. 374–385, 2007.

[21] G. Porenta, H. Schima, A. Pentaris et al., "Assessment of coronary stenoses by Doppler wires: a validation study using *in vitro* modeling and computer simulations," *Ultrasound in Medicine and Biology*, vol. 25, no. 5, pp. 793–801, 1999.

[22] T. D. S. Mabotuwana, L. K. Cheng, and A. J. Pullan, "A model of blood flow in the mesenteric arterial system," *BioMedical Engineering Online*, vol. 6, article 17, 2007.

[23] N. M. Maurits, G. E. Loots, and A. E. P. Veldman, "The influence of vessel wall elasticity and peripheral resistance on the carotid artery flow wave form: a CFD model compared to in vivo ultrasound measurements," *Journal of Biomechanics*, vol. 40, no. 2, pp. 427–436, 2007.

[24] K. Perktold, M. Hofer, G. Rappitsch, M. Loew, B. D. Kuban, and M. H. Friedman, "Validated computation of physiologic flow in a realistic coronary artery branch," *Journal of Biomechanics*, vol. 31, no. 3, pp. 217–228, 1997.

[25] A. Santamarina, E. Weydahl, J. M. Siegel, and J. E. Moore, "Computational analysis of flow in a curved tube model of the coronary arteries: effects of time-varying curvature," *Annals of Biomedical Engineering*, vol. 26, no. 6, pp. 944–954, 1998.

[26] S. A. Urquiza, P. J. Blanco, M. J. Vénere, and R. A. Feijóo, "Multidimensional modelling for the carotid artery blood flow," *Computer Methods in Applied Mechanics and Engineering*, vol. 195, no. 33–36, pp. 4002–4017, 2006.

[27] S. Z. Zhao, P. Papathanasopoulou, Q. Long, I. Marshall, and X. Y. Xu, "Comparative study of magnetic resonance imaging and image-based computational fluid dynamics for quantification of pulsatile flow in a carotid bifurcation phantom," *Annals of Biomedical Engineering*, vol. 31, no. 8, pp. 962–971, 2003.

[28] E. O. Kung, A. S. Les, C. A. Figueroa et al., "In vitro validation of finite element analysis of blood flow in deformable models," *Annals of Biomedical Engineering*, vol. 39, no. 7, pp. 1947–1960, 2011.

[29] N. H. J. Pijls, W. F. Fearon, P. A. L. Tonino et al., "Fractional flow reserve versus angiography for guiding percutaneous coronary intervention in patients with multivessel coronary artery disease: 2-year follow-up of the FAME (fractional flow reserve versus angiography for multivessel evaluation) study," *Journal of the American College of Cardiology*, vol. 56, no. 3, pp. 177–184, 2010.

Hindawi Publishing Corporation
BioMed Research International
Volume 2014, Article ID 490428, 10 pages
http://dx.doi.org/10.1155/2014/490428

Research Article

Spaceflight Affects Postnatal Development of the Aortic Wall in Rats

Shin-ichiro Katsuda,[1] Masao Yamasaki,[1,2] Hidefumi Waki,[1,3] Masao Miyake,[1] Hirotaka O-ishi,[1,4] Kiyoaki Katahira,[5] Tadanori Nagayama,[1,6] Yukako Miyamoto,[1] Masamitsu Hasegawa,[7] Haruyuki Wago,[1] Toshiyasu Okouchi,[1] and Tsuyoshi Shimizu[1,8]

[1] *Department of Cellular and Integrative Physiology, Fukushima Medical University, 1 Hikari–ga–oka, Fukushima 960-1295, Japan*
[2] *Department of Physiology, Faculty of Clinical Engineering, School of Health Sciences, Fujita Health University, 1-98 Dengakugakubo, Kutsukake-cho, Toyoake, Aichi 470-1192, Japan*
[3] *School of Health and Sports Science, Juntendo University, 1-1 Hiragagakuendai, Inzai, Chiba 270-1695, Japan*
[4] *Medical Corporations Tenshindo Shida Hospital, 2134-4 Oaza-Nakamura, Kashima, Saga 849-1304, Japan*
[5] *Medical-Industrial Translational Research Center, Fukushima Medical University, 1 Hikari–ga–oka, Fukushima 960-1295, Japan*
[6] *Nihonmatsu Hospital, 1-553 Narita-cho, Nihonmatsu, Fukushima 964-0871, Japan*
[7] *National Cerebral and Cardiovascular Center Research Institute, 5-7-1 Fujishiro-dai, Suita, Osaka 565-0873, Japan*
[8] *Shimizu Institute of Space Physiology, Suwa Maternity Clinic, 112-13 Shimosuwa, Suwa-gun, Nagano 393-0077, Japan*

Correspondence should be addressed to Shin-ichiro Katsuda; skatsuda@fmu.ac.jp

Received 24 April 2014; Revised 13 June 2014; Accepted 13 June 2014; Published 19 August 2014

Academic Editor: Bruno Levy

We investigated effect of microgravity environment during spaceflight on postnatal development of the rheological properties of the aorta in rats. The neonate rats were randomly divided at 7 days of age into the spaceflight, asynchronous ground control, and vivarium control groups (8 pups for one dam). The spaceflight group rats at 9 days of age were exposed to microgravity environment for 16 days. A longitudinal wall strip of the proximal descending thoracic aorta was subjected to stress-strain and stress-relaxation tests. Wall tensile force was significantly smaller in the spaceflight group than in the two control groups, whereas there were no significant differences in wall stress or incremental elastic modulus at each strain among the three groups. Wall thickness and number of smooth muscle fibers were significantly smaller in the spaceflight group than in the two control groups, but there were no significant differences in amounts of either the elastin or collagen fibers among the three groups. The decreased thickness was mainly caused by the decreased number of smooth muscle cells. Plastic deformation was observed only in the spaceflight group in the stress-strain test. A microgravity environment during spaceflight could affect postnatal development of the morphological and rheological properties of the aorta.

1. Introduction

It is well known that blood shifts headward immediately after exposure to a microgravity (μG) environment and thereafter decreases in volume to adapt to the environment, which could affect cardiovascular hemodynamics and associated regulatory mechanisms [1, 2]. Central venous pressure (CVP) [3, 4], cardiac output (CO) [5, 6], and arterial pressure (AP) [7, 8] have been reported to instantaneously increase after exposure to μG and then decrease in the process of adapting to μG environment during spaceflight in humans.

On the other hand, cardiovascular function changes concomitant with growth after the birth [9]. Blood pressure has been shown to gradually elevate to almost the mature level by the age of 8 weeks [10] or 45 days [11] in Sprague-Dawley (SD) rats and at 4 weeks of age in Wistar Kyoto rats [12]. Baroreceptor sensitivity has also been reported to develop with growth [10, 11]. AP is determined by the rheological

properties of the aortic wall as well as by cardiovascular hemodynamics. Baroreflex function is susceptible to the rheological properties of the aortic wall in which they lie [13, 14]. The rheological properties are closely related to alteration in the fine structure of the wall [15–20]. Baroreceptor function and rheological properties of the aortic wall are considered to develop with morphological growth of the heart, blood vessels, and other cardiovascular components. In our research group, postnatal development of the baroreflex system has been studied under ordinary gravitational conditions [9] and simulated microgravity conditions such as head-down tilt (HDT) [21, 22] and parabolic flight [22, 23]. Yamasaki and Shimizu [24] showed previously in 3-4-week-old rabbits raised in HDT posture in a simulated μG environment for 34–36 days that the number of unmyelinated fibers of the left aortic nerve was significantly reduced compared to the control rabbits, which suggested that development of the aortic baroreflex sensitivity was depressed by exposure to HDT posture. It is thus possible that a similar phenomenon is observed during spaceflight in neonate animals. Therefore, we suspected that the rheological and histological properties of the aortic wall as well as cardiovascular hemodynamics could be modulated by exposure to a μG environment during growth and investigated to verify the hypothesis in the NASA Neurolab Programs (STS-90) [25] where we joined with the theme "development of the aortic baroreflex in microgravity."

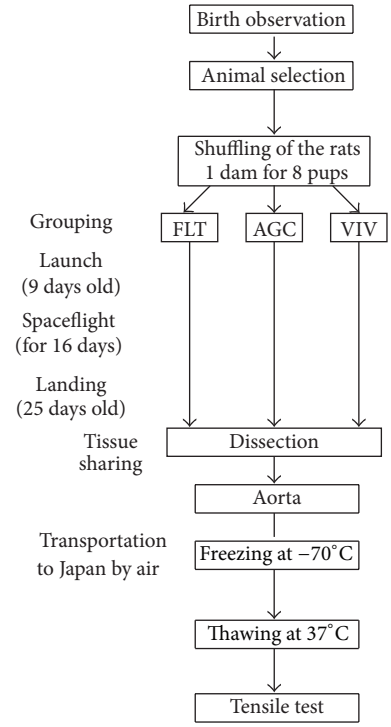

Figure 1: Flowchart of the experiment from the birth of rats to the tensile test. FLT: spaceflight, AGC: asynchronous ground control, and VIV: vivarium control.

2. Materials and Methods

2.1. Animals and Animal Care. Figure 1 shows a flowchart of the period from the birth to tensile test of the rats after the spaceflight. Eight neonate Sprague-Dawley rats in a good state of health and development, selected from a large colony 5 days after birth, were randomly assigned to one mother rat as one litter. A total of 18 litters were randomly and equally divided into three groups at 7 days after the birth: the spaceflight (FLT), asynchronous ground control (AGC), and vivarium control (VIV) groups. One litter out of the 6 litters in each group was assigned for the present study. The FLT group rats were bred in the specially designed Research Animal Holding Facility (RAHF) [26] loaded on board of the Space Shuttle. The RAHF cage is $4.00 \times 4.25 \times 10.00$ inches and can accommodate one dam and eight pups. The AGC and VIV group rats were housed in simulated RAHF and standard commercial ($18.50 \times 10.25 \times 8.50$ inches) cages, respectively, under one-G conditions and the same temperature ($23 \pm 1^{\circ}$C) and light and dark cycle as the FLT group rats. All rats were given SLO Foodbars and were cared for by a veterinarian crewmember during spaceflight and specialized personnel before and after the flight. The FLT group rats were exposed to a μG environment in the Space Shuttle "Columbia" for 16 days from 9 to 25 days after the birth. The FLT group rats were examined for basic health conditions immediately after landing and then dissected within 10 hrs after sampling blood under pentobarbital anesthesia (50 mg/kg body weight, i.p.). The tissues and organs were shared among some research teams joined to the Neurolab Programs (STS-90). In the AGC and VIV group rats, the same experimental procedures were employed, except for breeding under μG conditions. The aorta was excised from the origin of the ascending aorta to the thoracic aorta, gradually frozen to -70°C, transported to Japan by air, and stored at -85°C to minimize damage due to freezing. All experimental procedures were performed according to the guidelines for Animal Care and Use in NASA and NIH.

2.2. Tensile Test. Prior to the tensile test, we investigated the differences in the tensile characteristics between the fresh and thawed proximal descending thoracic aorta in premature rats aged 3 weeks. There were no observable differences in the tension-strain or stress-strain relations between the fresh and thawed rat aorta (Katsuda and Hasegawa unpublished observations). The experimental procedure was similar to that described previously [19, 20, 27]. The proximal descending thoracic aorta was cut from the bifurcation of the left subclavian artery to the third intercostal arteries and cut longitudinally into 3 mm wide strips after rapid thawing to 37°C. The rheological properties of the strips were measured by a tensile testing instrument (TOM-30J, Minebea, Inc., Japan) which mainly consists of a load cell, a movable crosshead, a driving unit, and a chamber [19]. One end of the strip was mounted between the jaws of a chuck and it was suspended on a load cell with a flexible wire. Another end was held by another chuck attached to the organ bath of the tensile testing instrument. The sample was immersed in saline solution consisting of NaCl (147.2), KCl (2.7), $MgCl_2$ (0.5), $CaCl_2$ (1.8), NaH_2PO_4 (1.0), Na_2HPO_4 (3.0), and glucose (5.6)

(mM) at 37°C. Initially, the strip was held at the maximum length where the tension just exceeded 0 N. After holding at the initial length, the strip was subjected to force-strain test. The tensile force in the sample was generated by mechanical stretching to about 1 N at a speed of 4.2 mm/min, relaxed to the initial length immediately after the stretching, and kept relaxed for 5 min. After plastic deformation was measured at 5 min after the relaxation of the strip, the strip was subjected to a stress-relaxation test. The strip was stretched by 50% of the initial length at a speed of 83.3 mm/min and sustained for 5 min. Immediately after the test, the strip was cut off at the margin of each chuck and weighed on a precision balance. Strain of the wall strip (ε) was defined as $\varepsilon = (\Delta + L_0)/L_0$, where L_0 and Δ were initial length of the strip and increment from the initial length, respectively. The stress value (σ) at any moment during the stretching was determined using the following formula: $\sigma = 1.06 \times L_0(1 + \varepsilon) \times T/W$, where T was the tension (g) of the strip, W the sample weight, L_0 initial length of the strip (cm), and ε strain of the strip. Poisson's ratio and density of the aortic wall were assumed to be 0.50 [28] and 1.06 g/cm^3 [29], respectively. The incremental elastic moduli of the wall (E) at strain levels of 0.25, 0.50, and 0.75 with respect to the unstressed length were selected as the mean gradient of the stress-strain curve at strains between 0.20 and 0.30, between 0.45 and 0.55, and between 0.70 and 0.80, respectively. For example, the value of E at the strain of 0.5 was expressed as $(\sigma_{0.55} - \sigma_{0.45})/(\varepsilon_{0.55} - \varepsilon_{0.45})$, where $\sigma_{0.55}$ and $\sigma_{0.45}$ were stress at strains of 0.55 and 0.45 and $\varepsilon_{0.55} - \varepsilon_{0.45}$ difference in strains (e.g., 0.1), respectively. The relaxation strength was calculated by $(\tau_0 - \tau_{5\,\mathrm{min}})/\tau_0 \times 100$ (%), where τ_0 was the maximal tension generated immediately after stretching and $\tau_{5\,\mathrm{min}}$ the tension at 5 min after the stretching (Figure 4). The plastic deformation of the strip was measured at 5 min after the relaxation of the sample in the stress-strain test. Wall thickness of the strip (h) was calculated as $h = W/(1.06 \times L_0 \times Wd)$, where Wd was the width of the sample (cm). Internal radius of the descending proximal thoracic aorta was estimated as $l/2\pi$, where l was the circumferential length of the excised wall strip.

2.3. Histological Sections. The strips were fixed in 10% neutral buffered formalin solution and embedded in paraffin. Circumferential and longitudinal histological sections were sliced at 5 μm thickness and stained with Elastica-van Gieson (EVG) and hematoxylin-eosin (HE).

2.4. Image Analysis. The images of smooth muscle cells (SMC), elastin fiber, and collagen fiber in the longitudinal histological sections stained with EVG, which were displayed at yellow, black, and red, respectively, were sampled by an image analysis system (LUZEX FS, Nireco Corporation, Tokyo, Japan) through a microscope (Olympus BX-50, Olympus Corporation, Tokyo, Japan) at a magnification of 40 times and a CCD-video camera operated by a camera control unit. The image within a frame of an image analysis system (2.52×10^{-4} μm^2 in area) was converted to the sliced video images prior to processing by the main processor. An outline image of each element was discriminated by the adjusting intensity, hue, and purity of its color and was selectively extracted. The three components and the entire sectional area were binarized and the intensity and tint were adjusted to the background. The SMC, elastin fiber, collagen fiber, and entire sectional area were measured with the main processor. The area of each component was expressed as a percentage of the entire sectional area in each histological section. These procedures for analyzing the three major components were repeated in at least two microscopic fields of each histological section. The image of the SMC stained with HE was taken into an image analysis system and binarized in a similar way to images of the longitudinal sections stained with EVG at a magnification of 40 times. The outline image of the nucleus in a given frame area (2.52×10^{-4} μm^2 in area) was emphasized for discrimination by adjusting the intensity, hue, and purity of its color, displayed in blue, and selectively extracted. The number of nuclei seen within one frame for one section stained with HE system was counted using an image analysis system. These procedures were repeated in three microscopic fields for each histological section. The number of nuclei in three microscopic fields was averaged within each rat group.

2.5. Statistical Analysis. The experimental data, for example, FLT versus ACG, FLT versus VIV, and ACG versus VIV, were compared by Scheffe's multiple comparison tests after confirming significant differences by one-way analysis of variance (ANOVA).

3. Results

Total number of pups available for all areas of research decreased after the landing of Space Shuttle, so that we were consequently forced to reduce the number of pups for a series of experiments. Six pups were ultimately allotted to the FLT, AGC, and VIV groups in the present study, respectively, after number of pups had been readjusted to share as fairly as possible.

Table 1 summarizes body weight and physical characteristics of the proximal thoracic descending aorta. Internal diameter was estimated from the excised strip of the proximal thoracic aorta. Body weight in the FLT group was about half of that in the two control groups and significantly lower than that in the AGC ($P < 0.001$) and VIV ($P < 0.001$) groups. Weight of the proximal descending thoracic aorta per unit area (cm^2) tended to be small in the FLT group compared with that in the two control groups, which was not statistically significant. Cross-sectional area of the aortic wall in the FLT group was significantly small compared with that in the AGC ($P < 0.01$) and VIV ($P < 0.01$) groups. Internal diameter was significantly smaller in the FLT group than in the AGC ($P < 0.001$) and VIV ($P < 0.01$) groups.

Figure 2(a) shows the force-strain curves in the longitudinal strips excised from the descending proximal thoracic aorta in the FLT, AGC, and VIV group rats. As the strain increased, the tensile force gradually elevated in the three groups. The difference in tensile force between the FLT and the two control groups gradually widened as strain increased. The tensile force in the FLT group rats was significantly

Table 1: Body weight and estimated weight and internal diameter of the proximal descending thoracic aorta in the FLT, AGC, and VIV group rats.

	Pups number	#1	#2	#3	#4	#5	#6	Mean	SE
Body weight (g)	FLT	54.1	31.1	24.5	32.7	43.7	53.9	40.0***a,b	5.1
	AGC	83.0	78.8	71.2	71.4	78.7	81.9	77.5	2.1
	VIV	87.4	80.3	81.4	88.8	80.9	78.9	83.0	1.7
Weight of the aorta per cm^2 (mg)	FLT	14.2	16.0	13.9	16.4	13.6	10.9	14.2	0.8
	AGC	17.1	16.5	23.3	24.1	22.4	16.4	20.0	1.5
	VIV	19.5	14.0	14.3	26.4	24.9	20.0	19.9	2.1
Cross-sectional area (mm^2)	FLT	0.51	0.46	0.40	0.51	0.46	0.37	0.45**a,**b	0.02
	AGC	0.69	0.65	0.84	0.93	0.88	0.68	0.78	0.05
	VIV	0.69	0.58	0.57	1.12	0.91	0.74	0.77	0.09
Internal diameter (mm)	FLT	1.20	0.97	0.97	1.05	1.13	1.17	1.08***a,**b	0.04
	AGC	1.37	1.33	1.22	1.30	1.32	1.38	1.32	0.02
	VIV	1.19	1.39	1.35	1.43	1.24	1.26	1.31	0.04

**$P < 0.01$, ***$P < 0.001$, [a]FLT versus AGC, and [b]FLT versus VIV. Body weight was measured on the day of the landing. Internal diameter was estimated from circumferential width of the wall strip excised from the proximal descending thoracic aorta. The cross-sectional area was calculated from width and thickness of the wall strip. The diameter is expected to be stretched approximately 50% in situ.

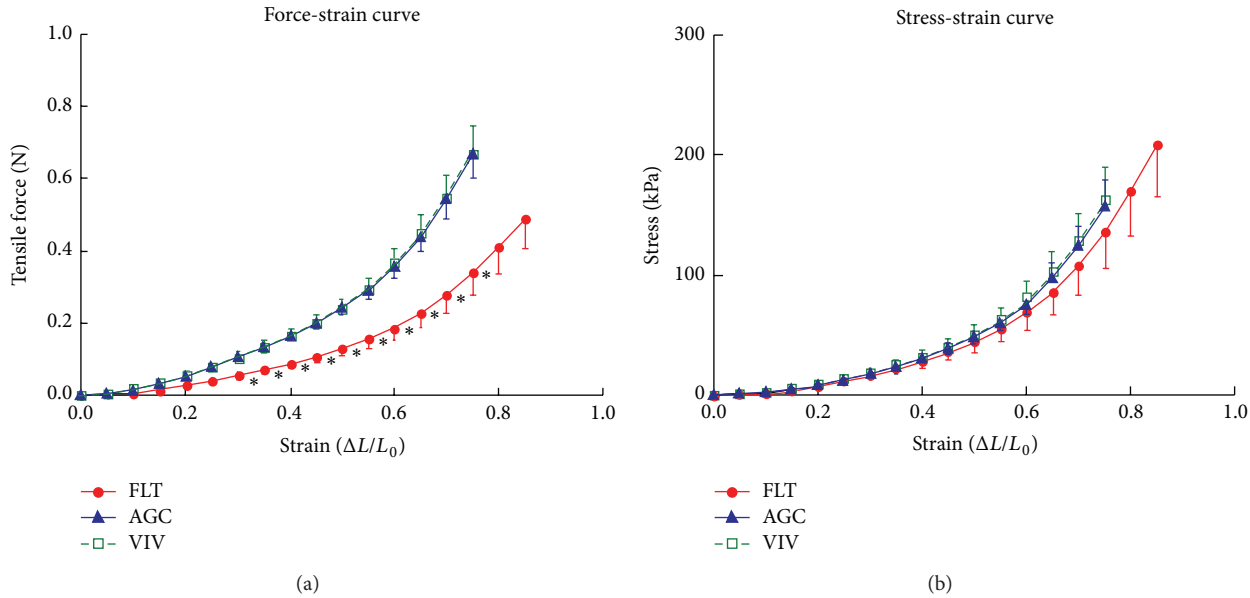

Figure 2: Force-strain (a) and stress-strain (b) curves of the longitudinal strips excised from the proximal thoracic aorta in the FLT, AGC, and VIV group rats. Values are mean ± SE. *: $P < 0.05$ (FLT versus AGC and FLT versus VIV), L_0: initial length of the strip, and ΔL: increment by stretching.

smaller than those in the AGC and VIV group rats at a strain range between 0.30 and 0.75 ($P < 0.05$). Figure 2(b) illustrates stress-strain curves derived from the corresponding force-strain curves in the three groups. The contour of the stress-strain curve resembles that of the force-strain curve. There were no significant differences in stress value between any two groups at any strain value ($P > 0.05$). The values of E at strains of 0.25, 0.50, and 0.75, which correspond to low, medium, and high physiological strain values of the aorta, respectively, are depicted in Figure 3. The value of E was about 100 kPa at a strain of 0.25, nearly doubled at a strain of 0.50, and at 0.75 drastically increased to about three times the strain at 0.50 in the three groups. There was no significant difference in the value of E between any two groups at any strain ($P > 0.05$). Figure 4 shows examples of stress-relaxation curves in FLT, AGC, and VIV rats. The pattern of the curve was almost similar among the three groups. Relaxation strength at 5 min after 50% stretching beyond the initial length in the FLT, AGC, and VIV groups ($n = 6$ in each group, mean ± SE) was 8.4 ± 1.7, 7.7 ± 0.9, and 7.6 ± 1.0 (%), respectively, which showed almost the same value (about 8.0%) in the three groups and was not significantly different between any two groups ($P > 0.05$). Plastic deformation of the strip measured at 5 min after the relaxation following the stress-strain test was observed in all the strips of the FLT group (0.12 ± 0.03 mm, mean ± SE) only despite showing no significant difference in the value of E compared to the two control groups, whereas

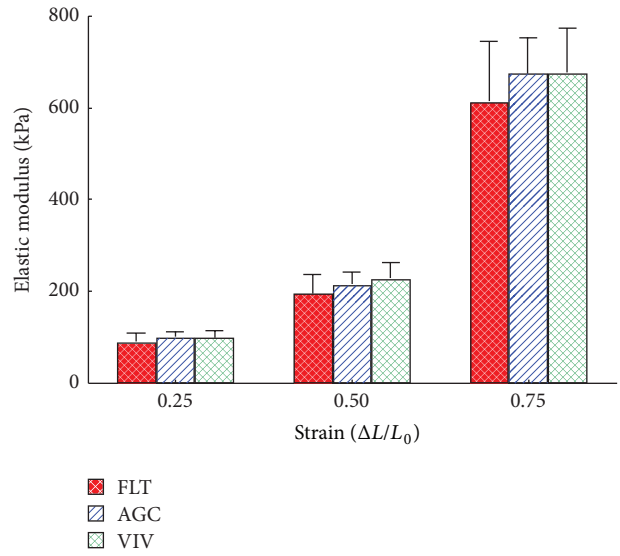

Figure 3: Incremental elastic modulus of the longitudinal strips excised from the proximal thoracic aorta in the FLT, AGC, and VIV group rats. Values are mean ± SE. Abbreviations are similar to those in Figure 2. Incremental elastic modulus was determined at strains of 0.25, 0.50, and 0.75.

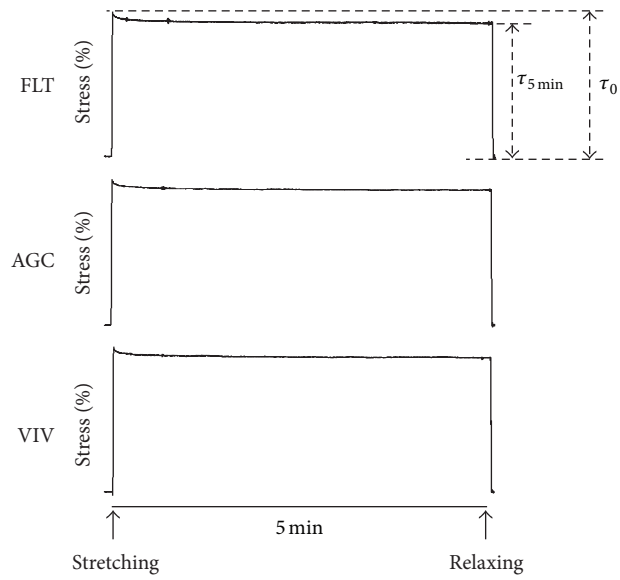

Figure 4: Examples of stress-relaxation of the longitudinal strips excised from the proximal thoracic aorta in the FLT, AGC, and VIV group rats. The strips were stretched by 50% from the initial length. Relaxation strength was defined as a percent ratio of $\tau_0/(\tau_0 - \tau_{5\,\mathrm{min}})$, where τ_0 was peak stress immediately after the stretching and $\tau_{5\,\mathrm{min}}$ stress at 5 min after the stretching.

plastic deformation was not detected in the two control groups. Figures 5(a) and 5(b) are photomicrographs of the longitudinal and circumferential histological sections of the proximal descending thoracic aorta stained with EVG and HE stain in the three groups, respectively. It is interesting that the smooth muscle layer in the FLT group was thin compared to that in the two control groups. The thick elastin fibers in the FLT group were almost the same in number, thickness, and amount as in the two control groups. The fine elastin fibers connecting the thick elastin fibers and smooth muscle cells to each other were circumferentially and longitudinally fast woven in the two control groups, whereas they were poorer in number and networking in the FLT group than in the control groups. The collagen fibers were also similar in amount and arrangement among the three groups, although the wall was considerably compressed in the FLT group rats. The number of nuclei in the smooth muscle cells was considerably smaller in the FLT group than in the two control groups. No histological alteration in the smooth muscle cells, for example, change in size or shape, was clearly detected by microscopic observation. Figures 6(a) and 6(b) illustrate estimated wall thickness and internal radius of the proximal descending thoracic aorta in FLT, AGC, and VIV groups. Wall thickness in the FLT group was 133.3 ± 17.8 μm (mean ± SE) and significantly decreased to about 70% of that in the two control groups (193.4 ± 11.5 for AGC group, $P < 0.05$, and 188.4 ± 18.2 μm for VIV group, $P < 0.05$). Internal radius was significantly smaller in the FLT group rats than that in the AGC and VIV group rats. Figure 7(a) illustrates the areas of elastin and collagen fibers and smooth muscle cells as measured in the longitudinal histological sections in the three groups using an image analysis system. The area of smooth muscle in the longitudinal histological section was significantly smaller in the FLT group than in the AGC ($P < 0.001$) and VIV ($P < 0.001$) groups, whereas the areas of the elastin and collagen fibers were not significantly different between any two groups ($P > 0.05$). The number of nuclei in one microscopic field in the image analysis system was 134.3 ± 3.6, 179.3 ± 5.5, and 166.2 ± 5.2 (mean ± SE) in the FLT, AGC, and VIV groups, respectively (Figure 7(b)). The number of nuclei was significantly smaller in the FLT group than in the AGC ($P < 0.01$) and VIV ($P < 0.05$) groups, respectively.

4. Discussion

The extracellular fluid first shifts headward in exposure to μG environment and decreases in volume in the course of acclimatizing to the environment. The decrease in fluid volume induced a decrease in CO, which could partly involve lowering of blood pressure [1, 2]. CO has been demonstrated to reduce by approximately 15% from the preflight level in astronauts during sustained spaceflight [5, 6]. Fritsch-Yelle et al. [7] reported that diastolic pressure and heart rate significantly decreased and that systolic pressure tended to fall during spaceflight in humans. Gazenko et al. [8] also observed the decrease in diastolic pressure in humans during spaceflight.

AP could be estimated by the rheological properties of the wall as well as by the parameters of cardiovascular hemodynamics such as cardiac output and peripheral vascular resistance. AP can theoretically be expressed by Laplace's law, for example, $\mathrm{AP} = T/R = Eh\varepsilon/R$, where T is tension of the wall, E elastic modulus of the wall, h thickness of

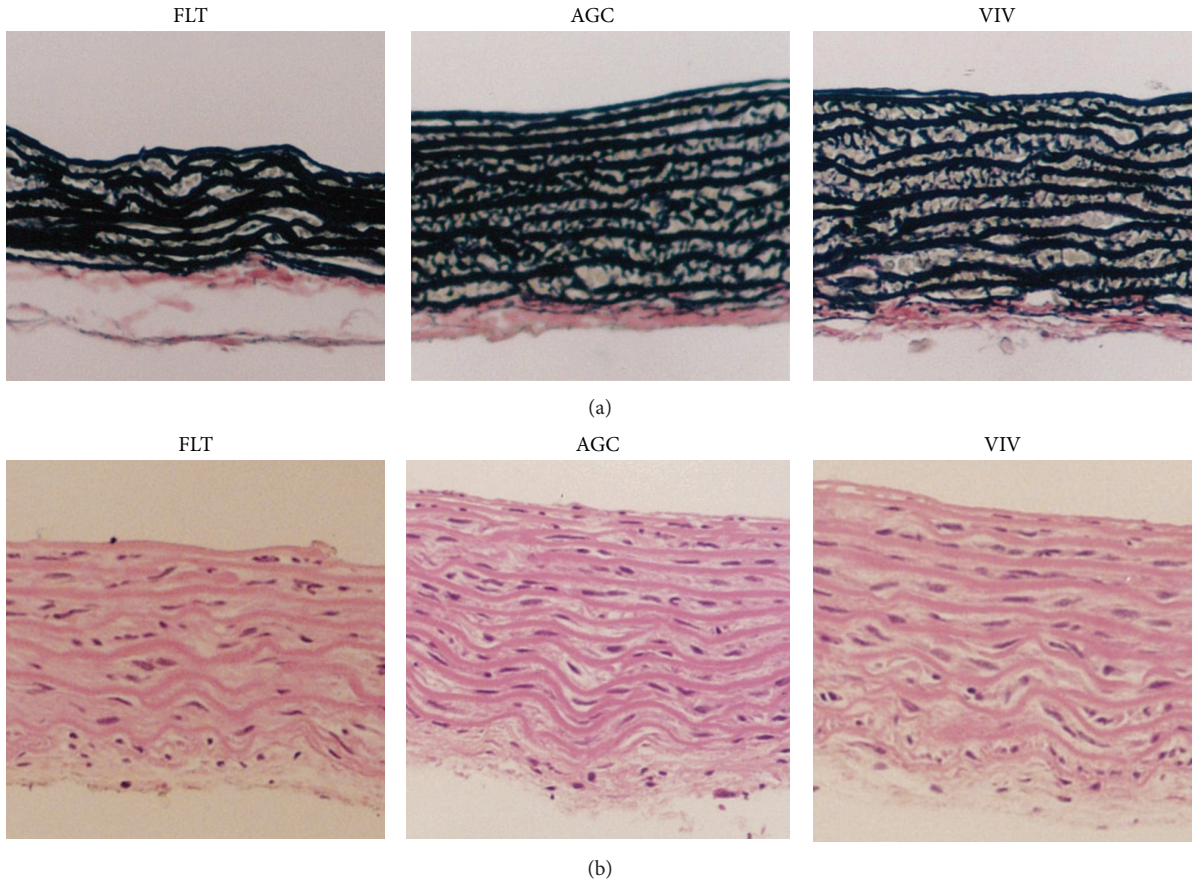

Figure 5: Photomicrographs of the longitudinal (a) and circumferential (b) histological sections of the proximal descending thoracic aorta stained with EVG (a) and HE (b) stains in the FLT, AGC, and VIV group rats. Perpendicular bar: 100 μm.

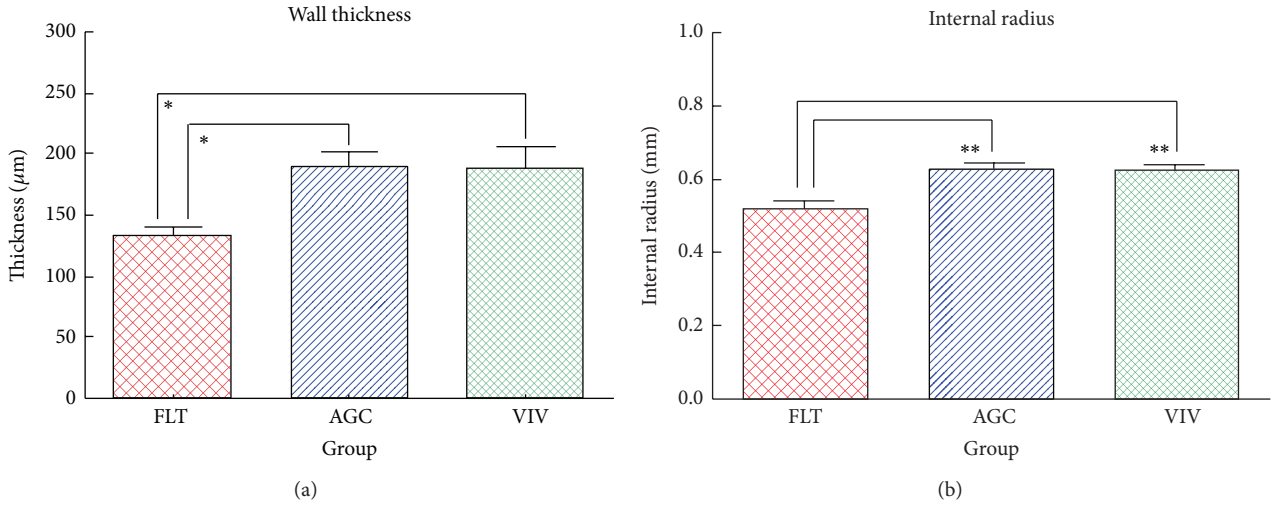

Figure 6: Estimated wall thickness (a) and internal radius (b) of the proximal thoracic aorta in the FLT, AGC, and VIV group rats. Values are mean ± SE. $^{*}P < 0.05$, $^{**}P < 0.01$.

the wall, ε strain of the wall, and R radius of the blood vessel. In our other analysis of cardiovascular function in Neurolab Program (STS-90), mean arterial pressure (MAP) measured about 12 hrs after the landing of the Space Shuttle was significantly lower in the FLT group rats than in the other AGC and VIV group rats, respectively [30, 31]. The time lag between the landing and arterial pressure measurement seems insufficient to adapt completely to the one-gravity (one-G) environment. There was no significant difference in the values of E among the FLT, AGC, and VIV groups,

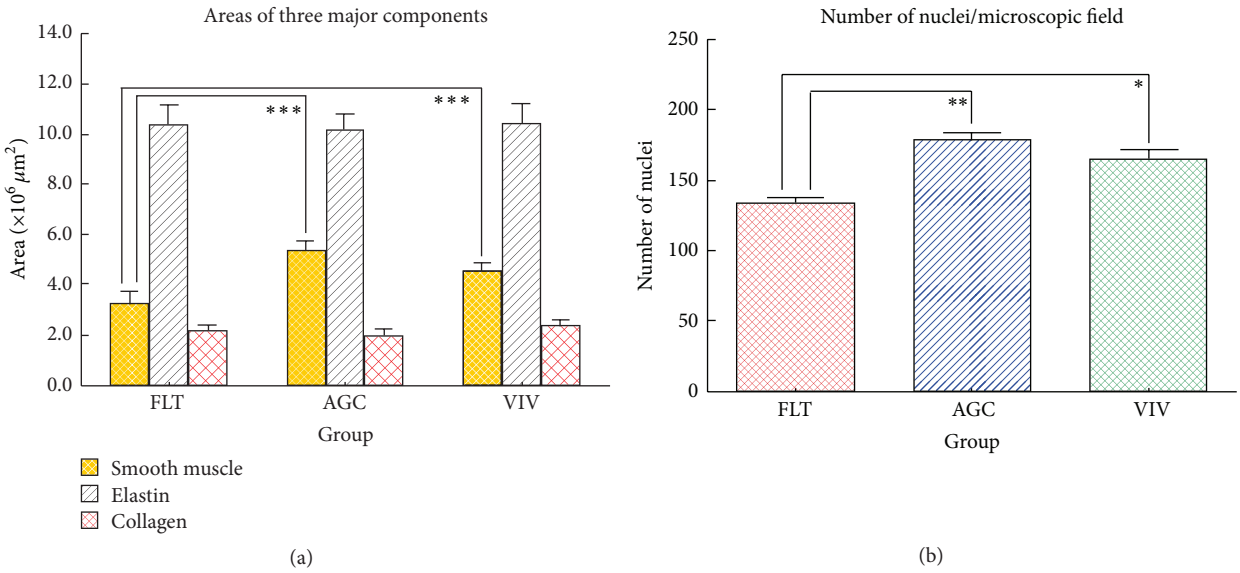

Figure 7: Area of the smooth muscle, elastin, and collagen fibers (a) in the longitudinal histological sections and number of nuclei of the smooth muscle cells (b) in the circumferential histological sections excised from the proximal thoracic aorta in the FLT, AGC, and VIV group rats. Values are mean ± SE. $^{*}P < 0.05$. $^{**}P < 0.01$. $^{***}P < 0.001$. Area of each component was measured in three given microscopic fields for one histological section stained with EVG with an image analysis system and then averaged within each group. The number of nuclei was measured in three given microscopic fields for one section stained with HE with an image analysis system and then averaged within each rat group.

respectively, although it tended to show a slight decrease in the FLT group. The significantly decreased wall tension in the FLT group mainly due to the reduction in wall thickness could partly be responsible for the fall in MAP level in the FLT group during the spaceflight.

The aortic wall consists in major part of the elastin and collagen fibers and SMC, whose content and arrangement have been morphologically demonstrated by optical and electron microscopic studies [16, 32]. The elastin fibers form a robust network in the proximal aortic region, while the network becomes sparser with increasing longitudinal cracks in the distal region of the aorta [19, 20]. The collagen fibers also show strong network structure in all aortic regions, though they were crimped or relaxed in an ordinarily stretched state [19, 20]. SMC are arranged in a spiral or helical manner. The number of turns of SMC spirals for a given length increases and the angle between the spiral plane and the transactional plane decreases with increasing distance from the heart [19, 20]. The elastin fiber and SMC are considered to contribute in major part to the elastic and viscous properties, respectively, of the aorta within the normal range of arterial pressure. The collagen fibers are thought to protect the aortic wall from rupturing when exposed to abnormally high pressure [15, 33].

The static rheological properties of the aortic wall have been shown to differ by arterial segment, direction of the wall, age, species, and other factors [34–40]. Azuma and Hasegawa [19, 20] previously investigated the difference in the rheological properties of the aorta between circumferential and longitudinal directions. The static rheological characteristics of the aortic wall become gradually viscoelastic in the circumferential direction with increasing distance from the heart, while they were elastic in the longitudinal direction irrespective of the portion of the aortic tree. There was no marked difference in the viscoelastic properties between the circumferential and longitudinal directions in the proximal aortic region. These mean that the proximal aorta behaves as an elastic vessel to achieve auxiliary pumping function.

In the present study, wall stress did not differ at any strain level between any two groups, though wall tensile force was significantly smaller in the FLT group than in the two control groups. This was caused by the significant decrease in wall thickness in the FLT group, which was considered to be chiefly due to the reduction in the amount of SMC. The number of SMC nuclei was significantly decreased in the FLT group in comparison to the two control groups, which contributed to the decrease in the SMC layer. Other important factors affecting the thickness of the SMC layer were the size of the SMC and the volume of the extracellular fluid surrounding the SMC. It is not plausible that a large amount of intracellular fluid was deprived to alter the contour of the SMC in the μG environment because severe dehydration in neonate rats over the period of lactation would not allow maintaining their lives in space. The size of the SMC may be well preserved; however, we did not investigate the size with an electron microscope in the present study. A decrease in the extracellular volume during spaceflight would partly contribute to the decrease in the SMC layer in addition to the reduction in the number of the SMC. The significant decrease in the internal diameter of the aorta and body weight in the FLT group rats would partly support a decrease in the extracellular volume during spaceflight. The decreasing trend of the weight of the aorta and the significant decrease in

cross-sectional area of the aorta in the FLT rats are considered to mainly reflect the decreased SMC layer. The lower mass of the aortic wall possibly affects the rheological properties of the aortic wall through the decreased SMC layer in FLT rats. It is unlikely that the lower mass of the aorta per se alters overall rheological characteristics of the aortic wall in the FLT group because the elastin and collagen contents were almost the same as those in the two control groups.

The relaxation strength was about 8% in the three groups, which suggested that the wall in the proximal thoracic aorta was almost elastic regardless of the presence or absence of spaceflight. The elastic properties would reflect the histological findings that there were no significant differences in the elastin and collagen fiber content and that the arrangement of thick elastin fibers was not markedly altered in any of the three groups. The plastic deformation was observed in all strips in the FLT group, whereas it was not detected in the two control groups. This was likely caused in part by the decrease in the elastic recoil due to the insufficient formation of the fine elastin fibers connecting the thick elastin fibers or SMC.

Cardiovascular function and rheological properties of the aortic wall are known to gradually develop with growth after birth [9–12, 24, 27]. Waki et al. [10] investigated changes in the MAP level and baroreceptor function with postnatal development in SD rats at 3, 8, and 20 weeks of age and reported that MAP level reached mature level by 8 weeks, although the sensitivity of baroreceptors was significantly smaller at 3 and 8 weeks than at 20 weeks. Dickhout and Lee [12] showed an increase in MAP level with postnatal development and reaching approximately mature level at 4 weeks of age in Wistar Kyoto rats. Kasparov and Paton [11] also reported progressive increase in MAP level with growth from 6 to 25 days after birth. We previously observed that the value of relaxation strength at 5 min after the stretching was 9.3%, 8.2%, and 4.6% on average in SD rats at 3, 8, and 20 weeks of age, respectively, and that wall tensile force at a given strain and thickness gradually increased with growth by the age of 20 weeks [27]. These support strongly that cardiovascular function and rheological properties are still in development at least at 3 weeks of age.

An important question arises whether breeding in μG environment affects growth or not. Nutritional state could have significant impact on growth. In the present study, the body weight in the FLT rats was significantly low compared with that in the two control groups on the day of the landing on the ground. The most likely cause seemed to be lack of nursing due to a reduced interaction between the dam and pups during spaceflight. However, it was extraordinarily difficult for the astronauts to measure daily milk intake and body weight in a confined cabin of the Space Shuttle under microgravity conditions. They could only check physical conditions of rats by appearance in the μG environment. However, some scientific bases have been shown that nutritional disturbance during spaceflight was not a major cause of the morphological and functional alterations in the FLT rats. Walton et al. [41] showed that the body weight in the FLT rats reached that of the AGC rats and VIV rats by 8 and 13 days after the landing, respectively. Adams et al. [42] demonstrated that the myosin heavy chain (MHC) genes, very sensitive to lack of nutrition, were not expressed in the FLT rats in the Neurolab experiment (STS-90), whereas expression of cardiac β-MHC was predominant in malnourished status. We investigated the rheological properties in the same pups as those shared with the team examined MHC gene expression. Oishi et al. [43] reported that the aortic ring in the FLT rats showed smaller or no vasoconstriction response to phenylephrine compared with that in the AGC and VIV rats. Furthermore, the phenylephrine-induced vasoconstriction response in the lactation-restricted rats little changed compared with that in the normal rats. Stein et al. [44] compared morphological findings of SMC of the aorta using an electron microscope in growth-arrested rats at 18 and 33 weeks of age by either inhibition of thyroid function or caloric restriction at 5 weeks with those in age- and body-weight-matched controls. They reported that the ultrastructural appearance was similar among these groups, though aortic weight, DNA, cholesterol, and phospholipid contents differed. We previously investigated the effects of malnutrition on the rheological characteristics of the proximal descending aorta in 16-day-old neonate rats restricted from nursing for 9 days (Katsuda et al. unpublished observations). There were no significant differences in wall tensile force, wall stress, incremental elastic modulus, wall thickness, or number of nuclei in the SMC between the nursing-restricted and control rat groups, although body weight was significantly smaller in the suckling-restricted groups than that in the control groups. It cannot be denied that the μG conditions affect the morphology and function of the vascular system, although detailed study on nutritional matter in the μG environment is required in the future.

Most investigators have reported the μG environment could affect growth of the nervous and muscular system in neonate rats in the Neurolab study (STS-90) [31, 41, 42, 45, 46]. Adams et al. [45] demonstrated that the growth of body and limb skeletal muscles of neonate rats was impaired under μG environment and that systemic and body expression of insulin-like growth factor-I (IGF-I) was suppressed by spaceflight for 16 days. Yamasaki et al. [46] reported that the number of high-threshold unmyelinated fibers of the aortic nerve was significantly smaller in the neonate rats exposed to μG environment for 16 days than in the control rats bred under one-G conditions. Waki et al. [31] also demonstrated that the baroreflex function in neonate rats was attenuated at 12 hrs after the returning from the spaceflight for 16 days. In the present study, the diameter of the aorta, the wall thickness, and the number of SMC in the proximal thoracic aortic wall were significantly reduced in the FLT group compared to those in the control groups. Morphological and rheological properties are considered to be affected by exposure to a μG environment in the course of development. The neonate rat might not need to develop the aortic wall thickness, internal diameter, and strength much to increase blood pressure and to pump out a large amount of blood toward peripherals under μG conditions because the rat would not fully move muscles against gravity in the process of growth during spaceflight.

In conclusion, the μG environment in the space could affect the morphological and rheological properties of the

aorta in the process of growth in neonate rats. The present study offers fundamental data on vascular physiology and morphology in animals and humans for long-term stay in space station.

Conflict of Interests

There is no conflict of interests regarding the publication of this paper.

Acknowledgments

The authors express their gratitude to the members of research support teams from NASA Ames Research Center and the John F. Kennedy Space Center, the National Aerospace Exploration Agency of Japan (present Japan Aerospace Exploration Agency (JAXA)), and the Japan Space Forum (JSF) for supporting the present study. They are also grateful to Ms. E. Wagner, Dr. S. Nagaoka, Dr. C. Mukai, Ms. M. Satoh, Ms. M. Yamasaki, and Ms. K. Takahashi for kind support in the present study. Part of this work was also supported by JSPS KAKENHI Grant no. 08407004 and by the Japan Space Forum "Ground Research Announcement for Space Utilization."

References

[1] A. R. Hargens and D. E. Watenpaugh, "Cardiovascular adaptation to spaceflight," *Medicine and Science in Sports and Exercise*, vol. 28, no. 8, pp. 977–982, 1996.

[2] D. E. Watenpaugh and A. R. Hargens, " The cardiovascular system in microgravity," in *Handbook of Physiology*, M. J. Fregly and C. M. Blatteis, Eds., vol. 1, section 4, pp. 631–674, Americ an Physiological Society, Oxford University Press, Oxford, UK, 1996.

[3] J. C. Buckey Jr., F. A. Gaffney, L. D. Lane et al., "Central venous pressure in space," *Journal of Applied Physiology*, vol. 81, no. 1, pp. 19–25, 1996.

[4] K. A. Kirsch, L. Rocker, and O. H. Gauer, "Venous pressure in man during weightlessness," *Science*, vol. 225, no. 4658, pp. 218–219, 1984.

[5] D. S. O'Leary, G. M. Pantalos, and M. K. Sharp, "Feedback control of mean aortic pressure in a dynamic model of the cardiovascular system," *ASAIO Journal*, vol. 45, no. 6, pp. 587–594, 1999.

[6] G. K. Prisk, H. J. B. Guy, A. R. Elliott, R. A. Deutschman III, and J. B. West, "Pulmonary diffusing capacity, capillary blood volume, and cardiac output during sustained microgravity," *Journal of Applied Physiology*, vol. 75, no. 1, pp. 15–26, 1993.

[7] J. M. Fritsch-Yelle, J. B. Charles, M. M. Jones, and M. L. Wood, "Microgravity decreases heart rate and arterial pressure in humans," *Journal of Applied Physiology*, vol. 80, no. 3, pp. 910–914, 1996.

[8] O. G. Gazenko, E. B. Shulzhenko, V. F. Turchaninova, and A. D. Egorov, "Central and regional hemodynamics in prolonged space flights," *Acta Astronautica*, vol. 17, no. 2, pp. 173–179, 1988.

[9] T. Shimizu, "Postnatal development of regulatory function of the circulation," *Journal of the Physiological Society of Japan*, vol. 51, no. 5, pp. 137–152, 1989 (Japanese).

[10] H. Waki, M. Yamasaki, K. Katahira, S. Katsuda, M. Maeda, and T. Shimizu, "Developmental changes in functional characteristics of aortic baroreceptor afferents in rats," *Experimental Physiology*, vol. 93, no. 3, pp. 319–324, 2008.

[11] S. Kasparov and J. F. R. Paton, "Changes in baroreceptor vagal reflex performance in the developing rat," *Pflugers Archiv*, vol. 434, no. 4, pp. 438–444, 1997.

[12] J. G. Dickhout and R. M. K. W. Lee, "Blood pressure and heart rate development in young spontaneously hypertensive rats," *American Journal of Physiology. Heart and Circulatory Physiology*, vol. 274, no. 3, pp. H794–H800, 1998.

[13] J. E. Angell-James, "The responses of aortic arch and right subclavian baroreceptors to changes of non-pulsatile pressure and their modification by hypothermia," *The Journal of Physiology*, vol. 214, no. 2, pp. 201–223, 1971.

[14] J. E. Angell-James, "Arterial baroreceptor activity in rabbits with experimental atherosclerosis," *Circulation Research*, vol. 34, no. 1, pp. 27–39, 1974.

[15] A. C. Burton, "Relation of structure to function of the tissues of the wall of blood vessels," *Physiological Reviews*, vol. 34, no. 4, pp. 619–642, 1954.

[16] J. T. Apter and E. Marquez, "Correlation of visco-elastic properties of large arteries with microscopic structure," *Circulation Research*, vol. 22, no. 3, pp. 393–404, 1968.

[17] F. M. Attinger, "Two-dimensional in-vitro studies of femoral arterial walls of the dog," *Circulation Research*, vol. 22, no. 6, pp. 829–840, 1968.

[18] H. Bader, "The anatomy and physiology of the vascular wall," in *Handbook of Physiology*, W. F. Hamilton, Ed., vol. 2 of *Circulation, Section 2*, pp. 865–889, American Physiological Society, Washington, DC, USA, 1963.

[19] T. Azuma and M. Hasegawa, "A rheological approach to the architecture of arterial walls," *Japanese Journal of Physiology*, vol. 21, no. 1, pp. 27–47, 1971.

[20] M. Hasegawa and T. T. Azuma, "Rheological properties of the main vascular system: with special reference to the fine structure of walls," in *Proceedings of the Symposium on Biomaterials*, pp. 1–13, The Society of Materials Science, Tokyo, Japan, 1975.

[21] T. Shimizu, M. Yamasaki, T. Nagayama et al., "Changes in the common carotid arterial flow in the rabbit and rat during parabolic flight," in *Proceedings of the 33th International Congress of Physiological Sciences*, Christchurch, NewZealand, 1997.

[22] T. Nagayama, S. Katsuda, H. Waki et al., "Changes in femoral arterial flow in the rabbit under conditions of microgravity elicited during parabolic flight," *Japanese Journal of Physiology*, vol. 47, supplement, p. S233, 1997.

[23] H. Waki, T. Shimizu, K. Katahira, T. Nagayama, M. Yamasaki, and S. Katsuda, "Effects of microgravity elicited by parabolic flight on abdominal aortic pressure and heart rate in rats," *Journal of Applied Physiology*, vol. 93, no. 6, pp. 1893–1899, 2002.

[24] M. Yamasaki and T. Shimizu, "Effects of the head-down tilt posture on postnatal development of the aortic baroreflex in the rabbit," *Japanese Journal of Physiology*, vol. 52, no. 2, pp. 149–161, 2002.

[25] J. C. Buckey Jr., R. M. Linnehan, and A. W. Dunlap, *The Neurolab Spacelab Mission: Neuroscience Research in Space, Results From the STS-90, Neurolab Spacelab Mission*, edited by J. C. Buckey and J. L. Homic, pp. 1–309, Lyndon B, NASA Johnson Space Center, Huston, Tex, USA, 2003.

[26] J. C. Buckey Jr., R. M. Linnehan, and A. W. Dunlap, "Animal care on neurolab," in *The Neurolab Spacelab Mission: Neuroscience Research in Space*, J. C. Buckey and J. L. Homic, Eds., pp. 295–298, Lyndon B, NASA Johnson Space Center, Huston, Tex, USA, 2003.

[27] S. Katsuda, H. Waki, M. Yamasaki et al., "Postnatal changes in the rheological properties of the aorta in Sprague-Dawley rats," *Experimental Animals*, vol. 51, no. 1, pp. 83–93, 2002.

[28] R. W. Lawton, "The thermoelastic behavior of isolated aortic strips of the dog," *Circulation Research*, vol. 3, no. 4, pp. 403–408, 1955.

[29] D. A. McDonald, *Blood Flow in Arteries*, Edward Arnold, London, UK, 1st edition, 1961.

[30] T. Shimizu, "Development of the aortic baroreflex system under conditions of microgravity," *Journal of Gravitational Physiology*, vol. 6, no. 1, pp. 55–58, 1999.

[31] H. Waki, K. Katahira, M. Yamasaki et al., "Effects of spaceflight on postnatal development of arterial baroreceptor reflex in rats," *Acta Physiologica Scandinavica*, vol. 184, no. 1, pp. 17–26, 2005.

[32] M. L. Harkness, R. D. Harkness, and D. A. McDonald, "The collagen and elastin content of the arterial wall in the dog," *Proceedings of the Royal Society of London B*, vol. 146, no. 925, pp. 541–551, 1957.

[33] J. Krafka Jr., "Comparative study of histophysics of the aorta," *American Journal of Physiology*, vol. 125, no. 1, pp. 1–14, 1938.

[34] T. H. Cox, "Effects of age on the mechanical properties of rat carotid artery," *The American Journal of Physiology—Heart and Circulatory Physiology*, vol. 233, no. 2, pp. H256–H263, 1977.

[35] R. H. Cox, "Comparison of carotid artery mechanisms in the rat, rabbit, and dog," *The American Journal of Physiology—Heart and Circulatory Physiology*, vol. 234, no. 3, pp. H280–H288, 1978.

[36] R. H. Cox, "Regional variation of series elasticity in canine arterial smooth muscles," *The American Journal of Physiology*, vol. 234, no. 5, pp. H542–H551, 1978.

[37] R. H. Cox, "Regional, species, and age related variations in the mechanical properties of arteries," *Biorheology*, vol. 16, no. 1-2, pp. 85–94, 1979.

[38] M. Hasegawa and Y. Watanabe, "Rheological properties of the thoracic aorta in normal and WHHL rabbits," *Biorheology*, vol. 25, no. 1-2, pp. 147–156, 1988.

[39] M. Roach and A. C. Burton, "The reason for the shape of the distensibility curves of arteries," *Canadian Journal of Biochemistry and Physiology*, vol. 35, no. 8, pp. 681–690, 1957.

[40] M. R. Roach and A. C. Burton, "The effect of age on the elasticity of human iliac artery," *Canadian Journal of Biochemistry and Physiology*, vol. 37, no. 4, pp. 557–570, 1959.

[41] K. D. Walton, R. G. Kalb, J. D. Luis et al., "Motor system development depends on experience: a microgravity study of rats," in *Neurolab Spacelab Mission: Neuroscience Research in Space, Results From the STS-90, Neurolab Spacelab Mission*, J . C. Buckey and J . L. Homick Jr., Eds., pp. 95–103, 2003.

[42] G. R. Adams, F. Haddad, and K. M. Baldwin, "Gravity plays an important role in muscle development and the differentiation of contractile protein phenotype," in *Neurolab Spacelab Mission: Neuroscience Research in Space, Results From the STS-90, Neurolab Spacelab Mission*, J. C. Buckey and J. L. Homick Jr., Eds., pp. 111–122, 2003.

[43] H. Oishi, T. Shimizu, K. Katahira et al., "Effects of microgravity to the mechanical changes in the rat aorta," Fy1997 Ground-based Research Announcement for Space Utilization Research Report, Japan Space Forum, Tokyo, Japan, 1998, (Japanese).

[44] O. Stein, S. Eisenberg, and Y. Stein, "Morphologic and biochemical changes in smooth muscle cells of aortas in growth-restricted rats," *Laboratory Investigation*, vol. 25, no. 2, pp. 149–157, 1971.

[45] G. R. Adams, S. A. McCue, P. W. Bodell, M. Zeng, and K. M. Baldwin, "Effects of spaceflight and thyroid deficiency on hindlimb development. I. Muscle mass and IGF-I expression," *Journal of Applied Physiology*, vol. 88, no. 3, pp. 894–903, 2000.

[46] M. Yamasaki, T. Shimizu, K. Katahira et al., "Spaceflight alters the fiber composition of the aortic nerve in the developing rat," *Neuroscience*, vol. 128, no. 4, pp. 819–829, 2004.

Hindawi Publishing Corporation
BioMed Research International
Volume 2014, Article ID 385082, 9 pages
http://dx.doi.org/10.1155/2014/385082

Research Article

Angiotensin Converting Enzyme Inhibition Reduces Cardiovascular Responses to Acute Stress in Myocardially Infarcted and Chronically Stressed Rats

A. Cudnoch-Jedrzejewska,[1] K. Czarzasta,[1] L. Puchalska,[1] J. Dobruch,[1] O. Borowik,[1] J. Pachucki,[2] and E. Szczepanska-Sadowska[1]

[1] *Department of Experimental and Clinical Physiology, Medical University of Warsaw, Ulica Pawinskiego 3c, 02-106 Warsaw, Poland*
[2] *Department of Internal Medicine and Endocrinology, Medical University of Warsaw, Ulica Banacha 1a, 02-097 Warsaw, Poland*

Correspondence should be addressed to A. Cudnoch-Jedrzejewska; agnieszka.cudnoch@wum.edu.pl

Received 28 February 2014; Revised 29 May 2014; Accepted 1 June 2014; Published 19 June 2014

Academic Editor: Alain Broccard

Previous studies showed that chronically stressed and myocardially infarcted rats respond with exaggerated cardiovascular responses to acute stress. The present experiments were designed to elucidate whether this effect can be abolished by treatment with the angiotensin converting enzyme (ACE) inhibitor captopril. Sprague Dawley rats were subjected either to sham surgery (Groups 1 and 2) or to myocardial infarction (Groups 3 and 4). The rats of Groups 2 and 4 were also exposed to mild chronic stressing. Four weeks after the operation, mean arterial blood pressure (MABP) and heart rate (HR) were measured under resting conditions and after application of acute stress. The cardiovascular responses to the acute stress were determined again 24 h after administration of captopril orally. Captopril significantly reduced resting MABP in each group. Before administration of captopril, the maximum increases in MABP evoked by the acute stressor in all (infarcted and sham-operated) chronically stressed rats and also in the infarcted nonchronically stressed rats were significantly greater than in the sham-operated rats not exposed to chronic stressing. These differences were abolished by captopril. The results suggest that ACE may improve tolerance of acute stress in heart failure and during chronic stressing.

1. Introduction

Prolonged activation of the renin-angiotensin system (RAS) plays a pivotal role in the pathogenesis of cardiovascular diseases [1, 2]. Introduction of angiotensin converting enzyme 1 inhibitors (ACEI) and angiotensin AT1 receptor blockers (AT1RB) into the treatment of cardiovascular diseases markedly reduced morbidity and mortality of cardiovascular patients [3–5]. Although large clinical trials did not indicate significant differences between the effectiveness of ACEI and effectiveness of AT1RB [6], there were also reports showing that some patients manifest preference to ACEI while others respond better to AT1RB or require supplementary treatment [7, 8]. Thus far, the reasons of individual differences in preference of AT1RB or ACEI are not fully recognized. One of the causes of individual differences in effectiveness of AT1 receptors blockers and ACE inhibitors in the cardiovascular diseases might result from different role of these compounds in the regulation of cardiovascular reactions to stress.

In recent years, evidence has been provided that angiotensin II (Ang II) may be an important stress hormone. Therefore, Yang et al. [9] reported that rats exposed to a short-lasting compulsive water swim or to prolonged stressing (5-day exposure to low ambient temperature) manifest significantly higher concentration of Ang II in the brain, adrenals, heart, vessels, and blood than the control animals. In addition, several groups of investigators provided evidence that angiotensin II and angiotensin AT1 receptors play an essential role in the stimulation of neuroendocrine responses to stress [10–13]. With regard to the regulation of blood pressure, Saiki et al. [14] reported that the blockade of AT1 receptors in the brain by intracerebroventricular (ICV) administration of losartan or saralasin reduces the cardiovascular responses to immobilization stress, whereas De Matteo et al. [15] and

Mayorov and Head [16] have found that the blockade of AT1 receptors in the rostral ventrolateral medulla (RVLM) and dorsomedial hypothalamus with candesartan or losartan reduces significantly the pressor response to 7-minute exposure to air jet stressor in rabbits. Furthermore, the studies of Zhang et al. [17] and Cudnoch-Jedrzejewska et al. [18, 19] revealed that the blockade of AT1 receptors with losartan abolishes elevation of cardiovascular responses to stress in rats with myocardial infarction.

In the present study we tested the hypothesis that cardiovascular responses to stress might also be significantly influenced by orally applied ACE inhibitors. The rationale to address this question was based on the following premises. Firstly, the spectrum of ACE inhibitors action markedly differs from that of AT1RB [7, 20]. Angiotensin converting enzyme inhibitors abolish the formation of Ang II, preventing thereby activation of both AT1 and AT2 receptors, while AT1RB selectively interferes with the stimulation of AT1 receptors. In addition, ACE interferes with the destruction of kinins [21]. Secondly, chronic stressing is frequently an unavoidable attribute of everyday life and it was reported that it might aggravate the cardiovascular pathology [22]. Therefore, in this investigation, we aimed to elucidate whether oral administration of ACE inhibitors may effectively reduce cardiovascular responses to acute stress in the postinfarct heart failure, during chronic stress and during combination of these two challenges. In order to solve this question we compared effects of administration of captopril, which effectively inhibits ACE1 in rats [23, 24], on the cardiovascular responses to acute stress in infarcted and sham-operated rats, and in the rats exposed either to chronic stressing alone or to chronic stressing combined with myocardial infarction.

2. Material and Methods

2.1. Animal Husbandry. Male Sprague Dawley rats (SPRD/Möl/Lod) were used as experimental animals. They were obtained from the Department of Animal Breeding and kept under 12 h light/12 h dark rhythm (light on at 6:00 a.m.) and in a room with regulated temperature (range 22–25°C). The rats were fed standard rat chow containing 0.3% sodium chloride (NaCl) and had free access to water. All experimental and surgical procedures described below were approved by the Local Ethical Committee on Animal Research and conducted in accordance with the international/EU guidelines and regulations on the use and care of laboratory animals.

2.2. Surgical Procedures. All surgical procedures were carried out under barbiturate anesthesia (pentobarbital, Biowet, Puławy, 5 mg/100 g of body wt, i.p.). Immediately after surgery, the rats were given an analgesic (buprenorphine 3 μg/100 g of body wt, i.p.; 2 times daily for 2-3 days) and antibiotic (penicillin, Polfa 10,000 IU/100 g of body wt, i.m.) and were placed in their own home cages.

At an age of 8–10 weeks, the rats were subjected either to a permanent left coronary artery ligation or to sham surgery. The coronary ligation was performed according to our own modification [25] of the surgical procedure described by Selye et al. [26]. Briefly, the heart was exteriorized through a surgical incision made between the 4th and 5th intercostal space while ventilation of the lungs was maintained by frequent administration of air jet puffs by means of a small rubber balloon connected to the rat's nose by means of a plastic tube. The left coronary artery was permanently ligated with a suture thread (Ethicon 6.0). The heart was placed back into the thoracic cavity and the wound was closed with surgical sutures (Ethicon 4.0). The rate of survival from the surgery was 48%. In the sham-operated rats the coronary artery was not ligated—instead the pericardium was touched with a needle. The rate of survival of the sham-operated rats was 95%.

Five weeks after the thoracic surgery, rats at the age of 13–15 weeks had an arterial line implanted for the measurement of mean arterial blood pressure (MABP) and heart rate (HR). The line consisted of an intra-arterial portion, made from a 3.5–4.0 cm tubing (i.d., 0.12 mm; o.d., 0.25 mm), and the external portion (i.d., 0.25 mm; o.d., 0.4 mm), made from a polyvinyl tubing (Scientific Commodities Inc.). The arterial catheter was inserted into the aorta through the femoral artery so that its end was located 2 cm below the renal arteries. The external tubing was tunnelled under the skin and exteriorized on the neck. The catheter was filled with 0.9% physiological NaCl, containing 500 U/mL of heparin, and closed with a stopper.

2.3. Course of Experiments and Experimental Groups

2.3.1. Course of Experiments. Five weeks after the myocardial infarction or sham surgery and 48 h after implantation of the arterial catheter, the rats were divided into four experimental groups (29 rats, body weight: 327–343 g) and four supplementary groups (19 rats, body weight: 335–345 g). During the experiments, the rats remained in their home cages but food and fluid were removed. For the experimental group, each experiment consisted of two parts performed on two consecutive days (Figure 1). During part 1, the rat was connected to the arterial line and the resting MABP and HR as well as MABP and HR responses to the air jet stressor were recorded. After 30 minutes allowed for adaptation, MABP and HR were recorded continuously for 40 minutes under resting conditions and for 10 minutes after the application of the alarming stressor (Figure 1). Subsequently, the rat was disconnected from the line and offered free access to food and water containing captopril (15 mg/35 mL/24 h/rat; approximately 45 mg/kg/24 h; that is, 0.207 mmol/kg/24 h). This dose of captopril was previously found to normalize arterial blood pressure in spontaneously hypertensive rats by [24, 27]. The amount of water in the bottle corresponded to an average 24 h water intake consumed by the rats receiving the same diet [28]. In all experiments, the rats ingested the total amount of captopril contained in the drinking fluid. Measurements of the cardiovascular parameters were repeated 24 hours later during the second part of the experiment as shown in Figure 1. At the end of each experiment, the rat was anesthetized with pentobarbital and a thin catheter (i.d., 0.5 mm; o.d., 0.8 mm; Dural Plastics and Engineering, Auburn, Australia)

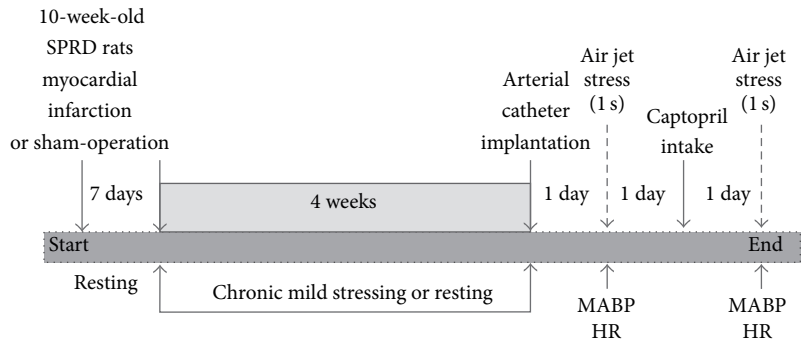

Figure 1: Experimental procedures. MABP: mean arterial blood pressure; HR: heart rate.

was inserted into the left ventricle of the heart via the right carotid artery and the aortic arch. The catheter served to determine the left ventricle end-diastolic pressure (LVEDP).

2.3.2. Measurements and Procedures. Blood pressure, heart rate, and end-diastolic left ventricle pressure (LVEDP) were determined by means of the blood pressure recording system (BIOPAC, MP 100, Santa Barbara, CA, USA). MABP was determined as the area under the arterial pressure curve divided by the cardiac cycle duration. Heart rate (beats/min) was calculated from the number of the systolic pressure peaks.

The cardiovascular response to acute stress was estimated using our own modification [25] of the air jet stress procedure described by Zhang et al. [17]. The air jet was blown on the top of the rat's head for 1 second via a laboratory-made device. The device consisted of a tank containing compressed air (10 atmospheres) and connected by a plastic tube (i.d., 3.0 mm) to a funnel (i.d., 41.5 mm) held 1.5–2.0 cm above the rat's head. The cardiovascular measurements were collected continuously for 10 minutes following the air jet application. The magnitude of the cardiovascular responses to the air jet stressor was evaluated by measuring the maximum increases in MABP (ΔMABPmax) and heart rate (ΔHRmax) after application of the stressor. The maximum increases in these parameters were determined by subtracting the resting values (found immediately before the application of the air jet) from the maximum values of MABP and HR recorded during the first 5 seconds after application of the air jet. The latency to the maximum increases in MABP and HR and the duration (time between the onset and the end) of the pressor and tachycardic responses were also determined.

LVEDP was determined at the end of the 2nd part of the experiment.

2.3.3. Groups of Experiments. Group 1 (control) was performed on 7 sham-operated rats with the purpose of determining the effect of ACE inhibition on MABP and HR under resting conditions and during the alarming (air jet) stress in the rats that were neither infarcted nor chronically stressed.

Group 2 was performed on 7 sham-operated, chronically stressed rats in order to determine the effects of captopril on resting cardiovascular parameters and cardiovascular responses to the alarming stressor in the sham-operated rats, exposed to chronic mild stressing.

The program of chronic stressing was similar to that used by Grippo et al. [29], except for some modifications described previously [30]. Briefly, the stressing was started one week after the thoracic surgery and consisted of five sessions per week (one session/day), which was followed by two days of rest. The following procedures were applied: (1) exposure of the rat to stroboscopic lamp flashes (300 flashes/min for 5 h); (2) placing the rat's cage in an oblique position (angle 40°) for 6 h; (3) visit of another rat in the home cage of the experimental rat for 3 h (during the visit the rats were separated by a transparent barrier); (4) water deprivation for 18 h followed by access to an empty bottle for 6 h; (5) placing the rat for 4 h in a new smaller cage (30 × 30 × 30 cm), in which it was exposed to an alien smell (deodorant placed in a perforated box). During each week, the sequence of the stressing procedures was altered. After four weeks of chronic stressing, the experiment was performed according to the protocol described in Group 1. Each stressing procedure started at 10:00 a.m. The same model of mild chronic stressing was found to induce anhedonia and significant changes in blood renin and corticosterone levels ([29] and our own unpublished data).

Group 3 was performed on 8 infarcted rats and was aimed at determining the effect of captopril on resting MABP and HR and on the cardiovascular responses to air jet stress in the infarcted rats, not exposed to chronic stressing. The experimental design was the same as in Group 1.

Group 4 was performed on 7 infarcted, chronically stressed rats in order to determine the effect of captopril on resting MABP and HR and on the cardiovascular responses to acute stress during combined exposure to the postinfarct heart failure and chronic stressing. The experimental protocol and the program of stressing were the same as in Group 2.

2.3.4. Supplementary Experiments. Supplementary experiments were performed to find out whether the rats could adapt to the air jet stressor when it was applied with 24 h intervals. Eight 10-week-old rats were subjected to the sham surgery (Group 5; $n = 4$ and Group 6; $n = 4$) or to a permanent coronary ligation (Group 7; $n = 5$ and Group 8; $n = 4$). Subsequently, the rats of Groups 5 and 7 were staying at rest for four weeks whereas the rats of Groups 6 and 8 were

exposed to chronic stressing. After this time all rats had an arterial catheter implanted. One day after implantation of the arterial catheter, the rats were connected to the BIOPAC system for recording MABP and HR at rest and during exposure to acute stress as in Groups 1–4. Subsequently, the rats of both groups were disconnected from the recording system and returned to their home cages where they had free access to food and water without captopril. After 24 h, measurements of MABP and HR at rest and during application of acute stress were repeated.

2.4. Postmortem Examination. After the experiments, the rats were killed by an overdose of pentobarbital (pentobarbital 10 mg/100 g of body wt, i.p.) and the heart was excised from the thorax. The wall of the left ventricle (including septum) was separated from the right ventricle and both atria. The infarct surface on the external and internal wall of the ventricle was measured and the measurements were averaged. The size of the infarct was determined planimetrically [31] with some modifications described previously [25] and expressed as a percentage of the total left ventricle surface. Fragments of the infarcted and noninfarcted left ventricle wall were harvested for histological verification of the presence of postinfarct fibrosis. The fragments were placed in a 4% formaldehyde solution and embedded in paraffin.

Tissue blocks were sectioned at 4 μm and stained with hematoxilin and eosin for routine morphological examination [28, 30]. The abdomen was opened to check whether the end of the arterial catheter was located below the renal arteries and did not obstruct the lumen of the aorta or the renal artery.

2.5. Statistical Analysis. Statistical software (release 10) was used for statistical analysis of the results using recommendations of Curran-Everett and Benos [32] and Ludbrook [33] for independent and repeated measurements and the post hoc analysis of data. The Shapiro-Wilk test was used to check whether the data follow a normal distribution. Multiple-way ANOVA (two levels of rats: infarcted versus sham-operated; 2 levels of repeated measurements: before and after captopril intake; and 4 levels of experimental design: sham-operated nonchronically stressed, sham-operated chronically stressed, infarcted nonchronically stressed, and infarcted chronically stressed) was used to determine the significance of differences between the resting cardiovascular parameters and between the maximum increases, latencies, and durations of the cardiovascular parameters produced by the air jet stressor. The horizontal and vertical multiple pairwise comparisons were made using the post hoc Tukey test; t-test (paired or unpaired) was used if two groups of measurements were compared. The differences were considered significant if P was <0.05. Values presented in the text and figures correspond to means and standard errors.

3. Results

3.1. Effect of Captopril Intake on Resting MABP and HR. Significant differences were found between the individual experimental groups both before [$F(3.25) = 10.32$; $P < 0.001$] and after captopril ingestion [$F(3.25) = 13.47$; $P < 0.001$]. The resting MABP was significantly lower in the rats drinking water containing captopril than in those drinking pure water. A comparison between the individual groups showed that before the administration of captopril the resting MABP was significantly lower in the infarcted nonchronically stressed rats than in the sham-operated nonchronically stressed rats (Figure 2). MABP was also lower in the infarcted chronically stressed rats than in the sham-operated chronically stressed rats (Figure 2).

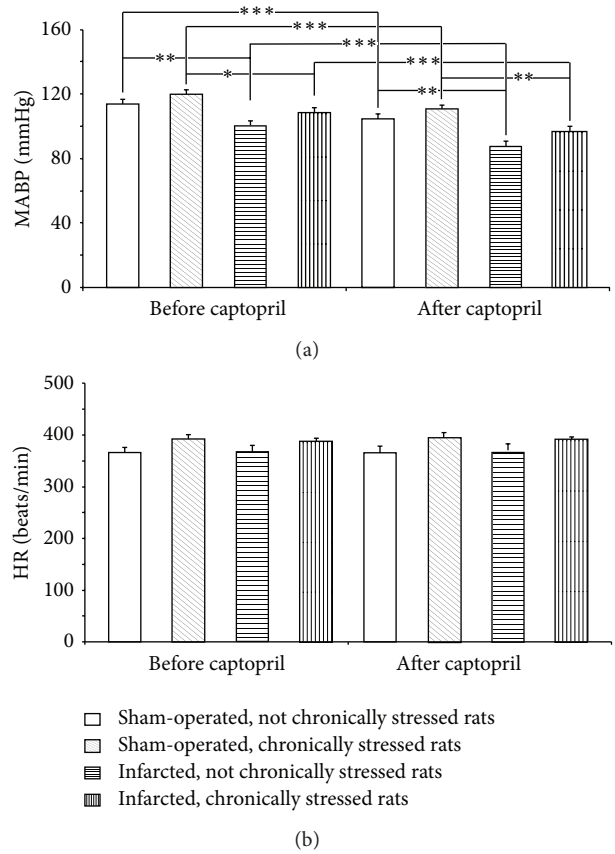

Figure 2: Changes in resting mean arterial blood pressure (MABP) and heart rate (HR) before and after captopril intake in the infarcted or sham-operated rats, exposed or not exposed to mild chronic stressing. Means ± SE are shown; $^{*}P < 0.05$; $^{**}P < 0.01$; $^{***}P < 0.001$.

There were no significant differences in the resting heart rate, which did not differ either before or after administration of captopril (Figure 2).

3.2. Effect of Captopril on Air Jet Stress-Induced Maximum Changes in MABP and HR. As shown in Figure 3 the baseline MABP were stable during 40 min preceding application of the acute stress. The corresponding changes of HR were also not significant (data not shown). The acute stress elicited significant increases of MABP and HR (Figure 4). One-way ANOVA revealed that before ingestion of captopril significant differences in the magnitude of cardiovascular responses to stress were present between the individual experimental groups [$F(3.25) = 6.61$; $P < 0.001$]. Individual comparisons

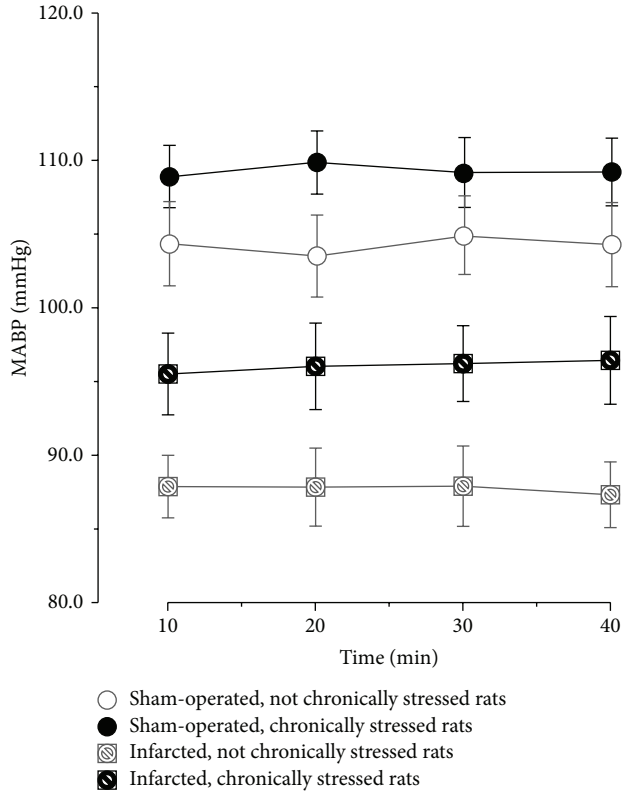

Figure 3: Fluctuations of baseline mean arterial blood pressure (MABP) during 40 min preceding application of the acute stress in the infarcted or sham-operated rats, exposed or not exposed to mild chronic stressing.

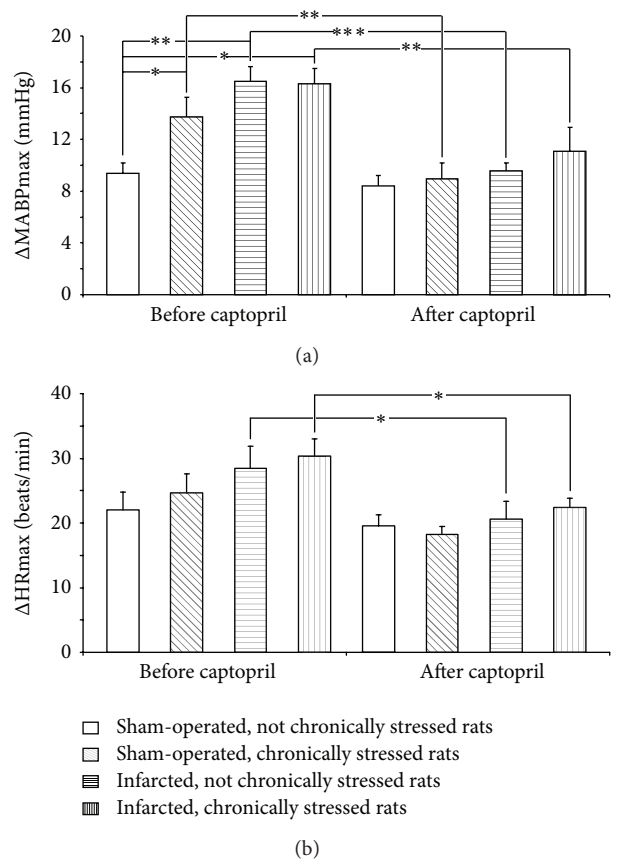

Figure 4: Maximum increases in mean arterial blood pressure (ΔMABPmax) and heart rate (ΔHRmax) after application of air jet stressor before and after captopril intake in the infarcted or sham-operated rats, exposed or not exposed to mild chronic stressing. Means ± SE are shown; $^{*}P < 0.05$; $^{**}P < 0.01$; $^{***}P < 0.001$.

showed that ΔMABPmax values were significantly higher in the sham-operated chronically stressed, infarcted nonchronically stressed, and the infarcted chronically stressed rats than in the sham-operated nonchronically stressed rats (Figure 4).

Captopril decreased the air jet stress-induced ΔMABPmax in each experimental group except for the sham-operated Group 1 (Figure 4). Before captopril administration, the intergroup differences in ΔHRmax were not significant. Ingestion of captopril resulted in significant decrease of ΔHRmax in the infarcted nonchronically stressed rats and in the infarcted chronically stressed rats ($P < 0.05$) (Figure 4).

3.3. Duration and Latency of the Pressor and Tachycardic Responses to Air Jet Stressor. A comparison of ΔMABP and ΔHR durations before and after administration of captopril by multiple-way repeated measures ANOVA revealed the presence of significant differences {ΔMABP: [$F(1.25) = 6.69$; $P < 0.05$]; ΔHR: [$F(1.25) = 8.51$; $P < 0.05$]} (Figure 5). Individual comparisons demonstrated that captopril reduced the duration of ΔMABP and ΔHR in each group (Figure 5).

A comparison of the latencies to ΔMABPmax before and after administration of captopril by multiple-way repeated measures showed significant differences [$F(1.25) = 13.92$; $P < 0.01$]. As shown in Figure 6, the latencies to ΔMABPmax after administration of captopril were significantly lower than before administration of this compound. Administration of captopril did not affect latencies of ΔHRmax in any of the experimental groups (Figure 6).

3.3.1. Supplementary Experiments (Groups 5–8). As shown in Figure 7, acute stress produced the same maximum increases of MABP in the rats drinking water without captopril when it was repeated with 24 h intervals. Repeatability of responses was present both in the sham-operated and in the infarcted rats.

3.3.2. Other Measurements. Left ventricle end-diastolic pressure in the infarcted, nonchronically stressed rats (24.88 ± 1.93) was significantly higher than in the sham-operated, nonstressed rats (3.88 ± 0.61; $P < 0.001$). Similarly, LVEDP in the infarcted, chronically stressed rats (22.56 ± 1.56) was significantly higher than in the sham-operated, chronically stressed rats (3.38 ± 0.63; $P < 0.001$). Left ventricle end-diastolic pressure in the infarcted, nonchronically stressed rats, receiving captopril (18.33 ± 0.95), was higher than in the sham-operated, nonstressed rats, receiving captopril (2.88 ± 0.35; $P < 0.001$). Similarly, LVEDP in the infarcted, chronically stressed rats, receiving captopril (16.38 ± 0.84), was significantly higher than in the sham-operated, chronically

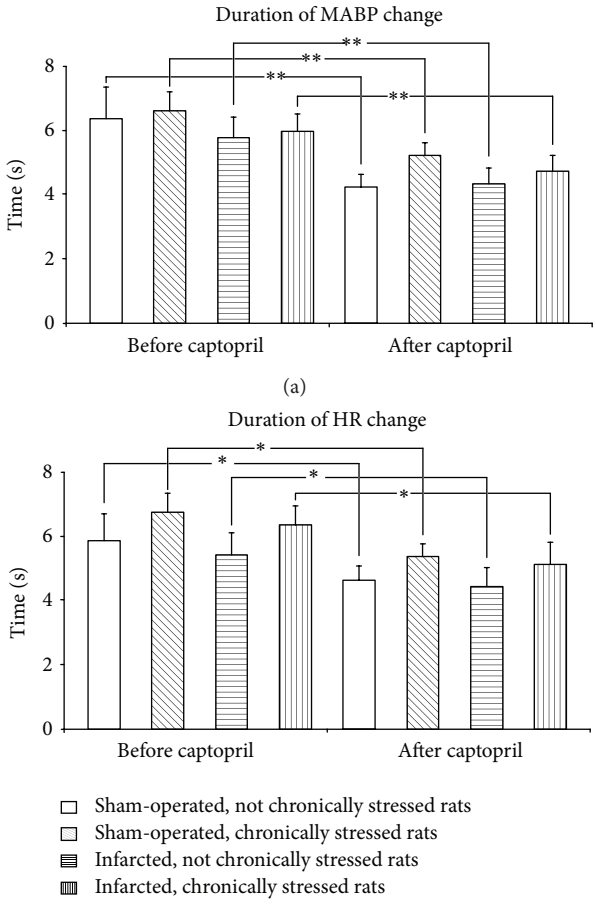

Figure 5: Duration of air jet stress-induced increases in mean arterial blood pressure (ΔMABP) and heart rate (ΔHR) before and after captopril intake in the infarcted or sham-operated rats, exposed or not exposed to mild chronic stressing. Means ± SE are shown; $^{*}P < 0.05$; $^{**}P < 0.01$.

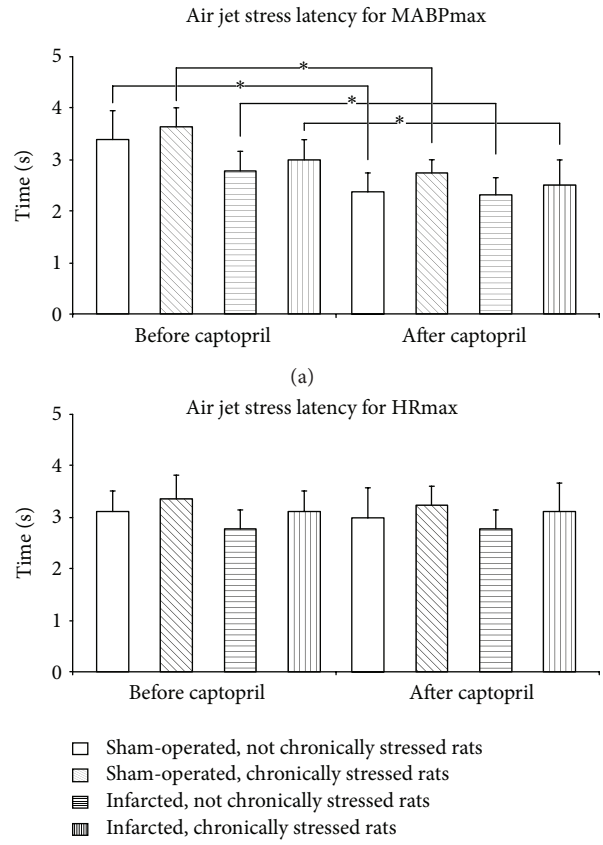

Figure 6: Latency of air jet stress-induced maximum increases in mean arterial blood pressure (ΔMABPmax) and heart rate (ΔHRmax) before and after captopril intake in the infarcted or sham-operated rats, exposed or not exposed to mild chronic stressing. Means ± SE are shown; $^{*}P < 0.05$.

stressed rats, receiving captopril (2.75 ± 0.37; $P < 0.001$). Captopril significantly reduced LVED in all infarcted rats ($P < 0.01$) but did not exert significant effect on LVEDP in the sham-operated chronically stressed rats.

The *postmortem* measurements showed that the infarct surfaces were similar in the all-infarcted, nonchronically stressed rats (range 25–45%) and in the all-infarcted, chronically stressed rats (range 26–47.5%).

4. Discussion

A novel finding in the present study is that the oral administration of ACE inhibitors normalizes cardiovascular responses to acute stress in infracted and chronically stressed rats.

4.1. Hypotensive Effect of Short-Term Administration of Captopril on Resting Blood Pressure. In the present study, we decided to evaluate the effect of oral administration of captopril as it is the routine way for the application of ACE inhibitors during the treatment of cardiovascular diseases.

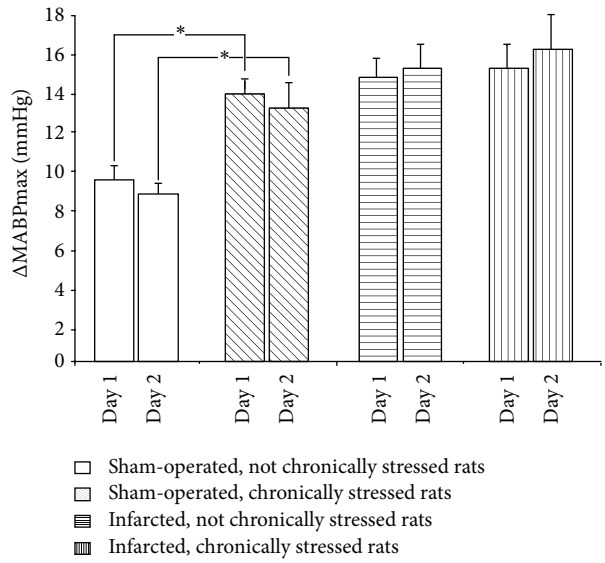

Figure 7: Maximum increases of blood pressure during application of air jet stress in the infarcted or sham-operated rats, exposed or not exposed to mild chronic stressing. Air jet stressor was applied twice with 24 h interval (day 1 and day 2). Means ± SE are shown; $^{*}P < 0.05$.

In our study, the dose of captopril ingested in 24 h water supply was sufficient to decrease the resting blood pressure in all experimental groups, including the sham-operated nonstressed rats. The finding that captopril decreases the resting blood pressure in the infarcted and chronically stressed rats fits with the activation of the systemic and local renin-angiotensin systems during postinfarct heart failure [17, 34, 35] and during chronic stress [29]. For instance, Ahmad et al. [35] have found that systematically applied lisinopril—one of the hydrophilic ACE inhibitors—reduces ACE activity, both in the brain and in the kidney of the infarcted rats. A decrease of the resting blood pressure after captopril indicates that the dose of captopril, which was applied, was sufficient to exert the hypotensive effect in the control nondisturbed animals. Previously, a significant hypotensive effect was also observed after chronic application of captopril in conscious Sprague Dawley control rats [23] and after administration of 25 mg of this compound into healthy human subjects in an upright position [36].

4.2. Suppression of Exaggerated Cardiovascular Responses to Acute Stress by Captopril in Infarcted and Chronically Stressed Rats. Our results confirm previous findings showing enhanced cardiovascular responses to acute stress in myocardially infarcted rats [17, 18, 25, 30] and in chronically stressed rats [30]. In previous studies, it was demonstrated that this effect significantly depends on the activation of the brain renin-angiotensin system as it could be abolished by ICV administration of AT1 receptor blockers and potentiated by central administration of Ang II [17–19]. The present study shows that significant attenuation of exaggerated cardiovascular responses to acute stress may be achieved both in infarcted and in chronically stressed rats by oral administration of captopril.

It cannot be excluded that the suppression of cardiovascular responses to stress by captopril could result from the inhibition of the brain ACE. Indirect evidence indicates that peripheral administration of ACE inhibitors, including captopril, may inhibit the brain renin-angiotensin system [35, 37, 38]. Moreover, autoradiographic studies have shown that chronic oral administration of ACE inhibitor quinapril lowers ACE density in several brain structures by 35–38% [39]. On the other hand, there are also studies showing that Ang II modulates sympathoadrenal activity through peripheral action [1, 40]. Thus, the stress-suppressing inhibitory effect of captopril might be partly related to the suppression of the stimulation of the sympathoadrenal system, which is significantly stimulated both during postinfarct heart failure [17] and during chronic stressing [22, 29, 41, 42].

The present study shows that oral administration of captopril significantly reduces exaggerated cardiovascular responses to acute stress during chronic stressing. Previous studies provided evidence for pronounced activation of the renin-angiotensin system during stress. Thus, significant increases in Ang II content in the hypothalamus, medulla oblongata, heart, and adrenal medulla were found in the rats subjected to acute and prolonged stress by Yang et al. [9]. Moreover, it has been shown that a restraint stress enhances expression of AT1 receptors mRNA in the paraventricular nucleus (PVN) [43]. It was also demonstrated that AT1 receptors play a significant role in the activation of the hypothalamo-pituitary-adrenal axis during stress [10, 11, 13]. Previous studies showed that the blockade of central AT1 receptors in the rostral, ventrolateral medulla (RVLM) significantly attenuates pressor responses to short-lasting emotional stress in rabbits [15, 16]. In addition, Saiki et al. [14] reported that the blockade of central AT1 receptors suppresses stimulation of the sympathetic nervous system and reduces pressor and tachycardic responses elicited by immobilization stress. The present study implies the involvement of Ang II in the regulation of blood pressure during chronic stressing; however its action may be mediated by other compounds.

Our previous studies provided evidence for interaction of vasopressin and angiotensin II in the regulation of cardiovascular responses to acute stress. We have also found that vasopressin and stimulation of V1 receptors participate in Ang II-induced potentiation of the cardiovascular responses to acute stress in infarcted rats [18, 19]. Thus, reduction of the cardiovascular responses to acute stress by captopril could result from its inhibitory effect on generation of Ang II in vasopressin secreting neurons. In this line, it has been shown that inhibition of ACE by oral application of quinapril or ramipril reduces the content of vasopressin in the supraoptic and paraventricular (PVN) nuclei as well as in the brain regions innervated by vasopressin secreting neurons [39, 44].

Apart from inhibition of Ang II formation, ACE inhibitors may also act by activation of the kinins system and release of bradykinin [21, 45] and through the stimulation of nitric oxide synthase and 20-HETE pathway [46, 47].

Interestingly, captopril significantly shortened the duration of the pressor and tachycardic responses to the air jet stressor in all experimental groups and reduced the latency to the maximum increase in arterial blood pressure (Figures 5 and 6). Reduced duration of the pressor and tachycardic responses to acute stress may be considered as a positive result of ACE treatment because most likely it was associated with reduced cardiac workload. The shortening of the latency to the air jet stress-induced maximum elevation in MABP by captopril may suggest that the blockade of ACE enhances alertness to the alarming stressor.

In conclusion, the present study shows that orally administered captopril significantly decreases resting arterial blood pressure and significantly reduces the pressor and tachycardic responses to the acute stressor in chronically stressed rats and in infarcted rats exposed and not exposed to chronic stressing. Thus, the study discloses a new aspect of beneficial action of orally administered ACE inhibitors in the postinfarct cardiac failure and during chronic exposure to stress.

Conflict of Interests

The authors report no conflict of interests regarding the publication of this paper. The authors alone are responsible for the content and the writing of the paper.

Acknowledgments

The authors are indebted to Mrs. Marzanna Tkaczyk and Mr. Marcin Kumosa for their skillful technical assistance. The

study was supported by Grants from the Ministry of Science and Education (Grant 2P05 182 29).

References

[1] M. E. Fabiani, D. T. Dinh, L. Nassis, and C. I. Johnston, "Angiotensin-converting enzyme: basic properties, distribution, and functional role," in *Hypertension: A Companion to Brenner and Rector's the Kidney*, S. Oparil and M. A. Weber, Eds., pp. 90–100, WB Saunders, Philadelphia, Pa, USA, 2000.

[2] D. Fournier, F. C. Luft, M. Bader, D. Ganten, and M. A. Andrade-Navarro, "Emergence and evolution of the renin-angiotensin-aldosterone system," *Journal of Molecular Medicine*, vol. 90, no. 5, pp. 495–508, 2012.

[3] M. A. Pfeffer, J. J. V. McMurray, E. J. Velazquez et al., "Valsartan, captopril, or both in myocardial infarction complicated by heart failure, left ventricular dysfunction, or both," *The New England Journal of Medicine*, vol. 349, no. 20, pp. 1893–1906, 2003.

[4] J. Schrader, A. Kulschewski, and A. Dendorfer, "Inhibition of the renin-angiotensin system and the prevention of stroke," *The American Journal of Cardiovascular Drugs*, vol. 7, no. 1, pp. 25–37, 2007.

[5] R. Ferrari, "RAAS inhibition and mortality in hypertension: from pharmacology to clinical evidence," *Kardiologia Polska*, vol. 71, no. 1, pp. 1–7, 2013.

[6] S. Ueda, "New approaches to blockade of the renin-angiotensin-aldosterone system: evidence from randomized controlled trials (RCTs) of angiotensin-converting enzyme inhibitors and angiotensin II-receptor blockers-questions remain unsolved," *Journal of Pharmacological Sciences*, vol. 113, no. 4, pp. 292–295, 2010.

[7] H. Makani, S. Bangalore, K. A. Desouza, A. Shah, and F. H. Messerli, "Efficacy and safety of dual blockade of the renin-angiotensin system: meta-analysis of randomised trials," *British Medical Journal*, vol. 346, no. 7896, article f360, 2013.

[8] U. Shah, K. A. Mergenhagen, and K. Kellick, "Effectiveness and safety of dual renin-angiotensin system blockade: a comparison between younger and older cohorts," *Consultant Pharmacist*, vol. 28, no. 6, pp. 383–389, 2013.

[9] G. Yang, Z.-X. Xi, Y. Wan, H. Wang, and G. Bi, "Changes in circulating and tissue angiotensin II during acute and chronic stress," *Biological Signals*, vol. 2, no. 3, pp. 166–172, 1993.

[10] I. Armando, S. Volpi, G. Aguilera, and J. M. Saavedra, "Angiotensin II AT1 receptor blockade prevents the hypothalamic corticotropin-releasing factor response to isolation stress," *Brain Research*, vol. 1142, no. 20, pp. 92–99, 2007.

[11] J. M. Saavedra and J. Benicky, "Brain and peripheral angiotensin II play a major role in stress," *Stress*, vol. 10, no. 2, pp. 185–193, 2007.

[12] J. Pavel, J. Benicky, Y. Murakami, E. Sanchez-Lemus, and J. M. Saavedra, "Peripherally administered angiotensin II AT1 receptor antagonists are anti-stress compounds in vivo," *Annals of the New York Academy of Sciences*, vol. 1148, pp. 360–366, 2008.

[13] J. M. Saavedra, E. Sánchez-Lemus, and J. Benicky, "Blockade of brain angiotensin II AT1 receptors ameliorates stress, anxiety, brain inflammation and ischemia: therapeutic implications," *Psychoneuroendocrinology*, vol. 36, no. 1, pp. 1–18, 2011.

[14] Y. Saiki, T. Watanabe, N. Tan, M. Matsuzaki, and S. Nakamura, "Role of central ANG II receptors in stress-induced cardiovascular and hyperthermic responses in rats," *The American Journal of Physiology—Regulatory Integrative and Comparative Physiology*, vol. 272, no. 1, part 2, pp. R26–R33, 1997.

[15] R. De Matteo, G. A. Head, and D. N. Mayorov, "Angiotensin II in dorsomedial hypothalamus modulates cardiovascular arousal caused by stress but not feeding in rabbits," *The American Journal of Physiology—Regulatory Integrative and Comparative Physiology*, vol. 290, no. 1, pp. R257–R264, 2006.

[16] D. N. Mayorov and G. A. Head, "AT1 receptors in the RVLM mediate pressor responses to emotional stress in rabbits," *Hypertension*, vol. 41, no. 5, pp. 1168–1173, 2003.

[17] W. Zhang, B. S. Huang, and F. H. H. Leenen, "Brain renin-angiotensin system and sympathetic hyperactivity in rats after myocardial infarction," *The American Journal of Physiology—Heart and Circulatory Physiology*, vol. 276, no. 5, part 2, pp. H1608–H1615, 1999.

[18] A. Cudnoch-Jedrzejewska, J. Dobruch, L. Puchalska, and E. Szczepańska-Sadowska, "Interaction of AT1 receptors and V1a receptors-mediated effects in the central cardiovascular control during the post-infarct state," *Regulatory Peptides*, vol. 142, no. 3, pp. 86–94, 2007.

[19] A. Cudnoch-Jedrzejewska, E. Szczepanska-Sadowska, J. Dobruch et al., "Differential sensitisation to central cardiovascular effects of angiotensin II in rats with a myocardial infarct: relevance to stress and interaction with vasopressin," *Stress*, vol. 11, no. 4, pp. 290–301, 2008.

[20] T. Unger, "Targeting cardiovascular protection: the concept of dual renin-angiotensin system control," *MedGenMed Medscape General Medicine*, vol. 10, supplement, p. S4, 2008.

[21] A. Kuoppala, K. A. Lindstedt, J. Saarinen, P. T. Kovanen, and J. O. Kokkonen, "Inactivation of bradykinin by angiotensin-converting enzyme and by carboxypeptidase N in human plasma," *The American Journal of Physiology—Heart and Circulatory Physiology*, vol. 278, no. 4, pp. H1069–H1074, 2000.

[22] J. E. Dimsdale, "Psychological stress and cardiovascular disease," *Journal of the American College of Cardiology*, vol. 51, no. 13, pp. 1237–1246, 2008.

[23] S. Elkouri, P. Demers, M. G. Sirois, A. Couturier, and R. Cartier, "Effect of chronic exercise and angiotensin-converting enzyme inhibition on rodent thoracic aorta," *Journal of Cardiovascular Pharmacology*, vol. 44, no. 5, pp. 582–590, 2004.

[24] A. L. M. Swislocki, T. L. Kinney Lapier, D. T. Khuu, K. Y. Fann, M. Tait, and K. J. Rodnick, "Metabolic, hemodynamic, and cardiac effects of captopril in young, spontaneously hypertensive rats," *The American Journal of Hypertension*, vol. 12, no. 6, pp. 581–589, 1999.

[25] J. Dobruch, A. Cudnoch-Jedrzejewska, and E. Szczepanska-Sadowska, "Enhanced involvement of brain vasopressin V1 receptors in cardiovascular responses to stress in rats with myocardial infarction," *Stress*, vol. 8, no. 4, pp. 273–284, 2005.

[26] H. Selye, E. Bajusz, S. Grasso, and P. Mendell, "Simple techniques for the surgical occlusion of coronary vessels in the rat," *Angiology*, vol. 11, pp. 398–407, 1960.

[27] M. A. Pfeffer, J. M. Pfeffer, C. Steinberg, and P. Finn, "Survival after an experimental myocardial infarction: beneficial effects of long-term therapy with captopril," *Circulation*, vol. 72, no. 2, pp. 406–412, 1985.

[28] A. Cudnoch-Jędrzejewska, E. Szczepańska-Sadowska, J. Dobruch et al., "Fluid consumption, electrolyte excretion and heart remodeling in rats with myocardial infarct maintained on regular and high sodium intake," *Journal of Physiology and Pharmacology*, vol. 56, no. 4, pp. 599–610, 2005.

[29] A. J. Grippo, J. Francis, T. G. Beltz, R. B. Felder, and A. K. Johnson, "Neuroendocrine and cytokine profile of chronic mild stress-induced anhedonia," *Physiology and Behavior*, vol. 84, no. 5, pp. 697–706, 2005.

[30] A. Cudnoch-Jedrzejewska, E. Szczepanska-Sadowska, J. Dobruch, R. Gomolka, and L. Puchalska, "Brain vasopressin V1 receptors contribute to enhanced cardiovascular responses to acute stress in chronically stressed rats and rats with myocardial infarcton," *The American Journal of Physiology—Regulatory Integrative and Comparative Physiology*, vol. 298, no. 3, pp. R672–R680, 2010.

[31] F. H. H. Leenen, B. Yuan, and B. S. Huang, "Brain "ouabain" and angiotensin II contribute to cardiac dysfunction after myocardial infarction," *The American Journal of Physiology—Heart and Circulatory Physiology*, vol. 277, no. 5, part 2, pp. H1786–H1792, 1999.

[32] D. Curran-Everett and D. J. Benos, "Guidelines for reporting statistics in journals published by the American Physiological Society," *Physiological Genomics*, vol. 18, no. 3, pp. 249–251, 2004.

[33] J. Ludbrook, "Repeated measurements and multiple comparisons in cardiovascular research," *Cardiovascular Research*, vol. 28, no. 3, pp. 303–311, 1994.

[34] S. Y. Chai, J. Zhuo, and F. A. O. Mendelsohn, "Localization of components of the renin-angiotensin system and site of action of inhibitors," *Arzneimittel-Forschung/Drug Research*, vol. 43, no. 2A, pp. 214–221, 1993.

[35] M. Ahmad, R. White, J. Tan, B. S. Huang, and F. H. Leenen, "Angiotensin-converting enzyme inhibitors, inhibition of brain and peripheral angiotensin-converting enzymes, and left ventricular dysfunction in rats after myocardial infarction," *Journal of Cardiovascular Pharmacology*, vol. 51, no. 6, pp. 565–572, 2008.

[36] R. Fagard, P. Lijnen, L. Vanhees, and A. Amery, "Hemodynamic response to converting enzyme inhibition at rest and exercise in humans," *Journal of Applied Physiology Respiratory Environmental and Exercise Physiology*, vol. 53, no. 3, pp. 576–581, 1982.

[37] P. Geppetti, M. G. Spillantini, S. Frilli, U. Pietrini, M. Fanciullacci, and F. Sicuteri, "Acute oral captopril inhibits angiotension converting enzyme activity in human cerebrospinal fluid," *Journal of Hypertension*, vol. 5, no. 2, pp. 151–154, 1987.

[38] J. Tan, J. M. Wang, and F. H. H. Leenen, "Inhibition of brain angiotensin-converting enzyme by peripheral administration of trandolapril versus lisinopril in Wistar rats," *The American Journal of Hypertension*, vol. 18, no. 2, part 1, pp. 158–164, 2005.

[39] F. Muders, D. Elsner, K. Jandeleit et al., "Chronic ACE inhibition by quinapril modulates central vasopressinergic system," *Cardiovascular Research*, vol. 34, no. 3, pp. 575–581, 1997.

[40] A. Dendorfer, A. Thornagel, W. Raasch, O. Grisk, K. Tempel, and P. Dominiak, "Angiotensin II induces catecholamine release by direct ganglionic excitation," *Hypertension*, vol. 40, no. 3, pp. 348–354, 2002.

[41] G. F. DiBona and S. Y. Jones, "Analysis of renal sympathetic nerve responses to stress," *Hypertension*, vol. 25, no. 4, part 1, pp. 531–538, 1995.

[42] A. J. Grippo, J. A. Moffitt, and A. K. Johnson, "Cardiovascular alterations and autonomic imbalance in an experimental model of depression," *The American Journal of Physiology—Regulatory Integrative and Comparative Physiology*, vol. 282, no. 5, pp. R1333–R1341, 2002.

[43] D. S. Leong, J. A. Terrón, and A. Falcón-Neri at al, "Restraint stress modulates brain, pituitary and adrenal expression of angiotensin II AT(1A), AT(1B) and AT(2) receptors," *Neuroendocrinology*, vol. 75, no. 4, pp. 227–240, 2002.

[44] F. Muders, D. Elsner, H. Schunkert, G. A. J. Riegger, and M. Palkovits, "Central vasopressin is modulated by chronic blockade of the renin-angiotensin system in experimental left ventricular hypertrophy," *The American Journal of Hypertension*, vol. 12, no. 3, pp. 311–314, 1999.

[45] J. V. Gainer, J. D. Morrow, A. Loveland, D. J. King, and N. J. Brown, "Effect of bradykinin-receptor blockade on the response to angiotensin-converting-enzyme inhibitor in normotensive and hypertensive subjects," *The New England Journal of Medicine*, vol. 339, no. 18, pp. 1285–1292, 1998.

[46] O. Ito, K. Omata, S. Ito, K. M. Hoagland, and R. J. Roman, "Effects of converting enzyme inhibitors on renal P-450 metabolism of arachidonic acid," *The American Journal of Physiology—Regulatory Integrative and Comparative Physiology*, vol. 280, no. 3, pp. R822–R830, 2001.

[47] F. Qadri, T. Arens, E.-C. Schwarz, W. Häuser, A. Dendorfer, and P. Dominiak, "Brain nitric oxide synthase activity in spontaneously hypertensive rats during the development of hypertension," *Journal of Hypertension*, vol. 21, no. 9, pp. 1687–1694, 2003.

Hindawi Publishing Corporation
BioMed Research International
Volume 2014, Article ID 363756, 8 pages
http://dx.doi.org/10.1155/2014/363756

Review Article

Hemodynamic Indexes Derived from Computed Tomography Angiography to Predict Pulmonary Embolism Related Mortality

Gregor John,[1] Christophe Marti,[1] Pierre-Alexandre Poletti,[2] and Arnaud Perrier[3]

[1] *Department of Internal Medicine, Rehabilitation and Geriatrics, Geneva University Hospitals (HUG), Gabrielle-Perret-Gentil 4, 1205 Geneva, Switzerland*
[2] *Department of Radiology, Emergency-Room Radiology Unit, Geneva University Hospitals (HUG), Gabrielle-Perret-Gentil 4, 1205 Geneva, Switzerland*
[3] *Department of Internal Medicine, Rehabilitation and Geriatrics, Geneva University Hospitals (HUG) and Geneva Faculty of Medicine, Gabrielle-Perret-Gentil 4, 1211 Geneva, Switzerland*

Correspondence should be addressed to Gregor John; gregor.john@hcuge.ch

Received 24 April 2014; Accepted 2 June 2014; Published 18 June 2014

Academic Editor: Karim Bendjelid

Pulmonary embolism (PE) induces an acute increase in the right ventricle afterload that can lead to right-ventricular dysfunction (RVD) and eventually to circulatory collapse. Hemodynamic status and presence of RVD are important determinants of adverse outcomes in acute PE. Technologic progress allows computed tomography angiography (CTA) to give more information than accurate diagnosis of PE. It may also provide an insight into hemodynamics and right-ventricular function. Proximal localization of emboli, reflux of contrast medium to the hepatic veins, and right-to-left short-axis ventricular diameter ratio seem to be the most relevant CTA predictors of 30-day mortality. These elements require little postprocessing time, an advantage in the emergency room. We herein review the prognostic value of RVD and other CTA mortality predictors for patients with acute PE.

1. Introduction

Pulmonary embolism (PE) has a wide spectrum of presentations and severity. Some patients present with shock, requiring urgent thrombolysis [1], while others can be safely treated on an outpatient basis with anticoagulation alone [2]. Guidelines propose tailoring management of PE depending on the risk of adverse outcomes, which depends on hemodynamic status (presence of shock or hypotension), biomarkers (brain natriuretic peptide or cardiac troponin levels), and imagery [1, 3]. Among normotensive patients, right-ventricular dysfunction (RVD) has been shown to carry a higher mortality [4–6]. Echocardiography has become the standard procedure to evaluate RVD but requires skilled specialists and is not available around the clock in many hospitals [7].

Nowadays, computed tomography angiography (CTA) is by far the most commonly used modality to diagnose pulmonary embolism. CTA also allows appreciating vessel and cardiac chamber size. Furthermore, contrast medium flow is a dynamic process. Abnormal flow dynamics can manifest in two ways: diverted hyperdense venous opacification and an altered temporal relationship of vascular opacification [8]. Thus even if CTA produces static images, it provides clues for dynamic or functional parameters, therefore making multislice chest CTA an attractive alternative to echocardiography for prognostic assessment. Using information given by a single test also avoids time consuming and often costly supplemental procedures.

We will herein review indirect hemodynamic signs given by chest CTA and their impact on risk stratification.

2. Hemodynamic Consequence of Pulmonary Arterial Obstruction at a Glance

In the pulmonary circulation, cardiac output (3 L/min/m^2) faces low arterial resistance (80 dynes·s/cm^5) and generates low pressure (mean pulmonary arterial pressure, 15 mmHg). The blood flow can eventually triple to face an increased

demand without changing pulmonary pressure by recruitment of new vascular beds.

The burden of pulmonary arterial obstruction and previous cardiorespiratory state determine the hemodynamic consequences of PE. In previously healthy subjects, there is a nonlinear correlation between the degree of pulmonary arterial obstruction and pulmonary pressure. Pulmonary pressure elevation is negligible until obstruction involves more than 30–50% of the arterial bed but increases rapidly above that threshold [9]. This increase is steeper in case of previous pulmonary or left-heart disease. Arterial obstruction and reflex vasoconstriction induced by hypoxia or locally released cytokines cause pulmonary hypertension and enlargement of proximal arterial vessels [10].

Increased central venous return related to hypoxia-induced peripheral venoconstriction in addition to reflex tachycardia increases right- ventricular preload and stroke volume. Therefore, in medium-sized PE, cardiac output remains normal or even slightly increased despite the higher afterload. However, when the right ventricle (RV) can no longer accommodate this pressure increase, signs of right-ventricular failure occur. The blood stasis will cause vein enlargement (e.g., superior and inferior vena cava and azygos vein). Contrast medium reflux in the inferior vena cava on chest CTA (Figure 1) is an indirect sign of tricuspid valve insufficiency with elevated right atrial pressure [11].

The right-ventricular wall is thin, in comparison to that of the left ventricle. Wall stress generated by an acute increase in mean pulmonary arterial pressure above 40 mmHg results in right-ventricular dilatation (Figure 2) [9]. RV pressure and dilatation can induce a shift of the septum that will abnormally bow to the left (Figure 2). Because the pericardium is inextensible, this results in an acute decrease of left-ventricular (LV) compliance. In addition, a decrease in coronary blood flow leads to myocardial ischemia that first affects the RV due to an already increased oxygen demand and then exacerbates abnormal LV compliance. The decrease in stroke volume of the RV can lead to a decrease in pulmonary venous return to the left ventricle, causing a drop in systemic blood pressure. Syncope or shock occurs in 5–10% of patients with acute PE [12].

Chest CTA gives indirect signs of right-heart afterload (size of the main pulmonary arteries and emboli burden) or preload (size of azygos vein and vena cava) and allows an estimate of right-ventricular dysfunction through right-to-left ventricular ratios (diameter, surface, volume, or even function), interventricular septum bowing, and retrograde reflux of contrast into the veins. All these signs are interdependent (e.g., right-to-left ventricle ratios and embolic burden or retrograde reflux of contrast into the veins) and may give information on more than one of the following physiologic entities: preload, afterload, and ventricular function.

3. Computed Tomography Angiography Signs of Right-Ventricular Dysfunction

In the late nineties, ventricular dilatation [13] and interventricular septum bowing [12] were recognized on helical computed tomography. RV dilatation and LV reduced volume both contribute to a high right-to-left ventricle diameter ratio [14].

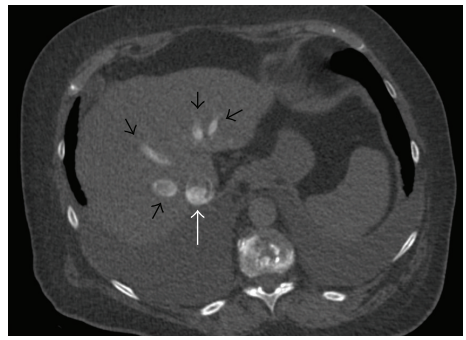

Figure 1: Computed tomography showing significant (grade 5) reflux of contrast media in the inferior vena cava (white arrow) and hepatic veins (black arrows) seen in a 75-year-old man diagnosed with pulmonary embolism and right-ventricular dysfunction.

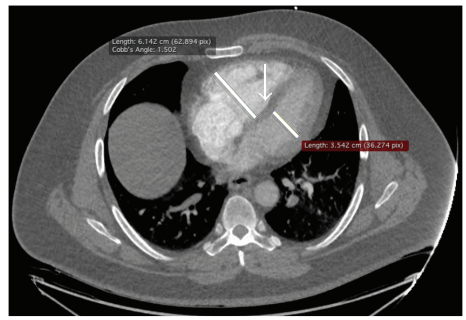

Figure 2: Computed tomography of a 75-year-old man with right-ventricular dysfunction showing increased right-to-left diameter ratio. The short-axis is measured at the widest points between the inner surface of the free wall and the surface of the interventricular septum, in axial transverse images used to diagnose procedure, without reconstructions. The right and left ventricle diameters selected to calculate the ratio are by definition the largest transverse diameters and are therefore often measured in different CTA slices. Note the interventricular septum bowing to the left (arrow).

3.1. Right-to-Left Ventricular Ratios. Right ventricle dilatation can be assessed by different methods on CTA. The right-to-left ventricular diameter ratio is more commonly used because it is simple to measure and mirrors the concept of right ventricle dilatation at echocardiography. The fastest method is to measure the heart chambers' minor axis at the widest points between the inner surface of the free wall and the surface of the interventricular septum in the same images used for diagnosis, without reconstructions (Figure 2). The right and left ventricle diameters selected to calculate the ratio are by definition the largest transverse diameters and are therefore often measured in different CTA slices. However, "submassive pulmonary embolism," as defined by the American Heart Association criteria, requires the use of reconstructed images in order to obtain

a four-chamber view, comparable to echocardiography [3, 15]. The latter method is more time consuming and is dependent on manipulations of workstation by the radiologist that can result in different divergent planes of four-chamber views and its incremental value is limited [16, 17]. The European guidelines do not define the method for calculating the right-to-left ventricle diameter ratio [1].

Since ventricles have a complex tridimensional shape that is not considered when the ratio is measured in two dimensions, some authors have proposed to measure volumetric ratios [18, 19]. This volume ratio might be more accurate in predicting mortality [20]. However, it demands manual outlining of endocardial contour, which needs an additional 4 to 11 minutes [18], a practical issue limiting its generalisation. A further step for improving the assessment of heart function by CTA is to synchronize it with the ECG in order to obtain diastolic and systolic ventricular images. Stroke volume and ejection fraction can be calculated accurately with a good reproducibility compared to MRI [21]. However, ECG-driven CTA did not demonstrate a statistically different area under the receiver-operator curve compared to axial ratio for predicting adverse clinical outcomes [22]. This technique results in an extra amount of contrast agent and radiation exposure. Ejection fraction derived from the ECG-synchronized CTA is time consuming (around 20 minutes [21]) and requires expertise [22].

Indeed, all those methods (axial ratio with or without reconstruction and volumetric ratio) can be used to measure ventricular dilatation and stratify the risk associated with PE, with a good interobserver reproducibility (kappa > 0.8 for RVD and Spearman's rank correlation > 0.8) [16, 17]. In their meta-analysis on the association between right-ventricular dysfunction and mortality, Becattini et al. found similar results for the different methods used to estimate the right-to-left ventricle ratio [17].

Studies exploring CTA include very different patient populations with a mortality ranging from 5 to 18% [4]. Also, the thresholds used to define RVD are not uniform. The most frequently used cut-off point for axial and four-chamber view right-to-left ventricular ratio is 1.0 [4] and 1.2 for volume ratio [18]. Higher cut-off points select a population at increased risk of death [17]. The American Heart Association recommends a cut-off of 0.9 while the ESC proposes a cut-off of 0.9 or 1.0 for the right-to-left ventricle diameter ratio [1, 3]. Whatever the cut-off used is, overall RVD assessed by CTA is observed in more than 50% of patients diagnosed with PE [4]. In their meta-analyses, Becattini et al. [17] and Trujillo-Santos et al. [4] confirmed an increased mortality associated with RVD in all-comers [17] and in the normotensive subset of patients with pulmonary embolism [4, 17]. The risk of death at 30 days after diagnosis doubles (Table 1) for patients with an increased right-to-left ventricle ratio (diameter, surface, or volume ratio) determined by CTA, a result comparable to RV dysfunction assessed by echocardiography [5, 6]. The absolute risk increases from 5.1% (105/2049) to 11.2% (293/2612) in all-comers including patients with shock and from 3.3% (33/984) to 5.4% (69/1270) in normotensive patients with an increased right-to-left ventricle ratio [17].

3.2. Septum Bowing. This nonspecific sign of increased right-sided pressure is found roughly in 20% of patients with PE (Figure 2) [14, 16, 27]. Septum bowing has an excellent specificity (100%) but a poor sensitivity (26%) for predicting RV dysfunction [11]. Furthermore, it is the right-ventricular CTA sign with the poorest interobserver reproducibility (kappa: 0.32), thus limiting its clinical application [16]. It has been shown to confer a greater risk of ICU admission [27, 28] and short-term death (Table 1) [17, 18].

4. Computed Tomography Angiography Estimate of Afterload

4.1. Embolic Obstruction Burden Score and Localization. The number of emboli and their locations are expected to correlate with prognosis. Computed tomography angiography allows an accurate visualisation of emboli up to the subsegmental portions of the pulmonary arteries [29]. Many different CTA scores integrate the number of occluded vessels and the degree of obstruction (complete versus incomplete) with conflicting results concerning their association with death. Vedovati et al. found no association with mortality [23]. However, this recent meta-analysis explored only one scoring system, the Qanadli score [30], and was limited by a small number of studies and a high degree of heterogeneity with many outliers. Moreover, all emboli burden scores are laborious to perform and simpler information can be readily obtained on CTA, namely, the central position (main or lobar arteries) of the emboli. The central location of the emboli seems to have a greater influence on the risk of 30-day mortality than the presence of multiple minor emboli (included in burden scores) [23]. This is confirmed in the same meta-analysis (Table 1) [23].

4.2. Pulmonary Artery Size. In small heterogeneous populations, the diameter of the main pulmonary artery [26] and the ratio between the pulmonary artery and the ascending aorta were proposed as indicators of pulmonary hypertension [10], since the size of the main pulmonary artery increases in severe PE [28, 31]. The diameter of the main pulmonary artery and the ratio between the pulmonary artery and the ascending aorta failed to demonstrate a correlation with mortality in the context of acute PE in a large study and meta-analysis [14, 23].

4.3. Blood Flow Distribution on Dual-Energy CTA. Standard CTA uses a single X-ray beam at a fixed potential (single-energy), which gives useful structural information, but is sometimes limited in differentiating between tissues with similar attenuation. The principle of dual-energy imaging has been established a long time ago [32] but was only recently implemented on modern CT scanner devices [33–35]. Dual-energy CT analyses simultaneously the X-ray attenuation at low- and high-energy levels (usually 80 and 140 kV), which brings specific information about a particular structure or tissue (e.g., used to differentiate calcium from iodine, iodine from blood clot, and so forth). Dual-energy chest CTA has many applications [35]. In suspected acute PE, it provides

Table 1: Computed tomography angiography (CTA) signs, involved mechanism, association with short-term mortality, and level of evidence.

CTA sign	Pathophysiology	Proportion of patients with PE and positive sign	30-day mortality OR (95% CI)	Data based on	Interobserver variability*	Level of evidence†
Main pulmonary artery size	Extension of arterial obstruction and pulmonary hypertension/right ventricular afterload	Variable	Not statistically significant	4 small retrospective studies and two meta-analyses [17, 23]	Fair	Low
Emboli burden			Not statistically significant	Meta-analysis of 9 studies [23]	Fair	Good
Emboli position			2.2 (1.3–3.9) for main or lobar arteries localisation	Meta-analysis of 3 studies [23]	Excellent	Good
Blood flow on dual-energy CTA			3.8 (1.0–14.6)‡ for a defect >5%	2 small retrospectives studies	Unknown	Low
Right-to-left ventricular ratio	Right-ventricular dysfunction	>50%	2.1 (1.6–2.8) for all-comers with pulmonary embolism	One meta-analysis (>5000 patients) [17]	Excellent	Good
			1.7 (1.1–2.7) for normotensive patients	Two meta-analyses (>2000 patients each) [4, 17]	Excellent	Good
Interventricular septal bowing		20%	1.8 (1.2–2.7)	One meta-analysis (1422 patients) [17]	Poor	Low
Retrograde reflux of contrast	Tricuspid regurgitation, increased atrial pressure/right- ventricular preload	20%	3.1 (1.2–7.7)§	>6 small and 1 intermediate-size retrospective study	Fair-excellent	Low
Azygos vein size		Variable	1.5 (1.1–2.0)‖	1 small retrospective study	Fair	Low

*Based on kappa statistic: <0.4 poor; 0.4–0.75 fair; >0.75 excellent; †global appreciation of scientific evidence based on the number, size, quality of the studies, and availability of a meta-analysis; ‡calculated from Bauer et al. [24]; §calculated from Aviram et al. [25]; ‖14-day mortality [26].
CTA: computed tomography angiography; OR: odds ratio; 95% CI: 95% confidence interval.

excellent morphologic details while allowing the identification of small peripheral thrombi [36].

By isolating the iodine component of the tissue, dual-energy CTA gives the distribution of contrast medium within the lung parenchyma (parallel to the blood perfusion of the lung). Lung perfusion scores derived from dual-energy CTA and number of pulmonary segments with reduced blood flow have been shown to correlate with CTA obstruction score [37–40], troponin I [38], D-dimer [24], and right-to-left ventricular ratio [24, 37–42]. Only one retrospective study suggested a link with mortality (7/18 deaths in the group with a perfusion defect of more than 5% and 5/35 death in the group with smaller defect, Table 1) [24]. Another study showed greater perfusion defects among the 10/60 patients admitted to ICU or dying from PE compared to normotensive patients with PE [37]. However, the dual-energy CTA increases the postprocessing time, the number of images to be stored, and requires expertise. Numerous artefacts also limit its interpretation (e.g., heart and diaphragmatic movement and parenchymal abnormalities) [35]. Irradiation dose seems not to be increased compared to single-energy CTA but depends on type of dual-energy (single source or dual source) and protocol used [35, 43]. The usefulness of dual-energy CTA in risk stratification for acute PE deserves further study.

5. Computed Tomography Angiography Estimate of Preload

Preload is more difficult to appreciate on CTA. Saugel et al. found a disappointing correlation between invasive measurement (transpulmonary thermodilution) and CTA determined parameters of left-sided hemodynamics (preload and lung water content) [44]. Contrast reflux in vena cava and vein size integrate information on ventricular pressure overload, dilatation, and decreased function. These are arbitrarily classified as preload for the conceptual purposes of this paper. Cardiac chambers are also related to preload.

5.1. Retrograde Reflux of Contrast into the Veins. Reflux of medium contrast into the inferior vena cava (IVC) is an indirect CTA sign of increased RV pressure that can be seen in various underlying conditions (Figure 1) [8]. It is present in around 20% of patients with acute PE [25]. The severity of the reflux of contrast medium can be graded as 1 = no reflux to 6 = reflux into IVC with opacification that extends down to the distal hepatic veins [25]. Only reflux down to the hepatic veins (grade ≥ 4) seems to have prognostic significance [25]. Interobserver reproducibility is good when high grades of reflux are considered ($\geq$4) (Kappa: 0.57–0.78) [16, 25]. Reflux of contrast medium into the IVC is a significant predictor of RVD determined by echocardiography or biomarkers (94% sensitivity and 55% specificity) [11] and of 30-day mortality (Table 1) [18].

5.2. Vein Size. An increased pressure in the right atrium results in the widening of dependent veins such as the azygos vein, coronary sinus, and superior and inferior vena cava (IVC) [28, 45]. All of these vein sizes were significantly different in patients with RVD assessed by echocardiography compared to those without [45]. IVC size incorporated in a multivariate model predicted better RVD than as a single parameter or ratio measured on CTA [45]. In a small retrospective study, the azygos vein and SVC sizes were different between deceased patients and survivors from an acute PE [31]. However evidence is lacking on the real utility of those CTA parameters to predict 30-day mortality.

6. Clinical Implication for PE Risk Stratification

An ideal risk stratification tool should be able to identify patients at higher risk of death deserving admission to a monitored unit and/or thrombolysis and safely select low-risk patients eligible for short hospital stay or outpatient treatment.

As previously discussed, the most validated CTA sign is the right-to-left ventricle diameter ratio, other signs having no utility (obstruction score), lacking evidence (contrast reflux) or having a high interobserver variability (septum bowing) (Table 1). However the absolute 30-day mortality risk increases only slightly for patients with an increased right-to-left ventricle ratio [17]. Thus, the pooled estimated positive predictive value for right-to-left ventricle diameter ratio measured in transverse images is only 10% (95% CI 6–15%) [17]. With a positive likelihood ratio of 1.3 (95% CI 1.1–1.4) this result has little utility in practice, since the posttest probability is only little different from the pretest probability. CTA performances are comparable to those of echocardiography, which thus adds little for further risk stratification after CTA. Some data suggest that combination of CTA with cardiac biomarkers [20, 46] or clinical scores may further optimize risk stratification [47, 48]. Nevertheless, in the recently published PEITHO study in which the intermediate-risk population was selected based on evidence of both myocardial injury (elevated troponin) and RVD assessed by CTA or US, the 30-day mortality in the heparin-alone arm was low (2.8%) [46].

The pooled estimated negative predictive value for right-to-left ventricle diameter ratio measured in transverse images is 95% (95% CI 93–97%) [17], making CTA a good candidate to identify low-risk patients. However, the negative likelihood ratio is only 0.7 (95% CI 0.6–0.9) [4], a result comparable to echocardiography (NLR 0.6 (95% CI 0.4–0.9)) [5]. This apparent discrepancy between high negative predictive value and poorly discriminative NLR is due to the low overall mortality associated with PE. Therefore, it should be recognized that a number of patients with PE and no RVD on CTA are still at risk of dying. On the other hand, a simple score, the PESI score, based only on clinical variables, is able to accurately identify patients with a 30-day mortality below 3% and has been extensively validated. Therefore, risk stratification by imaging whatever the index used is not clinically relevant for identifying low-risk patients eligible for short hospital stay or outpatient treatment [2].

In summary, available evidence suggests a role for CTA as an alternative to echocardiography for identifying patients

with intermediate-risk PE eligible for closer monitoring. In contrast, low-risk patient should be identified with PESI score (I or II) [2].

7. Conclusion

This review shows the prognostic values that can be gathered on an already available CTA, which is (fast) always done for diagnosis. However, the choice of CTA or echocardiography for risk stratification remains dependent on their institutional availability. Right-to-left short-axis ventricular ratio is the most relevant CTA-parameter for predicting short-term mortality (within 30 days) and can replace echocardiography for RVD assessment. However, its incremental value for risk stratification in acute PE is low (likelihood ratios close to 1).

Further research should focalize on management strategies depending on CTA-based risk categories, in combination with clinical scores or biomarkers. Although proximal location of emboli, septum bowing, and reflux of contrast medium into the hepatic veins may be of interest, there is insufficient evidence to recommend their clinical use. Right-to-left short-axis ventricular ratio measurement on CTA demands little postprocessing time, a useful feature in the emergency room.

Conflict of Interests

All authors declare no support from any organisation for the submitted work, no financial relationships with any organisations that might have an interest in the submitted work in the previous three years, and no other relationships or activities that could appear to have influenced the submitted work.

Acknowledgments

The authors gratefully acknowledge Claire Bardini and Stephan Von Düring for their correction of the English paper.

References

[1] A. Torbicki, A. Perrier, S. Konstantinides et al., "Guidelines on the diagnosis and management of acute pulmonary embolism: the Task Force for the Diagnosis and Management of Acute Pulmonary Embolism of the European Society of Cardiology (ESC)," *European Heart Journal*, vol. 29, no. 18, pp. 2276–2315, 2008.

[2] D. Aujesky, P.-M. Roy, F. Verschuren et al., "Outpatient versus inpatient treatment for patients with acute pulmonary embolism: an international, open-label, randomised, non-inferiority trial," *The Lancet*, vol. 378, no. 9785, pp. 41–48, 2011.

[3] M. R. Jaff, M. S. McMurtry, S. L. Archer et al., "Management of massive and submassive pulmonary embolism, iliofemoral deep vein thrombosis, and chronic thromboembolic pulmonary hypertension: a scientific statement from the american heart association," *Circulation*, vol. 123, no. 16, pp. 1788–1830, 2011.

[4] J. Trujillo-Santos, P. L. den Exter, V. Gomez et al., "Computed tomography-assessed right ventricular dysfunction and risk stratification of patients with acute non-massive pulmonary embolism: systematic review and meta-analysis," *Journal of Thrombosis and Haemostasis*, vol. 11, no. 10, pp. 1823–1832, 2013.

[5] G. Coutance, E. Cauderlier, J. Ehtisham, M. Hamon, and M. Hamon, "The prognostic value of markers of right ventricular dysfunction in pulmonary embolism: a meta-analysis," *Critical Care*, vol. 15, no. 2, article R103, 2011.

[6] O. Sanchez, L. Trinquart, I. Colombet et al., "Prognostic value of right ventricular dysfunction in patients with haemodynamically stable pulmonary embolism: a systematic review," *European Heart Journal*, vol. 29, no. 12, pp. 1569–1577, 2008.

[7] S. Z. Goldhaber, "Echocardiography in the management of pulmonary embolism," *Annals of Internal Medicine*, vol. 136, no. 9, pp. 691–700, 2002.

[8] M. V. Gosselin and G. D. Rubin, "Altered intravascular contrast material flow dynamics: clues for refining thoracic CT diagnosis," *American Journal of Roentgenology*, vol. 169, no. 6, pp. 1597–1603, 1997.

[9] K. M. McIntyre and A. A. Sasahara, "The hemodynamic response to pulmonary embolism in patients without prior cardiopulmonary disease," *The American Journal of Cardiology*, vol. 28, no. 3, pp. 288–294, 1971.

[10] C. S. Ng, A. U. Wells, and S. P. G. Padley, "A CT sign of chronic pulmonary arterial hypertension: the ratio of main pulmonary artery to aortic diameter," *Journal of Thoracic Imaging*, vol. 14, no. 4, pp. 270–278, 1999.

[11] H. J. Seon, K. H. Kim, W. S. Lee et al., "Usefulness of computed tomographic pulmonary angiography in the risk stratification of acute pulmonary thromboembolism: comparison with cardiac biomarkers," *Circulation Journal*, vol. 75, no. 2, pp. 428–436, 2011.

[12] K. E. Wood, "Major pulmonary embolism: review of a pathophysiologic approach to the golden hour of hemodynamically significant pulmonary embolism," *Chest*, vol. 121, no. 3, pp. 877–905, 2002.

[13] J. H. Reid and J. T. Murchison, "Acute right ventricular dilatation: a new helical CT sign of massive pulmonary embolism," *Clinical Radiology*, vol. 53, no. 9, pp. 694–698, 1998.

[14] R. W. van der Meer, P. M. T. Pattynama, M. J. L. van Strijen et al., "Right ventricular dysfunction and pulmonary obstruction index at helical CT: prediction of clinical outcome during 3-month follow-up in patients with acute pulmonary embolism," *Radiology*, vol. 235, no. 3, pp. 798–803, 2005.

[15] R. Quiroz, N. Kucher, U. J. Schoepf et al., "Right ventricular enlargement on chest computed tomography: prognostic role in acute pulmonary embolism," *Circulation*, vol. 109, no. 20, pp. 2401–2404, 2004.

[16] D. K. Kang, L. Ramos-Duran, U. J. Schoepf et al., "Reproducibility of CT signs of right ventricular dysfunction in acute pulmonary embolism," *American Journal of Roentgenology*, vol. 194, no. 6, pp. 1500–1506, 2010.

[17] C. Becattini, G. Agnelli, F. Germini, and M. C. Vedovati, "Computed tomography to assess risk of death in acute pulmonary embolism: a meta-analysis," *The European Respiratory Journal*, vol. 43, no. 6, pp. 1678–1690, 2014.

[18] D. K. Kang, C. Thilo, U. J. Schoepf et al., "CT signs of right ventricular dysfunction: prognostic role in acute pulmonary embolism," *JACC: Cardiovascular Imaging*, vol. 4, no. 8, pp. 841–849, 2011.

[19] H. Doğan, L. J. M. Kroft, M. V. Huisman, R. J. van der Geest, and A. de Roos, "Right ventricular function in patients with

acute pulmonary embolism: analysis with electrocardiography-synchronized multi-detector row CT," *Radiology*, vol. 242, no. 1, pp. 78–84, 2007.

[20] D. K. Kang, J. S. Sun, K. J. Park, and H. S. Lim, "Usefulness of combined assessment with computed tomographic signs of right ventricular dysfunction and cardiac troponin T for risk stratification of acute pulmonary embolism," *American Journal of Cardiology*, vol. 108, no. 1, pp. 133–140, 2011.

[21] M. Müller, F. Teige, D. Schnapauff, B. Hamm, and M. Dewey, "Evaluation of right ventricular function with multidetector computed tomography: comparison with magnetic resonance imaging and analysis of inter- and intraobserver variability," *European Radiology*, vol. 19, no. 2, pp. 278–289, 2009.

[22] N. van der Bijl, F. A. Klok, M. V. Huisman et al., "Measurement of right and left ventricular function by ECG-synchronized CT scanning in patients with acute pulmonary embolism: usefulness for predicting short-term outcome," *Chest*, vol. 140, no. 4, pp. 1008–1015, 2011.

[23] M. C. Vedovati, F. Germini, G. Agnelli, and C. Becattini, "Prognostic role of embolic burden assessed at computed tomography angiography in patients with acute pulmonary embolism: systematic review and meta-analysis," *Journal of Thrombosis and Haemostasis*, vol. 11, no. 12, pp. 2092–2102, 2013.

[24] R. W. Bauer, C. Frellesen, M. Renker et al., "Dual energy CT pulmonary blood volume assessment in acute pulmonary embolism—correlation with D-dimer level, right heart strain and clinical outcome," *European Radiology*, vol. 21, no. 9, pp. 1914–1921, 2011.

[25] G. Aviram, O. Rogowski, Y. Gotler et al., "Real-time risk stratification of patients with acute pulmonary embolism by grading the reflux of contrast into the inferior vena cava on computerized tomographic pulmonary angiography," *Journal of Thrombosis and Haemostasis*, vol. 6, no. 9, pp. 1488–1493, 2008.

[26] K. Kuriyama, G. Gamsu, R. G. Stern, C. E. Cann, R. J. Herfkens, and B. H. Brundage, "CT-determined pulmonary artery diameters in predicting pulmonary hypertension," *Investigative Radiology*, vol. 19, no. 1, pp. 16–22, 1984.

[27] P. A. Araoz, M. B. Gotway, R. L. Trowbridge et al., "Helical CT pulmonary angiography predictors of in-hospital morbidity and mortality in patients with acute pulmonary embolism," *Journal of Thoracic Imaging*, vol. 18, no. 4, pp. 207–216, 2003.

[28] D. Collomb, P. J. Paramelle, O. Calaque et al., "Severity assessment of acute pulmonary embolism: evaluation using helical CT," *European Radiology*, vol. 13, no. 7, pp. 1508–1514, 2003.

[29] P. D. Stein, S. E. Fowler, L. R. Goodman et al., "Multidetector computed tomography for acute pulmonary embolism," *The New England Journal of Medicine*, vol. 354, no. 22, pp. 2317–2327, 2006.

[30] S. D. Qanadli, M. El Hajjam, A. Vieillard-Baron et al., "New CT index to quantify arterial obstruction in pulmonary embolism: comparison with angiographic index and echocardiography," *American Journal of Roentgenology*, vol. 176, no. 6, pp. 1415–1420, 2001.

[31] B. Ghaye, A. Ghuysen, V. Willems et al., "Severe pulmonary embolism: pulmonary artery clot load scores and cardiovascular parameters as predictors of mortality," *Radiology*, vol. 239, no. 3, pp. 884–891, 2006.

[32] G. N. Hounsfield, "Computerized transverse axial scanning (tomography): I. Description of system," *British Journal of Radiology*, vol. 46, no. 552, pp. 1016–1022, 1973.

[33] R. K. Kaza, J. F. Platt, R. H. Cohan, E. M. Caoili, M. M. Al-Hawary, and A. Wasnik, "Dual-energy ct with single- and dual-source scanners: current applications in evaluating the genitourinary tract," *Radiographics*, vol. 32, no. 2, pp. 353–369, 2012.

[34] C. A. Coursey, R. C. Nelson, D. T. Boll et al., "Dual-energy multidetector CT: how does it work, what can it tell us, and when can we use it in abdominopelvic imaging?" *Radiographics*, vol. 30, no. 4, pp. 1037–1055, 2010.

[35] G. M. Lu, Y. Zhao, L. J. Zhang, and U. J. Schoepf, "Dual-energy CT of the lung," *American Journal of Roentgenology*, vol. 199, no. 5, supplement, pp. S40–S53, 2012.

[36] A. Foncubierta-Rodriguez, O. A. Jimenez Del Toro, A. Platon, P. A. Poletti, H. Muller, and A. Depeursinge, "Benefits of texture analysis of dual energy CT for Computer-Aided pulmonary embolism detection," in *Proceedings of the 35th Annual International Conference of the IEEE Engineering in Medicine and Biology Society (EMBC '13)*, pp. 3973–3976, 2013.

[37] P. Apfaltrer, V. Bachmann, M. Meyer et al., "Prognostic value of perfusion defect volume at dual energy CTA in patients with pulmonary embolism: correlation with CTA obstruction scores, CT parameters of right ventricular dysfunction and adverse clinical outcome," *European Journal of Radiology*, vol. 81, no. 11, pp. 3592–3597, 2012.

[38] S. F. Thieme, N. Ashoori, F. Bamberg et al., "Severity assessment of pulmonary embolism using dual energy CT—correlation of a pulmonary perfusion defect score with clinical and morphological parameters of blood oxygenation and right ventricular failure," *European Radiology*, vol. 22, no. 2, pp. 269–278, 2012.

[39] E. J. Chae, J. B. Seo, Y. M. Jang et al., "Dual-energy CT for assessment of the severity of acute pulmonary embolism: pulmonary perfusion defect score compared with CT angiographic obstruction score and right ventricular/left ventricular diameter ratio," *American Journal of Roentgenology*, vol. 194, no. 3, pp. 604–610, 2010.

[40] M. Okada, Y. Nakashima, Y. Kunihiro et al., "Volumetric evaluation of dual-energy perfusion CT for the assessment of intrapulmonary clot burden," *Clinical Radiology*, vol. 68, no. 12, pp. e669–e675, 2013.

[41] S. Miura, Y. Ohno, H. Kimura, and K. Kichikawa, "Quantitative lung perfused blood volume imaging on dual-energy CT: capability for quantitative assessment of disease severity in patients with acute pulmonary thromboembolism," *Acta Radiologica*, 2014.

[42] L. J. Zhang, G. F. Yang, Y. E. Zhao, C. S. Zhou, and G. M. Lu, "Detection of pulmonary embolism using dual-energy computed tomography and correlation with cardiovascular measurements: a preliminary study," *Acta Radiologica*, vol. 50, no. 8, pp. 892–901, 2009.

[43] T. De Zordo, K. von Lutterotti, C. Dejaco et al., "Comparison of image quality and radiation dose of different pulmonary CTA protocols on a 128-slice CT: high-pitch dual source CT, dual energy CT and conventional spiral CT," *European Radiology*, vol. 22, no. 2, pp. 279–286, 2012.

[44] B. Saugel, K. Holzapfel, J. Stollfuss et al., "Computed tomography to estimate cardiac preload and extravascular lung water. A retrospective analysis in critically ill patients," *Scandinavian Journal of Trauma, Resuscitation and Emergency Medicine*, vol. 19, article 31, 2011.

[45] G. Staskiewicz, E. Czekajska-Chehab, S. Uhlig, J. Przegalinski, R. Maciejewski, and A. Drop, "Logistic regression model for

identification of right ventricular dysfunction in patients with acute pulmonary embolism by means of computed tomography," *European Journal of Radiology*, vol. 82, no. 8, pp. 1236–1239, 2013.

[46] G. Meyer, E. Vicaut, T. Danays et al., "Fibrinolysis for patients with intermediate-risk pulmonary embolism," *The New England Journal of Medicine*, vol. 370, no. 15, pp. 1402–1411, 2014.

[47] C. Bova, O. Sanchez, P. Prandoni et al., "Identification of intermediate-risk patients with acute symptomatic pulmonary embolism," *The European Respiratory Journal*, 2014.

[48] D. Jimenez, D. Kopecna, V. Tapson et al., "Derivation and validation of multimarker prognostication for normotensive patients with acute symptomatic pulmonary embolism," *American Journal of Respiratory and Critical Care Medicine*, vol. 189, no. 6, pp. 718–726, 2014.

Hindawi Publishing Corporation
BioMed Research International
Volume 2014, Article ID 598029, 7 pages
http://dx.doi.org/10.1155/2014/598029

Research Article

Evaluation of Cardiac Function Index as Measured by Transpulmonary Thermodilution as an Indicator of Left Ventricular Ejection Fraction in Cardiogenic Shock

Jessica Perny,[1] Antoine Kimmoun,[1,2,3] Pierre Perez,[1] and Bruno Levy[1,2,3]

[1] *CHU Nancy, Service de Reanimation Medicale Brabois, Pole Cardiovasculaire et Reanimation Medicale, Hopital Brabois, 54511 Vandoeuvre-les-Nancy, France*
[2] *INSERM, CHU Nancy, Groupe Choc Inserm, U1116, Faculté de Médecine, 54511 Vandoeuvre-les-Nancy, France*
[3] *Université de Lorraine, 54000 Nancy, France*

Correspondence should be addressed to Bruno Levy; b.levy@chu-nancy.fr

Received 27 February 2014; Revised 7 May 2014; Accepted 19 May 2014; Published 11 June 2014

Academic Editor: Karim Bendjelid

Introduction. The PiCCO transpulmonary thermodilution technique provides two indices of cardiac systolic function, the cardiac function index (CFI) and the global ejection fraction (GEF). Both appear to be correlated with left ventricular ejection fraction (LVEF) measured by echocardiography in patients with circulatory failure, especially in septic shock. The aim of the present study was to test the reliability of CFI as an indicator of LVEF in patients with cardiogenic shock. *Methods*. In thirty-five patients with cardiogenic shock, we performed (i) simultaneous measurements of echocardiography LVEF and cardiac function index assessed by transpulmonary thermodilution ($n = 72$) and (ii) transpulmonary thermodilution before/after increasing inotropic agents ($n = 18$). *Results*. Mean LVEF was 31% (+/−11.7), CFI 3/min (+/−1), and GEF 14.2% (+/−6). CFI and GEF were both positively correlated with LVEF ($P < 0.0001$, $r^2 = 0.27$). CFI and GEF were significantly increased with inotropic infusion (resp., $P = 0.005$, $P = 0.007$). A cardiac function index <3.47/min predicted a left ventricular ejection fraction ≤35% (sensitivity 81.1% and specificity 63%). In patients with right ventricular dysfunction, CFI was not correlated with LVEF. *Conclusion*. CFI is correlated with LVEF provided that patient does not present severe right ventricular dysfunction. Thus, the PiCCO transpulmonary thermodilution technique is useful for the monitoring of inotropic therapy during cardiogenic shock.

1. Introduction

Hemodynamic monitoring is essential for the diagnosis and therapeutic management of critically ill patients [1]. There are several different methods and techniques for monitoring patients with circulatory failure, although none are ideal (namely non-invasive, safe, reproducible, assessing cardiac preload and myocardial function) [2–5]. Considering the systolic function of the left ventricle, Doppler echocardiography has become the standard tool for measuring left ventricular ejection fraction (LVEF) [6, 7]. Unfortunately, echocardiography for hemodynamic monitoring is limited by the availability of equipment and/or experienced examiners on a 24/24 hour basis. As a result, the PiCCO system (Pulsion Medical System, Munich, Germany) based on the use of a specific thermodilution arterial catheter and a central venous line has emerged as an interesting monitoring approach and could be proposed as an alternative to echocardiography for the estimation of LVEF; indeed, this system allows on the one hand the assessment of cardiac output [5], of cardiac preload [3, 8–13], and on the other hand two indices of cardiac systolic function, the cardiac function index (CFI) and the global ejection fraction (GEF). Both appear to be correlated with left ventricular systolic ejection fraction measured with echocardiography in patients with circulatory failure [14–16]. However, these latter studies essentially pertained to patients with septic shock, and less than 15% of the patients presented severe heart failure (cardiogenic shock).

The aim of the present study was thus to evaluate the reliability of CFI as a marker of left ventricular ejection fraction in patients with cardiogenic shock. We hypothesized that CFI is correlated with LVEF, increases with inotropic

infusion and is not altered with fluid expansion in patients with cardiogenic shock.

2. Material and Methods

2.1. Study Population. This prospective observational study was conducted in a 13-bed ICU in a university hospital.

Patients were included if they met the following criteria: presence of a cardiogenic shock and monitoring by a transpulmonary thermodilution device. Inclusion was possible during the initial evolution of cardiogenic shock (i.e., when inotropic agent was introduced and/or when dobutamine posology was increased).

Cardiogenic shock was defined as a persistent hypotension resulting from heart failure in the presence of adequate intravascular volume [17]. Circulatory shock was diagnosed by observing hypotension, tachycardia, poor tissue perfusion such as oliguria, cool skin, mottled extremities, and cerebral hypoperfusion. Associated hemodynamic criteria included the following:

(i) persistent hypotension (systolic blood pressure ≤90 mm Hg or decrease in systolic arterial pressure >30% in known hypertensive patients),

(ii) cardiac index (CI) less than 2.2 L/min per m^2 without dobutamine infusion and/or patient already receiving inotropic agent because of a low CI. CI was assessed either by echocardiography or by transpulmonary thermodilution [17, 18].

Exclusion criteria included the following: age <18 years; no available echocardiography (absence of sufficient echogenicity); septic shock and/or septic cardiomyopathy; and patient treated with intra-aortic balloon pumping (given that the thermodilution technique requires interrupting the treatment and real time arterial pulse contour analysis is not possible). Nonsinus rhythm (atrial fibrillation), right ventricular failure, and therapeutic hypothermia for cardiac arrest were not considered as exclusion criteria.

The following data were recorded: age, sex, past medical history (such as chronic cardiac insufficiency and nonsinus rhythm), simplified acute physiology score (SAPS II), cause of cardiogenic shock, need for mechanical support, renal replacement therapy, and use of vasopressor and/or inotropic agent during measurement and during the ICU stay.

2.2. Transpulmonary Thermodilution and Calculation of CFI and GEF. A 5-French thermistor-tipped catheter was placed into the femoral artery and a central venous catheter was inserted into a central vein (jugular or subclavian vein); both were connected to the PiCCO system. Cardiac output (CO) and volumetric parameters were measured with the thermodilution technique and obtained after injection of 15 mL of cold isotonic saline 0.9% (<8°C) via the central venous catheter.

The CO was calculated from the thermodilution curves, according to the Stewart-Hamilton algorithm; the mean of three consecutive injections was recorded.

Volumetric parameters were calculated from the mean transit time (MTt) and the exponential downslope time (DSt) of the thermodilution curve: (i) intrathoracic thermal volume (ITTV) was obtained by the product of CO × MTt; (ii) pulmonary thermal volume (PTV) was obtained by the product of CO × DSt; (iii) the global end-diastolic volume (GEDV) represented the difference between ITTV and PTV: GEDV = ITTV − PTV = CO ∗ MTt − CO ∗ DSt.

The PiCCO monitor automatically calculated the two cardiac systolic function indices, namely, CFI and GEF.

(i) CFI is the ratio between CO and GEDV: CFI = CO/GEDV, expressed in min^{-1}.

(ii) GEF is defined as the ratio of the stroke volume (SV) to the quarter of the GEDV: GEF = SV/(GEDV/4), expressed as a percentage.

The transpulmonary thermodilution parameters were recorded in 3 different situations:

(1) each time an echocardiography was performed,

(2) before and 30 minutes after the initiation or increase in inotropic agent,

(3) before and immediately after a volume loading: the reason for administering fluid infusion was systematically recorded (response to a passive leg-raising, presence of respiratory changes in pulse pressure).

2.3. Echocardiography. A transthoracic echocardiography was performed with a Vivid 3 (Philips) by a specially trained cardiologist. LVEF was obtained by the biplane Simpson's method or was visually estimated [19, 20].

The operator systematically looked for evidence of a right ventricular dysfunction; a severe right heart failure was defined in this study by the association of three abnormalities [21, 22]:

(1) visually right ventricular dilatation and/or right ventricular wall motion abnormalities,

(2) tricuspid annular plane systolic excursion (TAPSE) ≤15 mm,

(3) systolic pulmonary artery pressure (PAPs) ≥35 mmHg.

2.4. Statistical Analysis. Statistical analyses were performed using the GraphPad software, version 4.0, and STATA software, version 9.0.

Continuous variables are expressed as mean (+/− standard derivation). Categorical variables are expressed as percentages. The correlations were tested using a Pearson test.

The comparison of variables between before and after therapeutic intervention was performed with a nonparametric test (Wilcoxon matched pairs signed-rank test).

The receiver operating characteristic (ROC) curve was constructed to study the ability of CFI to predict a LVEF ≤35%.

A $P < 0.05$ was considered statistically significant.

Table 1: Patient characteristics ($n = 35$).

$n = 35$		
Sex ratio	1.2	
Men (n; %)	19	(54.3%)
Age (years; SD)	66	±16
Underlying cardiovascular disease:		
(i) Preexisting cardiomyopathy (n; %)	21	(60%)
LVEF (%; SD)	39.7	±14
(ii) Chronic atrial fibrillation (n; %)	11	(31.5%)
SAPSII (n; SD)	54	±21
Causes of cardiogenic shock: (n; %)		
(i) Acute myocardial infarction	15	(42.9%)
(ii) End-stage cardiomyopathy	6	(17.1%)
(iii) Treatment toxicity (chemotherapy)	5	(14.3%)
(iv) Myocarditis	2	(5.7%)
(v) Complex heart rhythm disorder	2	(5.7%)
(vi) Thyrotoxicosis	1	(2.9%)
(vii) Unknown	4	(11.4%)
Need for life support techniques in ICU: (n; %)		
(i) Renal replacement therapy	12	(34.3%)
(ii) Mechanical ventilation	22	(62.8%)
(iii) Norepinephrine use	25	(71%)
(iv) Epinephrine use	1	(2.8%)
(v) Dobutamine use	35	(100%)
Mortality in the ICU (n; %)	19	(54%)

LVEF: left ventricular ejection function; SAPSII: simplified acute physiology score II; ICU: intensive care unit.

3. Results

Thirty-five patients were studied between January 2009 and November 2012. Table 1 summarizes the characteristics of the population. Of the 19 men (54.3%) and 16 women (45.7%), 21 patients (60%) had a preexisting cardiomyopathy, with a mean LVEF of 39.7% (+/−14), and 11 patients (31.5%) had a past history of chronic atrial fibrillation. Mean SAPS II score at admission was 54 (+/−21). The causes of cardiogenic shock were principally acute myocardial infarction ($n = 15$) and end-stage cardiomyopathy ($n = 6$). Overall ICU mortality rate was 54%.

Seventy-two pairs of CFI/LVEF measurements were obtained, for which thermodilution and echocardiography variables are described in Table 2. In 38 pairs, patients were treated with norepinephrine (mean dosage of 0.72 μg/kg/min), and 63 were under dobutamine infusion (mean dosage of 9.4 μg/kg/min). For the 72 pairs of measurements, mean LVEF was 31% (+/−11.7), whereas mean CI, CFI, and GEF were, respectively, 2.6 L/min/m^2 (+/−0.8), 3/min (+/−1), and 14.2 (+/−6). As shown in Figure 1, a significant correlation between CFI and LVEF was observed ($P < 0.0001$, $r = 0.52$ (95% confidence interval: 0.32–0.67), $r^2 = 0.27$) in the 72 pairs of measurements. A significant correlation was also established between GEF and LVEF ($P < 0.0001$, $r = 0.52$ (95% confidence interval: 0.33–0.67), $r^2 = 0.27$).

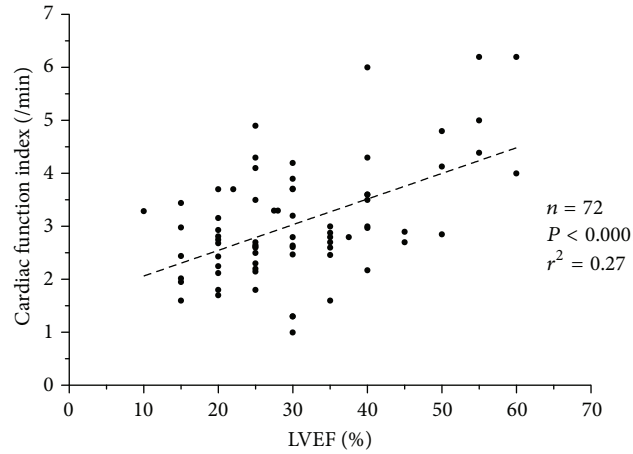

Figure 1: Correlation between cardiac function index (CFI) and left ventricular ejection fraction (LVEF). Dashed line: linear regression line.

Eighteen thermodilution measurements were obtained before and after the onset or increase in dobutamine infusion (Table 3). CI, CFI, and GEF were significantly increased with inotropic infusion, whereas there was no change in heart rate and GEDV (Table 3 and Figures 2 and 3).

Only 4 measurements before and after volume expansion were performed: 3 fluid loadings were decided because the patient was deemed to respond positively to fluid administration (presence of respiratory variation in pulse pressure in one patient; positive hemodynamic response to passive leg-raising in 2 others). CI, CFI, GEF, and GEDV were not altered by volume expansion (Table 4).

In the 72 pairs of measurements, a CFI value <3.47 allowed diagnosing a LVEF ≤35% with a sensitivity of 81.1% (95% confidence interval: 0.68–0.9) and a specificity of 63% (95% confidence interval: 0.38–0.83). The area under the ROC curve was 0.8 (95% confidence interval: 0.69–0.91) (Figure 4).

Among the 72 CFI/LVEF measurements, 14 pertained to 9 patients with a right ventricular dysfunction. Reasons for the cardiogenic shock associated myocarditis and acute myocardial ischemia with right ventricular impairment, chemotherapy toxicity, and end-stage chronic heart failure. In these patients, CI and CFI were not correlated with LVEF (resp., $P = 0.28$; $P = 0.34$) (Table 5).

4. Discussion

The present study shows that CFI, obtained by the transpulmonary thermodilution function, is a reliable indicator of left ventricular ejection fraction in cardiogenic shock. Indeed, CFI was found to be statistically correlated with LVEF and to increase with inotropic infusion while not altered by fluid expansion. Moreover, a CFI <3.47 allowed predicting a LVEF ≤35% with good sensibility (81.1%) and specificity (63%).

Assessing LVEF in critically ill patients admitted to the ICU is a key aspect of their hemodynamic management, since detecting a low LVEF may lead to specific therapy

Table 2: Hemodynamic characteristics of pairs of CFI/LVEF measurements ($n = 72$).

	Mean	SD	
Patient data			
Norepinephrine (μg/kg/min)	0.72	±0.79	$n = 38$
Epinephrine (μg/kg/min)	0.77	—	$n = 1$
Dobutamine (μg/kg/min)	9.4	±4.8	$n = 63$
Systolic arterial pressure (mmHg)	121	±20	$n = 72$
Diastolic arterial pressure (mmHg)	60	±12	$n = 72$
Mean arterial pressure (mmHg)	80	±15	$n = 72$
Heart rate (/min)	100	±19	$n = 72$
Echocardiography data			
Left ventricular ejection fraction (%)	31%	±11.7	$n = 72$
Pulmonary systolic arterial pressure (mmHg)	44	±12.3	$n = 38$
TAPSE (mm)	18.4	±4.7	$n = 63$
Transpulmonary thermodilution data			
Cardiac index (L/min/m^2)	2.6	±0.8	$n = 72$
Cardiac function index (/min)	3	±1	$n = 72$
Global ejection fraction (%)	14.2	±6	$n = 72$
Global end diastolic volume (mL/m^2)	820	±190	$n = 72$

CFI: cardiac function index; LVEF: left ventricular ejection function; TAPSE: tricuspid annular plane systolic excursion.

Table 3: Evolution of hemodynamic parameters before and after increasing dobutamine infusion; $n = 18$.

$n = 18$	Before		After		
	Mean	SD	Mean	SD	
Systolic arterial pressure (mmHg)	115	±19	117	±17.7	—
Diastolic arterial pressure (mmHg)	57	±11	55	±8.4	—
Mean arterial pressure (mmHg)	76	±13	75	±10	—
Heart rate/(min)	101	±25	105	±23	$P = 0.078$
Cardiac index (L/min/m^2)	2.21	±0.55	2.95	±0.92	$P = 0.0008$
Cardiac function index (/min)	2.75	±0.87	3.28	±1.26	$P = 0.0046$
Global ejection function (%)	11.4	±3.9	13.6	±4.5	$P = 0.0074$
Global end-diastolic volume (L/m^2)	788	±185	879	±255	$P = 0.22$
Dobutamine (μg/kg/min)	5.3	±4.7	10.1	±5.7	—
Left ventricular ejection fraction % ($n = 11$)	27	±9	30.2	±9.4	—

Table 4: Measurements before and immediately after fluid infusion; $n = 4$.

$n = 4$	Before		After		
	Mean	SD	Mean	SD	
Systolic arterial pressure (mmHg)	124	±22	125	±24	—
Diastolic arterial pressure (mmHg)	65	±13	60	±18	—
Mean arterial pressure (mmHg)	83	±13	82	±17	—
Heart rate (/min)	95	±6	95	±6.2	—
Cardiac index (L/min/m^2)	2.54	±1.18	2.45	±1.19	$P = 0.62$
Cardiac function index (/min)	4.4	±3	4.25	±2.9	$P = 0.62$
Global ejection function (%)	18.8	±11	19	±11	$P = 0.85$
Global end-diastolic volume (L/m^2)	570	±140	610	±117	$P = 0.62$

such as inotropic infusion. Echocardiography is the gold standard for LVEF estimation: it is a reliable, safe, and noninvasive technique; however, echocardiography requires specific equipment and a competent operator 24/24 h, which is currently not possible in all ICUs. Thus, by providing two cardiac function indices, the PiCCO system could provide an interesting alternative to echocardiography in the assessment of LVEF. Our work confirmed the results of the two previous studies regarding the validity of CFI as an indicator of LVEF in critically ill ICU patients: Combes et al. [14] first

Table 5: Patients with a right ventricular dysfunction; 14 measurements, 9 patients.

$n = 14$	Mean	SD
Echocardiography data		
Left ventricular ejection fraction (%)	29.9%	±9.8
Pulmonary systolic arterial pressure (mmHg)	47	±6.8
TAPSE (mm)	12.9	±1.5
Thermodilution		
Cardiac index (L/min/m^2)	3	±1.1
Cardiac function index (/min)	2.95	±0.8
Global ejection function (%)	12	±3.7

TAPSE: tricuspid annular plane systolic excursion.

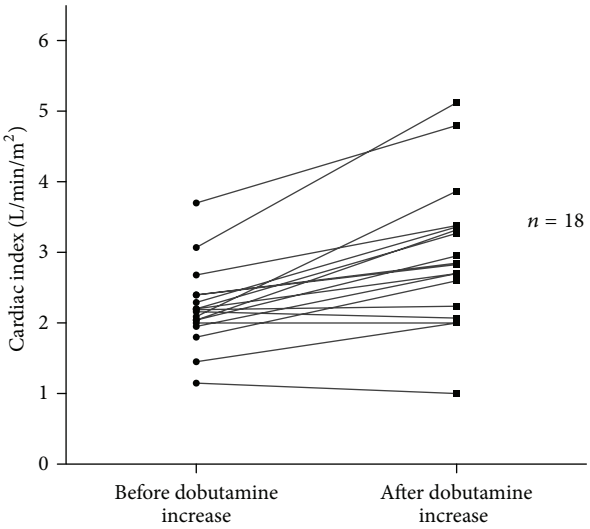

Figure 2: Changes in cardiac index with dobutamine infusion ($n = 18$): $P = 0.0008$.

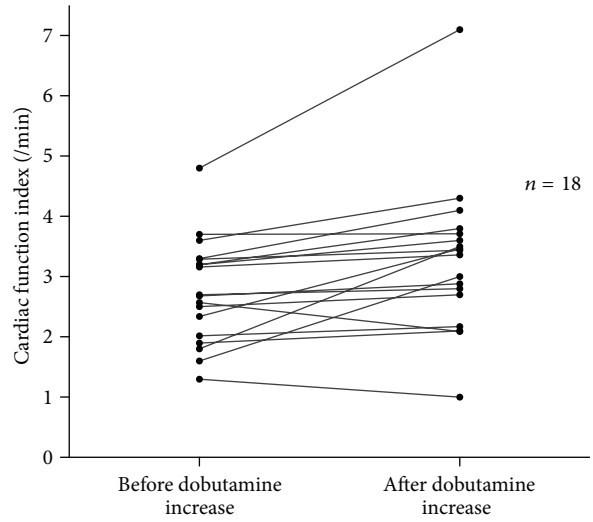

Figure 3: Changes in cardiac function index with dobutamine infusion ($n = 18$): increase in CFI under dobutamine ($P = 0.0046$).

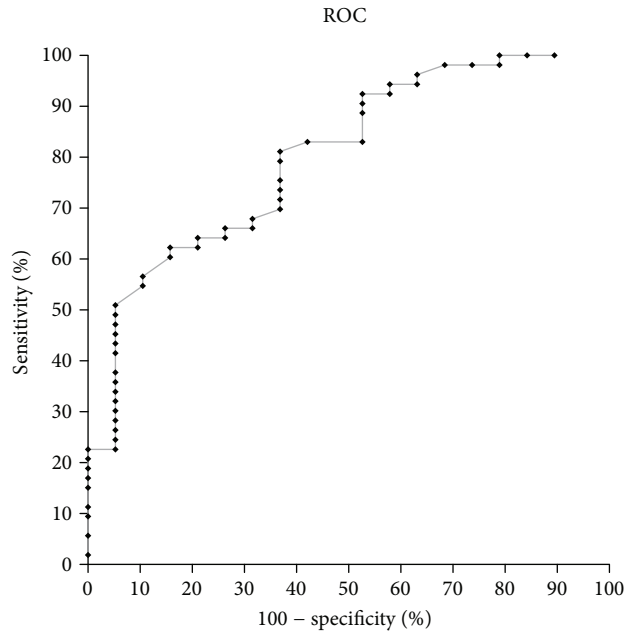

Figure 4: Receiver operating characteristic curve showing the ability of CFI to predict a LVEF ≤ 35%.

demonstrated in 30 patients that CFI was correlated with LVEF assessed by transesophageal echocardiography ($r = 0.87$; $P < 0.0001$). A similar correlation was also described in 2009 by Jabot et al. [15] from 96 CFI/LVEF measurements ($r = 0.67$; $P < 0.0001$) involving 39 patients in which LVEF was obtained by transparietal echocardiography. In these studies, however, few patients presented severe cardiac dysfunction, as only 15% of the population was admitted for cardiogenic shock. Our study is the only study to assess CFI as a marker of LVEF in patients with severe cardiac impairment, as witnessed by a mean LVEF of 31%. Interestingly, the correlation between CFI and LVEF was slightly lower in our study than in the two previous studies ($r = 0.52$ versus 0.87 and 0.67, resp.). Because CFI represents the ratio between CO and GEDV, a severe dilatation of cardiac cavity such as that observed in chronic atrial fibrillations may underestimate CFI (and thus LVEF estimated with CFI). Combes et al. [14] excluded patients with nonsinus rhythm or with a known abdominal aortic aneurysm, whereas we did not exclude patients with a past history of arrhythmia or aneurysm. Moreover, in our population, we noted 31.5% chronic atrial fibrillation, which may explain the lower correlation between CFI and LVEF. Thus, CFI is correlated with LEVF even if the patient has a low LVEF or a past history of nonsinus rhythm. These patients are furthermore likely representative of the general ICU patient population.

In addition, CFI may also track the changes in LVEF under inotropic agent. Indeed, as previously demonstrated by Jabot et al. [15], we show herein that CFI statistically improved with inotropic treatment, whereas it was not altered by fluid infusion. The fact that only 4 fluid expansions were studied could be considered as a limitation of our study; however, it nevertheless confirms that these patients are representative

of a population with cardiogenic shock, for example, with adequate intravascular volume.

A serious weakness of CFI is probably the existence of a right ventricular (RV) impairment. Since CFI represents the ratio between CO and GEDV, it reflects global myocardial contraction, in other words, left and right ventricular function [7, 23]. Hence, an isolated or preponderant RV impairment might underestimate CFI and consequently LVEF. In our series, CFI and LVEF in patients with severe RV impairment were not correlated, whereas Combes et al. excluded three patients with RV failure: for these patients, PiCCO clearly underestimated LVEF (more than 20% difference with the true LVEF) [14]. On the other hand, Jabot et al. [15] did not exclude patients with significant right heart failure: in their subgroup, CFI and LVEF were statistically correlated ($r = 0.46$); while the observed correlation coefficient was lower than the correlation for the whole population ($r = 0.69$), the difference between the two values was not statistically significant. In the present study, when considering the patients without a severe RV dysfunction ($n = 58$), CFI and LVEF are positively correlated ($r = 0.55$); this correlation coefficient is closed to the rate for the whole studied population ($r = 0.52$).

Considering that RV failure may underestimate LVEF or lead to a false negative, the PiCCO system cannot surrogate echocardiography for the assessment of LVEF. In clinical practice, a low CFI should alert the clinician to an impairment in systolic function (left and/or right): an echocardiography must therefore be performed to discriminate between right or left ventricular dysfunction; echocardiography can also provide critical information regarding diagnosis such as segmental wall-motion or valve abnormalities.

In conclusion, this study demonstrates that CFI is significantly correlated to LVEF in cardiogenic shock provided that patient does not present severe isolated right ventricular dysfunction. The PiCCO system is a simple and easily reproducible technique, which provides a consistent estimation of LVEF. However, it does not replace echocardiography: a low CFI should alert the physician to a possible impairment of LV systolic function, and an echocardiography must be performed to exclude right ventricular impairment. Once the LV dysfunction is confirmed, CFI allows a consistent monitoring of LV function under inotropic treatment.

Conflict of Interests

On behalf of all authors, the corresponding author states that there is no conflict of interest.

References

[1] M. Antonelli, M. Levy, P. J. D. Andrews et al., "Hemodynamic monitoring in shock and implications for management. International Consensus Conference, Paris, France, 27-28 April 2006," *Intensive Care Medicine*, vol. 33, no. 4, pp. 575–590, 2007.

[2] G. Cotter, O. M. Cotter, and E. Kaluski, "Hemodynamic monitoring in acute heart failure," *Critical Care Medicine*, vol. 36, supplement 1, pp. S40–S43, 2008.

[3] S. G. Sakka, C. C. Rühl, U. J. Pfeiffer et al., "Assessment of cardiac preload and extravascular lung water by single transpulmonary thermodilution," *Intensive Care Medicine*, vol. 26, no. 2, pp. 180–187, 2000.

[4] S. Ritter, A. Rudiger, and M. Maggiorini, "Transpulmonary thermodilution-derived cardiac function index identifies cardiac dysfunction in acute heart failure and septic patients: an observational study," *Critical Care*, vol. 13, no. 4, article R133, 2009.

[5] S. Sakka, K. Reinhart, and A. Meier-Hellmann, "Comparison of pulmonary artery and arterial thermodilution cardiac output in critically ill patients," *Intensive Care Medicine*, vol. 25, no. 8, pp. 843–846, 1999.

[6] J. M. Brown, "Use of echocardiography for hemodynamic monitoring," *Critical Care Medicine*, vol. 30, no. 6, pp. 1361–1364, 2002.

[7] Y. Beaulieu, "Bedside echocardiography in the assessment of the critically ill," *Critical Care Medicine*, vol. 35, supplement 5, pp. S235–S249, 2007.

[8] F. Michard, S. Alaya, V. Zarka, M. Bahloul, C. Richard, and J. Teboul, "Global end-diastolic volume as an indicator of cardiac preload in patients with septic shock," *Chest*, vol. 124, no. 5, pp. 1900–1908, 2003.

[9] F. Michard and J. Teboul, "Predicting fluid responsiveness in ICU patients: a critical analysis of the evidence," *Chest*, vol. 121, no. 6, pp. 2000–2008, 2002.

[10] D. A. Reuter, T. W. Felbinger, E. Kilger, C. Schmidt, P. Lamm, and A. E. Goetz, "Optimizing fluid therapy in mechanically ventilated patients after cardiac surgery by on-line monitoring of left ventricular stroke volume variations. Comparison with aortic systolic pressure variations," *British Journal of Anaesthesia*, vol. 88, no. 1, pp. 124–126, 2002.

[11] D. A. Reuter, T. W. Felbinger, K. Moerstedt et al., "Intrathoracic blood volume index measured by thermodilution for preload monitoring after cardiac surgery," *Journal of Cardiothoracic and Vascular Anesthesia*, vol. 16, no. 2, pp. 191–195, 2002.

[12] D. A. Reuter, T. W. Felbinger, C. Schmidt et al., "Stroke volume variations for assessment of cardiac responsiveness to volume loading in mechanically ventilated patients after cardiac surgery," *Intensive Care Medicine*, vol. 28, no. 4, pp. 392–398, 2002.

[13] D. A. Reuter, A. Kirchner, T. W. Felbinger et al., "Usefulness of left ventricular stroke volume variation to assess fluid responsiveness in patients with reduced cardiac function," *Critical Care Medicine*, vol. 31, no. 5, pp. 1399–1404, 2003.

[14] A. Combes, J.-B. Berneau, C.-E. Luyt, and J.-L. Trouillet, "Estimation of left ventricular systolic function by single transpulmonary thermodilution," *Intensive Care Medicine*, vol. 30, no. 7, pp. 1377–1383, 2004.

[15] J. Jabot, X. Monnet, L. Bouchra, D. Chemla, C. Richard, and J. Teboul, "Cardiac function index provided by transpulmonary thermodilution behaves as an indicator of left ventricular systolic function," *Critical Care Medicine*, vol. 37, no. 11, pp. 2913–2918, 2009.

[16] S. G. de Hert, D. Robert, S. Cromheecke, F. Michard, J. Nijs, and I. E. Rodrigus, "Evaluation of left ventricular function in anesthetized patients using femoral artery dP/dtmax," *Journal of Cardiothoracic and Vascular Anesthesia*, vol. 20, no. 3, pp. 325–330, 2006.

[17] S. M. Hollenberg, C. J. Kavinsky, and J. E. Parrillo, "Cardiogenic shock," *Annals of Internal Medicine*, vol. 131, no. 1, pp. 47–59, 1999.

[18] S. Topalian, F. Ginsberg, and J. E. Parrillo, "Cardiogenic shock," *Critical Care Medicine*, vol. 36, supplement 1, pp. S66–S74, 2008.

[19] R. M. Lang, M. Bierig, R. B. Devereux et al., "Recommendations for chamber quantification: a report from the American Society of Echocardiography's Guidelines and Standards Committee and the Chamber Quantification Writing Group, developed in conjunction with the European Association of Echocardiography, a branch of the European Society of Cardiology," *Journal of the American Society of Echocardiography*, vol. 18, no. 12, pp. 1440–1463, 2005.

[20] J. H. McGowan and J. G. F. Cleland, "Reliability of reporting left ventricular systolic function by echocardiography: a systematic review of 3 methods," *American Heart Journal*, vol. 146, no. 3, pp. 388–397, 2003.

[21] B. Lamia, J.-L. Teboul, X. Monnet, C. Richard, and D. Chemla, "Relationship between the tricuspid annular plane systolic excursion and right and left ventricular function in critically ill patients," *Intensive Care Medicine*, vol. 33, no. 12, pp. 2143–2149, 2007.

[22] C. Selton-Suty and Y. Juillière, "Non-invasive investigations of the right heart: how and why?" *Archives of Cardiovascular Diseases*, vol. 102, no. 3, pp. 219–232, 2009.

[23] A. Vieillard-Baron, M. Slama, B. Cholley, G. Janvier, and P. Vignon, "Echocardiography in the intensive care unit: from evolution to revolution?" *Intensive Care Medicine*, vol. 34, no. 2, pp. 243–249, 2008.

Hindawi Publishing Corporation
BioMed Research International
Volume 2014, Article ID 514729, 10 pages
http://dx.doi.org/10.1155/2014/514729

Research Article

Numerical Simulation and Clinical Implications of Stenosis in Coronary Blood Flow

Jun-Mei Zhang,[1] Liang Zhong,[1,2] Tong Luo,[3] Yunlong Huo,[4] Swee Yaw Tan,[1,2] Aaron Sung Lung Wong,[1,2] Boyang Su,[1] Min Wan,[1] Xiaodan Zhao,[1] Ghassan S. Kassab,[3] Heow Pueh Lee,[5] Boo Cheong Khoo,[5] Chang-Wei Kang,[6] Te Ba,[6] and Ru San Tan[1,2]

[1] *National Heart Center Singapore, 5 Hospital Drive, Singapore 169609*
[2] *Duke-NUS Graduate Medical School Singapore, 8 College Road, Singapore 169857*
[3] *Department of Biomedical Engineering, Indiana University-Purdue University Indianapolis, Indianapolis, IN 46202, USA*
[4] *Department of Mechanics and Engineering Science, College of Engineering, Peking University, Beijing 100871, China*
[5] *Department of Mechanical Engineering, National University of Singapore, 1 Engineering Drive 2, Singapore 117576*
[6] *Fluid Dynamics Department, Institute of High Performance Computing, 1 Fusionopolis Way, No. 16-16 Connexis North, Singapore 138632*

Correspondence should be addressed to Liang Zhong; zhong.liang@nhcs.com.sg

Received 28 February 2014; Accepted 29 April 2014; Published 2 June 2014

Academic Editor: Bruno Levy

Fractional flow reserve (FFR) is the gold standard to guide coronary interventions. However it can only be obtained via invasive angiography. The objective of this study is to propose a noninvasive method to determine FFR_{CT} by combining computed tomography angiographic (CTA) images and computational fluid dynamics (CFD) technique. Utilizing the method, this study explored the effects of diameter stenosis (DS), stenosis length, and location on FFR_{CT}. The baseline left anterior descending (LAD) model was reconstructed from CTA of a healthy porcine heart. A series of models were created by adding an idealized stenosis (with DS from 45% to 75%, stenosis length from 4 mm to 16 mm, and at 4 locations separately). Through numerical simulations, it was found that FFR_{CT} decreased (from 0.89 to 0.74), when DS increased (from 45% to 75%). Similarly, FFR_{CT} decreased with the increase of stenosis length and the stenosis located at proximal position had lower FFR_{CT} than that at distal position. These findings are consistent with clinical observations. Applying the same method on two patients' CTA images yielded FFR_{CT} close to the FFR values obtained via invasive angiography. The proposed noninvasive computation of FFR_{CT} is promising for clinical diagnosis of CAD.

1. Introduction

As the most common type of cardiovascular disease, coronary artery disease (CAD) is caused by the build-up of plaques on the endothelial walls of coronary arteries, which leads to a reduction in arteries cross-sectional area and blood supply to the myocardium [1]. Pathology studies of CAD have revealed that coronary stenosis is the predominant factor leading to cardiovascular-related events such as myocardial infarction (MI), stroke, and unstable angina. Therefore it is vital to physiologically characterize and quantify functional coronary stenosis.

The rapid development of noninvasive imaging technologies, such as computed tomography angiography (CTA) and magnetic resonance imaging (MRI), has proven valuable to characterize the anatomic severity of CAD with fair cost and less complication. Diameter stenosis (DS) is commonly applied to quantify the anatomic severity of CAD. It expresses the ratio of the lumen diameter at a stenotic region over that of a "normal" segment. However, DS cannot characterize hemodynamic functional significance of coronary stenosis on myocardial blood supply. Among the stenoses discriminated with the threshold of 50% for DS, fewer than half are ischemic [2].

In terms of hemodynamic indexes to quantify the functional significance of coronary stenosis, fractional flow reserve (FFR) is the gold standard to guide coronary interventions [3–6] because of its significantly fewer follow-up coronary events over DS. FFR is calculated as a ratio of the pressure distal versus pressure proximal to a stenosis following vasodilation. Revascularization is commonly recommended when the coronary stenosis leads to FFR ≤ 0.80. However, FFR can only be measured via invasive coronary catheterization, which may result in higher medical cost and complications [4]. This is not ideal, because only one-third of the intermediate stenosis (DS = 40–70%) is classified as functional significant with FFR ≤ 0.80 [5].

In view of the abundant hemodynamic information provided by computational fluid dynamics (CFD) simulations, considerable insights have been gained on understanding the physiology of CAD through CFD studies [7]. Tremendous progress has been made in applying the CFD method to simulate the blood flow in patient-specific coronary artery models for elucidating the role of hemodynamics in CAD development and progression [8–10].

As proper boundary conditions are necessary for CFD simulations of CAD, both prescribed profiles [11, 12] and sophisticated reduced-ordered models [13–15] have been attempted. For the latter, the downstream vasculature is represented by flow-dependent formulation. For example, the static pressure at the outlet may be calculated from the corresponding flow rate and resistance. Since resistance, compliance, or impedance values of the downstream vasculature are assumed to be decided by their own anatomy rather than by the upstream stenosis, these parameters obtained from the normal vessel (without stenosis) can be applied to the diseased vessel [15].

With the development of CFD techniques, numerous CFD studies have been coupled with clinical imaging techniques to provide detailed hemodynamic information and link CAD with vortices [16], wall shear stress (WSS) [12, 17], oscillatory shear index (OSI) [18], and so forth. However, the application of CFD method to predict clinical diagnosis indexes is still limited. A landmark study was carried out by HeartFlow Company [19–22] to derive noninvasive FFR_{CT} from CT images by applying sophisticated reduced-ordered models as the boundary conditions for transient numerical simulations. Because the calculation of FFR is based on the time-averaged pressure over several cardiac cycles in clinics [23], this study explored a method to combine CT images and steady flow simulation for calculating noninvasive FFR_{CT} with lower computational cost. The method is firstly applied on a left anterior descending (LAD) model reconstructed from CTA of a healthy porcine heart and then tested on two patient-specific left coronary artery trees reconstructed from patients' CTA images to examine whether the approach can be applied for noninvasively assessing the hemodynamic significance of coronary stenosis in clinics.

As the anatomical severity of CAD is believed to be related not only to DS but also to the location and length of the stenosis, which can affect the hemodynamics [24], a series of models were created by adding an idealized stenosis (with DS from 45% to 75%, stenosis length from 4 mm to 16 mm, and at 4 locations separately) on the baseline porcine LAD model. In this manner, the effects of DS, stenosis length, and location (proximal to distal) on FFR_{CT} are investigated. The results may be useful to aid the clinician in making the decision of revascularization.

This paper is organized as follows: the detailed computational methodologies were described in Section 2. In Section 3, the detailed hemodynamic information (flow patterns, flow rate, pressure, and FFR_{CT} distributions) for a series of stenosed porcine LAD models was provided to explore the effect of DS, stenosis length, and location on FFR_{CT}. The results of two case studies were also presented to demonstrate the applicability of the current methodologies on clinical diagnosis of human CAD. Finally, the conclusions were drawn in Section 4.

2. Computational Methodologies

In this study, a left anterior descending (LAD) model was used as the baseline model, which was reconstructed from CTA of a healthy porcine heart. The detailed description on animal preparation, CTA, and image processing can be found in [25]. As shown in Figure 1(a), the baseline model embodied the LAD main trunk (≥2 mm in diameter) and 7 primary branches ("a"–"g" in Figure 1) (≥1 mm in diameter). To investigate the effect of DS, the trunk between side branches "a" and "b" was narrowed to represent stenosed model with DS of 45%, 55%, 65%, and 75% separately as shown in Figure 2. All of these stenoses were located at the same location (Location A) with the same stenosis length of 4 mm. To investigate the effect of stenosis location, a 4 mm length stenosis with DS of 55% was created at 4 locations (Location "A" to "D") from proximal to distal LAD trunk, as shown in Figure 3. Another series of models were constructed with a 55% stenosis located downstream the branch "a" and having the stenosis lengths of 4 mm, 8 mm, 12 mm, and 16 mm separately, as shown in Figure 4.

After generating these LAD models with SpaceClaim, their computational domains were discretized with commercial software ANSYS workbench. Meshes near the branch junctions, at the stenosis and near the walls, were refined for adequate resolution of flow in the boundary layers (as shown in Figure 1(b)). After mesh dependency test conducted on the baseline model, a total of about 0.5 million volume cells were found to be adequate, as further grid refinement led to less than 1% relative error in the maximum velocity. The same setting for mesh generation was applied for all other LAD models.

In order to simulate the blood flow in normal and diseased LAD models, the continuity (1) and Navier-Stokes (2) equations were solved by FLUENT using finite volume approximation:

$$\frac{\partial u_j}{\partial x_j} = 0 \tag{1}$$

$$\frac{\partial \left(\rho u_j u_i\right)}{\partial x_j} = -\frac{\partial P}{\partial x_i} + \frac{\partial}{\partial x_j}\left(\mu\left(\frac{\partial u_i}{\partial x_j} + \frac{\partial u_j}{\partial x_i}\right)\right), \tag{2}$$

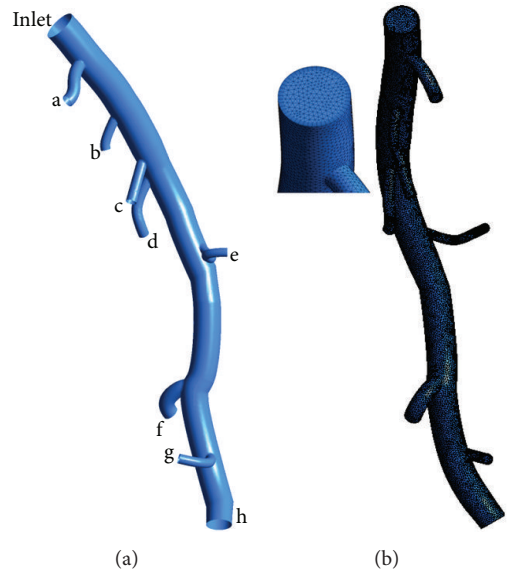

Figure 1: (a) Baseline LAD model reconstructed from CT and (b) the generated meshes for the baseline model with enlarged view.

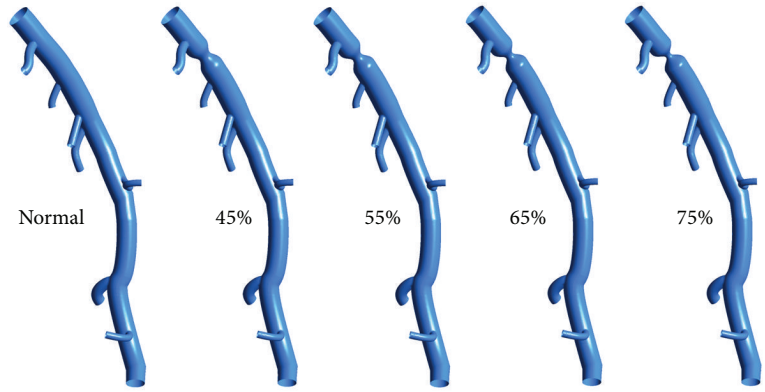

Figure 2: Baseline and stenosed LAD models with the 4 mm length stenoses located at the same location (Location A) with DS of 45%, 55%, 65%, and 75% separately.

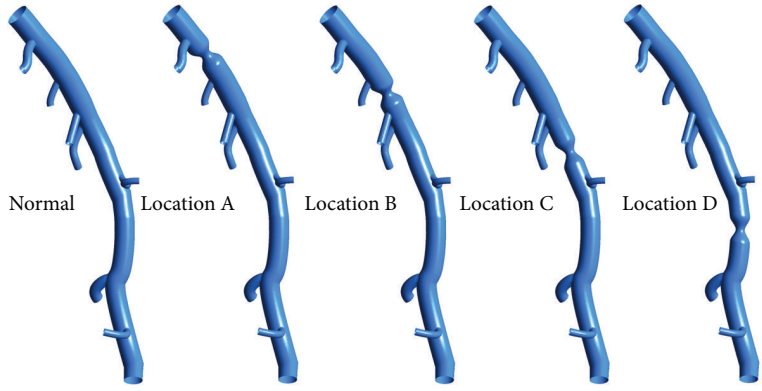

Figure 3: Baseline and stenosed LAD models with the 4 mm length stenoses located at A, B, C, and D separately (having the DS of 55%).

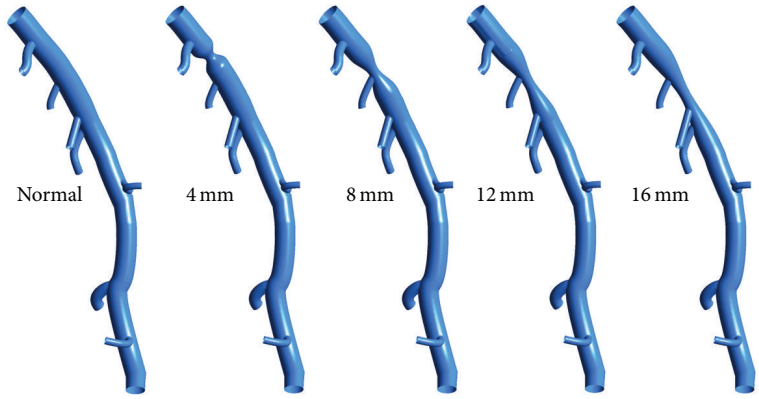

Figure 4: Baseline and stenosed LAD models with 55% DS located downstream the branch "a" with the stenosis lengths of 4 mm, 8 mm, 12 mm, and 16 mm separately.

Here x_j and u_j (or u_i) were the location in Cartesian coordinate and the Cartesian component of velocity, respectively. P represented the static pressure. ρ and μ were density and dynamic viscosity of the fluid, which were set as 1060 kg/m^3 and 4.5×10^{-3} Pa·s, respectively, to mimic the blood properties in large epicardial arteries [25, 26].

Proper boundary conditions are required for CFD simulations to closely mimic the real physiological condition [13]. In general, the total pressure was specified at the inlet of each model, and resistance boundary condition was assigned to every coronary outlet to enforce a relationship between pressure and flow.

According to the pulsatile pressure and flow velocity waveforms measured in vivo at the inlet of the porcine LAD [25], the time-averaged inflow rate and pressure were 66.75 mL/min and 69.54 mmHg, respectively.

In order to derive the resistance values of downstream vasculatures, the steady-state simulations under two sets of boundary conditions were carried out on the baseline model prior to the simulation on stenosed LAD models. One of the simulations represents the peak phase of systole, when the inlet pressure is at the maximum [25]. The other simulation represents the peak diastole phase with minimum pressure at the inlet. For both simulations, the flow rate distributions between the primary branches were believed to obey the generalized Murray's law [27], as it was the baseline LAD, which represents normal (healthy) coronary arteries without stenosis. Based on these two steady-state flow simulations, the pressure and flow rate information at the outlets of primary branches could be obtained. Accordingly the resistance of the vasculature downstream each primary branch was obtained via

$$R_i = \frac{P_i - P_{0,i}}{Q_i}, \tag{3}$$

where P_i and Q_i represent the pressure and flow rate at the ith outlet, respectively. Here, R_i is the resistance of the downstream vasculature and $P_{0,i}$ is the back pressure at ith outlet.

In clinics, FFR measurement is done following vasodilation, which leads to the decrease of coronary resistance. To resemble this physiological situation, the resistance of downstream vasculature of each primary branch was assumed to be reduced to 0.21 times of its resting value, which was within the physiological range measured by Wilson et al. [24]. Accordingly the total pressure at the inlet was assumed to be 69.87 mmHg for all the porcine LAD models with the consideration of flow rate increment following vasodilation. Because the epicardial stenosis severity was found to be not affecting the minimal microvascular resistance [28], the resistance of downstream vascular for a stenosed LAD model was assumed to be the same as that of the baseline model [22].

User defined function (UDF) was compiled to supply the resistance boundary conditions at the outlets. In this manner, the downstream vasculature of the primary branches was coupled to the LAD model, and the static pressure at each outlet was solved iteratively. To ensure smooth convergence, the pressure gradient calculated at the outlet was attenuated several times to couple iterative underrelaxation-based resistance boundary conditions with those outlets; namely, an implicit algorithm was applied to the outlet with an underrelaxation factor of ω given as

$$P_i^{n+1} = P_i^n + \omega \left(R_i Q_i^{n+1} + P_{o,i} - P_i^n \right). \tag{4}$$

In addition, no-slip boundary condition was applied at the wall, as all these LAD models were assumed to be stationary and rigid. All the computations were executed in a Dell T7500 workstation and it took around half hour computational time for one case.

3. Results and Discussion

To elucidate the role of stenosis on hemodynamics of coronary artery, Figure 5 shows the streamline distributions in the normal and stenosed LAD models with DS increasing from 45% to 75% at interval of 10%. When the LAD was free of stenosis, part of the inflow diverted in the primary branches along its way downstream. Most of the blood flowed through

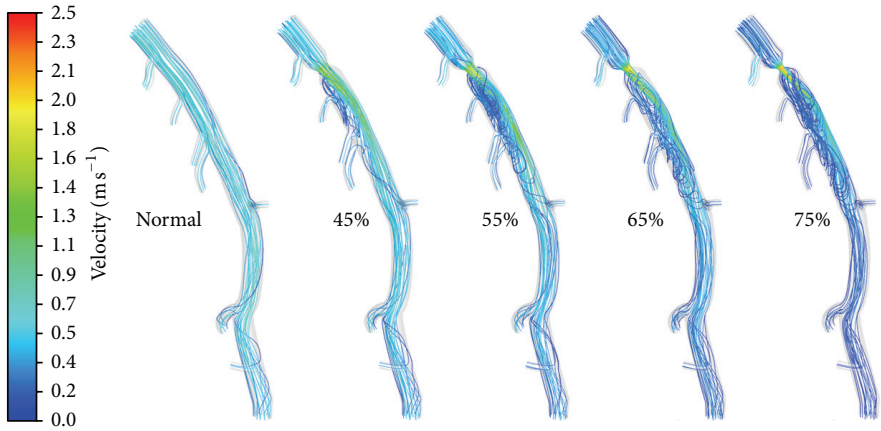

FIGURE 5: Streamline distributions on the baseline and stenosed LAD models with the 4 mm length stenoses located at the same location (Location A) with DS of 45%, 55%, 65%, and 75% separately.

the LAD main trunk smoothly, with streamlines parallel to the walls. In other words, there was no obvious presence of vortex in the normal LAD model.

Once there was a stenosis in the LAD trunk, the streamlines diverted into the center of the LAD main trunk due to the shrinking of the cross-sectional area from the beginning to the throat of the stenosis region. Downstream the throat of the stenosis, the cross-sectional area of the LAD main trunk increased gradually. Due to the inertia momentum, the fluid moved downstream with slight divergence of the streamlines. Hence flow recirculation region was formed near the wall downstream the stenosis, which was filled by vortices and reverse flow derived from the downstream streamlines as shown in Figure 5. With the increase of DS, the throat diameter became smaller leading to more significant divergence of the streamlines and larger flow recirculation in size downstream the stenosis. These vortices and flow recirculation were suspected to promote thrombus formation and potentially myocardial infarction [16].

An interesting phenomenon was found for the flow rate distribution among the primary branches. With the increase of DS, less blood flowed downstream to perfuse the myocardium downstream the first primary branch (labeled as "a" in Figure 1). This is because, for this series of models, the stenosis was located at the main trunk downstream the first primary branch. The vortices and flow recirculation developed downstream the stenosis result in energy diffusion and dissipation, which makes it difficult to perfuse the blood downstream. Hence less blood was distributed to the regions downstream the stenosis. However, there was a slight increase of blood flow to the first primary branch, with the increase of DS as shown in Figure 6. Similar phenomenon is named as "branch steal" by Gould et al. [29] to describe the situation when a nonstenotic branch between proximal and distal stenoses shunts flow away from the stenotic parallel daughter branch to an extent depending on their relative size and severities of the 2 stenoses, which leads to less flow in the stenotic daughter branch. It was also found that the sum of

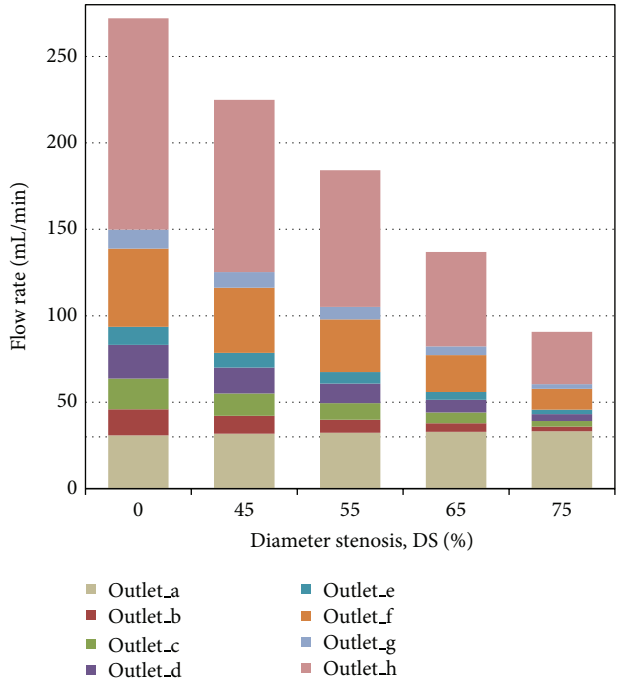

FIGURE 6: Flow rate distributions for the baseline and stenosed LAD models with the 4 mm length stenoses located at the same location (Location A) with DS of 45%, 55%, 65%, and 75% separately.

the total blood flow through the outlets reduced with the increase of DS, which implied that stenosis led to a reduction in blood supply to the myocardium. This was the most important physiological complication of coronary stenosis.

To quantify the hemodynamic significance of stenosis, Figure 7 shows the pressure distribution for different models. For normal LAD, the pressure drop along the main trunk was mainly due to the viscous force, which was less than 3.3 mmHg. Due to the diffusion and dissipation of

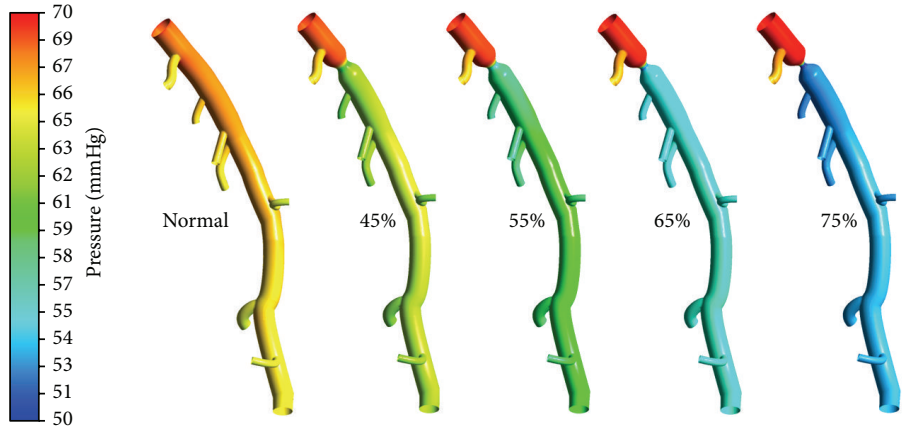

Figure 7: Pressure distributions on the baseline and stenosed LAD models with the 4 mm length stenoses located at the same location (Location A) with DS of 45%, 55%, 65%, and 75% separately.

the recirculation vortices formed downstream the stenosis, the pressure therein decreased much more. With the increase of DS, pressure downstream the stenosis became much lower as shown in Figure 7.

To resemble FFR values measured via invasive angiography, FFR_{CT} is calculated as P_d/P_a. Here P_d and P_a represent the pressure distal and proximal to the stenosis, respectively. As shown in Figure 8(a), FFR_{CT} decreased from 0.89 to 0.74, when DS increased from 45% to 75%. As revascularization is commonly recommended when coronary stenosis leads to FFR $\leq$ 0.8 in clinical applications [5], the LAD with DS $\geq$ 60% was suggested to receive revascularization procedures according to Figure 8(a). This is in line with the clinical findings that the diagnostic performance of CTA can be improved by rating coronary stenosis as significant with the threshold of 60% rather than 50% [30].

To assess the effect of stenosis location and length on the hemodynamic severity of CAD, Figures 8(b) and 8(c) show the relationship between stenosis location and length with FFR_{CT}, respectively. Comparing with the stenosis located more distally, those stenoses located at proximal portion led to lower P_d/P_a, namely, FFR_{CT}. Therefore the stenosis located at proximal portion resulted in more significant reduction in blood supply to the myocardium, which was suspected to promote the further accumulation of plaques. This result is consistent with the clinical findings that the adverse events of coronary artery disease occurred most frequently in a proximal position [31].

In addition, the FFR_{CT} values decreased with the increase of stenosis length, which implies higher fractional losses over the stenosis. However the effect of lesion length on hemodynamics is not significant as shown in Figure 8(c). Similar finding was reported by Wilson et al. [24]. However it is worth noting that fractional losses at longer stenosis may depend on the ruggedness of the surface and local geometry of the stenosis in real life. Hence simulation on the realistic coronary artery tree is critically important.

Therefore, we have also attempted to apply the same CFD methodologies on the patients' CTA images. The detailed information on image reconstruction and numerical simulation was presented in [32, 33]. Figures 9(a) and 9(b) show the predicted FFR_{CT} on the patient-specific left coronary artery trees reconstructed from two patients' CTA images, respectively. The first patient has a moderate stenosis at proximal LAD, which is not ischemia-causing, as its FFR was 0.97 measured via invasive angiography. Its FFR_{CT} predicted by CFD was 0.98. The other patient has an ischemia-causing moderate stenosis at mid LAD, whose FFR was less than 0.8, that is, at 0.73, and its FFF_{CT} was found to be 0.74. These two examples demonstrated that the noninvasive methodologies presented in this study were applicable to assess the hemodynamic significance of stenosis in clinics.

4. Conclusions

In recent years, tremendous progress has been made on invasive and noninvasive medical imaging techniques to diagnose the anatomical and hemodynamic significance of coronary stenosis. Although FFR is the gold standard to diagnose the hemodynamic significance of the CAD, it can only be obtained via invasive coronary angiography. Combining CTA with CFD methods, the flow pattern and pressure distributions can be predicted for a baseline LAD model reconstructed from the CTA of a healthy porcine heart.

By adding stenosis on this baseline model, the effects of DS, stenosis location, and length on the hemodynamics of stenosed coronary artery were explored. It was found that the flow recirculation vortices were formed downstream the throat of stenosis due to the divergence of the streamline, which led to the decrease of flow rate and pressure downstream the stenosis due to energy diffusion and dissipation. The phenomenon of "branch steal" was observed, which was previously reported by Gould et al. [29] when a nonstenotic

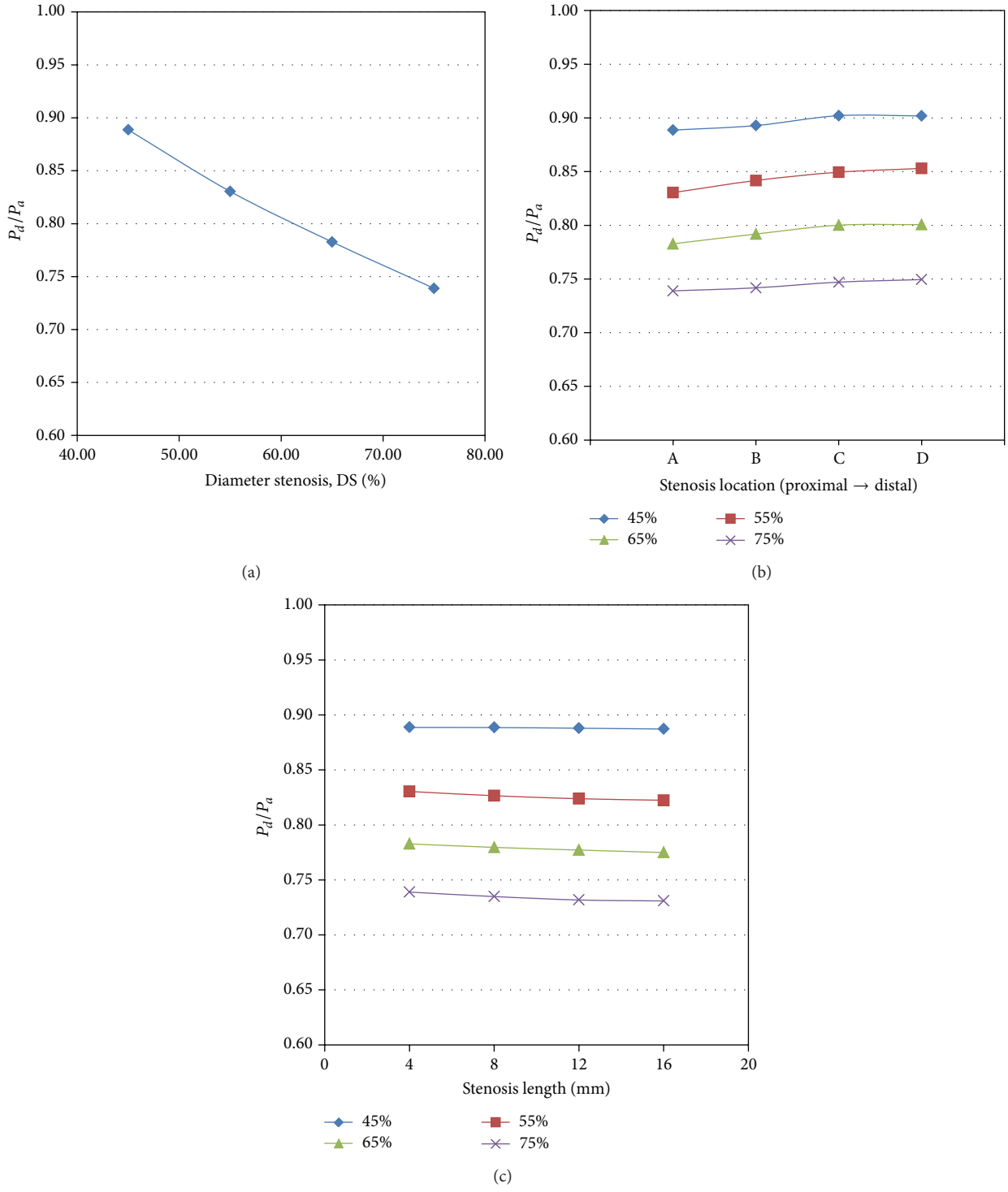

Figure 8: Effect of (a) diameter stenosis, (b) stenosis location, and (c) length on FFR_{CT}.

branch between proximal and distal stenoses shunts flow away from the stenotic parallel daughter branch [28].

With the increase of DS, the flow recirculation region increased in size, which led to lower pressure and FFR_{CT} downstream stenosis. Using a threshold of 0.8, the LAD with DS ≥ 60% was suggested to receive revascularization procedure rather than DS ≥ 50%, which is in line with the clinical finding [30].

In addition, the stenosis location and length were found to affect the hemodynamics in coronary artery trees.

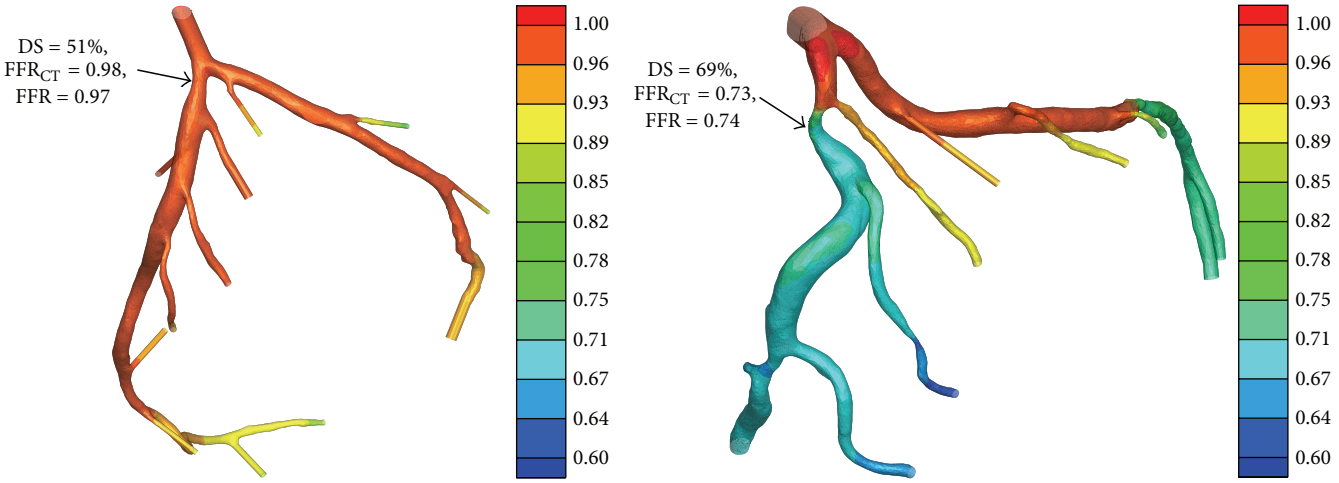

Figure 9: Distributions of FFR_{CT} based on numerical simulations on patient-specific left coronary trees reconstructed from two patients' CTA images. (a) The patient has a moderate stenosis (DS = 51%) at proximal LAD, whose FFR is 0.97 via invasive angiography and its FFR_{CT} is 0.98 predicted by CFD. (b) The patient has a moderate stenosis (DS = 69%) at mid LAD, whose FFR is 0.73 via invasive angiography and its FFR_{CT} is 0.74 predicted by CFD.

Lower FFR_{CT} was associated with the stenosis located in the proximal position and/or with longer stenosis length. This was in line with the clinical observations [24, 31].

Further application of the methodologies on two patient-specific left coronary artery trees reconstructed from CTA images demonstrated that the methodology utilized in this study was promising in facilitating the patient-specific non-invasive diagnosis of hemodynamic significance of coronary stenosis with affordable computational cost. Currently, the computation time was half hour for one case study with a Dell T7500 workstation, which is much longer than an invasive clinical setting, but it is acceptable for noninvasive diagnostics. If a more powerful workstation with larger number of compute nodes is applied, the computation time can be much less than 30 minutes.

Although efforts have been made to mimic the physiological condition as close as possible, there are several possible sources of limitation inherent in the assumptions made in the present study. First, the determination of downstream vascular resistance is argumentative. Intracoronary resistance has been reported to be fluctuating in a phasic pattern, even after administration of vasodilation medicine [23, 34, 35], due to the interaction between the myocardium and microvasculature during systole and diastole. However a mean resistance value was estimated (by iterative approximation at two time points) in this study. To justify the effect of resistance value on FFR_{CT}, a series of simulations were carried out on one model. It was found that the 24–71% variations of resistance values only led to less than 2.4% differences of FFR_{CT}. Therefore the error in the estimated downstream vascular resistance may only result in limited effect on the results of FFR_{CT}. In addition, the method in this study does not consider the circumference with microvascular disease, which is an interesting topic to be explored in the future.

Secondly, the compliance effect of the vessel walls was ignored in this study, as compliance was reported to be less important in affecting the hemodynamics of the coronary arteries [36]. Thirdly, the blood flow was assumed to be laminar with Newtonian fluid. Since the vessels investigated in this study had a diameter greater than 1 mm and the blood flow in the elderly was generally correlated with the low hematocrit, the assumption of Newtonian fluid can be justified. In addition, as the peak Reynolds number in coronary arteries was lower than the critical value proposed by Peacock et al. [37], the flow can be assumed to be laminar in this study.

Last but not least, the impact of errors in image processing on the simulation results is worth exploring in the future. Current clinical imaging processing techniques have difficulty in reconstructing accurate 3D models for small vessels (e.g., with a diameter less than 0.5 mm) owing to the limitation of the imaging resolution. With the development of medical imaging techniques, the breakthrough in this area should be achievable in the near future.

Abbreviations

CAD: Coronary artery disease
CFD: Computational fluid dynamics
CT: Computed tomography
DS: Diameter stenosis
FFR: Fractional flow reserve
LAD: Left anterior descending
MI: Myocardial infarction
OSI: Oscillatory shear index
WSS: Wall shear stress.

Conflict of Interests

The authors declare that there is no conflict of interests regarding the publication of this paper.

Acknowledgments

This research is supported by the SingHealth Foundation, Singapore, under its Translational Research Grant, and administered by the SingHealth (SHF/FG503P/2012) and by National Heart Center Singapore under its NHCS Centre Grant Seed Funding (NHCS-CGSF/2014/003), and by Biomedical Research Council Research Grant (14/1/32/24/002). The financial supports of NMRC/EDG/1037/2011 by the National Research Foundation, Singapore, under its Cooperative Basic Research Grant, and Duke-NUS-GCR/2013/0009, and by the Goh Cardiovascular Research Grant are gratefully acknowledged. The authors acknowledge the support of all staff at the National Heart Centre, Singapore, especially Fong Ching Teck, Max Wu Bing Huang, and Ho Pei Yi and the staff in catheter laboratory and CT departments.

References

[1] T. Heitzer, T. Schlinzig, K. Krohn, T. Meinertz, and T. Münzel, "Endothelial dysfunction, oxidative stress, and risk of cardiovascular events in patients with coronary artery disease," *Circulation*, vol. 104, no. 22, pp. 2673–2678, 2001.

[2] W. B. Meijboom, C. A. G. Van Mieghem, N. van Pelt et al., "Comprehensive assessment of coronary artery stenoses: computed tomography coronary angiography versus conventional coronary angiography and correlation with fractional flow reserve in patients with stable angina," *Journal of the American College of Cardiology*, vol. 52, no. 8, pp. 636–643, 2008.

[3] N. H. J. Pijls, J. A. M. Van Son, R. L. Kirkeeide, B. De Bruyne, and K. L. Gould, "Experimental basis of determining maximum coronary, myocardial, and collateral blood flow by pressure measurements for assessing functional stenosis severity before and after percutaneous transluminal coronary angioplasty," *Circulation*, vol. 87, no. 4, pp. 1354–1367, 1993.

[4] N. P. Johnson, R. L. Kirkeeide, and K. L. Gould, "Is discordance of coronary flow reserve and fractional flow reserve due to methodology or clinically relevant coronary pathophysiology?" *Cardiovascular Imaging*, vol. 5, no. 2, pp. 193–202, 2012.

[5] P. A. L. Tonino, B. De Bruyne, N. H. J. Pijls et al., "Fractional flow reserve versus angiography for guiding percutaneous coronary intervention," *The New England Journal of Medicine*, vol. 360, no. 3, pp. 213–224, 2009.

[6] N. H. J. Pijls and J.-W. E. M. Sels, "Functional measurement of coronary stenosis," *Journal of the American College of Cardiology*, vol. 59, no. 12, pp. 1045–1057, 2012.

[7] J. M. Zhang, L. Zhong, B. Su et al., "Perspective on CFD studies of coronary artery disease lesions and hemodynamics—a review," *International Journal for Numerical Methods in Biomedical Engineering*, 2014.

[8] U. Olgac, D. Poulikakos, S. C. Saur, H. Alkadhi, and V. Kurtcuoglu, "Patient-specific three-dimensional simulation of LDL accumulation in a human left coronary artery in its healthy and atherosclerotic states," *American Journal of Physiology—Heart and Circulatory Physiology*, vol. 296, no. 6, pp. H1969–H1982, 2009.

[9] E. Wellnhofer, J. Osman, U. Kertzscher, K. Affeld, E. Fleck, and L. Goubergrits, "Flow simulation studies in coronary arteries-Impact of side-branches," *Atherosclerosis*, vol. 213, no. 2, pp. 475–481, 2010.

[10] T. Chaichana, Z. Sun, and J. Jewkes, "Computation of hemodynamics in the left coronary artery with variable angulations," *Journal of Biomechanics*, vol. 44, no. 10, pp. 1869–1878, 2011.

[11] R. Torii, N. B. Wood, N. Hadjiloizou et al., "Stress phase angle depicts differences in coronary artery hemodynamics due to changes in flow and geometry after percutaneous coronary intervention," *American Journal of Physiology—Heart and Circulatory Physiology*, vol. 296, no. 3, pp. H765–H776, 2009.

[12] H. Samady, P. Eshtehardi, M. C. McDaniel et al., "Coronary artery wall shear stress is associated with progression and transformation of atherosclerotic plaque and arterial remodeling in patients with coronary artery disease," *Circulation*, vol. 124, no. 7, pp. 779–788, 2011.

[13] I. E. Vignon-Clementel, C. A. Figueroa, K. E. Jansen, and C. A. Taylor, "Outflow boundary conditions for three-dimensional finite element modeling of blood flow and pressure in arteries," *Computer Methods in Applied Mechanics and Engineering*, vol. 195, no. 29-32, pp. 3776–3796, 2006.

[14] H. J. Kim, I. E. Vignon-Clementel, C. A. Figueroa et al., "On coupling a lumped parameter heart model and a three-dimensional finite element aorta model," *Annals of Biomedical Engineering*, vol. 37, no. 11, pp. 2153–2169, 2009.

[15] H. J. Kim, I. E. Vignon-Clementel, J. S. Coogan, C. A. Figueroa, K. E. Jansen, and C. A. Taylor, "Patient-specific modeling of blood flow and pressure in human coronary arteries," *Annals of Biomedical Engineering*, vol. 38, no. 10, pp. 3195–3209, 2010.

[16] D. G. Katritsis, A. Theodorakakos, I. Pantos et al., "Vortex formation and recirculation zones in left anterior descending artery stenoses: computational fluid dynamics analysis," *Physics in Medicine and Biology*, vol. 55, no. 5, pp. 1395–1411, 2010.

[17] P. H. Stone, S. Saito, S. Takahashi et al., "Prediction of progression of coronary artery disease and clinical outcomes using vascular profiling of endothelial shear stress and arterial plaque characteristics: the PREDICTION study," *Circulation*, vol. 126, no. 2, pp. 172–181, 2012.

[18] J. Knight, U. Olgac, S. C. Saur et al., "Choosing the optimal wall shear parameter for the prediction of plaque location—a patient-specific computational study in human right coronary arteries," *Atherosclerosis*, vol. 211, no. 2, pp. 445–450, 2010.

[19] B.-K. Koo, A. Erglis, J.-H. Doh et al., "Diagnosis of ischemia-causing coronary stenoses by noninvasive fractional flow reserve computed from coronary computed tomographic angiograms: results from the prospective multicenter DISCOVER-FLOW (Diagnosis of Ischemia-Causing Stenoses Obtained Via Noninvasive Fractional Flow Reserve) study," *Journal of the American College of Cardiology*, vol. 58, no. 19, pp. 1989–1997, 2011.

[20] J. K. Min, B.-K. Koo, A. Erglis et al., "Usefulness of noninvasive fractional flow reserve computed from coronary computed tomographic angiograms for intermediate stenoses confirmed by quantitative coronary angiography," *American Journal of Cardiology*, vol. 110, no. 7, pp. 971–976, 2012.

[21] J. K. Min, J. Leipsic, M. J. Pencina et al., "Diagnostic accuracy of fractional flow reserve from anatomic CT angiography," *Journal of the American Medical Association*, vol. 308, no. 12, pp. 1237–1245, 2012.

[22] C. A. Taylor, T. A. Fonte, and J. K. Min, "Computational fluid dynamics applied to cardiac computed tomography for

noninvasive quantification of fractional flow reserve," *Journal of American College of Cardiology*, vol. 61, no. 22, pp. 2233–2241, 2013.

[23] S. Sen, J. Escaned, I. S. Malik et al., "Development and validation of a new adenosine-independent index of stenosis severity from coronary waveintensity analysis: results of the ADVISE (ADenosine Vasodilator Independent Stenosis Evaluation) study," *Journal of the American College of Cardiology*, vol. 59, no. 15, pp. 1392–1402, 2012.

[24] R. F. Wilson, M. L. Marcus, and C. W. White, "Prediction of the physiologic significance of coronary arterial lesions by quantitative lesion geometry in patients with limited coronary artery disease," *Circulation*, vol. 75, no. 4, pp. 723–732, 1987.

[25] Y. Huo, T. Wischgol, and G. S. Kassab, "Flow patterns in three-dimensional porcine epicardial coronary arterial tree," *American Journal of Physiology—Heart and Circulatory Physiology*, vol. 293, no. 5, pp. H2959–H2970, 2007.

[26] J.-M. Zhang, L. P. Chua, D. N. Ghista, S. C. M. Yu, and Y. S. Tan, "Numerical investigation and identification of susceptible sites of atherosclerotic lesion formation in a complete coronary artery bypass model," *Medical and Biological Engineering and Computing*, vol. 46, no. 7, pp. 689–699, 2008.

[27] Y. Zhou, G. S. Kassab, and S. Molloi, "On the design of the coronary arterial tree: a generalization of Murray's law," *Physics in Medicine and Biology*, vol. 44, no. 12, pp. 2929–2945, 1999.

[28] W. Aarnoudse, W. F. Fearon, G. Manoharan et al., "Epicardial stenosis severity does not affect minimal microcirculatory resistance," *Circulation*, vol. 110, no. 15, pp. 2137–2142, 2004.

[29] K. L. Gould, R. Kirkeeide, and N. P. Johnson, "Coronary branch steal experimental validation and clinical implications of interacting stenosis in branching coronary arteries," *Circulation: Cardiovascular Imaging*, vol. 3, no. 6, pp. 701–709, 2010.

[30] O. F. Donati, P. Stolzmann, L. Desbiolles et al., "Coronary artery disease: which degree of coronary artery stenosis is indicative of ischemia?" *European Journal of Radiology*, vol. 80, no. 1, pp. 120–126, 2011.

[31] S. Jost, J. W. Deckers, P. Nikutta et al., "Progression of coronary artery disease is dependent on anatomic location and diameter," *Journal of the American College of Cardiology*, vol. 21, no. 6, pp. 1339–1346, 1993.

[32] J. M. Zhang, T. Luo, Y. Huo et al., "Area stenosis associated with non-invasive fractional flow reserve obtained from Coronary CT Images," in *Proceedings of the 35th Annual International Conference of the IEEE Engineering in Medicine and Biology Society (EMBC '13)*, pp. 3865–3868, 2013.

[33] L. Zhong, B. Su, J. M. Zhang et al., "Effects of stenosis on the porcine left anterior descending arterial tree," in *Proceedings of the 35th Annual International Conference of the IEEE Engineering in Medicine and Biology Society (EMBC '13)*, pp. 3869–3872, 2013.

[34] J. E. Davies, Z. I. Whinnett, D. P. Francis et al., "Evidence of a dominant backward-propagating "suction" wave responsible for diastolic coronary filling in humans, attenuated in left ventricular hypertrophy," *Circulation*, vol. 113, no. 14, pp. 1768–1778, 2006.

[35] S. B. Bender, M. J. Van Houwelingen, D. Merkus, D. J. Duncker, and M. Harold Laughlin, "Quantitative analysis of exercise-induced enhancement of early- and late-systolic retrograde coronary blood flow," *Journal of Applied Physiology*, vol. 108, no. 3, pp. 507–514, 2010.

[36] D. Zeng, E. Boutsianis, M. Ammann, K. Boomsma, S. Wildermuth, and D. Poulikakos, "A study on the compliance of a right coronary artery and its impact on wall shear stress," *Journal of Biomechanical Engineering*, vol. 130, no. 4, Article ID 041014, 11 pages, 2008.

[37] J. Peacock, T. Jones, C. Tock, and R. Lutz, "The onset of turbulence in physiological pulsatile flow in a straight tube," *Experiments in Fluids*, vol. 24, no. 1, pp. 1–9, 1998.

Hindawi Publishing Corporation
BioMed Research International
Volume 2014, Article ID 459269, 10 pages
http://dx.doi.org/10.1155/2014/459269

Research Article

Relationship between Stroke Volume and Pulse Pressure during Blood Volume Perturbation: A Mathematical Analysis

Ramin Bighamian and Jin-Oh Hahn

Department of Mechanical Engineering, University of Maryland, 2181 Glenn L. Martin Hall, College Park, MD 20742, USA

Correspondence should be addressed to Jin-Oh Hahn; jinoh.hahn@alum.mit.edu

Received 13 February 2014; Revised 15 April 2014; Accepted 24 April 2014; Published 20 May 2014

Academic Editor: Karim Bendjelid

Arterial pulse pressure has been widely used as surrogate of stroke volume, for example, in the guidance of fluid therapy. However, recent experimental investigations suggest that arterial pulse pressure is not linearly proportional to stroke volume. However, mechanisms underlying the relation between the two have not been clearly understood. The goal of this study was to elucidate how arterial pulse pressure and stroke volume respond to a perturbation in the left ventricular blood volume based on a systematic mathematical analysis. Both our mathematical analysis and experimental data showed that the relative change in arterial pulse pressure due to a left ventricular blood volume perturbation was consistently smaller than the corresponding relative change in stroke volume, due to the nonlinear left ventricular pressure-volume relation during diastole that reduces the sensitivity of arterial pulse pressure to perturbations in the left ventricular blood volume. Therefore, arterial pulse pressure must be used with care when used as surrogate of stroke volume in guiding fluid therapy.

1. Introduction

Stroke volume (SV) is the volume of blood pumped out by the heart to the arterial tree. It is known to be highly correlated with cardiac function in that it typically decreases in the presence of diseases such as cardiogenic shock [1], hemorrhage [2], sepsis [3], spinal cord injury [4], and hypothyroid [5]. It is also an important determinant of cardiac output, which is modulated by the demand for oxygen delivery to the tissues in the body [6] and the capacitance of the arteriovenous system [7]. Regarding its clinical applications, the interpretation of SV (or correspondingly cardiac output) can help caregivers to better understand the complex pathophysiological alterations in the critical illness, thereby helping to avoid deleterious effects of inotropic therapy [8], potentially harmful effects of vasopressor agents [9], and the detrimental edema in fluid administration [10].

Despite its clinical significance, SV has not been widely utilized for routine diagnostic and therapeutic purposes due to the difficulty in its measurement [11]. In fact, most state-of-the-art methods to directly measure SV (e.g., thermodilution technique and bioimpedance method) are invasive, expensive, and/or uncomfortable and necessitate trained experts for reliable measurement [12–15].

To exploit SV in clinical applications without encountering the problems listed above, there have been numerous efforts to indirectly estimate SV from minimally invasive or noninvasive arterial circulatory measurements, which are collectively called the pulse wave analysis (PWA) methods [16–19]. In a typical PWA method, arterial blood pressure (BP) and/or flow signals are analyzed via cardiovascular models [20–22], signal processing techniques [23, 24], feature extraction techniques [25], and so on.

In one of its simplest form, PWA is based on the assumption that SV is proportional to arterial pulse pressure (hereafter called pulse pressure (PP)) [16–19]. In fact, there are many existing evidences supporting this assumption [20, 21, 26]. Due to this reason, PP has been widely used as a convenient surrogate of SV during diagnostic and therapeutic procedures, such as fluid therapy [27], ventricular resynchronization therapy [28], and vasopressor/inotrope therapy [29].

Some recent experimental investigations suggest that although SV and PP are proportionally correlated during blood volume perturbation, the relationship may not be

strictly linear, and PP may underestimate SV in response to blood volume changes [27, 30, 31]. It is possible that the underestimation of SV during fluid therapy may potentially require substantial correction for dosage regimen, since brute-force fluid administration based on linear SV-PP assumption is likely suboptimal. Indeed, the essential challenge in fluid therapy is to avoid the administration of too little or too much volume, since there is a relatively narrow range for safe fluid therapy and both overload and underhydration can adversely affect the patient outcome. In fact, it has been shown that patients receiving proper fluid therapy, compared with those receiving restricted fluid regimens due to underestimation of SV, have more than 50% fewer complications and shorter length of hospital stay [32]. In order for PP to be used as a reliable surrogate of SV during fluid therapy, the relationship between SV and PP in response to blood volume changes must be clearly understood. The goal of this study was to unveil the mechanisms underlying the relation between pulse pressure and stroke volume based on a systematic mathematical analysis in order to elucidate how pulse pressure and stroke volume respond to a perturbation in blood volume and validate our analysis with experimental data.

This paper is organized as follows. In Section 2, the left-ventricular pressure-volume loop is introduced as a framework for our analysis. In Section 3, the responses of SV and PP to blood volume perturbation are analyzed, based on which the relationship between SV and PP during blood volume change is elucidated. The mathematical analysis is compared with experimental data in Section 4.

2. Left-Ventricular Pressure-Volume Framework

We use the left ventricular (LV) pressure-volume loop (*P-V* loop) framework [33] to mathematically analyze how changes in SV and PP are related during volume perturbation. In the context of LV *P-V* loop, the so-called "maximum" LV pressure [33–35] is given by the weighted average of end-systolic and end-diastolic pressures:

$$P_{\mathrm{LV}}^{\max} = \phi(t)\, P_S(V(t)) + \left(1 - \phi(t)\right) P_D(V(t)), \tag{1}$$

where $\phi(t)$ is the activation function [33, 35, 36] and P_S and P_D are the pressures corresponding to end-systolic and end-diastolic *P-V* relationships at a LV volume $V(t)$ [33, 35]. P_S and P_D are given by (see red and blue dashed lines in Figure 1)

$$\begin{aligned} P_S(V(t)) &= E_S\left(V(t) - V_0\right), \\ P_D(V(t)) &= B\left[e^{A(V(t)-V_0)} - 1\right], \end{aligned} \tag{2}$$

where E_S is the end-systolic LV elastance, A and B are constants specifying the end-diastolic *P-V* relationship, and V_0 is the LV volume corresponding to zero LV pressure [33, 35, 36].

In Section 3, we exploit the above well-established mathematical model to elucidate the relationship between the changes in SV and PP during volume perturbation.

3. Relationship between SV and PP during Volume Perturbation

In this study, the mechanisms underlying the relation between SV and PP during volume perturbation are elucidated as follows. First, we show how SV changes in response to changes in end-diastolic volume (due to volume perturbation). Second, we show how PP changes in response to changes in end-diastolic volume. Using these two results, we finally explain how PP changes relative to SV in response to changes in end-diastolic volume.

3.1. SV Response to Volume Perturbation. In the context of *P-V* loop, SV can be computed from end-diastolic volume as follows. By definition, SV is given by the difference between end-diastolic and end-systolic volumes:

$$\delta V = V_{\mathrm{ed}} - V_{\mathrm{es}} = V\left(t_{\mathrm{ed}}\right) - V\left(t_{\mathrm{es}}\right), \tag{3}$$

where $V_{\mathrm{ed}} = V(t_{\mathrm{ed}})$ and $V_{\mathrm{es}} = V(t_{\mathrm{es}})$ are end-diastolic and end-systolic volumes and t_{ed} and t_{es} are the time instants corresponding to end-diastole and end-systole, respectively. Alternatively, SV is given from mean arterial pressure (MAP) as follows:

$$\delta V = \frac{P_m}{R} T, \tag{4}$$

where P_m is MAP, R is total peripheral resistance (TPR), and T is heart period. At end-systole ($t = t_{\mathrm{es}}$), the *P-V* loop intersects with the systolic *P-V* relationship $P_S = E_S(V(t) - V_0)$ [33, 35], where $P_S = P_{\mathrm{es}}$ and $V(t) = V(t_{\mathrm{es}}) = V_{\mathrm{es}}$. Therefore, we have

$$P_{\mathrm{es}} = E_S\left(V_{\mathrm{es}} - V_0\right). \tag{5}$$

On the other hand, since end-systolic pressure is typically very close in value to MAP [37, 38], we have, from (4),

$$\delta V = V_{\mathrm{ed}} - V_{\mathrm{es}} \cong \frac{P_{\mathrm{es}}}{R} T. \tag{6}$$

Combining (5) and (6) yields the following expression for V_{es}:

$$V_{\mathrm{es}} = \frac{E_A}{E_S + E_A} V_{\mathrm{ed}} + \frac{E_S}{E_S + E_A} V_0, \tag{7}$$

where $E_A = R/T$ is called the arterial elastance [33, 35, 38]. Therefore, SV can be computed from end-diastolic volume as

$$\delta V = V_{\mathrm{ed}} - V_{\mathrm{es}} = \frac{E_S}{E_S + E_A}\left(V_{\mathrm{ed}} - V_0\right). \tag{8}$$

Thus, SV is related to end-diastolic volume by the proportionality constant $E_S/(E_S+E_A)$, which depends on LV and arterial elastances. Therefore, it can be concluded that a change in end-diastolic volume caused by volume perturbation results in a change in SV whose magnitude is linearly proportional to that of end-diastolic volume, *if LV and arterial elastances remain constant* during volume perturbation. In Figure 1, this can be illustrated as the linear proportionality between the triangles defined by $(V_{\mathrm{ed},j}, 0)$, $(V_0, 0)$, and $(V_{\mathrm{es},j}, P_{\mathrm{es},j})$, $j = 0, 1, 2$: as long as E_S and E_A remain constant, SV ($= V_{\mathrm{ed},j} - V_{\mathrm{es},j} = P_{\mathrm{es},j}\cot^{-1}E_A = (E_S E_A/(E_S + E_A))(V_{\mathrm{ed},j} - V_0)\cot^{-1}E_A$) is proportional to the end-diastolic volume ($= V_{\mathrm{ed},j} - V_0$).

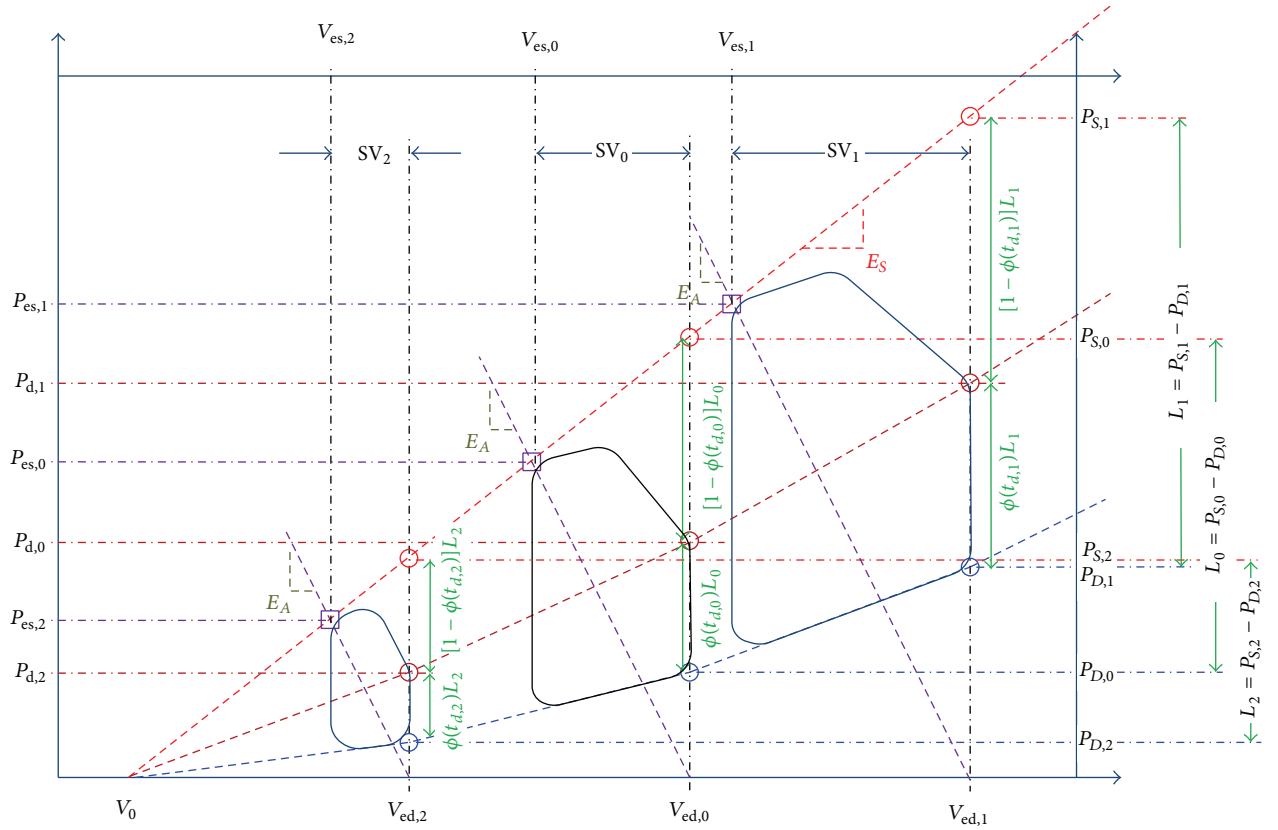

FIGURE 1: Left ventricular pressure-volume loop for different end-diastolic volumes.

3.2. PP Response to Volume Perturbation. To understand the PP response to volume perturbation, we first analyze the responses of end-systolic and diastolic (DP) pressures to changes in end-diastolic volume and then show the response of PP by formulating it to the difference between end-systolic pressure response and DP response. The rationale for using end-systolic pressure and DP rather than systolic pressure (SP) and DP is because, in contrast to end-systolic pressure and DP which always occur at end-systolic and end-diastolic volumes (see Figure 1), the value of volume on the P-V loop where SP occurs is not straightforward to specify. It will be demonstrated that PP can be, at least approximately, obtained from end-systolic pressure and DP by assuming that end-systolic pressure is typically very close in value to MAP.

At diastole ($t = t_d$ where t_d is the time instant corresponding to DP), the maximum LV pressure is equal to DP, and LV volume is equal to end-diastolic volume (V_{ed}). Therefore, (1) reduces to

$$\begin{aligned} P_d(V_{ed}) &= \phi(t_d) P_S(V_{ed}) + (1-\phi(t_d)) P_D(V_{ed}) \\ &= \phi(t_d) E_S(V_{ed} - V_0) \\ &\quad + (1-\phi(t_d)) B\left[e^{A(V_{ed}-V_0)} - 1\right]. \end{aligned} \tag{9}$$

For simplicity of analysis, assume that t_d relative to T remains constant during volume perturbation (see Section 3.4 for what happens if this assumption is relaxed). Then, it is obvious from (9) that, for a given value of end-diastolic volume, DP is determined as the weighted average of end-systolic and end-diastolic pressures corresponding to that end-diastolic volume:

$$\begin{aligned} P_d(V_{ed}) &= \sigma P_S(V_{ed}) + (1-\sigma) P_D(V_{ed}) \\ &= \sigma E_S(V_{ed} - V_0) + (1-\sigma) B\left[e^{A(V_{ed}-V_0)} - 1\right], \end{aligned} \tag{10}$$

where $\sigma = \phi(t_d)$ is constant *if t_d relative to T remains constant*. Now, if we note that the end-systolic P-V relationship, $E_S(V_{ed} - V_0)$, is linear in V_{ed}, whereas the end-diastolic P-V relationship, $B[e^{A(V_{ed}-V_0)} - 1]$, is exponential in V_{ed}, and also that $P_d(V_{ed})$ is simply the weighted average between the two, it can be concluded that the rate of change in DP increases as end-diastolic volume increases (see Figure 1). This is illustrated in Figure 1 by the brown dashed line connecting $P_{d,j} = P_d(V_{ed,j})$, $j = 0, 1, 2$, whose slope becomes steeper as end-diastolic volume increases.

The response of end-systolic pressure to changes in end-diastolic volume can be obtained by combining (5) and (7), which yields

$$P_{es}(V_{ed}) = E_S(V_{es} - V_0) = \frac{E_S E_A}{E_S + E_A}(V_{ed} - V_0). \tag{11}$$

Thus, end-systolic pressure is related to end-diastolic volume by the proportionality constant $E_S E_A/(E_S + E_A)$, which depends on LV and arterial elastances. Therefore, it can be concluded that end-systolic pressure is linearly proportional

to end-diastolic volume *if LV and arterial elastances remain constant* during volume perturbation.

To relate end-systolic pressure and DP to PP, we use a widely accepted relationship between SP, MAP, and DP: $P_m \cong P_d + (1/3)(P_s - P_d)$. As for Section 3.1, if we assume that end-systolic pressure is very close to MAP ($P_{es} \approx P_m$), we get the following relationship between PP, end-systolic pressure, and DP:

$$\begin{aligned} P_{es} &\cong P_d + \frac{1}{3}\left(P_s - P_d\right) \longrightarrow P_p \\ &= P_s - P_d \\ &\cong 3\left(P_{es} - P_d\right) \end{aligned} \tag{12}$$

which indicates that PP is linearly proportional to the difference between end-systolic pressure and DP.

Finally, combining the conclusions drawn from (10)–(12), we can conclude that the rate of change in PP decreases as end-diastolic volume increases, because the rate of change in DP becomes steeper than that in end-systolic pressure as end-diastolic volume increases (see Figure 1). This can be illustrated in Figure 1 as follows: as long as LV and arterial elastances as well as $\phi(t_d)$ remain constant, the rate of change in $P_{es,j} - P_{d,j}$ decreases with an increase in end-diastolic volume (see the left vertical axis), since the difference between the slopes of red (P_{es}) and brown (P_D) lines decreases as end-diastolic volume increases.

3.3. Relationship between SV and PP. The analyses performed in Sections 3.1 and 3.2 indicate that, under the assumption that (1) both LV and arterial elastances as well as t_d relative to T remain constant during volume perturbation, and (2) end-systolic pressure is close in value to MAP, SV shows constant proportionality to end-diastolic volume as indicated in (8) (i.e., it is a linear function of end-diastolic volume). In contrast, PP exhibits decreasing proportionality to end-diastolic volume with an increase in end-diastolic volume, thereby decreasing the rate of change in PP response to end-diastolic volume as it increases (in other words, PP shows a gradually decreasing slope when it is plotted against end-diastolic volume). Since SV and PP exhibit constant versus decreasing slopes against end-diastolic volume, respectively, the relationship between SV and PP is concave towards SV. Therefore, SV and PP are not linearly proportional to each other, and the rate of change in PP is not a good quantitative indicator of the rate of change in SV. In fact, our analyses suggest that the rate of change in PP underestimates the rate of change in SV in the neighborhood of a given operating end-diastolic volume (see Figure 2). Indeed, Figure 2 illustrates that the slope of SV with respect to end-diastolic volume is steeper than that of PP around the vicinity of an operating end-diastolic volume.

3.4. Relaxation of Assumptions. In our analysis, we made the following assumptions: during changes in end-diastolic volume due to volume perturbation, (i) the time instant corresponding to DP relative to the heart period (t_d/T) is constant (A1); (ii) end-systolic pressure is close in value to MAP (A2); and (iii) LV and arterial elastances remain

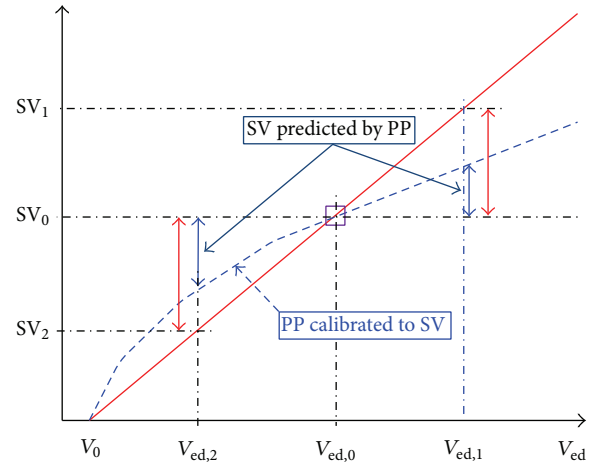

Figure 2: Relationship between SV and PP.

constant (A3). In this section, these assumptions are relaxed and their effects are incorporated to the conclusion drawn in Section 3.3.

3.4.1. Relaxation of Assumption (A1). It has been suggested that the shape of the activation function $\phi(t)$ is highly consistent among different individuals that is, its inter-individual variability is small [39, 40]. However, the timing values associated with cardiac events, for example, diastole ($t = t_d$) may be subject to change due to mechanisms such as baroreflex. This may invalidate the assumption (A1) above. Thus, it is worthwhile to examine how the timing-related variability in $\phi(t)$ alters the relationship between SV and PP.

It is obvious from (8) that SV is not influenced by $\phi(t)$. In addition, (10)–(12) indicate that PP is related to $\phi(t)$ only via DP but not via end-systolic pressure. So, uncertainty in $\phi(t)$ affects the relationship between SV and PP by altering DP (which occurs at $t = t_d$). Consequently, variability in the time instant corresponding to diastole ($t = t_d$) turns out to be the main parameter to be analyzed. In this study, we perform sensitivity analysis to quantitatively assess how significantly the relationship between SV and PP is altered by the variability in t_d. Using (10)–(12), PP can be rewritten as follows:

$$\begin{aligned} P_p &= P_s - P_d \\ &\cong 3\left(P_{es} - P_d\right) \\ &= 3\left\{\frac{E_S E_A}{E_S + E_A}\left(V_{ed} - V_0\right)\right. \\ &\qquad \left. - \left[\sigma P_S\left(V_{ed}\right) + (1-\sigma) P_D\left(V_{ed}\right)\right]\right\}. \end{aligned} \tag{13}$$

Then, the sensitivity of PP with respect to t_d/T is given by

$$\begin{aligned} \frac{\partial P_p}{\partial\left(t_d/T\right)} &\cong -3\frac{\partial P_d}{\partial\left(t_d/T\right)} \\ &= -3\frac{\partial \sigma}{\partial\left(t_d/T\right)}\left[P_S\left(V_{ed}\right) - P_D\left(V_{ed}\right)\right]. \end{aligned} \tag{14}$$

Table 1: Effect of arterial elastance on the responses of end-systolic pressure, PP, and SV.

	R	T	E_A	$E_S E_A/(E_S + E_A)$	$E_S/(E_S + E_A)$	P_{es}	P_p	δV
$V_{ed} \uparrow$	$\downarrow$	$\uparrow$	$\downarrow$	$\downarrow$	$\uparrow$	$\downarrow$	$\downarrow$	$\uparrow$
$V_{ed} \downarrow$	$\uparrow$	$\downarrow$	$\uparrow$	$\uparrow$	$\downarrow$	$\uparrow$	$\uparrow$	$\downarrow$

Table 2: Effect of LV elastance on the responses of end-systolic pressure, PP, and SV.

	E_S	$E_S E_A/(E_S + E_A)$	$E_S/(E_S + E_A)$	P_{es}	P_d	P_p	δV
$V_{ed} \uparrow$	$\downarrow$	$\downarrow$	$\downarrow$	$\downarrow$	$\downarrow$	$\uparrow$	$\downarrow$
$V_{ed} \downarrow$	$\uparrow$	$\uparrow$	$\uparrow$	$\uparrow$	$\uparrow$	$\downarrow$	$\uparrow$

In (14), $[P_S(V_{ed}) - P_D(V_{ed})]$ does not depend on t_d; it is a function of V_{ed} only. Since the term $\partial\sigma/\partial(t_d/T)$ (i.e., the sensitivity of the activation function with respect to t_d/T) is always positive [34], it can be concluded that PP decreases as t_d/T increases.

3.4.2. Relaxation of Assumption (A2). The effect of discrepancy between MAP and end-systolic pressure on the relationship between SV and PP can be examined as follows. It is clear from (8) and (12) that only PP but not SV is affected. The error in PP ($\tilde{P}_p$) due to the difference between MAP and end-systolic pressure is given by

$$\begin{aligned}\tilde{P}_p &= 3\left(P_{es} - P_d\right) - 3\left(P_m - P_d\right)\\ &= 3\tilde{P}_m,\end{aligned} \tag{15}$$

where $\tilde{P}_m = P_{es} - P_m$. Thus, an error in MAP (caused by approximating it to end-systolic pressure) is propagated to the PP error with an amplification factor of 3 (e.g., 1% error in MAP results in 3% error in PP), which can be deleterious if the MAP error is large. However, the absolute magnitude of alteration in PP due to the discrepancy between MAP and end-systolic pressure is not expected to be significant, since MAP is indeed close in value to end-systolic pressure over a wide range of physiologic conditions [37, 38].

3.4.3. Relaxation of Assumption (A3). First, the effect of arterial elastance on the responses of end-systolic pressure, PP, and SV anticipated due to the changes in end-diastolic volume is summarized in Table 1. In theory, TPR and the heart rate (the inverse of heart period) are altered by the autonomic baroreflex in response to alterations in V_{ed} [41, 42]. Specifically, an increase in end-diastolic volume results in a decrease in TPR and heart rate, whereas they increase to a decrease in end-diastolic volume [41, 42]. Therefore, the arterial elastance decreases during an increase in end-diastolic volume, which then yields a decrease in end-systolic pressure (with respect to its value predicted under constant arterial elastance) via a decrease in $E_S E_A/(E_S + E_A)$. This then results in a decrease in PP, since DP is not affected by the arterial elastance. On the other hand, a decrease in arterial elastance yields an increase in SV (again, with respect to its value predicted under constant arterial elastance) via an increase in $E_S/(E_S + E_A)$. Therefore, should there be any notable impact of end-diastolic volume on arterial elastance, the underestimation of SV based on PP will be exacerbated during an increase in end-diastolic volume, for example, during fluid therapy. In contrast, it can be deduced, based on the reasoning consistent with the above, that PP and SV will, respectively, increase and decrease from their values predicted under constant arterial elastance if end-diastolic volume decreases. Thus, the underestimation of SV based on PP will be alleviated during a decrease in end-diastolic volume, for example, hemorrhage.

Second, the effect of LV elastance on the responses of end-systolic pressure, PP, and SV anticipated due to the changes in end-diastolic volume is summarized in Table 2. Similarly to TPR and heart rate, LV elastance is altered by the autonomic baroreflex in response to alterations in V_{ed} [43]. In particular, LV elastance typically decreases if end-diastolic volume increases, and it increases if end-diastolic volume decreases [43]. It can then be shown that both $E_S E_A/(E_S+E_A)$ and $E_S/(E_S + E_A)$ decrease in response to an increase in end-diastolic volume. Consequently, an increase in end-diastolic volume will result in a decrease in end-systolic pressure and SV (with respect to their values predicted under constant LV elastance), whereas a decrease in end-diastolic volume will result in an increase in end-diastolic pressure and SV (again, with respect to their values predicted under constant LV elastance). In addition, DP is also affected by the LV elastance, because a change in LV elastance alters the value of $P_S(V_{ed})$ (see Figure 1). Therefore, the effect of LV elastance on PP can be elucidated by combining its impacts on end-systolic pressure and DP. To quantify the effect of LV elastance on PP, consider the following equations for end-systolic pressure and DP in response to a perturbation on LV elastance:

$$\begin{aligned}\left(P_{es} + \Delta P_{es}\right) &= \frac{\left(E_S + \Delta E_S\right) E_A}{\left(E_S + \Delta E_S\right) + E_A}\left(V_{ed} - V_0\right),\\ \left(P_d + \Delta P_d\right) &= \sigma\left(E_S + \Delta E_S\right)\left(V_{ed} - V_0\right)\\ &\quad + (1 - \sigma)\, B\left[e^{A(V_{ed} - V_0)} - 1\right].\end{aligned} \tag{16}$$

Thus, alterations in end-systolic pressure and DP can be written as follows:

$$\begin{aligned}\Delta P_{es} &= \left[\frac{\left(E_S + \Delta E_S\right) E_A}{\left(E_S + \Delta E_S\right) + E_A} - \frac{\left(E_S\right) E_A}{\left(E_S\right) + E_A}\right]\left(V_{ed} - V_0\right)\\ &\approx \left(\frac{E_A}{E_S + E_A}\right)^2 \Delta E_S\left(V_{ed} - V_0\right),\\ \Delta P_d &= \sigma \Delta E_S\left(V_{ed} - V_0\right),\end{aligned} \tag{17}$$

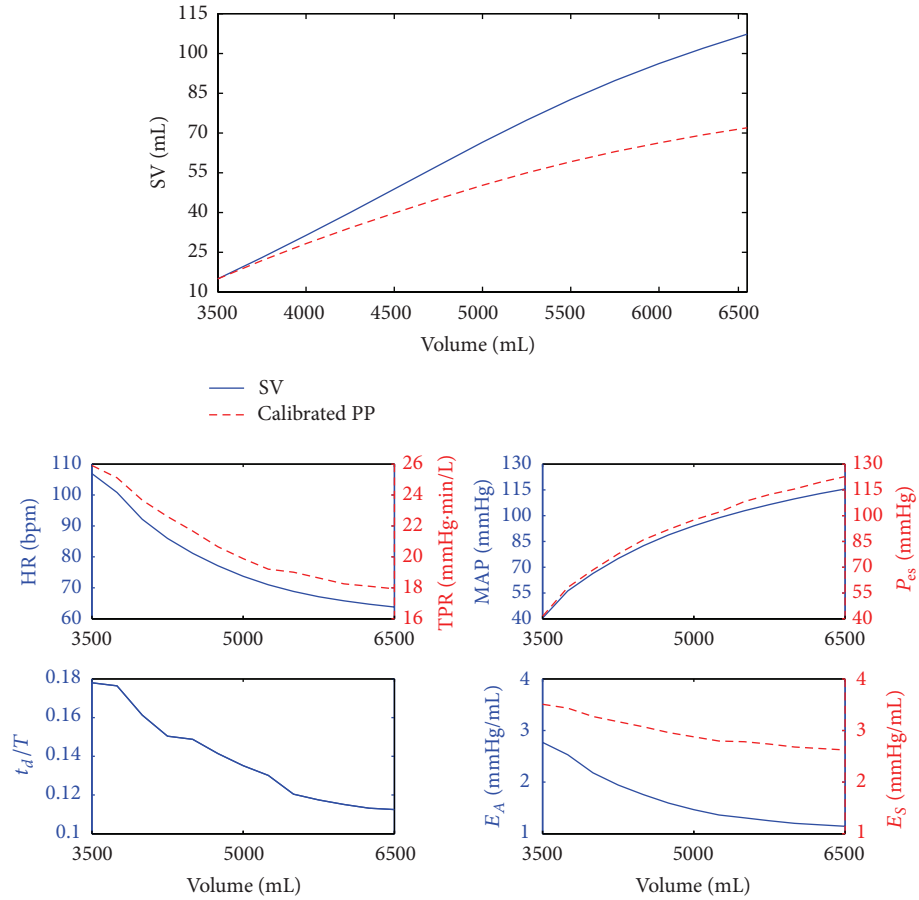

Figure 3: A representative result of SV, BP, and baroreflex responses to a wide range of perturbation in blood volume (3.5 L–6.5 L).

where the expression for ΔP_{es} was simplified using the Taylor series expansion. Consequently, the alteration of PP due to a perturbation in LV elastance can be quantified as follows:

$$\frac{\partial P_p}{\partial E_S} = 3\left[\left(\frac{E_A}{E_S + E_A}\right)^2 - \sigma\right](V_{ed} - V_0). \tag{18}$$

So, whether PP increases or decreases depends on the sign of $[(E_A/(E_S + E_A))^2 - \sigma]$. Though not definitive, it can be shown numerically that $[(E_A/(E_S + E_A))^2 - \sigma]$ takes negative values over the space of physiologically nominal parameter values. Therefore, should there be any notable impact of end-diastolic volume on LV elastance, the underestimation of SV based on PP will be alleviated during an increase in end-diastolic volume, for example, during fluid therapy. In contrast, the underestimation of SV based on PP will be exacerbated during a decrease in end-diastolic volume, for example, hemorrhage.

3.5. Simulation Study. To numerically examine the results of the analysis in this section, a simulation model developed by Ursino [44] and Ursino and Magosso [45, 46] was used to create SV and PP responses to a wide range of hypothetical volume perturbations. The model includes a time-varying elastance model of the heart, arterial and venous vessels lumped into 12 compartments, and a nonlinear baroreflex feedback model. In the simulation model, blood volume was varied from 3.5 L to 6.5 L (with nominal volume of 5.0 L), and the corresponding BP and SV responses in the steady state were obtained. A representative result is shown in Figure 3, where PP has been scaled to SV so that their values at 3.5 L match.

First of all, the simulation result shown in Figure 3 makes sure that the change in PP underestimates that in SV. For example, the change in SV as predicted by the change in PP in response to the added blood volume of 3.0 L (from 3.5 L to 6.5 L) was only ~60% of the actual change in SV. Therefore, PP must not be used as a linear predictor of SV.

It is noted that the result shown in Figure 3 was obtained in the presence of realistic variability in t_d/T, E_A, and E_S. Indeed, the baroreflex feedback responses in Figure 3 indicate that these parameters were subject to nonnegligible variability during blood volume perturbation. In particular, t_d/T decreased by large amount in response to an increase in blood volume, which was attributed to a large decrease in HR (thus a large increase in T). Also, TPR as well as arterial and LV elastances decreased as blood volume increased, which was anticipated. Compared with LV elastance, however, the variability in arterial elastance was significantly larger due to large changes in HR and TPR.

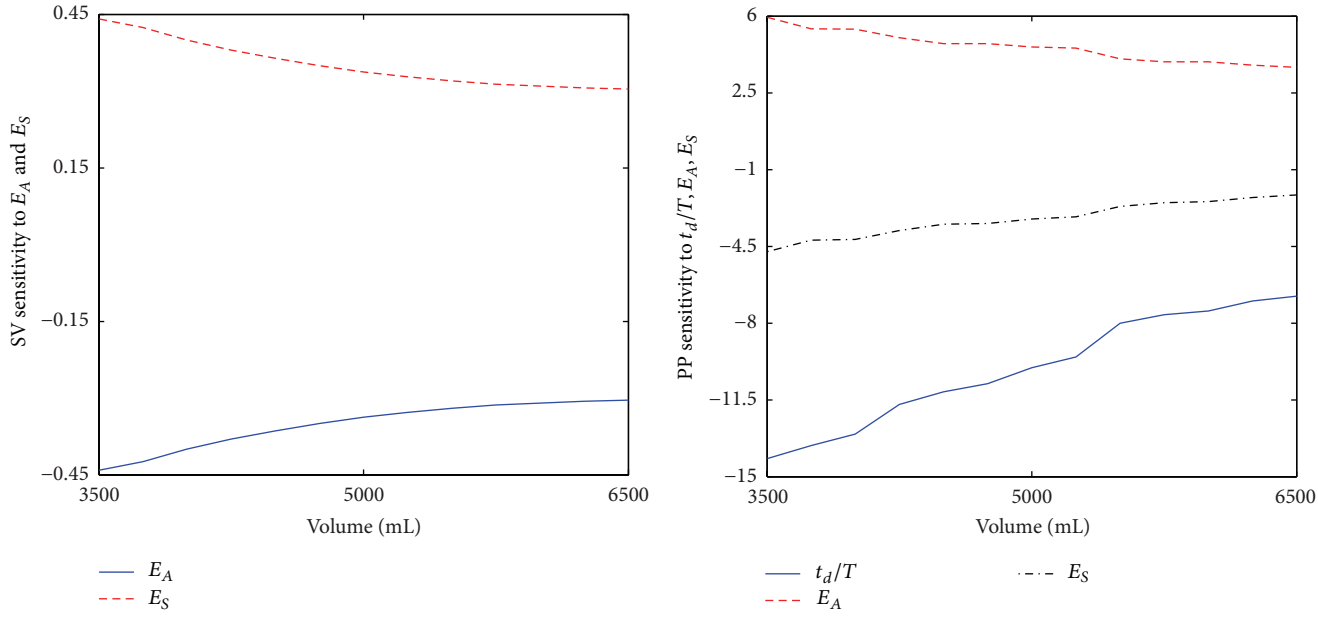

(a) SV (b) PP

Figure 4: Sensitivity of SV and PP to t_d/T, E_A, and E_S.

To quantitatively examine the effect of variability in t_d/T, E_A, and E_S on our analysis, the sensitivity of SV and PP to these parameters was computed and scrutinized (see Figure 4). Overall, the sensitivity of SV on E_A and E_S was very small (see Figure 4(a)). Also, it does not explicitly depend on t_d/T as indicated by (8). Thus, we predicted that the assumptions (A1)–(A3) made in Section 3 would not affect SV. Indeed, simulated SV as shown in Figure 3 was very close in value to SV predicted from (8) under constants E_A and E_S (not shown). On the other hand, PP turned out to be largely affected by these parameters (see Figure 4(b)). Considering that the absolute amount of change in E_A was much larger than that in E_S (see Figure 3), it turned out that the effect of changes in t_d/T and E_A on PP was dominant in comparison with the effect of change in E_S. Now that the direction of changes in t_d/T and E_A is the same (i.e., both decrease for positive volume perturbation but increase for negative volume perturbation) but their impact on PP is opposite (as indicated by opposite signs in sensitivity, see Figure 4(b)), it was observed that their effects were approximately canceled by each other. So, together with the observation that end-systolic pressure was consistently higher than MAP (see Figure 3), PP was overestimated based on (15). Summarizing all these observations, relaxation of the assumptions (A1)–(A3) made in Section 3 appears to further pronounce PP's underestimation of SV.

4. Experimental Data Analysis

To experimentally examine the validity of mathematical analysis conducted in this study, we analyzed a subset of *P-V* loop data collected in a previous study [47]. Data pertaining to 5 human subjects were analyzed, each of which had LV *P-V* loops associated with multiple LV volumes, electrocardiogram (ECG), and central aortic BP waveform. In each *P-V* loop, ECG was used to identify the beginning of diastole. The time instant at which LV pressure attains its maximum was regarded as the systolic peak (LV pressure = SP), from which the time instants corresponding to DP and end-systolic pressure were determined based on the time rate of change of LV pressure. Then, end-diastolic and end-systolic LV volumes were derived as average LV volume values during

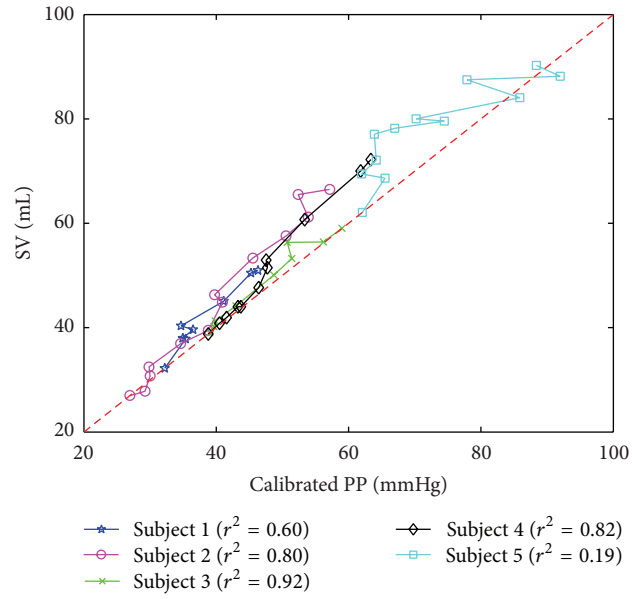

Figure 5: Experimental relation between SV and PP in humans.

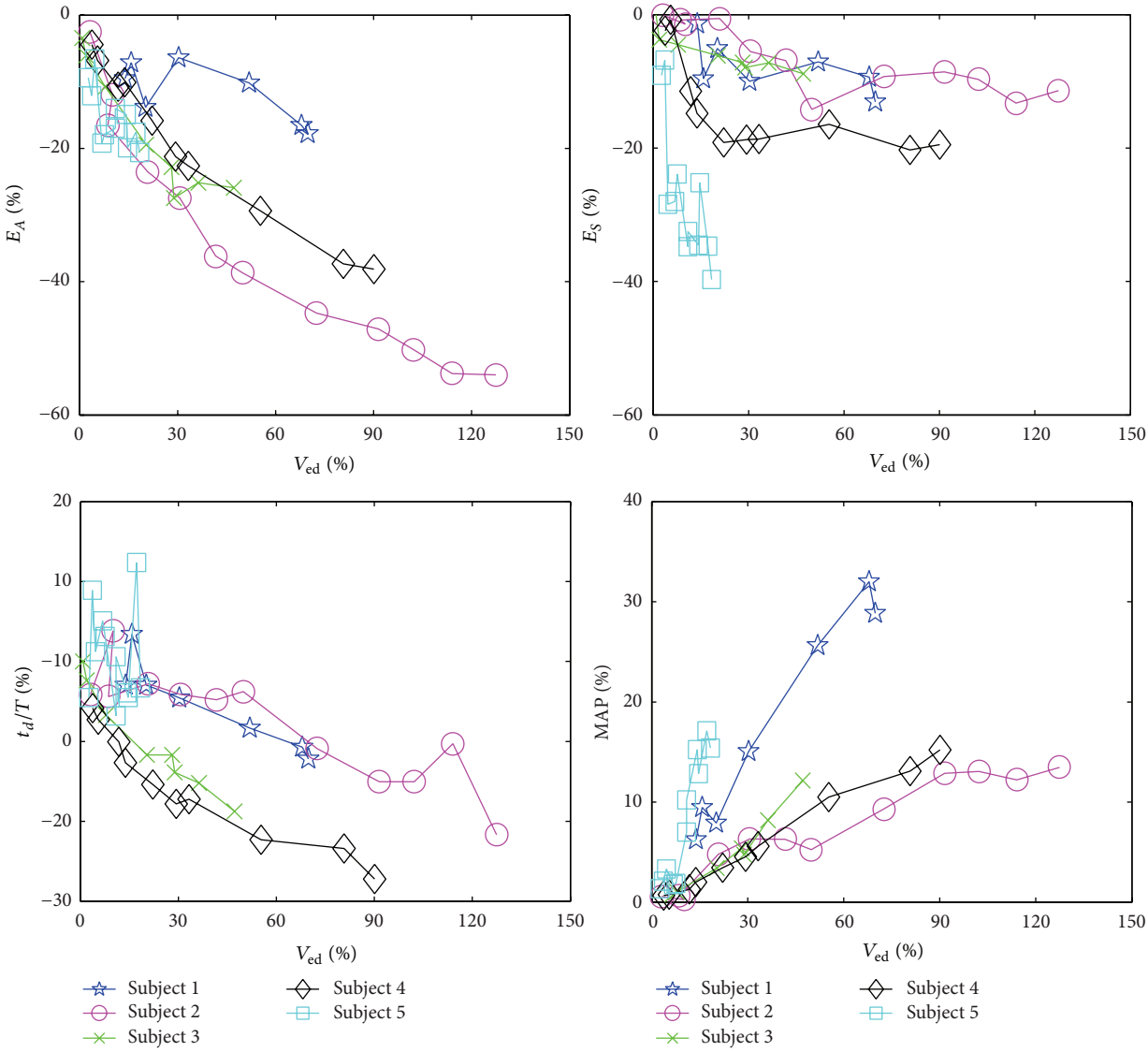

FIGURE 6: Behaviors of arterial (E_A) and LV (E_S) elastances, normalized DP time instant (t_d/T), and MAP in response to perturbations in end-diastolic volume.

isovolumetric contraction and relaxation phases, respectively. SV was then determined by subtracting end-systolic volume from end-diastolic volume. PP was derived directly from the central aortic BP waveform.

Figure 5 shows the relation between SV and calibrated (at the smallest SV) PP obtained from the data. The pairs of SV and PP mostly lie above the red dashed line corresponding to $\delta V = P_p$, meaning that PP indeed underestimates SV. On the average, the r^2 value between SV and calibrated PP was only 0.67, and the amount of change in SV was about 1.36 times larger than the amount of change in PP for a given perturbation in LV end-diastolic volume. It is also obvious in Figure 1 that the trend of underestimation was more significant as LV volume increased (especially in subjects 1, 2, 4, and 5, although in subject 5 outliers were observed due to noisy LV P-V loop measurement). All in all, observations from Figure 5 are highly consistent with the mathematical analysis conducted earlier in this study (Section 3).

It is also worth mentioning that the experimental data indicated that (i) MAP and end-systolic pressure were very close to each other, and that (ii) the experimentally observed behaviors of arterial (E_A) and LV (E_S) elastances, normalized DP time instant (t_d/T), and MAP in response to perturbations in end-diastolic volume were also consistent with the mathematical analysis conducted in Sections 3.4 and 3.5 (Figure 6). First, the difference between MAP and end-systolic pressure observed in the data was only 9 ± 4% of the end-systolic pressure. Second, the trends of E_A, E_S and t_d/T were all inversely proportional to end-diastolic volume, while MAP was proportional to end-diastolic volume. Third, comparing the amount of changes in E_A, E_S and t_d/T,

the change in E_A dominated those in E_S and t_d/T (see Figures 3 and 6), which, as discussed in Section 3.5, is the basis to justify that the assumptions (A1) and (A3) will not significantly affect the relation between SV and PP. Therefore, together with Figure 5, Figure 6 supports the validity of our mathematical analysis (see Section 3.3) to a large extent: (i) the underestimation of SV by PP is mainly due to the nonlinear LV *P-V* relation during diastole that ultimately reduces the sensitivity of PP to LV volume, and (ii) the assumptions made in Section 3.4 will not affect our analysis significantly.

5. Conclusion and Future Work

Pulse pressure has been observed to underestimate stroke volume in recent experimental studies, but the mechanisms underlying the relation between the two have not been clearly understood. In this study, we elucidated the mechanisms underlying the nonlinear dependence between SV and PP. In sum, the rate of change in PP decreases with end-diastolic volume, while SV depends linearly on end-diastolic volume. Therefore, PP underestimates SV. Considering that PP is frequently used as a direct surrogate of SV, this entails an important clinical implication: nonoptimal fluid therapy may result if there is no correction to PP to compensate for its nonlinear dependence on SV. In our opinion, the analysis conducted in this study may be useful for developing methods to enable such compensation in the follow-up studies.

Conflict of Interests

The authors declare that there is no conflict of interests regarding the publication of this paper.

Acknowledgments

This work was supported in part by the Young Investigator Grant from the Korean-American Scientists and Engineers Association. The authors appreciate Professor David A. Kass at the Johns Hopkins University for providing them with the experimental data for this study.

References

[1] H. R. Reynolds and J. S. Hochman, "Cardiogenic shock current concepts and improving outcomes," *Circulation*, vol. 117, no. 5, pp. 686–697, 2008.

[2] J. L. Lomas-Niera, M. Perl, C. S. Chung, and A. Ayala, "Shock and hemorrhage: an overview of animal models," *Shock*, vol. 24, no. 1, pp. 33–39, 2005.

[3] J. D. Hunter and M. Doddi, "Sepsis and the heart," *British Journal of Anaesthesia*, vol. 104, no. 1, pp. 3–11, 2010.

[4] M. J. Devivo, "Epidemiology of traumatic spinal cord injury: trends and future implications," *Spinal Cord*, vol. 50, no. 5, pp. 365–372, 2012.

[5] M. R. Gamberini, A. Meloni, G. Rossi et al., "Hypothyroidism and cardiac complications in thalassemia major patients," *Blood*, vol. 122, no. 21, pp. 2254–2254, 2013.

[6] J. Bisgaard, T. Gilsaa, E. Rønholm, and P. Toft, "Optimising stroke volume and oxygen delivery in abdominal aortic surgery: a randomised controlled trial," *Acta Anaesthesiologica Scandinavica*, vol. 57, no. 2, pp. 178–188, 2013.

[7] K. Tomsin, T. Mesens, G. Molenberghs, L. Peeters, and W. Gyselaers, "Characteristics of heart, arteries, and veins in low and high cardiac output preeclampsia," *European Journal of Obstetrics & Gynecology and Reproductive Biology*, vol. 169, no. 2, pp. 218–222, 2013.

[8] P. McCann and P. J. Hauptman, "Inotropic therapy: an important role in the treatment of advanced symptomatic heart failure," *Medical Clinics of North America*, vol. 96, no. 5, pp. 943–954, 2012.

[9] M. Hadian, D. A. Severyn, and M. R. Pinsky, "The effects of vasoactive drugs on pulse pressure and stroke volume variation in postoperative ventilated patients," *Journal of Critical Care*, vol. 26, no. 3, pp. 328.e1–328.e8, 2011.

[10] A. Watanabe, T. Tagami, S. Yokobori et al., "Global end-diastolic volume is associated with the occurrence of delayed cerebral ischemia and pulmonary edema after subarachnoid hemorrhage," *Shock Augusta Ga*, vol. 38, no. 5, pp. 480–485, 2012.

[11] J. Truijen, J. J. van Lieshout, W. A. Wesselink, and B. E. Westerhof, "Noninvasive continuous hemodynamic monitoring," *Journal of Clinical Monitoring and Computing*, vol. 26, no. 4, pp. 267–278, 2012.

[12] D. A. Reuter, C. Huang, T. Edrich, S. K. Shernan, and H. K. Eltzschig, "Cardiac output monitoring using indicator-dilution techniques: basics, limits, and perspectives," *Anesthesia and Analgesia*, vol. 110, no. 3, pp. 799–811, 2010.

[13] W. Alexander Osthaus, D. Huber, C. Beck et al., "Comparison of electrical velocimetry and transpulmonary thermodilution for measuring cardiac output in piglets," *Paediatric Anaesthesia*, vol. 17, no. 8, pp. 749–755, 2007.

[14] D. Tucker and M. F. Hazinski, "The nursing perspective on monitoring hemodynamics and oxygen transport," *Pediatric Critical Care Medicine*, vol. 12, supplement 4, pp. S72–S75, 2011.

[15] D. D. Backer and M. R. Pinsky, "Can one predict fluid responsiveness in spontaneously breathing patients?" in *Applied Physiology in Intensive Care Medicine 2*, M. R. Pinsky, L. Brochard, J. Mancebo, and M. Antonelli, Eds., pp. 385–387, Springer, Berlin, Germany, 2012.

[16] H. Ishihara, H. Okawa, K. Tanabe et al., "A new non-invasive continuous cardiac output trend solely utilizing routine cardiovascular monitors: comparison with the continuous thermodilution method early cardiovascular monitors," *Journal of Clinical Monitoring and Computing*, vol. 18, no. 5-6, pp. 313–320, 2004.

[17] B. Bataille, M. Bertuit, M. Mora et al., "Comparison of esCCO and transthoracic echocardiography for non-invasive measurement of cardiac output intensive care," *British Journal of Anaesthesia*, vol. 109, no. 6, pp. 879–886, 2012.

[18] T. G. Papaioannou, O. Vardoulis, and N. Stergiopulos, "The "systolic volume balance" method for the noninvasive estimation of cardiac output based on pressure wave analysis," *The American Journal of Physiology—Heart and Circulatory Physiology*, vol. 302, no. 10, pp. H2064–H2073, 2012.

[19] L. Mathews and K. R. K. Singh, "Cardiac output monitoring," *Annals of Cardiac Anaesthesia*, vol. 11, no. 1, pp. 56–58, 2008.

[20] T. A. Parlikar, T. Heldt, G. V. Ranade, and G. C. Verghese, "Model-based estimation of cardiac output and total peripheral

resistance," in *Proceedings of the Computers in Cardiology*, pp. 379–382, October 2007.

[21] N. Fazeli and J. O. Hahn, "Estimation of cardiac output and peripheral resistance using square-wave-approximated aortic flow signal," *Frontiers in Physiology*, vol. 3, article 298, 2012.

[22] T. Arai, K. Lee, and R. J. Cohen, "Cardiac output and stroke volume estimation using a hybrid of three Windkessel models," in *Proceedings of theAnnual International Conference of the IEEE Engineering in Medicine and Biology Society (EMBC '10)*, pp. 4971–4974, September 2010.

[23] D. Xu, N. Bari Olivier, and R. Mukkamala, "Continuous cardiac output and left atrial pressure monitoring by long time interval analysis of the pulmonary artery pressure waveform: proof of concept in dogs," *Journal of Applied Physiology*, vol. 106, no. 2, pp. 651–661, 2009.

[24] R. Mukkamala, A. T. Reisner, H. M. Hojman, R. G. Mark, and R. J. Cohen, "Continuous cardiac output monitoring by peripheral blood pressure waveform analysis," *IEEE Transactions on Biomedical Engineering*, vol. 53, no. 3, pp. 459–467, 2006.

[25] J. F. Martin, L. B. Volfson, V. V. Kirzon-Zolin, and V. G. Schukin, "Application of pattern recognition and image classification techniques to determine continuous cardiac output from the arterial pressure waveform," *IEEE Transactions on Biomedical Engineering*, vol. 41, no. 10, pp. 913–920, 1994.

[26] J. Marquez, K. McCurry, D. A. Severyn, and M. R. Pinsky, "Ability of pulse power, esophageal Doppler, and arterial pulse pressure to estimate rapid changes in stroke volume in humans," *Critical Care Medicine*, vol. 36, no. 11, pp. 3001–3007, 2008.

[27] V. A. Convertino, W. H. Cooke, and J. B. Holcomb, "Arterial pulse pressure and its association with reduced stroke volume during progressive central hypovolemia," *Journal of Trauma—Injury, Infection and Critical Care*, vol. 61, no. 3, pp. 629–634, 2006.

[28] D. A. Kass, "Ventricular dyssynchrony and mechanisms of resynchronization therapy," *European Heart Journal Supplements*, vol. 4, pp. D23–D30, 2002.

[29] R. Bighamian, A. T. Reisner, and J. O. Hahn, "An analytic tool for prediction of hemodynamic responses to vasopressors," *Transactions on Biomedical Engineering*, vol. 61, no. 1, pp. 109–118, 2014.

[30] A. T. Reisner, D. Xu, K. L. Ryan, V. A. Convertino, C. A. Rickards, and R. Mukkamala, "Monitoring non-invasive cardiac output and stroke volume during experimental human hypovolaemia and resuscitation," *British journal of anaesthesia*, vol. 106, no. 1, pp. 23–30, 2011.

[31] X. Monnet, A. Letierce, O. Hamzaoui et al., "Arterial pressure allows monitoring the changes in cardiac output induced by volume expansion but not by norepinephrine," *Critical Care Medicine*, vol. 39, no. 6, pp. 1394–1399, 2011.

[32] K. K. Varadhan and D. N. Lobo, "A meta-analysis of randomised controlled trials of intravenous fluid therapy in major elective open abdominal surgery: Getting the balance right," *Proceedings of the Nutrition Society*, vol. 69, no. 4, pp. 488–498, 2010.

[33] K. Sagawa, W. L. Maughan, H. Suga, and K. Sunagawa, *Cardiac Contraction and the Pressure-Volume Relationship*, Oxford University Press, Oxford, UK, 1988.

[34] I. Hay, J. Rich, P. Ferber, D. Burkhoff, and M. S. Maurer, "Role of impaired myocardial relaxation in the production of elevated left ventricular filling pressure," *The American Journal of Physiology—Heart and Circulatory Physiology*, vol. 288, no. 3, pp. H1203–H1208, 2005.

[35] W. P. Santamore and D. Burkhoff, "Hemodynamic consequences of ventricular interaction as assessed by model analysis," *The American Journal of Physiology—Heart and Circulatory Physiology*, vol. 260, no. 1, pp. H146–H157, 1991.

[36] H. Piene, "Impedance matching between ventricle and load," *Annals of Biomedical Engineering*, vol. 12, no. 2, pp. 191–207, 1984.

[37] D. A. Kass and R. Beyar, "Evaluation of contractile state by maximal ventricular power divided by the square of end-diastolic volume," *Circulation*, vol. 84, no. 4, pp. 1698–1708, 1991.

[38] M. S. Maurer, J. D. Sackner-Bernstein, L. E. Yushak et al., "Mechanisms underlying improvements in ejection fraction with carvedilol in heart failure," *Circulation: Heart Failure*, vol. 2, no. 3, pp. 189–196, 2009.

[39] K. E. Kjørstad, C. Korvald, and T. Myrmel, "Pressure-volume-based single-beat estimations cannot predict left ventricular contractility in vivo," *The American Journal of Physiology—Heart and Circulatory Physiology*, vol. 282, no. 5, pp. H1739–H1750, 2002.

[40] D. Georgakopoulos, W. A. Mitzner, C. H. Chen et al., "In vivo murine left ventricular pressure-volume relations by miniaturized conductance micromanometry," *The American Journal of Physiology—Heart and Circulatory Physiology*, vol. 274, no. 4, pp. H1416–H1422, 1998.

[41] J. C. Reil, G. H. Reil, and M. Böhm, "Heart rate reduction by if-channel inhibition and its potential role in heart failure with reduced and preserved ejection fraction," *Trends in Cardiovascular Medicine*, vol. 19, no. 5, pp. 152–157, 2009.

[42] A. Kumar, R. Anel, E. Bunnell et al., "Effect of large volume infusion on left ventricular volumes, performance and contractility parameters in normal volunteers," *Intensive Care Medicine*, vol. 30, no. 7, pp. 1361–1369, 2004.

[43] R. E. Klabunde, *Cardiovascular Physiology Concepts*, Lippincott Williams & Wilkins, Philadelphia, Pa, USA, 2005.

[44] M. Ursino, "Interaction between carotid baroregulation and the pulsating heart: a mathematical model," *The American Journal of Physiology—Heart and Circulatory Physiology*, vol. 275, no. 5, pp. H1733–H1747, 1998.

[45] M. Ursino and E. Magosso, "Short-term autonomic control of cardiovascular function: a mini-review with the help of mathematical models," *Journal of integrative neuroscience*, vol. 2, no. 2, pp. 219–247, 2003.

[46] M. Ursino and E. Magosso, "Acute cardiovascular response to isocapnic hypoxia. I. A mathematical model," *The American Journal of Physiology—Heart and Circulatory Physiology*, vol. 279, no. 1, pp. H149–H165, 2000.

[47] H. Senzaki, C. H. Chen, and D. A. Kass, "Single-beat estimation of end-systolic pressure-volume relation in humans. A new method with the potential for noninvasive application," *Circulation*, vol. 94, no. 10, pp. 2497–2506, 1996.

Hindawi Publishing Corporation
BioMed Research International
Volume 2014, Article ID 247054, 7 pages
http://dx.doi.org/10.1155/2014/247054

Research Article

Endothelium-Independent Vasorelaxant Effects of Hydroalcoholic Extract from *Nigella sativa* Seed in Rat Aorta: The Roles of Ca^{2+} and K^+ Channels

Saeed Niazmand,[1,2] Elahe Fereidouni,[2] Maryam Mahmoudabady,[2,3] and Seyed Mojtaba Mousavi[2]

[1] *Cardiovascular Research Center, School of Medicine, Mashhad University of Medical Sciences, Mashhad 9177948564, Iran*
[2] *Department of Physiology, School of Medicine, Mashhad University of Medical Sciences, Mashhad 9177948564, Iran*
[3] *Neurogenic Inflammation Research Centre, School of Medicine, Mashhad University of Medical Sciences, Mashhad 9177948564, Iran*

Correspondence should be addressed to Maryam Mahmoudabady; mahmoudabadym@mums.ac.ir

Received 4 February 2014; Revised 13 April 2014; Accepted 21 April 2014; Published 12 May 2014

Academic Editor: Karim Bendjelid

Objective. The aim of this study was to elucidate the mechanism(s) responsible for the vasorelaxant effect of *Nigella sativa* (*N. sativa*). *Methods.* The activity of different concentrations of *N. sativa* extract was evaluated on contractile responses of isolated aorta to KCl and phenylephrine (PE). *Results.* The extract (2–14 mg/mL) induced a concentration dependent relaxation both in endothelium-intact and endothelium-denuded aortic rings precontracted by PE (10^{-6} M) and KCl (6×10^{-2} M). Extract reduced PE- and KCl-induced contractions in presence of cumulative concentrations of calcium (10^{-5}–10^{-2} M) significantly. L-NAME and indomethacin had no effect on vasorelaxation effect of extract in PE-induced contraction. Diltiazem and heparin reduced significantly this vasorelaxation at a concentration of 14 mg/mL of extract; however, *N. sativa*-induced relaxation was not affected by ruthenium red. Tetraethylammonium chloride reduced the extract-induced relaxation in concentrations of 2–6 mg/mL of extract significantly but glibenclamide reduced this relaxative effect in all concentrations of extract. *Conclusions.* The inhibitory effect of *N. sativa* seed extract on the contraction induced by PE and KCl was endothelium-independent. This relaxation was mediated mainly through the inhibition of Ca^{2+} and K_{ATP} channels and also intracellular calcium release.

1. Introduction

Nigella sativa (N. sativa) which is commonly known as black cumin is a plant from the Ranunculaceae (buttercup) family. This plantisnative to Southern Europe, North Africa, and Southwest Asia and is cultivated in many countries in the world like those in the Middle Eastern Mediterranean region, Southern Europe, India, Pakistan, Iran, Syria, Turkey, and Saudi Arabia [1].

The seeds of *N. sativa* are used in folk (herbal) medicine all over the world for the treatment and prevention of a number of diseases and conditions that include asthma, diarrhea, and dyslipidemia [2]. *N. sativa* has been extensively studied for its biological activities and therapeutic potential and has been shown to possess a wide spectrum of activities such as anti-inflammatory [3], reduced ischemia-reperfusion injury [4], antioxidant [5, 6], antiepileptic [7], antibacterial [8], antihistaminic [9], antinociceptive [10], antidiabetic [11], hepatoprotective [12], and smooth muscle relaxant [9, 13] effects.

The seed oil of *N. sativa* was found to be rich in polyphenols and tocopherols [14, 15]. The seeds contain 36–38% fixed oils, 0.4–2.5% essential (volatile) oil, proteins, alkaloids, and saponins. The fixed oil is composed mainly of fatty acids, namely, linoleic (C18:2), oleic (C18:1), palmitic (C16:0), and stearic (C18:0) acids [16]. Thymoquinone (TQ) is the most pharmacologically active ingredient found abundantly (30–48%) in the black seeds, together with its derivatives such as dithymoquinone, thymohydroquinone, and thymol [17].

There is increasing evidence of the cardiovascular effect of *N. sativa* such asantihypertensive [18–21], hypotensive [22, 23], antihyperlipidemic [24–27], and ameliorative effect of endothelial dysfunction [28, 29]; however, the vasorelaxant effect of *N. sativa* was not evaluated. Thus, the present study investigated the effects of hydroalcoholic extract of *N. sativa* seed on the vasomotor tone of the aortic rings and its possible mechanism(s) of action.

2. Materials and Methods

2.1. Chemicals and Drugs. All chemicals were of analytical grade (Merck). Phenylephrine hydrochloride (PE), acetylcholine (ACh), N^G-nitro-L-arginine methyl ester (L-NAME), indomethacin, ruthenium red (RR), heparin (HP), tetraethylammonium chloride (TEA), and diltiazem were obtained from Sigma (Germany). Moreover, when necessary, the Krebs solution was used as solvent for all drugs.

2.2. Plant Material and Preparation of the Extract. *N. sativa* was collected from Nishabour city, Khorasan Province, Iran, and its seeds were dried at room temperature in the absence of sunlight. The plant was identified by botanists in the herbarium of the Ferdowsi University of Mashhad; the specimen number of the plant is 176-2013-9. The hydroethanolic extract was prepared using a maceration method as follows: 500 g of chopped *Nigella sativa* seeds were soaked in 500 cc of 50% ethanol for 48 hours at room temperature and the mixture was subsequently filtered and concentrated *in vacuo* at 40°C. The residue was suspended in saline solution to obtain 2, 4, 6, 8, 10, and 14 mg/mL concentrations.

2.3. Experimental Animals. Fourteen groups of Wistar rats (200 to 250 g, $n = 8$ for each group) were studied. The animals were group-housed in cages at 22 ± 2°C temperature and given water and food *ad libitum*, while a 12 h on/12 h off light cycle was maintained. All experiments were conducted in accordance with the internationally accepted principles for laboratory animal use and care and with institutional guidelines.

2.4. Preparation of Rat Aortas. The animals were anesthetized with 50 mg/kg Ketamine and decapitated by guillotine; after thoracotomy, the descending thoracic aorta was exposed and was rapidly dissected out and immersed in 95% O_2/5% CO_2-gassed (carbogen) ice-cold Krebs solution with the following composition (mM): NaCl (118.5), KCl (4.74), $MgSO_4$ (1.18), $NaHCO_3$ (24.9), KH_2PO_4 (1.2), $CaCl_2$ (2.5) and glucose (10), pH = 7.4. Aorta was then dissected free of periadventitial fat and connective tissue, with care taken to avoid touching the luminal surface and cut into four rings, each 5 mm in length. The aortic rings were mounted in 10 mL organ bath containing Krebs solution gassed with carbogen at 37°C. After a resting tension of 2 g, the vessel segments were allowed to equilibrate for 1 hour. Changes in tension were recorded by isometric transducers connected to a data acquisition system (AD instrument, Australia). In some rings, the endothelium was denuded by gently rubbing the intimal space with a thin metal rod. The absence of functional endothelium was verified by the inability of ACh (10^{-5} M) to induce the relaxation of rings precontracted with PE (10^{-6} M).

2.5. Experimental Procedure

2.5.1. Effect of N. sativa Extract on Aortic Contraction Induced by PE and KCl. These experiments were made to verify *N. sativa* extract induced relaxation effect. A steady contraction in rings with the endothelium intact or denuded was induced by 10^{-6} M PE or 6×10^{-2} M KCl, and *N. sativa* was added cumulatively (2, 4, 6, 8, 10, and 14 mg/mL). The *N. sativa* extract induced relaxation in the aortic rings which was calculated as a percentage of the relaxation in response to PE and KCl.

2.5.2. N. sativa Extract Induced Relaxation, L-NAME, and Indomethacin. To determine the nitric oxide (NO) or prostacyclin mediated relaxant effect of *N. sativa*, aortic rings were rinsed and exposed to L-NAME (10 μM), a nitric oxide synthase inhibitor, or indomethacin (10 μM), a cyclooxygenase (COX) inhibitor, for 30 min before induction of a steady contraction by 10^{-6} M PE, and final effects of cumulative concentrations of *N. sativa* extract (2, 4, 6, 8, 10, and 14 mg/mL) were evaluated for 25 minutes.

2.5.3. N. sativa Extract Induced Relaxation, Influx of Ca^{2+}, and Ca^{2+} Channels. In the first set of these experiments, an attempt was made to verify the relaxation induced by *N. sativa* involving Ca^{2+} influx. The endothelium-denuded aortic rings were washed four to five times with Ca^{2+}-free Krebs solution (containing 5×10^{-5} M EGTA) before PE (10^{-6} M) or KCl (6×10^{-2} M) was applied to produce a steady contraction, and then Ca^{2+} was added cumulatively to obtain a concentration-response curve (10^{-5} to 10^{-2} M) in the presence of 14 mg/mL *N. sativa* extract. In the second set of experiments, the aim was to evaluate the roles of voltage-dependent calcium channels in extract induced relaxation. Endothelium-denuded aortic rings were exposed to diltiazem (10^{-5} M), an L-type Ca^{2+} channel inhibitor, for 30 min before the application of PE (10^{-6} M) to induce a steady contraction; subsequently, the *N. sativa* extract (14 mg/mL) was added to evoke a relaxation.

2.5.4. N. sativa Extract Induced Relaxation and Intracellular Sources of Ca^{2+}. In this set of experiments, the aim was to clarify whether the relaxation induced by *N. sativa* was related to the inhibition of intracellular Ca^{2+} release.

Endothelium-denuded aortic rings were exposed to diltiazem (10^{-5} M), an L-type calcium blocker, for 30 min before the application of PE (10^{-6} M) to induce a steady contraction; subsequently, the *N. sativa* extract (14 mg/mL) was added to evoke relaxation. In the presence of diltiazem, ruthenium red (RR) (10^{-5} M), a ryanodine receptor inhibitor, or heparin (HP) (50 mg/L), an IP_3 receptor inhibitor, was added 30 min before the application of PE in separate experimental groups.

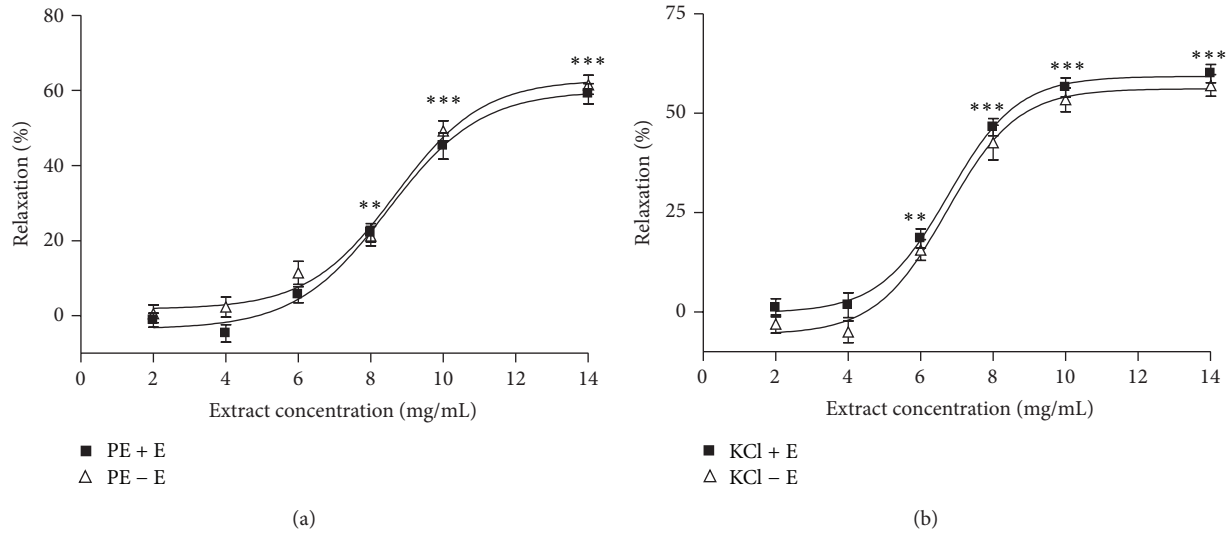

Figure 1: Effect of different concentrations of *Nigella sativa* extract (2, 4, 6, 8, 10, and 14 mg/mL) on PE (10^{-6} M) (a) and KCl (6×10^{-2} M) (b) precontracted rat aortic rings with (+E) or without (−E) endothelium. Data are expressed as mean ± S.E.M. ($n = 8$). $^{***}P < 0.001$, $^{**}P < 0.01$ compared to base.

2.5.5. N. sativa Extract Induced Relaxation and K^+ Channels. To examine the role of K^+channels in the extract induced relaxation, the aortic rings were rinsed and exposed to glibenclamide (10^{-5} M), an inhibitor of the ATP-dependent K^+channels (K_{ATP}), and tetraethylammonium chloride (TEA) (5 mM), a nonselective K^+ channel blocker, for 30 min before the application of 10^{-6} M PE to induce a steady contraction and finally the effects of cumulative concentrations of the extract (2, 4, 6, 8, 10, and 14 mg/mL) were evaluated for 25 min.

2.6. Data Analysis. All data are expressed as mean ± S.E.M. The EC_{50} was defined as the concentration of *N. sativa* that induced 50% of the maximum relaxation from the contraction elicited by PE (10^{-6} M) or KCl (6×10^{-2} M) and was calculated from the concentration-response curve, analyzed by nonlinear regression (curve fit) using GraphPad Prism (Version 4.0). Statistical comparisons were made using the Student's *t*-test and one-way ANOVA followed by the Tukey's test. *P* values less than 0.05 were considered to be statistically significant.

3. Results

3.1. Effect of N. sativa on PE and KCl Contracted Aorta. The *N. sativa* extract induced concentration-dependent relaxation in aortic rings precontracted by PE and KCl with a maximum relaxation of 62.3 ± 1.9% (EC_{50} = 8.5 mg/mL) and 60.2 ± 1.2% (EC_{50} = 7.6 mg/mL), respectively (Figures 1(a) and 1(b)). These inhibitory responses of extract were not significantly different in the intact and denuded aortic rings.

3.2. Effect of L-NAME and Indomethacin on Relaxant Response of N. sativa. Pretreatment of endothelium-intact aortic rings with L-NAME and indomethacin had no effect on the *N. sativa*-induced vasorelaxation at any concentration of extract (Figure 2).

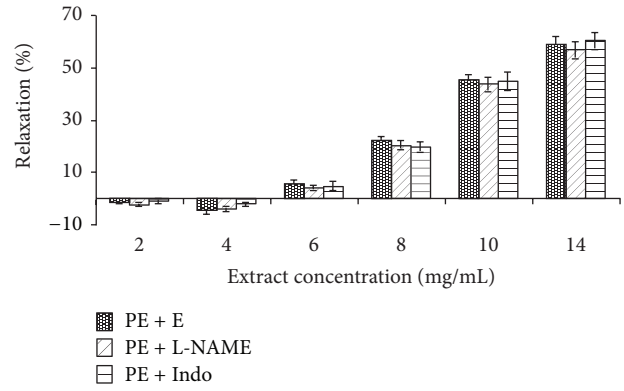

Figure 2: Effect of cumulative concentrations of *Nigella sativa* seed extract (2, 4, 6, 8, 10, and 14 mg/mL) on PE precontracted rat aortic rings with endothelium (PE + E) and after pretreatment with L-NAME (10 μM) (PE + L-NAME) or indomethacin (10 μM) (PE + Indo). Data are expressed as mean ± S.E.M. ($n = 8$).

3.3. Effect of N. sativa on Extracellular Ca^{2+}-Induced Contraction. Cumulative addition of Ca^{2+} in a Ca^{2+}-free medium containing PE or KCl induced a concentration-dependent contraction of aortic rings. Preincubation of the rings with 14 mg/mL of *N. sativa* significantly inhibited Ca^{2+}-induced contraction in both PE (Figure 3(a)) and KCl (Figure 3(b)) constricted rings.

3.4. Effect of N. sativa on Intracellular Sources of Ca^{2+}. The results of 30 min preincubation of endothelium-denuded aortic rings with RR or heparin in the presence of diltiazem

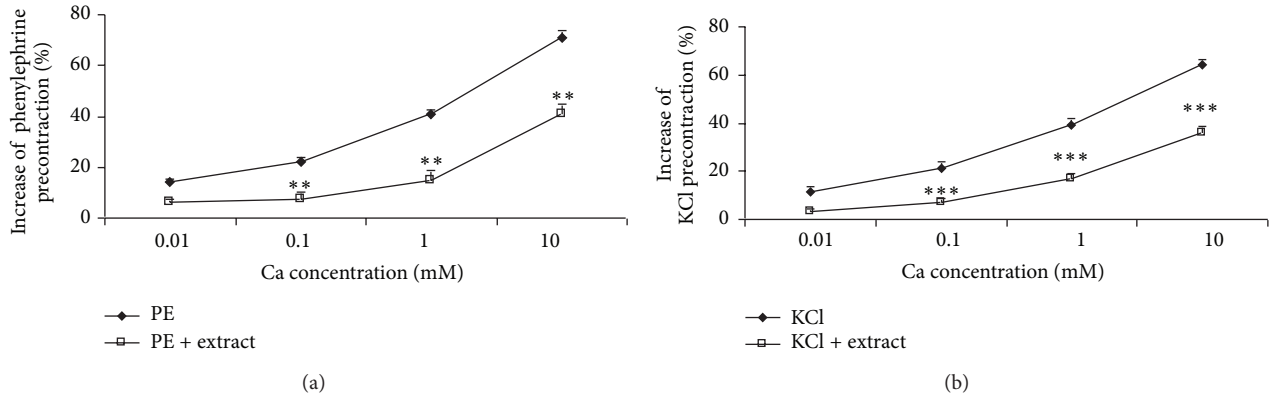

Figure 3: Effect of *Nigella sativa* seed extract at 14 mg/mL on the Ca^{2+}-induced (0.01–10 mM) contraction of rat aortic rings without endothelium pretreated with PE (10^{-6} M) (a) or KCl (6×10^{-2} M) (b). Data are expressed as mean ± S.E.M. ($n = 8$). $^{**}P < 0.01$, $^{***}P < 0.001$ compared tocontrol.

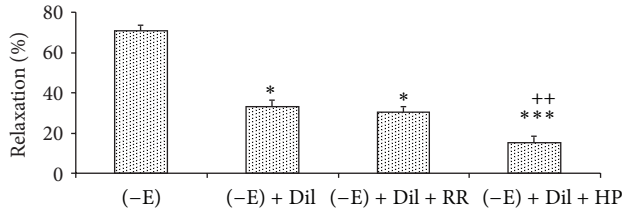

Figure 4: Effect of *Nigella sativa* seed extract (14 mg/mL) on endothelium-denuded rat aortic rings (−E) contracted with PE (10^{-6} M), in the presence of diltiazem (10^{-5} M) (−E + Dil), after ruthenium red (10^{-5} M) (−E + Dil + RR) or heparin (50 mg/L) (−E + Dil + HP) pretreatment. Data are expressed as mean ± S.E.M. ($n = 8$). $^{*}P < 0.05$, $^{***}P < 0.001$ compared to −En; $^{++}P < 0.01$ compared to −E + Dil.

with subsequent contraction by PE showed that diltiazem attenuated *N. sativa*-induced vasorelaxation in concentration of 14 mg/mL and RR did not change this reduction; however, heparin significantly diminished this effect of the extract (Figure 4).

3.5. Effect of N. sativa on K^+ Channels. 30 min preincubation of intact aortic rings with glibenclamide or TEA with a subsequent contraction by PE showed glibenclamide significantly reduced *N. sativa*-induced relaxation in all concentrations of extract but TEA reduced this relaxative effect only in concentrations of 2, 4, and 6 mg/mL (Figure 5).

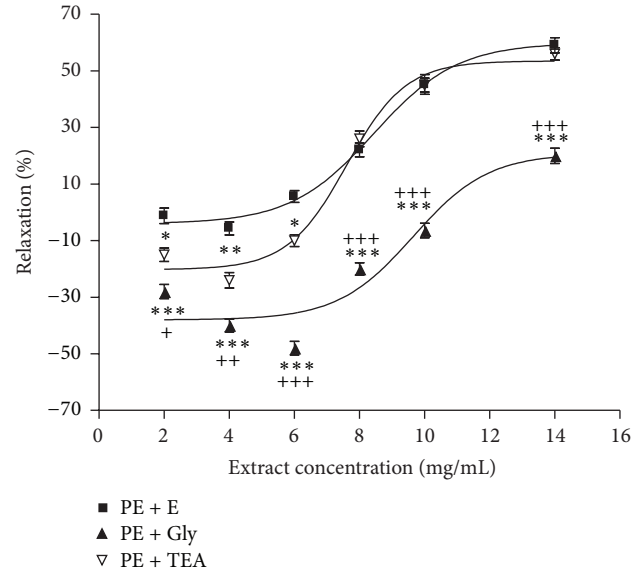

Figure 5: Effect of cumulative concentrations of *Nigella sativa* seed extract (2, 4, 6, 8, 10, and 14 mg/mL) on rat intact aortic rings contracted with PE (10^{-6} M) (PE + E), after pretreatment with glibenclamide (10^{-5} M) (PE + Gly) or tetraethylammonium chloride (5 mM) (PE + TEA). Data are expressed as mean ± S.E.M. ($n = 8$). $^{*}P < 0.05$, $^{**}P < 0.01$, and $^{***}P < 0.001$ compared to PE + E; $^{+}P < 0.05$, $^{++}P < 0.01$, and $^{+++}P < 0.001$ compared to PE + TEA.

4. Discussion

The results of the present study showed that *N. sativa* seed extract elicits vasorelaxation in aortic rings contracted by KCl and PE. Vasocontraction or vasorelaxation could be dependent on endothelium productions [30]. Endothelium through the production of substances such as nitric oxide (NO) and prostacyclin inhibits contraction and by secretion of endothelin can cause contraction in vascular smooth muscle cells (VSMCs) [31, 32].

The lack of variation between the vasorelaxation induced by *N. sativa* seed extract in intact- or denuded-endothelium of aortic rings suggests that this relaxant effect has been exerted on the VSMCs and not on the aorta endothelium (Figure 1).

The inhibitory effect of the extract on PE-induced contraction was not affected by the presence of L-NAME and indomethacin. NO and prostacyclin, the important factors of the vascular relaxant, are derived from the endothelium. Relaxant effect of NO is mainly due to an increase in cyclic guanosine monophosphate (cGMP). L-NAME as an inhibitor of NO production and indomethacin as a nonselective

inhibitor of COX had no effects on the vasorelaxant effect of the extract on PE-induced contractions, which indicated that the relaxant effect of the extract is dependent on neither NO nor prostacyclin (Figure 2). Also, the absence of difference between intact- or denuded-endothelium of aortic rings in extract induced vasorelaxation confirms the independency of this extract's effect on the endothelium. Moreover, the inhibitory effects of the extract on the contraction induced by KCl and PE in intact- and denuded-endothelium of aortic rings were not different which is in agreement with this recent claim.

Ca^{2+} is a critical factor in the excitation-contraction coupling in smooth muscle cells [33, 34]. Influx of extracellular Ca^{2+} through receptor-operated Ca^{2+} channels (ROCCs) and voltage-dependent Ca^{2+} channels (VDCCs) and release of Ca^{2+} from the sarcoplasmic reticulum by activation of 1,4,5 triphosphate inositol (IP_3) and ryanodine receptors (RYR) [35–37] result in increased intracellular Ca^{2+}, which causes contraction. On the other hand, the contraction elicited by KCl mainly results from the influx of extracellular Ca^{2+} induced by depolarization of the cell membrane and subsequent opening of the VDCCs [36].

PE, an adrenoreceptor agonist, causes aortic contraction by Ca^{2+} influx through ROCCs and by release of Ca^{2+} from the sarcoplasmic reticulum [37, 38]. The latter pathway involves PE stimulation of phospholipase C to produce diacylglycerol (DG) and IP3, and subsequently DG activates the light chain of myosin through activation of protein kinase C (PKC), and IP3 induces Ca^{2+} release from the sarcoplasmic reticulum by opening IP3 receptors [37]. In our experiments, *N. sativa* seed inhibited the contraction of aortic rings induced by PE, implying that *N. sativa* seed may inhibit the IP_3 and/or ryanodine receptor-dependent release of intracellular Ca^{2+}, reduce DG-PKC dependent myosin light chain kinase activity, and/or block ROCCs to decrease intracellular Ca^{2+} and relax the aorta. And, the finding that *N. sativa* seed reduced the aortic contraction when PE produced a steady contraction followed by gradual Ca^{2+} input in a Ca^{2+}-free solution, indicated that *N. sativa* seeds blockade of ROCCs to decrease the influx of extracellular Ca^{2+} may be a critical mechanism in relaxing the aorta.

Potassium chloride commonly causes a sustained contraction in isolated arteries. *N. sativa* seed extract had a concentration-dependent relaxant effect on this contraction which may be due to the effects on VDCCs in the VSMCs.

Results from previous studies have shown that the VDCCs are involved in KCl-induced contraction, so the inhibitory effects of vasorelaxant substances which affect this type of contractions may be through blocking VDCCs [33]. The relaxant effects of *N. sativa* seed extract on KCl-induced contraction in aortic rings in presence of cumulative concentrations of calcium are similar to the function of VDCCs in this suppressing effect.

To understand the effect of *N. sativa* seed on extracellular Ca^{2+} influx, experiments were conducted on rings contracted with PE or KCl in a Ca^{2+}-free Krebs solution in which Ca^{2+} was added subsequently. Our data reporting that *N. sativa* seed decreased Ca^{2+}-induced contractions after both PE- and KCl-induced contraction argue for the blockade of both ROCCs and VDCCs as part of the vasodilating effects of *N. sativa* seed. These results were verified by PE- or KCl-induced contraction in the presence of diltiazem as an L-type calcium blocker, in which the vasorelaxant effect of *N. sativa* seed decreased significantly (Figures 3(a) and 3(b)).

Relaxant effect of the extract was reduced significantly in the presence of heparin as an IP_3receptor inhibitor, which shows the importance of IP_3 signaling pathway in the relaxant effect of *N. sativa* seed.

Ruthenium red did not diminish the extract induced vasorelaxation in aortic rings precontracted by PE; thus, the ryanodine receptors did not have any role in the inhibitory effect of the extract.

Besides Ca^{2+} channels, K^+ channels contribute to the regulation of the membrane potential in electrically excitable cells including VSMCs [39]. Membrane hyperpolarization is due to an efflux of K^+ rises of the opening of the K^+ channels in the VSMCs. This effect is followed by the closure of VDCCs, leading to the reduction in Ca^{2+} entry and vasodilation [36]. VSMCs express both K_{ATP} and nonselective K^+ channel [40, 41]. Blockade of the K_{ATP} channel by glibenclamide significantly decreased the relaxant effects of the extract which confirmed the prominent role of these K^+ channels in the *N. sativa* seed induced vasorelaxation. Reduced inhibitory effect of the extract at concentrations of 2, 4, and 6 mg/mL by TEA showed implication of nonselective K^+ channel in the *N. sativa* seed induced vasorelaxation at lower concentrations of extract.

These results suggest that the relaxant effects of *N. sativa* seed extract on the contractions induced by PE and KCl in VSMCs are mediated by different signaling pathways. It seems that the most important mechanisms involved in this vasorelaxation are inhibition of extracellular Ca^{2+} influx, blockade of K_{ATP} channels, and also suppression of IP_3-mediated receptors. The previous study showed that cardiac inhibitory effect of *N. sativa* seed may be due to calcium channel inhibitory or an opening effect for the plant on potassium channels in isolated heart [42].

5. Conclusions

Based on the present data, the use of *N. sativa* seeds may be useful in traditional medicine for hypertension treatment that supports the previous studies which showed the antihypertensive effect of this plant.

Conflict of Interests

The authors declare that there is no conflict of interests regarding the publication of this paper.

Acknowledgment

The authors would like to thank the Research Affairs of Mashhad University of Medical Sciences for their financial support.

References

[1] A. Ahmad, A. Husain, M. Mujeeb et al., "A review on therapeutic potential of *Nigella sativa*: a miracle herb," *Asian Pacific Journal of Tropical Biomedicine*, vol. 3, no. 5, pp. 337–352, 2013.

[2] B. H. Ali and G. Blunden, "Pharmacological and toxicological properties of *Nigella sativa*," *Phytotherapy Research*, vol. 17, no. 4, pp. 299–305, 2003.

[3] M. H. Boskabady, N. Vahedi, S. Amery, and M. R. Khakzad, "The effect of *Nigella sativa* alone, and in combination with dexamethasone, on tracheal muscle responsiveness and lung inflammation in sulfur mustard exposed guinea pigs," *Journal of Ethnopharmacology*, vol. 137, no. 2, pp. 1028–1034, 2011.

[4] F. Yildiz, S. Coban, A. Terzi et al., "Protective effects of *Nigella sativa* against ischemia-reperfusion injury of kidneys," *Renal Failure*, vol. 32, no. 1, pp. 126–131, 2010.

[5] M. Burits and F. Bucar, "Antioxidant activity of *Nigella sativa* essential oil," *Phytotherapy Research*, vol. 14, no. 5, pp. 323–328, 2000.

[6] H. S. Aboul Ezz, Y. A. Khadrawy, and N. A. Noor, "The neuroprotective effect of curcumin and *Nigella sativa* oil against oxidative stress in the pilocarpine model of epilepsy: a comparison with valproate," *Neurochemical Research*, vol. 36, no. 11, pp. 2195–2204, 2011.

[7] N. A. Noor, H. S. Aboul Ezz, A. R. Faraag, and Y. A. Khadrawy, "Evaluation of the antiepileptic effect of curcumin and *Nigella sativa* oil in the pilocarpine model of epilepsy in comparison with valproate," *Epilepsy & Behavior*, vol. 24, no. 2, pp. 199–206, 2012.

[8] P. Landa, P. Marsik, J. Havlik, P. Kloucek, T. Vanek, and L. Kokoska, "Evaluation of antimicrobial and anti-inflammatory activities of seed extracts from six *Nigella* species," *Journal of Medicinal Food*, vol. 12, no. 2, pp. 408–415, 2009.

[9] M. H. Boskabady, B. Shirmohammadi, P. Jandaghi, and S. Kiani, "Possible mechanism(s) for relaxant effect of aqueous and macerated extracts from *Nigella sativa* on tracheal chains of guinea pig," *BMC Pharmacology*, vol. 4, article 3, 2004.

[10] A.-F. M. Abdel-Fattah, K. Matsumoto, and H. Watanabe, "Antinociceptive effects of *Nigella sativa* oil and its major component, thymoquinone, in mice," *European Journal of Pharmacology*, vol. 400, no. 1, pp. 89–97, 2000.

[11] A. Benhaddou-Andaloussi, L. Martineau, T. Vuong et al., "The *in vivo* antidiabetic activity of *Nigella sativa* is mediated through activation of the AMPK pathway and increased muscle Glut4 content," *Evidence-Based Complementary and Alternative Medicine*, vol. 2011, Article ID 538671, 9 pages, 2011.

[12] E. A. Al-Suhaimi, "Hepatoprotective and immunological functions of *Nigella sativa* seed oil against hypervitaminosis A in adult male rats," *International Journal for Vitamin and Nutrition Research*, vol. 82, no. 4, pp. 288–297, 2012.

[13] M. H. Boskabady, R. Keyhanmanesh, and M. A. E. Saadatloo, "Relaxant effects of different fractions from *Nigella sativa* L. on guinea pig tracheal chains and its possible mechanism(s)," *Indian Journal of Experimental Biology*, vol. 46, no. 12, pp. 805–810, 2008.

[14] G. Al-Naqeeb, M. Ismail, and A. S. Al-Zubairi, "Fatty acid profile, α-tocopherol content and total antioxidant activity of oil extracted from *Nigella sativa* seeds," *International Journal of Pharmacology*, vol. 5, no. 4, pp. 244–250, 2009.

[15] A. Mezit, H. Meziti, K. Boudiaf, B. Mustapha, and H. Bouriche, "Polyphenolic profile and antioxidant activities of *Nigella sativa* seed extracts *in vitro* and *in vivo*," *World Academy of Science, Engineering & Technology*, vol. 64, no. 6, pp. 24–32, 2012.

[16] C. Nergiz and S. Otles, "Chemical composition of *Nigella sativa* L. seeds," *Food Chemistry*, vol. 48, no. 3, pp. 259–261, 1993.

[17] O. A. Ghosheh, A. A. Houdi, and P. A. Crooks, "High performance liquid chromatographic analysis of the pharmacologically active quinones and related compounds in the oil of the black seed (*Nigella sativa L.*)," *Journal of Pharmaceutical and Biomedical Analysis*, vol. 19, no. 5, pp. 757–762, 1999.

[18] F. R. Dehkordi and A. F. Kamkhah, "Antihypertensive effect of *Nigella sativa* seed extract in patients with mild hypertension," *Fundamental & Clinical Pharmacology*, vol. 22, no. 4, pp. 447–452, 2008.

[19] M. M. Khattab and M. N. Nagi, "Thymoquinone supplementation attenuates hypertension and renal damage in nitric oxide deficient hypertensive rats," *Phytotherapy Research*, vol. 21, no. 5, pp. 410–414, 2007.

[20] X.-F. Leong, M. R. Mustafa, and K. Jaarin, "*Nigella sativa* and its protective role in oxidative stress and hypertension," *Evidence-Based Complementary and Alternative Medicine*, vol. 2013, Article ID 120732, 9 pages, 2013.

[21] A. Tahraoui, J. El-Hilaly, Z. H. Israili, and B. Lyoussi, "Ethnopharmacological survey of plants used in the traditional treatment of hypertension and diabetes in south-eastern Morocco (Errachidia province)," *Journal of Ethnopharmacology*, vol. 110, no. 1, pp. 105–117, 2007.

[22] R. Mohtashami, M. Amini, H. F. Huseini et al., "Blood glucose lowering effects of *Nigella sativa* L. seeds oil in healthy volunteers: a randomized, double-blind, placebo-controlled clinical trial," *Journal of Medicinal Plants*, vol. 10, no. 39, pp. 90–94, 2011.

[23] A. Zaoui, Y. Cherrah, M. A. Lacaille-Dubois, A. Settaf, H. Amarouch, and M. Hassar, "Diuretic and hypotensive effects of *Nigella sativa* on the spontaneously hypertensive rat," *Therapie*, vol. 55, no. 3, pp. 379–382, 2000.

[24] S. Ahmad and Z. H. Beg, "Elucidation of mechanisms of actions of thymoquinone-enriched methanolic and volatile oil extracts from *Nigella sativa* against cardiovascular risk parameters in experimental hyperlipidemia," *Lipids in Health and Disease*, vol. 12, article 86, 2013.

[25] A. Hamed and A. Alobaidi, "Effect of *Nigella sativa* and *Allium sativum* coadminstered with simvastatin in dyslipidemia patients: a prospective, randomized, double-blind trial," *Anti-Inflammatory & Anti-Allergy Agents in Medicinal Chemistry*, vol. 13, no. 1, pp. 68–74, 2014.

[26] P. M. Le, A. Benhaddou-Andaloussi, A. Elimadi, A. Settaf, Y. Cherrah, and P. S. Haddad, "The petroleum ether extract of *Nigella sativa* exerts lipid-lowering and insulin-sensitizing actions in the rat," *Journal of Ethnopharmacology*, vol. 94, no. 2-3, pp. 251–259, 2004.

[27] A. M. Sabzghabaee, M. Dianatkhah, N. Sarrafzadegan, S. Asgary, and A. Ghannadi, "Clinical evaluation of *Nigella sativa* seeds for the treatment of hyperlipidemia: a randomized, placebo controlled clinical trial," *Medical Archives*, vol. 66, no. 3, pp. 198–200, 2012.

[28] S. C. El-Saleh, O. A. Al-Sagair, and M. I. Al-Khalaf, "Thymoquinone and *Nigella sativa* oil protection against methionine-induced hyperhomocysteinemia in rats," *International Journal of Cardiology*, vol. 93, no. 1, pp. 19–23, 2004.

[29] N. Idris-Khodja and V. Schini-Kerth, "Thymoquinone improves aging-related endothelial dysfunction in the rat mesenteric artery," *Naunyn-Schmiedeberg's Archives of Pharmacology*, vol. 385, no. 7, pp. 749–758, 2012.

[30] M. Félétou and P. M. Vanhoutte, "Endothelial dysfunction: a multifaceted disorder (The Wiggers Award Lecture)," *American Journal of Physiology: Heart and Circulatory Physiology*, vol. 291, no. 3, pp. H985–H1002, 2006.

[31] R. Bello, S. Calatayud, L. Moreno, B. Beltran, E. Primo-Yúfera, and J. Esplugues, "Effects on arterial blood pressure of the methanol extracts from different *Teucrium* species," *Phytotherapy Research*, vol. 11, no. 4, pp. 330–331, 1997.

[32] S. Niazmand, M. Esparham, T. Hassannia, and M. Derakhshan, "Cardiovascular effects of *Teucrium polium* L. extract in rabbit," *Pharmacognosy Magazine*, vol. 7, no. 27, pp. 260–264, 2011.

[33] M. Lohn, M. Furstenau, V. Sagach et al., "Ignition of calcium sparks in arterial and cardiac muscle through caveolae," *Circulation Research*, vol. 87, no. 11, pp. 1034–1039, 2000.

[34] G. C. Wellman and M. T. Nelson, "Signaling between SR and plasmalemma in smooth muscle: sparks and the activation of Ca^{2+}-sensitive ion channels," *Cell Calcium*, vol. 34, no. 3, pp. 211–229, 2003.

[35] M. S. Imtiaz, C. P. Katnik, D. W. Smith, and D. F. van Helden, "Role of voltage-dependent modulation of store Ca^{2+} release in synchronization of Ca^{2+} oscillations," *Biophysical Journal*, vol. 90, no. 1, pp. 1–23, 2006.

[36] M. T. Nelson and J. M. Quayle, "Physiological roles and properties of potassium channels in arterial smooth muscle," *American Journal of Physiology: Cell Physiology*, vol. 268, no. 4, part 1, pp. C799–C822, 1995.

[37] K. S. Thorneloe and M. T. Nelson, "Ion channels in smooth muscle: regulators of intracellular calcium and contractility," *Canadian Journal of Physiology and Pharmacology*, vol. 83, no. 3, pp. 215–242, 2005.

[38] J. G. McCarron, K. N. Bradley, D. MacMillan, and T. C. Muir, "Sarcolemma agonist-induced interactions between InsP_3 and ryanodine receptors in Ca^{2+} oscillations and waves in smooth muscle," *Biochemical Society Transactions*, vol. 31, no. 5, pp. 920–924, 2003.

[39] E. A. Ko, J. Han, I. D. Jung, and W. S. Park, "Physiological roles of K^+ channels in vascular smooth muscle cells," *Journal of Smooth Muscle Research*, vol. 44, no. 2, pp. 65–81, 2008.

[40] S. F. Côrtes, B. A. Rezende, C. Corriu et al., "Pharmacological evidence for the activation of potassium channels as the mechanism involved in the hypotensive and vasorelaxant effect of dioclein in rat small resistance arteries," *British Journal of Pharmacology*, vol. 133, no. 6, pp. 849–858, 2001.

[41] W. F. Jackson, "Ion channels and vascular tone," *Hypertension*, vol. 35, no. 1, part 2, pp. 173–178, 2000.

[42] M. H. Boskabady, M. N. Shafei, and H. Parsaee, "Effects of aqueous and macerated extracts from *Nigella sativa* on guinea pig isolated heart activity," *Pharmazie*, vol. 60, no. 12, pp. 943–948, 2005.

Hindawi Publishing Corporation
BioMed Research International
Volume 2014, Article ID 129593, 9 pages
http://dx.doi.org/10.1155/2014/129593

Research Article

Haemodynamic Monitoring in the Intensive Care Unit: Results from a Web-Based Swiss Survey

Nils Siegenthaler,[1,2] Raphael Giraud,[1] Till Saxer,[1] Delphine S. Courvoisier,[3] Jacques-André Romand,[2] and Karim Bendjelid[1,2]

[1] *Intensive Care Unit, Department of Anaesthesiology, Pharmacology and Intensive Care, University Hospitals of Geneva, 4 Rue Gabrielle-Perret-Gentil, 1211 Geneva 14, Switzerland*
[2] *Faculty of Medicine, University of Geneva, 4 Rue Gabrielle-Perret-Gentil, 1211 Geneva 14, Switzerland*
[3] *Division of Clinical Epidemiology (Biostatistics), University Hospitals of Geneva, 4 Rue Gabrielle-Perret-Gentil 1211 Geneva 14, Switzerland*

Correspondence should be addressed to Nils Siegenthaler; nils.siegenthaler@hcuge.ch

Received 5 February 2014; Accepted 25 March 2014; Published 22 April 2014

Academic Editor: Bruno Levy

Background. The aim of this survey was to describe, in a situation of growing availability of monitoring devices and parameters, the practices in haemodynamic monitoring at the bedside. *Methods*. We conducted a Web-based survey in Swiss adult ICUs (2009-2010). The questionnaire explored the kind of monitoring used and how the fluid management was addressed. *Results*. Our survey included 71% of Swiss ICUs. Echocardiography (95%), pulmonary artery catheter (PAC: 85%), and transpulmonary thermodilution (TPTD) (82%) were the most commonly used. TPTD and PAC were frequently both available, although TPTD was the preferred technique. Echocardiography was widely available (95%) but seems to be rarely performed by intensivists themselves. Guidelines for the management of fluid infusion were available in 45% of ICUs. For the prediction of fluid responsiveness, intensivists rely preferentially on dynamic indices or echocardiographic parameters, but static parameters, such as central venous pressure or pulmonary artery occlusion pressure, were still used. *Conclusions*. In most Swiss ICUs, multiple haemodynamic monitoring devices are available, although TPTD is most commonly used. Despite the usefulness of echocardiography and its large availability, it is not widely performed by Swiss intensivists themselves. Regarding fluid management, several parameters are used without a clear consensus for the optimal method.

1. Introduction

Adequate haemodynamic assessment and management are cornerstones for the management of critically ill patients [1, 2]. However, the use of haemodynamic monitoring at the bedside faces many challenges. First, the methods, devices, and parameters available for haemodynamic monitoring have evolved over the last 30 years, and this may be responsible for the large heterogeneity in the types of techniques used by clinicians in various intensive care units (ICUs). Second, the proper use of these monitoring devices and the interpretation of the values displayed may be difficult and require a high level of knowledge and skill, resulting in heterogeneous interventions [3, 4]. Third, advanced methods for haemodynamic monitoring, per se, have not been associated with an improvement in patient survival [5–9], unless they are coupled with early and clinically relevant therapeutic strategies [1]. Consequently, the integration of measured parameters into the therapeutic strategy may also vary between physicians and ICUs. Finally, in some situations, the macrocirculation may be decoupled from the microcirculation [10, 11], thereby reducing the effectiveness of haemodynamic optimisation based only on commonly measured macrocirculatory parameters and complicating the haemodynamic management of critically ill patients.

Considerable heterogeneity in the availability and practice of haemodynamic monitoring exists at the bedside across

clinicians, ICUs, and countries, although studies investigating this issue are scarce [3, 12–15]. However, this type of study could allow for tailored training in intensive care and could help to adapt the clinical guidelines according to the techniques available. The goal of this study was, thus, to generate a first description of the availability and the use of bedside haemodynamic monitoring in Swiss ICUs, especially for the management of volume expansion.

2. Methods

This study was designed as a self-reported, internet-based survey. The questionnaire consisted of 36 multiple-choice questions (http://www.genevahemodynamic.com/) (research/swisshaemodynamicsurvey). Apart from general questions the questions investigated two topics: the monitoring techniques used by Swiss intensivists (16 questions) and the method by which Swiss intensivists address fluid management (8 questions). Advanced haemodynamic monitoring was defined as the use of techniques that allow the estimation of cardiac output. In questions reporting frequency of use, clinicians rate their utilisation on a scale from 1 to 10 (1 = never, 10 = in every case). In questions qualifying a device, clinicians were asked to scale their replies from 0 to 5 (0 = "the worst," 5 = "the best"). The questionnaire was first evaluated by two independent physicians specialised in critical haemodynamic care and then tested on 15 Swiss intensivists to improve the formulation of the questions.

We selected all adult ICUs (medical, surgical, and interdisciplinary) that conform to the recommendation of the Swiss Society of Intensive Medicine 2008-2009 (77 ICUs). We sent the questionnaire via e-mail to the physician responsible for the selected ICUs and/or to physicians working in the same centre that could be identified. The contacted physician could then decide to reply and/or to forward the questionnaire to some of his colleagues in the same ICU. To increase the return rate, the questionnaire was sent a second time to nonresponders. Replies were collected during the period from 2009 to 2010. As this survey was based on voluntary participation with an information disclosure, an ethics committee did not review this study.

2.1. Statistical Analysis. Data were analysed using R 2.14.1. We analysed the responses either at the physician level or the ICU level. Responses analysed at the physician level consider each physician's answer as having equivalent weight. Thus, ICUs with more responding physicians contributed more responses. To give equal weight to all ICUs, we also calculated the responses at the ICU level by determining the opinion of each centre, corresponding to the majority of replies in the centre, and then averaging the opinion of all ICUs. To determine the contribution of the number of replies per ICU to the results, we analysed the correlation between the responses averaged across ICUs versus that averaged across individual physicians. Regarding the description of replies concerning parameters that require a specific technique (e.g., extravascular lung water (EVLW), which can only be measured with the PiCCO device (PULSION Medical systems; Munich, Germany)), we selected only those replies from physicians working in ICUs where this device was available. To evaluate the degree of consensus for each question, we arbitrarily determined that a response rate greater than 65% for a single question represented a strong consensus, a response rate between 55 and 64% indicated a weak consensus, and a response rate less than 55% represented no consensus. For multiple-choice questions, a positive consensus was reached if the physicians who participated included the proposition, and a negative consensus was reached if the physicians who participated did not include the proposition.

3. Results

3.1. Descriptive Analysis. We obtained 130 replies from 55 ICUs (71.4%) from a total of 77 Swiss adult ICUs referenced during the study period. The median response rate was 1 per ICU (1–20 replies per ICU; mean response rate: 2.3; interquartile range: 1). Among the participating intensivists, 73% (n (Intensivists) = 95/130) declared to be specialists in intensive care medicine (certification from the Swiss Medical Association). In addition, 62% (n (Intensivists) = 81/130) reported more than 5 years of experience in critical care practice (5–10 years: 25% (n (Intensivists) = 33/130), >10 years: 37% (n (Intensivists) = 48/130)). The correlation between the replies reported by individual physicians and by ICUs was very high ($r = 0.997$, $P < 0.0001$), suggesting that the response rate of individual centres (i.e., the "size" of the ICU) did not influence the results.

3.2. Availability and Use of Haemodynamic Monitoring in Swiss ICUs. In Switzerland, intensivists reported frequent use of advanced haemodynamic monitoring during the shock state; for example, during cardiogenic and septic shock, the mean rate of use was 8.3/10 and 8.1/10, respectively. Three devices were most commonly available: echocardiography (95% (n (ICU) = 52/55)), right heart thermodilution with pulmonary artery catheter (PAC: 85% (n (ICU) = 47/55)), and transpulmonary thermodilution (TPTD) with the PiCCO device (82% (n (ICU) = 45/55)). FloTrac, oesophageal Doppler monitoring, and LiDCO were not widely available (20% (n (ICU) = 11/55), 13% (n (ICU) = 7/55), and 9% (n (ICU) = 5/55), resp.). Notably, in 67% (n (ICU) = 37/55) of Swiss ICUs, TPTD and PAC were both available, although TPTD was reported to be more commonly used (Figure 1). In ICUs where PAC was reported to be most frequently used, 78% (n (ICU) = 7/9) were leading centres recommended for critical care teaching (Swiss Medical Association class A ICUs).

Echocardiography was available in most ICUs (Figure 2) but was not routinely used, and in most cases, echocardiography was not performed by the intensivists themselves. In contrast to this result, a large majority of participating physicians considered that Swiss intensivists should be able to perform echocardiography in ICUs for haemodynamic management.

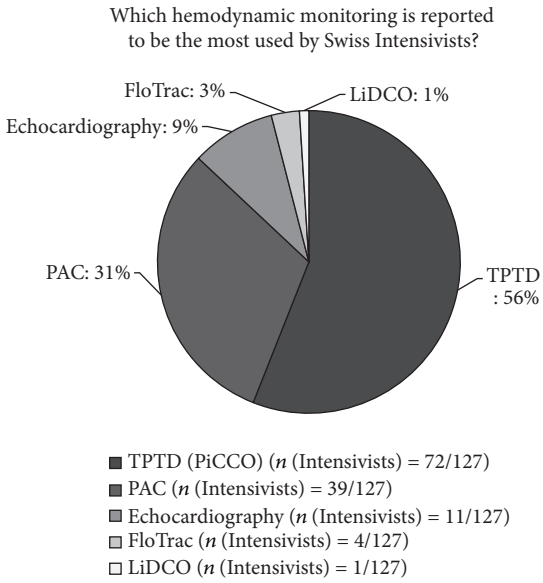

Figure 1: Haemodynamic monitoring techniques reported to be most commonly used by intensive care physicians. TPTD: transpulmonary thermodilution, PAC: pulmonary artery catheter. The results are presented as the mean number of replies from Swiss intensivists (in %) to the total number of intensivists who replied to the question (*n* (Intensivists)/total replies).

3.3. Clinically Oriented Selection of Haemodynamic Monitoring. The method considered optimal for haemodynamic monitoring varied according to the clinical situation (Figure 3). During cardiogenic shock, Swiss intensivists considered monitoring with PAC or echocardiography equally good and reported these two monitoring techniques superior to other techniques. During septic shock, intensivists considered TPTD to be the most appropriate monitoring technique. Finally, during acute respiratory distress syndrome (ARDS), intensivists considered TPTD and PAC to be the best techniques; interestingly, these two techniques were considered to be equivalent in this situation.

3.4. Parameters Used with TPTD and the PiCCO Device. Among all parameters associated with the PiCCO device, only cardiac index, EVLW, global end-diastolic volume (GEDV), stroke volume variation (SVV), and intrathoracic blood volume (ITBV) were used by a majority of clinicians (Figure 4).

3.5. Haemodynamic Parameters Used by Swiss Intensivists for Fluid Management. For the management of fluid therapy, guidelines were available in less than half of ICUs (45%, *n* (ICU) = 25/55). The mean arterial blood pressure targeted by the majority of intensivists was between 60 and 65 mmHg (40–50 mmHg: 2% (*n* (Intensivists) = 3/130), 50–55 mmHg: 2% (*n* (Intensivists) = 3/130), 55–60 mmHg: 8% (*n* (Intensivists) = 10/130), 60–65 mmHg: 56% (*n* (Intensivists) = 73/130), and 65–70 mmHg: 27% (*n* (Intensivists) = 35/130)

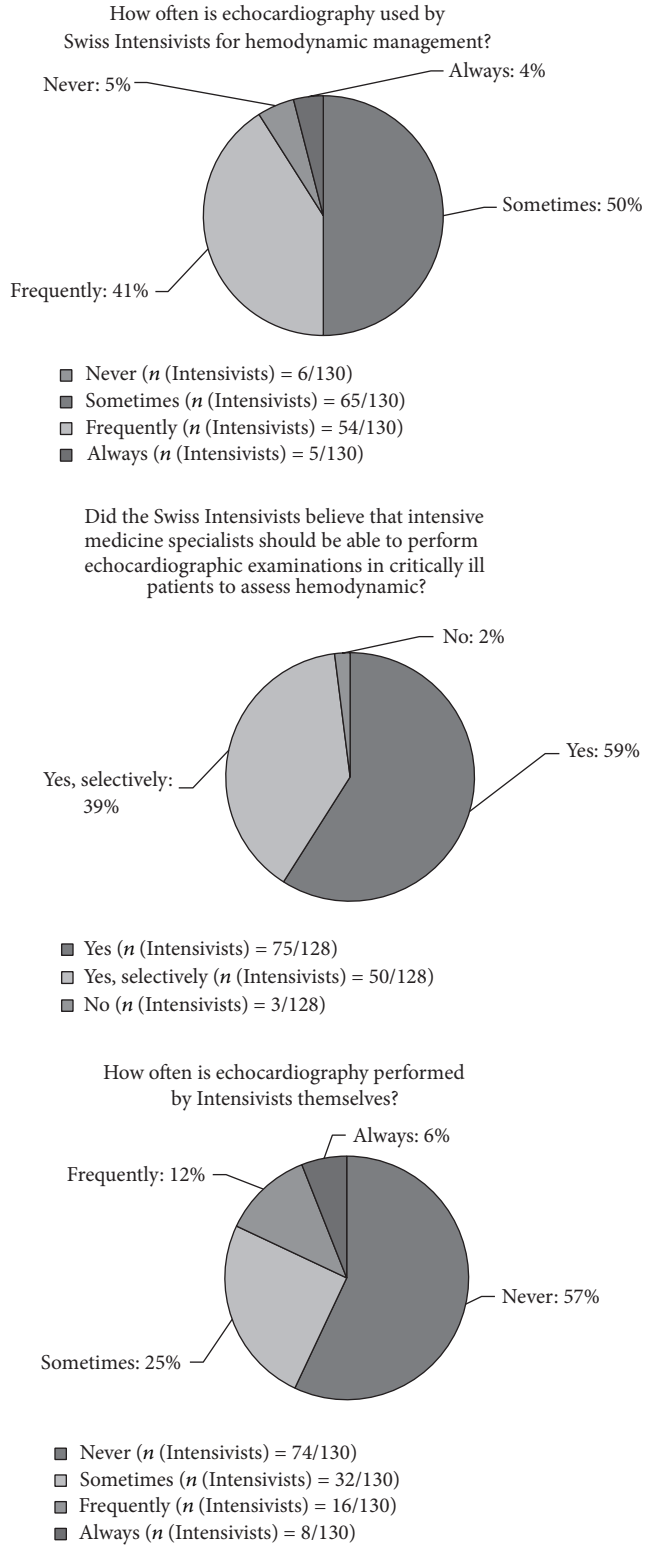

Figure 2: The use of echocardiography by intensivists. The results are presented as the mean number of replies from Swiss intensivists (in %) to the total number of intensivists who replied to the question (*n* (Intensivists)/total replies).

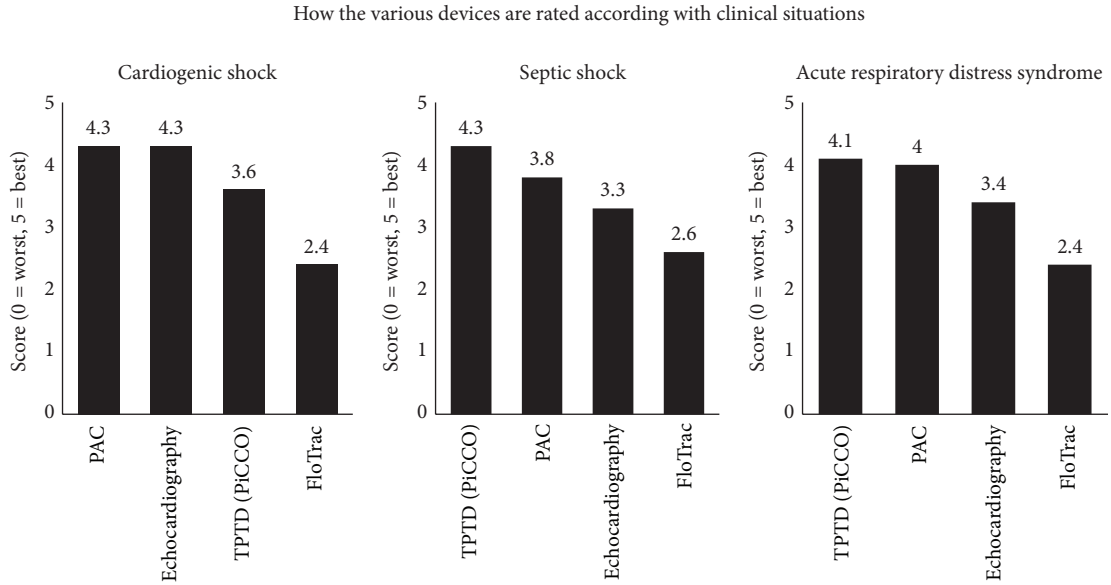

Figure 3: Evaluation of various devices by intensivists according to the clinical situation. Devices were rated on a scale from 1 "worst" to 5 "best." TPTD: transpulmonary thermodilution, PAC: pulmonary artery catheter.

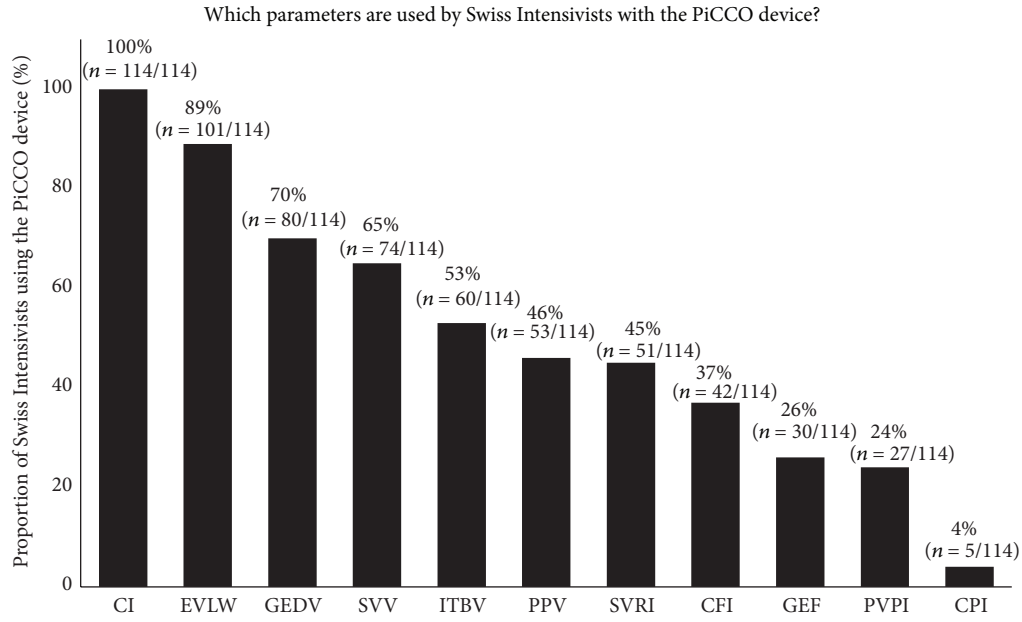

Figure 4: The use of various parameters available with transpulmonary thermodilution (PiCCO) by Swiss intensivists. CFI: cardiac function index; CI: cardiac index; CPI: cardiac power index; EVLW: extravascular lung water; GEDV: global end-diastolic volume; GEF: global ejection fraction; ITBV: intrathoracic blood volume; PPV: pulse pressure variation; PVPI: pulmonary vascular permeability index; SVRI: systemic vascular resistance index; SVV: stroke volume variation. The results of this multiple-choice question are presented as the mean number of replies from Swiss intensivists (in %) to the total number of intensivists who replied to the question (n (Intensivists)/total replies).

and 70–75 mmHg: 5% (n (Intensivists) = 6/130)). For the prediction of fluid responsiveness (Table 1), Swiss intensivists mainly used dynamic indices (i.e., indices which vary with respiration, e.g., pulse pressure variation, PPV), the passive leg rising manoeuvre (PLR), and/or echocardiographic parameters. Static parameters (i.e., parameters which did not varies with respiration) such as central venous pressure (CVP) and pulmonary artery occlusion pressure (PAOP) were also used by a significant number of intensivists (Table 1); however, when these methods were used, most intensivists considered that only low values indicated a state of preload dependency (CVP <

5 mmHg: 42% (n (Intensivists) = 55/130), CVP < 10 mmHg: 19% (n (Intensivists) = 25/130), CVP < 15 mmHg: 2% (n (Intensivists) = 2/130), and none: 37% (n (Intensivists) = 48/130); PAOP < 5 mmHg: 21% (n (Intensivists) = 24/114), PAOP < 10 mmHg: 31% (n(Intensivists) = 35/114), and PAOP < 15 mmHg: 21% (n (Intensivists) = 24/114), PAOP < 20 mmHg: 3% (n (Intensivists) = 3/114) and None: 25% (n (Intensivists) = 28/114)). On the other hand, to assess the possibility of further fluid filling, intensivists use different parameters, mainly EVLW and PAOP, according to the technique available (TPTD versus PAC).

3.6. Evaluation of Consensus. The results are displayed in Table 2.

4. Discussion

The present self-reported internet-based survey investigated the types of haemodynamic monitoring available in ICUs of a European country and reported how this monitoring is used at the bedside. We observed that, in Swiss ICUs, advanced haemodynamic monitoring is frequently used at the bedside. Among the techniques accessible, echocardiography, TPTD, and/or PAC were largely available in most ICUs; moreover, in a large majority of ICUs, both PAC and TPTD with PiCCO were available, but TPTD seemed to be the most frequently used technique. Echocardiography was largely available and considered a good technique in various situations, although this examination is generally not performed by intensivists themselves. Finally, for assessing fluid responsiveness, intensivists seemed to prefer dynamic indices instead of static parameters (Tables 1 and 2).

Limited data exists concerning the use of haemodynamic monitoring in critically ill patients at bedside across countries, but, as suggested by Torgersen et al., there seems to be considerable heterogeneity in the management and in the use of haemodynamic monitoring across centres and countries [15]. In our study, we observed a large utilisation of invasive haemodynamic monitoring in patients with shock. This practice is in accordance with the acknowledged importance of early and adequate haemodynamic optimisation in critically ill patients with shock [16]. In other European countries, during septic shock, Torgersen et al. reported that almost all responders asserted the cardiac output, even if the rate of invasive haemodynamic monitoring use was not reported. The fact that, in our country, echocardiography monitoring is less used may explain the higher rate of invasive technique observed in the present survey. Also, we may speculate that the skill and medical education of clinicians as well as the hospitals resources have a big influence on the way the critically ill patients are monitored.

The availability in a single centre of several types of haemodynamic monitoring techniques may allow the clinician, taking into account the specificities of each technique, to adapt the monitoring used in accordance with the clinical situation. However, as suggested by numerous previous studies [3, 14, 17], this implies the need for major training to ensure the proper use of different techniques and the adequate interpretation of measured parameters to correctly guide therapeutic interventions. Our observation of a large use of diverse techniques suggests that it may be interesting

Table 1: Haemodynamic parameters used by Swiss intensivists for fluid management.

Parameters	Average of replies by Swiss intensivists
Parameters used to predict fluid responsiveness	
PPV	59% (n = 76/130)
PLR	54% (n = 70/130)
Echocardiography	54% (n = 70/130)
SVV	48% (n = 62/130)
GEDV**	46% (n = 51/112)
CO	45% (n = 59/130)
$ScvO_2$	43% (n = 56/130)
Arterial pressure	42% (n = 54/130)
PAOP*	39% (n = 44/114)
EVLW**	33% (n = 37/111)
SvO_2*	32% (n = 36/113)
CVP	31% (n = 40/130)
RVVC	26% (n = 34/130)
ITBV**	21% (n = 24/112)
Global fluid balance	15% (n = 19/130)
Diameter of inferior vena cava	12% (n = 15/130)
Parameters used to stop further fluid infusion	
EVLW**	52% (n = 58/112)
PAOP*	51% (n = 58/114)
PPV	43% (n = 55/129)
GEDV**	42% (n = 47/112)
Lactate	42% (n = 54/129)
Echocardiography	38% (n = 49/128)
PLR	38% (n = 49/129)
ITBV**	30% (n = 34/112)
Other clinical parameters	27% (n = 35/129)
Oxygen requirement	26% (n = 33/129)
Normal CO	23% (n = 30/129)
$ScvO_2$	19% (n = 24/129)
SvO_2*	13% (n = 15/113)
High CO	6% (n = 8/129)

The results are presented as the mean response from Swiss intensivists in %, with the number of replies to the total number of intensivists responding to the question (n Intensivists/total replies). For parameters requiring a specific technique, only the replies from ICUs where this technique was available were selected: pulmonary artery catheter (PAC) available: indicated by*; transpulmonary thermodilution with PiCCO available: indicated by**. CO: cardiac output; CVP: central venous pressure; EVLW: extravascular lung water; GEDV: global end-diastolic volume; ITBV: intrathoracic blood volume; PAOP: pulmonary artery occlusion pressure; PLR: passive leg rising test; PPV: pulse pressure variation; RVVC: respiratory variation of inferior vena cava; $ScvO_2$: central venous blood saturation; SVV: stroke volume variation; SvO_2: mixed venous blood saturation.

Table 2: Consensus in the replies from Swiss intensivists concerning haemodynamic monitoring.

Strong consensus
On the availability of echocardiography, pulmonary artery catheter, or PiCCO in Swiss ICUs
On the nonavailability of FloTrac, oesophageal Doppler monitoring, or LiDCO in Swiss ICUs
On the use of echocardiography for haemodynamic monitoring
On the interest of Swiss intensivists to be able to perform echocardiography themselves in critically ill patients
On the use of cardiac index, EVLW, GEDV, or SVV when using the PiCCO device
On the nonuse of GEF, PVPI, or CPI when using the PiCCO device
On the nonuse of EVLW, SVO_2, CVP, RVVC, ITBV, global fluid balance, or the diameter of inferior vena cava for predicting fluid responsiveness
On the nonuse of ITBV, other clinical parameters, oxygen requirement, normal cardiac output, $ScVO_2$, SVO_2, or high cardiac output to stop further fluid infusion
Weak consensus
On the preference for the use of TPTD in haemodynamic monitoring
That Swiss intensivists do not perform themselves echocardiography
On the use of ITBV when using the PiCCO device
On the nonuse of CFI when using the PiCCO device
For a mean arterial blood pressure target between 60–65 mmHg
On the use of PPV for predicting fluid responsiveness
On the nonuse of cardiac output, $ScVO_2$, arterial pressure, or PAOP to predict fluid responsiveness
No consensus
On the frequency of use of echocardiography for haemodynamic monitoring
On the use of PPV or SVRI when using the PiCCO device
On the threshold of CVP that may indicate the need for fluid infusion
On the threshold of PAOP that may indicate the need for fluid infusion
On the use of PLR, echocardiography, SVV, or GEDV for predicting fluid responsiveness
On the use of EVLW or PAOP to stop further fluid infusion

A strong consensus was defined as a response rate greater than 65% for a single question; a weak consensus was defined as a response rate from 55–64%; and no consensus was declared when the response rate was under 55%. CVP: central venous pressure; EVLW: extravascular lung water; GEDV: global end-diastolic volume; ITBV: intrathoracic blood volume; PAOP: pulmonary artery occlusion pressure; PLR: passive leg rising test; PPV: pulse pressure variation; RVVC: respiratory variation of inferior vena cava; $ScvO_2$: central venous blood saturation; SVV: stroke volume variation; SvO_2: mixed venous blood saturation.

to assess the clinical and cost effectiveness of each technique in the management of critically ill patients. If further studies confirmed the availability of multiple devices in each ICU, a national program for teaching, maintenance of skills and regular evaluation of knowledge could be implemented to optimise the resources needed and maintain a high quality of use of these specific techniques. Indeed, in Switzerland there are no clear guidelines, specific recommendation, or nationally structured formation about the haemodynamic monitoring of patients in shock state. And the absence of any consensus on this issue makes the Swiss intensivist clinical practice associated to the local medical tradition.

Furthermore, as observed in other studies [9, 15], we noticed in our study that intensivists seemed to favour the use of new monitoring devices, such as TPTD with PiCCO, instead of the "historical" PAC method. The only exception concerned the leading centres involved in critical care teaching (Swiss Medical Association class A ICUs), where PAC remains largely used. Interestingly, in our study TPTD with PiCCO is considered by intensivists to be equivalent to PAC during ARDS and superior during septic shock, whereas during cardiogenic shock, PAC and echocardiography are considered the most appropriate techniques. Our results regarding the use of TPTD with PiCCO during septic shock are in accordance with the typical practice in European countries, in which most clinicians (65.5%) report the use of TPTD for the measurement of cardiac output in this situation [15]. Our observation of the clinical preference to use PAC or echocardiography during cardiogenic shock seems also in accordance with the study by Trof et al. comparing volume-limited (monitored by TPTD) versus pressure-limited (monitored by PAC) haemodynamic management in septic and nonseptic shock [18]. In this study, the authors did not observe any difference in ventilators-free days, lengths of stay, organ failures, and mortality between the two modes of haemodynamic monitoring. However, in the nonseptic shock patients, TPTD based algorithm (EVLW < 10 mL/kg, GEDV < 850 mL/m^2) resulted in more days on mechanical ventilation and ICU length of stay compared with PAC (PAOP < 18–20 mmHg).

Interestingly in our study, during ARDS the monitoring with TPTD (PiCCO) is considered, by the clinicians, to be equivalent with the monitoring with PAC. This observation may likely represent one of the characteristics of the evolution

in haemodynamic monitoring in critically ill patients. Traditionally, during ARDS, PAC has demonstrated certain advantages. First, the measurement of PAOP allows the exclusion of left ventricular dysfunction (PAOP of less than 18 mmHg), a criterion required for the diagnosis and definition of ARDS [19]. Second, PAC allows the evaluation of pulmonary artery hypertension, associated with the development of right ventricular failure [20], and enables the adjustment of pulmonary vasodilators (e.g., inhaled nitric oxide). Thus, during ARDS, other techniques such as echocardiography must be combined with TPTD to assess right ventricular function and pulmonary circulation. However, during ARDS, monitoring with TPTD may have benefits. For example, EVLW that was indexed to predicted body weight [21, 22] may allow a more precise evaluation of lung oedema than chest radiograph, where the presence of a bilateral infiltrate, which can be related to other diseases besides pulmonary oedema, may be difficult to identify. Moreover, EVLW may also be considered as a means to manage fluid balance during ARDS [21].

Echocardiography is a noninvasive advanced haemodynamic technique useful in the management of critically ill patients [23, 24]. In our study, we observed that even if echocardiography was widely available and considered to be reliable (Figure 3), this technique was not regularly used by intensivists themselves. This observation suggests that echocardiography is performed mainly by cardiologists in specific situations rather than as a true technique of haemodynamic monitoring used to regularly assess the evolution of the patient and the effect of treatment. However, we observed that a large majority of intensivists (98%) demonstrated a desire to become more independent in the practice of echocardiography in the critical care setting. This situation may be specific to countries where no specific echocardiographic training is intended for intensivists and where no specific descriptions of the skills required to practice this examination are accepted, as it is the case in Switzerland. In response to this situation, according to the will of clinicians and following the evolution of education and training in other European countries [24], the number of certified technicians and improved descriptions of the skills required to practice echocardiography in Swiss ICUs are growing [25, 26].

Among the difficulties associated with the use of haemodynamic monitoring, individual differences in the interpretation of parameters and related interventions could be significant. Apart from a high level of training, this issue may be improved by the implementation of clinical guidelines. However, as highlighted by the present survey, in most ICUs, guidelines for fluid resuscitation are not available. This underutilisation of guidelines during fluid resuscitation likely reflects the complexity of this issue and the lack of consensus on validated indices available to adequately predict fluid responsiveness in the large population of critically ill patients. Indeed, we failed to detect a strong consensus on the use of these indices among Swiss intensivists, although we did observe some consensus related to the nonuse of various parameters (Table 2). In the assessment of preload dependency, a slight majority of intensivists reported to use mainly dynamic indices (PPV), volumetric indices estimated with the TPTD technique (GEDV), or echocardiography, although a strong consensus was lacking. Notably, despite the amount of clinical data supporting the uselessness of static parameters (CVP, PAOP) as markers of fluid responsiveness [27, 28], a significant proportion of intensivists still use these static indices. Our reported utilisation of PAOP is comparable to that of other European countries, where 28.3% of clinicians still use PAOP to guide haemodynamic management during septic shock [15]. However, it should be noted that when these static measurements are used, intensivists consider only low values as a sign of hypovolemia-preload dependency, although there is no consensus as to the precise threshold. Similarly, to evaluate the safety of infusing further fluid, a slight majority of intensivists reported to use EVLW or PAOP, according to the technique available, as techniques to interrupt volume expansion, again without a consensus as to the preferred technique.

4.1. Limitations. First, it was not possible to determine the exact number of intensivists working in Switzerland and therefore to determine the true significance of our results. However, the response rate from all Swiss ICUs concerning the present survey was high, with the majority of responders experienced in intensive care medicine. Secondly, haemodynamic monitoring requires devices, accessories, consumables, and staff education that have financial implications. Indeed, economic characteristics of the institution and health economics of the country may influence the practice at bedside. Third, even if this survey is related to the 2009-2010 period, we consider that our results represent the actual evolution in the practice of haemodynamic monitoring at the bedside, as no major changes in hemodynamic monitoring practice and guidelines occur recently. Fourth, in order to describe the degree of consensus or agreement about the practice of haemodynamic monitoring, we used a simple method which, even if not well validated, allows to identify the "general opinion" of clinicians. Lastly, as demonstrated by a previous study [29], the difference between the perception of a practice and the real life practice at the bedside may be significant. Thus, our results are only indicative of self-reported practice in haemodynamic monitoring and only further prospective observational studies will be able to more precisely investigate this subject.

4.2. Conclusion. In our survey of haemodynamic monitoring in Swiss ICUs, we found that various types of monitoring techniques are available in ICUs, among which the "historical" PAC method seems to be progressively replaced by new monitoring techniques, such as TPTD.

As an alternative or complementary technique, echocardiography, which is largely available in Swiss ICUs, was not frequently used by intensivists themselves to regularly assess the haemodynamic state of critically ill patients. Concerning the utilisation of haemodynamic monitoring to guide the complex management of fluid therapy, clinical guidelines are underutilised and intensivists inconsistently refer essentially to dynamic indices of preload.

Conflict of Interests

Dr. Karim Bendjelid discloses that he was a consultant for Edwards Lifesciences Corporation during the period of this study (2009-2010). The other authors declare that they have no competing interests.

Acknowledgment

The authors wish to thank Professor Laurent Brochard for his advice and assistance in correcting the paper.

References

[1] E. Rivers, B. Nguyen, S. Havstad et al., "Early goal-directed therapy in the treatment of severe sepsis and septic shock," *The New England Journal of Medicine*, vol. 345, no. 19, pp. 1368–1377, 2001.

[2] N. Lees, M. Hamilton, and A. Rhodes, "Clinical review: goal-directed therapy in high risk surgical patients," *Critical Care*, vol. 13, no. 5, article 231, 2009.

[3] A. Gnaegi, F. Feihl, and C. Perret, "Intensive care physicians' insufficient knowledge of right-heart catheterization at the bedside: time to act?" *Critical Care Medicine*, vol. 25, no. 2, pp. 213–220, 1997.

[4] M. Jain, M. Canham, D. Upadhyay, and T. Corbridge, "Variability in interventions with pulmonary artery catheter data," *Intensive Care Medicine*, vol. 29, no. 11, pp. 2059–2062, 2003.

[5] A. F. Connors Jr., T. Speroff, N. V. Dawson et al., "The effectiveness of right heart catheterization in the initial care of critically ill patients," *Journal of the American Medical Association*, vol. 276, no. 11, pp. 889–897, 1996.

[6] M. R. Shah, V. Hasselblad, L. W. Stevenson et al., "Impact of the pulmonary artery catheter in critically ill patients: meta-analysis of randomized clinical trials," *Journal of the American Medical Association*, vol. 294, no. 13, pp. 1664–1670, 2005.

[7] S. Harvey, D. Young, W. Brampton et al., "Pulmonary artery catheters for adult patients in intensive care," *Cochrane Database of Systematic Reviews*, vol. 3, Article ID CD003408, 2006.

[8] C. Binanay, R. M. Califf, V. Hasselblad et al., "Evaluation study of congestive heart failure and pulmonary artery catheterization effectiveness: the ESCAPE trial," *JAMA*, vol. 294, no. 13, pp. 1625–1633, 2005.

[9] S. Harvey, K. Stevens, D. Harrison et al., "An evaluation of the clinical and cost-effectiveness of pulmonary artery catheters in patient management in intensive care: a systematic review and a randomised controlled trial," *Health Technology Assessment*, vol. 10, no. 29, pp. 1–133, 2006.

[10] D. De Backer, J. Creteur, J.-C. Preiser, M.-J. Dubois, and J.-L. Vincent, "Microvascular blood flow is altered in patients with sepsis," *American Journal of Respiratory and Critical Care Medicine*, vol. 166, no. 1, pp. 98–104, 2002.

[11] N. Siegenthaler, R. Giraud, V. Piriou, J. A. Romand, and K. Bendjelid, "Microcirculatory alterations in critically ill patients: pathophysiology, monitoring and treatments," *Annales Francaises d'Anesthesie et de Reanimation*, vol. 29, no. 2, pp. 135–144, 2010.

[12] J. Boldt, M. Lenz, B. Kumle, and M. Papsdorf, "Volume replacement strategies on intensive care units: results from a postal survey," *Intensive Care Medicine*, vol. 24, no. 2, pp. 147–151, 1998.

[13] M. Kastrup, A. Markewitz, C. Spies et al., "Current practice of hemodynamic monitoring and vasopressor and inotropic therapy in post-operative cardiac surgery patients in Germany: results from a postal survey," *Acta Anaesthesiologica Scandinavica*, vol. 51, no. 3, pp. 347–358, 2007.

[14] T. J. Iberti, E. P. Fischer, A. B. Leibowitz, E. A. Panacek, J. H. Silverstein, and T. E. Albertson, "A multicenter study of physicians' knowledge of the pulmonary artery catheter," *Journal of the American Medical Association*, vol. 264, no. 22, pp. 2928–2932, 1990.

[15] C. Torgersen, M. W. Dünser, C. A. Schmittinger et al., "Current approach to the haemodynamic management of septic shock patients in European intensive care units: a cross-sectional, self-reported questionnaire-based survey," *European Journal of Anaesthesiology*, vol. 28, no. 4, pp. 284–290, 2011.

[16] R. P. Dellinger, M. M. Levy, J. M. Carlet et al., "Surviving sepsis campaign: international guidelines for management of severe sepsis and septic shock: 2008," *Critical Care Medicine*, vol. 36, no. 1, pp. 296–327, 2008.

[17] I. G. Johnston, R. Jane, J. F. Fraser, P. Kruger, and K. Hickling, "Survey of intensive care nurses' knowledge relating to the pulmonary artery catheter," *Anaesthesia and Intensive Care*, vol. 32, no. 4, pp. 564–568, 2004.

[18] R. J. Trof, A. Beishuizen, A. D. Cornet, R. J. De Wit, A. R. J. Girbes, and A. B. J. Groeneveld, "Volume-limited versus pressure-limited hemodynamic management in septic and nonseptic shock," *Critical Care Medicine*, vol. 40, no. 4, pp. 1177–1185, 2012.

[19] G. R. Bernard, A. Artigas, K. L. Brigham et al., "The American-European Consensus Conference on ARDS: definitions, mechanisms, relevant outcomes, and clinical trial coordination," *American Journal of Respiratory and Critical Care Medicine*, vol. 149, no. 3 I, pp. 818–824, 1994.

[20] M. Monchi, F. Bellenfant, A. Cariou et al., "Early predictive factors of survival in the acute respiratory distress syndrome: a multivariate analysis," *American Journal of Respiratory and Critical Care Medicine*, vol. 158, no. 4, pp. 1076–1081, 1998.

[21] F. Michard, "Bedside assessment of extravascular lung water by dilution methods: temptations and pitfalls," *Critical Care Medicine*, vol. 35, no. 4, pp. 1186–1192, 2007.

[22] D. M. Berkowitz, P. A. Danai, S. Eaton, M. Moss, and G. S. Martin, "Accurate characterization of extravascular lung water in acute respiratory distress syndrome," *Critical Care Medicine*, vol. 36, no. 6, pp. 1803–1809, 2008.

[23] J. Poelaert, "Use of ultrasound in the ICU," *Best Practice and Research: Clinical Anaesthesiology*, vol. 23, no. 3, pp. 249–261, 2009.

[24] A. Vieillard-Baron, M. Slama, B. Cholley, G. Janvier, and P. Vignon, "Echocardiography in the intensive care unit: from evolution to revolution?" *Intensive Care Medicine*, vol. 34, no. 2, pp. 243–249, 2008.

[25] R. Giraud, N. Siegenthaler, D. Tagan, and K. Bendjelid, "Estimation of skills required to practice advanced level of echocardiography in intensive care," *Revue Medicale Suisse*, vol. 7, no. 282, pp. 413–416, 2011.

[26] R. Giraud, N. Siegenthaler, D. Tagan, and K. Bendjelid, "Evaluation of practical skills in echocardiography for intensivists," *Revue Medicale Suisse*, vol. 5, no. 229, pp. 2518–2521, 2009.

[27] K. Bendjelid and J.-A. Romand, "Fluid responsiveness in mechanically ventilated patients: a review of indices used in

intensive care," *Intensive Care Medicine*, vol. 29, no. 3, pp. 352–360, 2003.

[28] A. Coudray, J.-A. Romand, M. Treggiari, and K. Bendjelid, "Fluid responsiveness in spontaneously breathing patients: a review of indexes used in intensive care," *Critical Care Medicine*, vol. 33, no. 12, pp. 2757–2762, 2005.

[29] F. M. Brunkhorst, C. Engel, M. Ragaller et al., "Practice and perception a nationwide survey of therapy habits in sepsis," *Critical Care Medicine*, vol. 36, no. 10, pp. 2719–2725, 2008.